UNIVERSITÉ DE STRASBOURG

ÉCOLE DOCTORALE MSII

ICube (UMR 7357)

THÈSE présentée par :

Julien GARNON

soutenue le : **01 décembre 2020**

pour obtenir le grade de : **Docteur de l'université de Strasbourg**

Discipline/ Spécialité : Robotique

ASSISTANCE TO THE INJECTION OF A LARGE VOLUME OF ORTHOPEDIC BONE CEMENT

THÈSE dirigée par :
  M BAYLE Bernard   Professeur, université de Strasbourg
  M GANGI Afshin   Professeur, université de Strasbourg

RAPPORTEURS :
  M LEFEUVRE Elie   Professeur, université Paris-Sud
  M PEREIRA Philippe   Professeur, université de Heidelberg

AUTRES MEMBRES DU JURY :
  Mme MEYLHEUC Laurence   Maître de conférence, université de Strasbourg
  M GAUBERT Jean-Yves   Professeur, université de Marseille

Acknowledgements

List of figures

List of tables

Nomenclature

α degree of polymerization

α_g degree of polymerization at the gel point

T temperature (°K),

R gas constant 8.314 J/(mol.K)

$\dot{\gamma}$ shear rate

τ^* critical stress level at the transition to shear thinning

η_0 zero-shear viscosity

η dynamic iscosity

σ conductivity

ρ resistivity

q electric charge

μ free ion mobility

D diffusion coefficient

k Boltzman's constant

Q activation energy

τ dipole time constant

Introduction

Context

The principle of percutaneous image-guided cementoplasty is to inject bone cement within a pathological bone through a needle which is inserted under radiological monitoring. The goal is to reinforce the bony structure that can be weakened by various conditions, most frequently osteoporosis or cancer, with the intent to relieve the pain and provide local mechanical stabilization. The technique was first reported in 1987 for the management of an aggressive cervical hemangioma for which no other treatment remained feasible. Cement injection was initially performed in the spine, most specifically in the vertebral bodies, leading to the appellation vertebroplasty. A few years following the introduction of the technique, percutaneous cement injection started to be applied to the pelvic bone in order to treat painful acetabular metastases refractory to palliative radiation therapy and systemic analgesics. As it turned out to be effective with a minimal-invasive approach and with a low rate of complications, percutaneous cementoplasty was then increasingly performed, not only to manage the pain related to extra-spinal metastases but also to provide consolidation in case of an impending fracture.

Extra-spinal cementoplasty has mostly been reported in the pelvic bone and to a lesser extent in the long bones. The material (needles, image-guidance, cement) is usually the same as the one for vertebroplasty. Even though this might make sense regarding the similarities between the procedures, there are some specificities associated with cement injection outside the spine, particularly in the pelvic area. The anatomy and the biomechanics of the pelvic girdle is more complex than the one of a vertebral body. Moreover, it is a much bigger bone. The repartition and the volume of cement that is required to prevent from a pathological fracture and restore the transmission of loads may therefore differ greatly depending on whether the pelvic bone or the spine are considered.

Challenges and contributions

Several questions remain unanswered in the literature. There are very little data on the influence of the volume and repartition of cement on the restoration of strength. To the best of our knowledge, there is no experiment that seek to evaluate the influence of the number of cement plugs on the global coalescence of cement. Also, there is no standardized anatomical access and no dedicated device (needle, injection device) for the injection of a single large (more than 10 ml) cement volume through a single access site. Such injection comes indeed with specific constraints of time to manage the polymerization of the bone cement: a fast injection exposes to the risk of extravasation and leak, whereas a slow injection of the whole volume will be precluded by the increase of cement viscosity with time.

The goals of the present thesis are therefore:
- to review the literature on extra-spinal cementoplasty, was well as the properties of polymethylmetacrylate (PMMA) and the biomechanics of the bony pelvis, in order to understand the needs for an optimized approach;
- to review the clinical practice of cementoplasty in the pelvic bone, in order to identify the limitations of the actual technique of cementoplasty;

- to study the importance of injecting a large volume of cement in extra-spinal bones and most specifically the pelvic bone. This includes the evaluation of the influence of the volume and repartition of cement on bone stiffness, and the influence of the number of injection sites on the cohesion of cement using computer-assisted modeling and pre-clinical comparison on phantoms:

- to propose and evaluate standardized routes to the pelvic area and, as a result, optimize the injection through a single access site;

- to investigate the feasibility of in-situ measurement of cement viscosity;

- to develop and test a solution for the robot assisted injection of volumes of cement up to 30 ml.

Outline

In the first chapter of the present work, state-of-the-art reviews of the literature on extraspinal cementoplasty, PMMA bone cement and the biomechanics of the bony pelvis are presented. Analyses of the current clinical practice in our institution are also included in this section. In the second chapter, the mechanical importance of the volume of bone cement is studied. In the third chapter, different methods to achieve the injection of volume greater than 10 ml are compared. In the last chapter, different ways to improve the injection of volume greater than 10 ml through a single access site are analyzed. This includes the anatomical evaluation of two different approaches, the feasibility and potential interest of the measure of in-situ viscosity, and the development and testing of a robotic-assistance for the injection. Finally, the findings of this thesis are summed up and perspectives open by this work are proposed.

Publications

The present work has led to the following publications and presentations:

Garnon J et al. Percutaneous image-guided double oblique anterior approach to the acetabulum for cementoplasty. Clin Radiol. 2020 Sep 27:S0009-9260(20)30379-2. doi: 10.1016/j.crad.2020.09.001. Epub ahead of print. PMID: 32998833.

Garnon J et al. Biomechanics of the Osseous Pelvis and Its Implication for Consolidative Treatments in Interventional Oncology. Cardiovasc Intervent Radiol. 2020 Aug 26. doi: 10.1007/s00270-020-02624-0. Epub ahead of print. PMID: 32851425.

Garnon J et al. Subjective Analysis of the Filling of an Acetabular Osteolytic Lesion Following Percutaneous Cementoplasty: Is It Reliable? Cardiovasc Intervent Radiol. 2020 Mar;43(3):445-452. doi: 10.1007/s00270-019-02397-1. Epub 2019 Dec 19. PMID: 31858181.

Garnon J et al. Continuous Injection of Large Volumes of Cement Through a Single 10G Vertebroplasty Needle in Cases of Large Osteolytic Lesions. Cardiovasc Intervent Radiol. 2020 Apr;43(4):658-661. doi: 10.1007/s00270-019-02389-1. Epub 2019 Dec 2. PMID: 31792587.

Garnon J et al. Percutaneous extra-spinal cementoplasty in patients with cancer: A systematic review of procedural details and clinical outcomes. Diagn Interv Imaging. 2019 Dec;100(12):743-752. doi: 10.1016/j.diii.2019.07.005. Epub 2019 Aug 16. PMID: 31427218.

Garnon J et al. Injection Device for Percutaneous Osteoplasty. Seventh International Workshop on Medical and Service Robots" (MESROB2020)

Anselmini R. *Simulation de l'écoulement du ciment orthopédique en cimentoplastie*. Mémoire de diplôme d'ingénieur et de Master. Institut National des Sciences Appliquées de Strasbourg. Faculté de Physique et Ingénierie de l'Université de Strasbourg. 2020.

Harrer L, Husser M. *Conception d'un modèle de simulation de bassins et humérus*. Mémoire de Projet de Recherche et Technologique. Institut National des Sciences Appliquées de Strasbourg. 2020.

Marche C. *Etude de l'injection et de la tenue mécanique de gros volumes de PMMA pour la cimentoplastie*. Mémoire diplôme d'ingénieur. Institut National des Sciences Appliquées de Strasbourg. 2019.

Poursillie E. *Génération de phantom de bassin pour la cimentoplastie*. Mémoire de diplôme d'ingénieur et de Master. Institut National des Sciences Appliquées de Strasbourg. Faculté de Physique et Ingénierie de l'Université de Strasbourg. 2020.

1st Chapter – Extraspinal cementoplasty: generalities and review of the literature

This section seeks to describe the basic technique of percutaneous cementoplasty, as well as the main differences between its practice in the spine and outside the spine (mostly in the pelvic bone). Reviews of the literature on extraspinal cementoplasty, PMMA bone cement and the biomechanics of the bony pelvis are presented. The results of the retrospective analyses of our experience in extra-spinal cementoplasty regarding technical issues and long-term stability of the cement plug are exposed.

1.1. Percutaneous cementoplasty

1.1.1 Principle

Percutaneous cementoplasty has been described for the first time in 1987 for the management of an aggressive hemangioma of the axis [Galibert 1987]. The principle of the intervention is to insert a bone trocar inside the bone and to inject bone cement through the trocar (fig.1). The intervention is performed percutaneously (i.e without the need for an open surgical approach) under radiological guidance to ensure proper positioning of the needle and assess the correct diffusion of the cement.
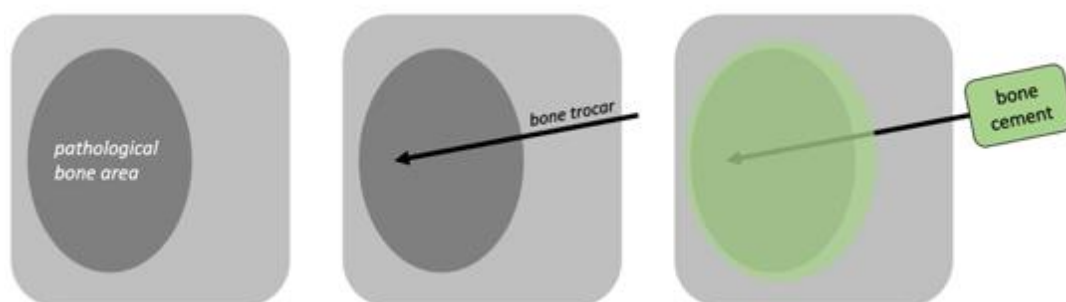
Fig.1: Principle of percutaneous cementoplasty: a bone trocar is inserted in a pathological bone area (most frequently due to osteoporosis or cancer). Bone cement is subsequently injected inside the bone through the trocar.

1.1.2. Main applications

Percutaneous cementoplasty is mostly applied in the spine (vertebroplasty) for the management of painful osteoporotic compression fractures of the vertebral body or painful malignant osteolysis (bone destruction due to cancer, mostly metastases) without or with impending/pathological fractures of the vertebral body (fig.2) [Cotten 1998]. The goal of vertebroplasty is to provide pain palliation and to a lesser extent to avoid secondary spinal kyphotic deformities.

16

Cementoplasty can also be used beyond the spine as a minimally invasive treatment of painful extra-spinal malignancies (extra-spinal cementoplasty), either as a first-line treatment or after failed radiation therapy. The main objective of such a treatment is to alleviate the pain of patients suffering from bone metastases (fig.3). In addition, bone cement may also provide bone consolidation in locations predominantly stressed with compression loads. It can also be used in combination with other devices such as nails or screws to enhance the biomechanical stability of the surgical device [Garnon 2019].

With the improvement of the life expectancy for many cancers and in an attempt to decrease the risk of skeletal related events, vertebroplasty and extra-spinal-cementoplasty are increasingly being performed in asymptomatic patients with the sole therapeutic goal of consolidation
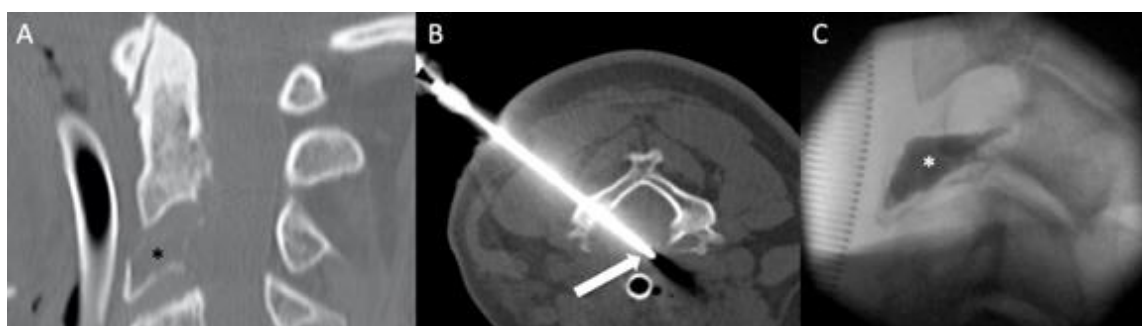
Fig.2: Vertebroplasty in the cervical spine. (A) Sagittal CT-scan shows a lytic metastasis of the vertebral body of C3 (black asterisk) at high risk of collapse. (B) A bone trocar (arrow) is inserted inside the lesion under image-guidance. (C) Bone cement (white asterisk) is injected inside the lesion with the double goals of pain treatment and bone consolidation.
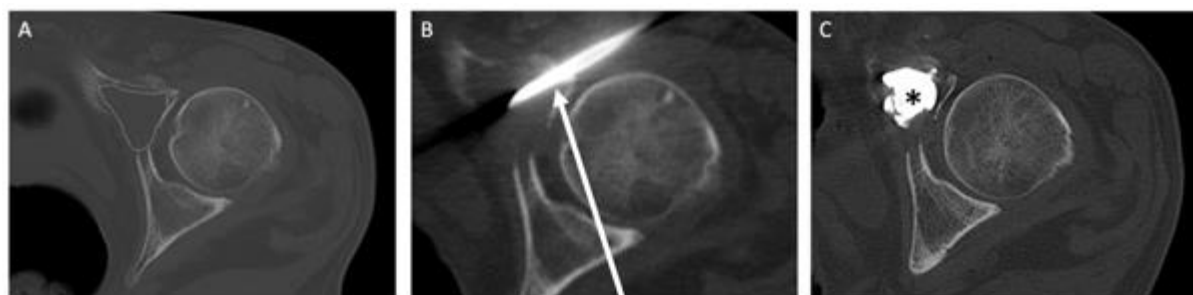
Fig.3: Extra-spinal cementoplasty. (A) Axial CT-scan shows a lytic metastasis in the anterior acetabulum (dotted circle). (B) A bone trocar (arrow) is inserted inside the lesion. (C) Bone cement (asterisk) inside the lesion.

1.1.3. Material

Percutaneous cementoplasty necessitates a bone trocar, bone cement and a device to inject the cement through the trocar.

1.1.3.1. Bone trocar

Any bone trocar can theoretically be used to inject bone cement. The tip may be bevel or diamond-tip (fig.4). A bevel needle is supposed to offer a better control on the direction of cement inflow. The diameter may range between 8G and 15G, a needle with a larger inner lumen having the advantage of facilitating the injection for the operator.
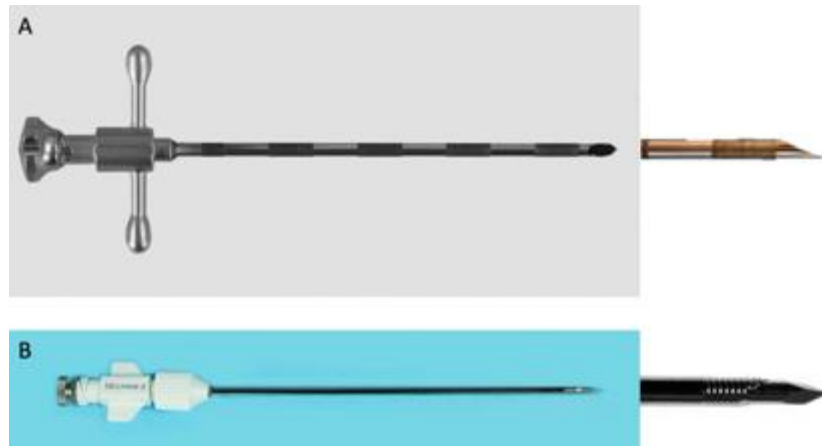
Fig.4: Examples of bone trocar for cementoplasty. (A) Bevel-tip trocar. (B) Diamond-tip trocar.

1.1.3.2. Bone cement

There are different types of bone cement on the market. Although there has been a trend to promote the use of biocompatible materials, PMMA is still by far the most frequently injected bone cement as it is cheap, easy to handle and offer long-term stability. PMMA bone cements may differ according to their viscosity, with high-viscosity bone cements offering a longer working time. For most cements, the application phase ranges between 10 to 20 minutes. The duration of the application phase of different PMMA bone cements is presented in table1.

Company	PMMA bone cement name	Duration of the application phase (min)	Room temperature (°C)
Merit	Osseoperm Mendec	17	21
	StabiliT ER[2]	35	20-23
Heraeus	Osteopal V	8	20
	Osteopal V +	20	20
		12	23
Optimed	CementoFixx M	9	20
Stryker	Vertaplex	20	20
	Vertaplex HV	18	20
	Spineplex	10	20

Table1: Duration of the application phase for a given room temperature of different PMMA bone cements

1.1.3.3. Injection device

The injection device helps to deliver the bone cement through the cannula. Various devices have been designed and range from basic models, such as standard 1 to 3 ml syringes, to more advanced handheld systems that allow the operator to control the injection while staying away from the injection site thereby decreasing radiation exposure. The delivery systems of main manufacturers and their capacity is presented in table2.

company	name of the delivery system	picture	maximal capacity (ml)
Optimed	Cemento-MP		10
J&J	Confidence		11
Merit	StabiliT VP		10
Stryker	Autoplex		12
Medtronic	Kyphon CDS		2x8

Table2: characteristics of the main delivery systems from different companies

1.1.4. Image guidance

Image-guidance is key for the technical success of the intervention. It is used throughout the entire phases of the intervention, i.e. for the placement of the needle and for the injection of bone cement. In this perspective, fluoroscopy and/or CT-scan may be used. Fluoroscopy offers real-time imaging with high spatial resolution but only with a two-dimension projection. CT-scan offers the possibility of 3 dimensions imaging, notably in the axial plane, at the cost of a higher radiation without (or with limited) access to real-time imaging. Both modalities may therefore be combined to get rid of the limitations of each technique taken separately (fig.5).
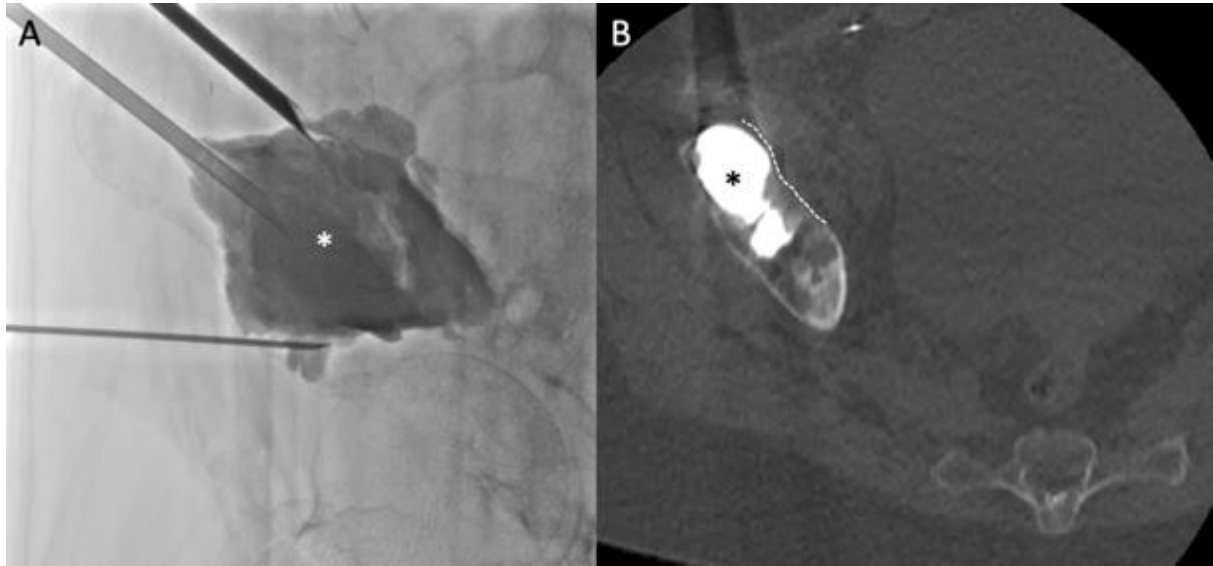
Fig.5: Combined fluoroscopic and cross-sectional imaging to guide an extra-spinal cementoplasty of the acetabular roof. (A) Fluoroscopy provides real-time monitoring of the bone cement (white asterisk). (B) CT-scan demonstrates very clearly the boundary (dotted line) between the soft tissue and the bone metastasis filled with cement (black asterisk). The combination increases the operator's confidence in the proper repartition of the PMMA bone cement.

For the insertion of the bone trocar, the choice of image guidance depends on the targeted area: fluoroscopy is most of the time sufficient to approach the spine or the long limbs whilst CT-scan offers increased precision to access the osseous pelvis. For the injection of cement, fluoroscopy should be considered as the gold-standard because of its real-time imaging capacities that allow to monitor for any extra-osseous leakage. For complex cases, i.e. those with destroyed anatomical landmarks secondary to cancer, CT-scan may be used in combination with fluoroscopy in order to assess proper repartition of the bone cement in 3 dimensions and rule out any extravasation in the surrounding soft tissue. Hence, the use of the combination of fluoroscopy and cross-sectional imaging to guide extra-spinal cementoplasty, particularly in the osseous pelvis, should be recommended. Such combination may be feasible with several solutions, such as Angio-CT, Cone-beam CT (CBCT), or a mobile C-arm and a regular CT-gantry (fig.6).
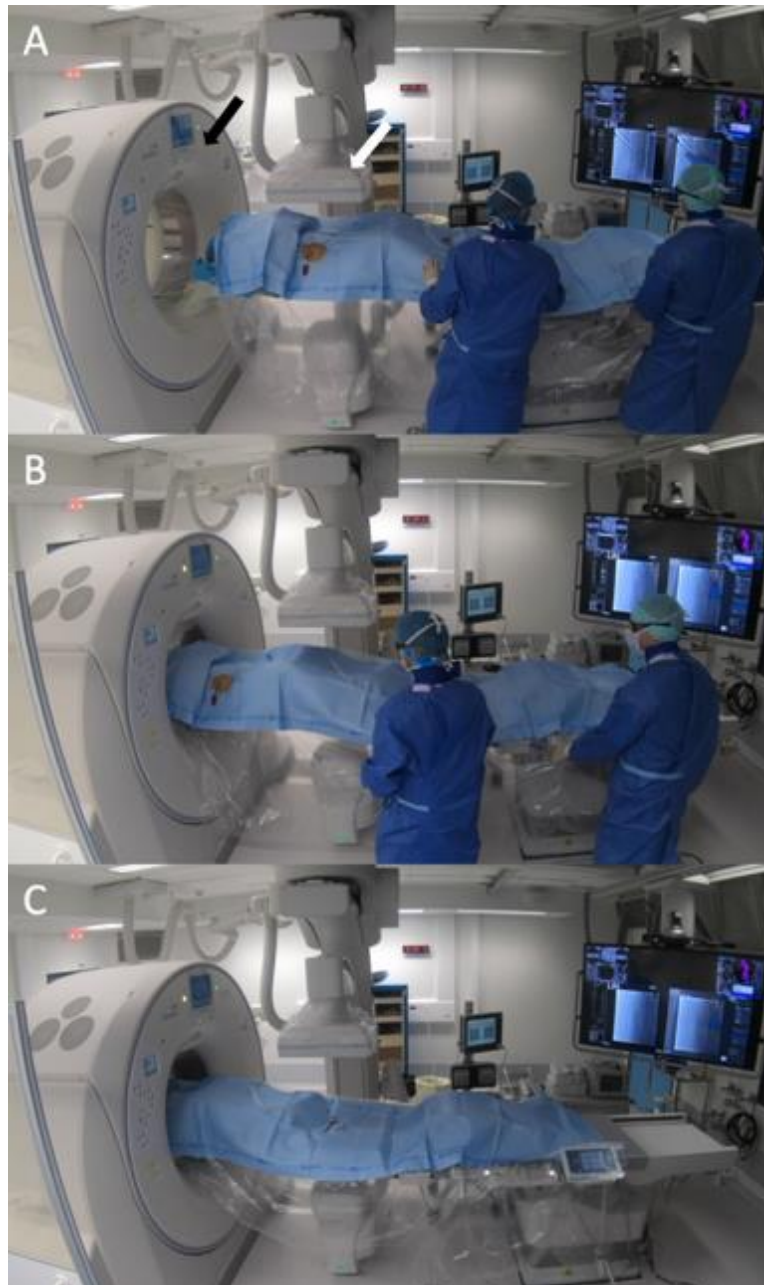
Fig.6: Example of the combination of fluoroscopy and CT-scan: Angio-CT. (A) Angio-CT includes a cone-beam (white arrow) fixed on the ceiling and a CT-scan (black arrow) mounted on rails. Imaging can be performed with fluoroscopy (A) and CT-scan (C), simply by displacing the table (B) between the two modalities. The transition takes less than 30 seconds.

1.2. Extra-spinal cementoplasty: technical considerations in comparison to vertebroplasty

Although the basic principle of the intervention remains similar, percutaneous cementoplasty in extra-spinal locations may differ from vertebroplasty notably concerning the access to the bone and the volume of required PMMA bone cement.

1.2.1. Approach to the lesion

The transpedicular or intercostovertebral approaches to the vertebral bodies are well standardized in the spine. On the other hand, access to extra-spinal lesions necessitate to adapt to the local anatomy that may be very complex (e.g. osseous pelvis). The ideal route for the bone trocar goes along the great axis of the tumor, which sometimes necessitates a double obliquity that might be challenging in the clinical practice. Hence, depending on the chosen pathway, several trocars may be required to optimize the chance of proper diffusion and filling of a lesion by the PMMA bone cement (fig.7).
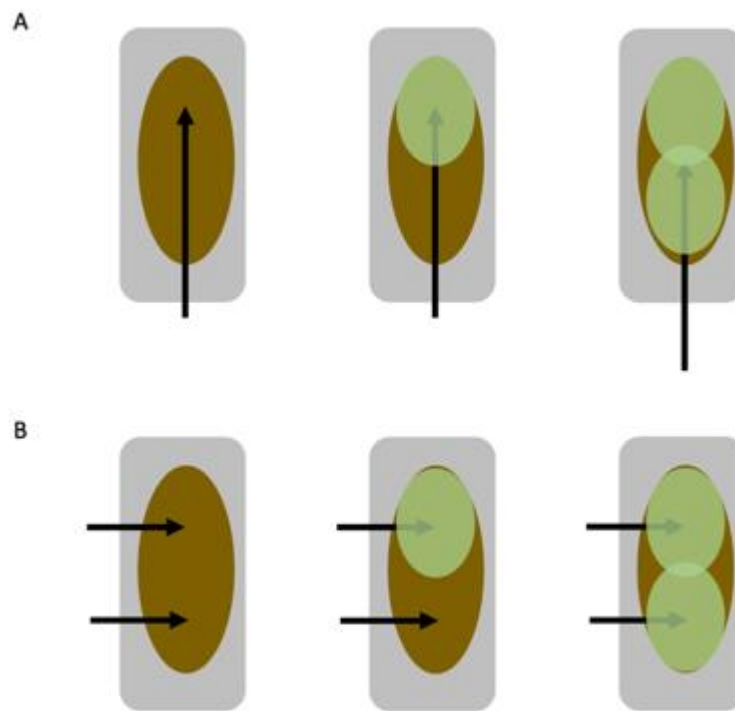
Fig.7: Different approaches to the same lesion in extra-spinal cementoplasty. (A) Approach in the great axis of the tumor. The volume of cement is delivered through a single needle while withdrawing the bone trocar. (B) Approach in the axial plane. It requires several needles to increase the chance of a good repartition of the bone cement. Approach in A is usually more challenging than the one in B.

1.2.2. Volume of PMMA bone cement

In the clinical practice, the volume of cement injected inside a vertebral body ranges from a few ml to 10 ml. Hence, the capacity of most delivery systems is adapted to inject such a quantity of bone cement. For extra-spinal locations, the volume of PMMA bone cement may exceed significantly the value of 10 ml, that will therefore be considered as the threshold value for the term "large volume of cement" throughout the present thesis. As extra-spinal cementoplasty is performed with bone cement and delivery systems designed for the spine, the maximal volume that can be injected with a single kit of cement does not exceed 10 to 15 ml for the majority of devices as seen previously. Even with a large containing system, the injection of a large volume of cement can be challenging

as it is associated with specific constraints of time to manage the polymerization of the bone cement: a fast injection exposes to the risk of extravasation outside the bone, whereas a slow injection of the whole volume will be precluded by the progressive hardening of the bone cement inside the delivery system. Hence, injection of a large volume of cement seems difficult to achieve in the daily practice.

1.3. Extra-spinal cementoplasty: systematic review of the literature

The aim of the following review is to perform a systematic analysis of the technical details and clinical outcomes of percutaneous extra-spinal cementoplasty in patients with malignant lesions, in order to understand if and where the injection of a large volume of cement was a clinical need.

1.3.1 Materials and methods

1.3.1.1 Selection criteria

Informed consent was not required for this retrospective systematic review. We searched PUBMED, MEDLINE, MEDLINE in-process, EMBASE and the Cochrane databases between January 1990 and February 2019 using the following keywords «percutaneous cementoplasty», «percutaneous osteoplasty» and «extra-spinal cementoplasty». After exclusion of duplicates, the titles and abstracts of publications identified by the database search were screened for studies that potentially met the inclusion/exclusion criteria. Final eligibility was based after examination of full text. The screening was performed by two of the authors. Disagreements were resolved by consensus.

The following criteria were used for selection: retrospective/prospective cohort of more than 4 patients; study published in English language; study reporting the use of percutaneous cementoplasty (i.e., percutaneous injection of cement inside a bone metastasis using a dedicated bone trocar, in extra-spinal locations); percutaneous cementoplasty was used as a stand-alone procedure or in combination with another percutaneous intervention and; percutaneous cementoplasty was used to provide pain palliation and/or bone consolidation.

Papers reporting the use of hollowed implants through which cement was injected (hollowed screws for example) were excluded from analysis, because the primary goal is to improve the material stability and not to fill the tumour. Studies including both spinal and extra-spinal procedures were only included if detailed data of extra-spinal interventions were accessible. Sacral cementoplasties were considered as extra-spinal cementoplasties. Commentaries, abstract, review articles and conference presentations were not included.

1.3.1.2. Methodological quality assessment

The quality of studies was evaluated with a modified version of the Newcastle-Ottawa scale [Wells 2015]. This system evaluates the quality of non-randomized studies included in a review using a ''star system'' from 0 to 6. The higher the number of stars, the lower the risk of bias. Papers awarded with less than four stars were excluded from the present review.

1.3.1.3. Data extraction and analysis

The full text of all included papers was reviewed to collect specific items in a dedicated spreadsheet (Excel 2011, Microsoft, Seattle, WA). For each study, data on:

- patient age;
- lesion characteristics (histology, size, localisation, Harrington classification for acetabular lesions, Mirel's score for lesions located in long bones);
- performing physician (surgeon/interventional radiologist);
- additional percutaneous intervention within the same session of treatment (balloon expansion, thermal ablation, implants);
- bone needle size in Gauge (G);
- volume of cement;
- degree of lesion filling;
- description of the technique for injection greater than 10 mL;
- rate of overall and symptomatic leakages;
- pain score before and after the intervention at last time point of assessment and;
- secondary fractures/surgery were extracted if available.

Case by case analysis was performed whenever possible. Descriptive statistics were computed to present results. The overall weighted mean method was used to calculate a mean value across studies whenever feasible.

1.3.2. Results

The first search query produced 2678 studies. After screening by title and abstracts, 65 studies were included for full text analysis. Of those, 30 fulfilled the inclusion/exclusion criteria and were therefore included for the present study (fig.8). No exclusions were made due to risk of bias.
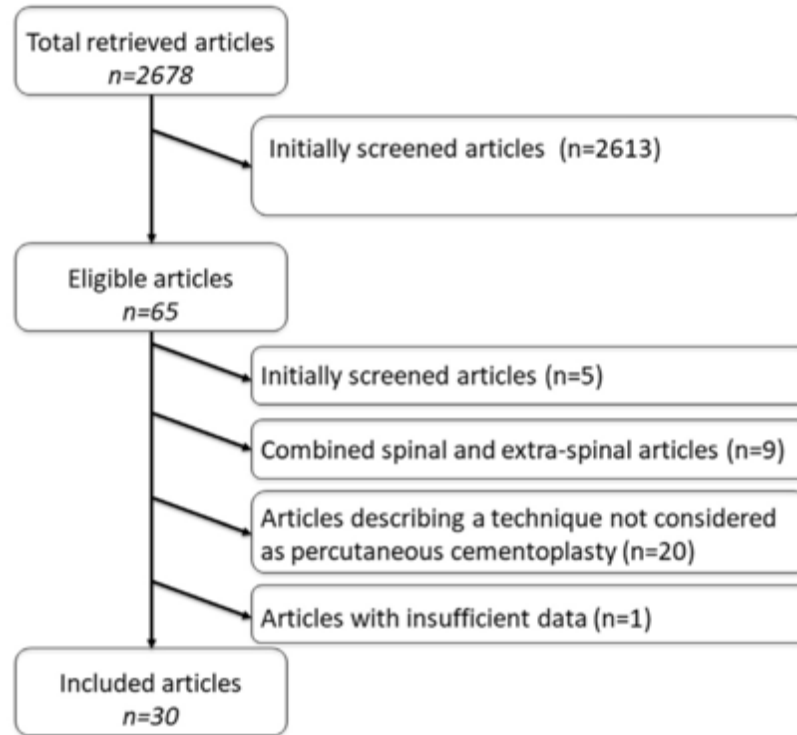
Fig.8: Flow chart of article selection

Included publications were issued between 1995 and 2019. There were 20 retrospective and 6 prospective studies, while 4 articles did not clearly state whether the study was prospective or retrospective.

1.3.2.1 Patients and lesions characteristics

A total of 761 extra-spinal lesions in 652 patients (data available from all studies; number of studies $n_p = 30$) were treated using percutaneous cementoplasty [Cotton 1995, Weill 1998, Marcy 2000, Hierholzer 2003, Toyota 2005, Kelekis 2005, Anselmetti 2008, Basile 2008, Hoffmann 2008, Maccauro 2008, Munk 2009, Masala 2011, Deschamps 2012, Gupta 2012, Iannessi 2012, Cazzato 2014, He 2014, Kim 2014, Sun 2014, Tian 2014, Colman 2015, Kurup 2015, Wei 2015, Kelekis 2016, Kim 2016, Wallace 2016, Durfee 2017, Couraud 2018, Fares 2018, Moser 2019]. The mean age of the patients at the time of treatment was available/could be extracted for all studies but one ($n_p = 29$) and ranged between 48.6- and 69.4-years old across publications. The most frequent histology was available/could be extracted for all studies ($n_p = 30$). Lung cancer was the most frequently reported primary tumor (11 articles), followed by breast (8 articles) and myeloma/kidney (7 articles).

Size of lesions was available in 9 studies ($n_p = 9$). The mean size was reported/could be calculated for 8 studies ($n_p = 8$), while one article reported only the volume of the lesions. The mean lesion size ranged from 29 mm to 73 mm across studies. The mean lesion size calculated among 315 lesions ($n_p = 8$) using the overall weighted mean method was 45 mm.

25

Localisation of the extra-spinal lesions was available for all studies and could be divided into lesions of the pelvis (coxal bone and sacrum), of the long bones and of other bones (rib, skull). Eleven studies focused on pelvic cementoplasties, 6 on cementoplasties of the long bones and 13 included all kind of locations. Overall, 489 lesions were located in the pelvis, 262 in the long bones of the limbs and 10 in other locations (n_p = 30) (Table3). The most frequently treated area in the coxal bone (n_p = 22) was the acetabulum (197 lesions). Only two studies over the 24 reporting percutaneous cementoplasty in the pelvis did not specify sublocation of the tumours within the coxal bone. Grading of acetabular lesions using the Harrington classification could be extracted from 3 studies, representing a total of 55 lesions with a mean score of 2.3. Lesions of the long bones were more frequently localized (n_p = 19) in the femur (166 lesions). The Mirel's score, which evaluates the risk of pathological fracture for lesions of the long bones, was reported in 5 articles, with a mean score greater than 9 (over 12) in all publications.

Palliative pain management was the main indication for 735 lesions (n_p = 27), while prevention of fracture was the major concern for 26 lesions (n_p = 3).

1.3.2.2. Procedure details

1.3.2.2.1 Performing physician

The performing physician could be evaluated in all studies but one (n_p = 29). Among the 728 treatments, 613 (84.2%) were performed by interventional radiologists and 115 (15.8%) by orthopedic surgeons. Lesions treated by surgeons (n_p = 5) were located either in the long bones (n = 63) or the acetabulum (n = 52). All 63 percutaneous cementoplasties performed by surgeons for lesions of the long bones (n_p = 2) were combined with surgical stabilization using flexible (n = 20) or closed intramedullary (n=43) nails. There was no other extra-spinal lesion treated by surgeons. Interventional radiologists (n_p = 24) treated more lesions in the pelvis (n = 408) than in the long bones (n = 195). Cementoplasty without any additional implanted device was used in the majority of lesions (n = 166, representing 85% of the lesions) treated by interventional radiologists in the long bones. Implant-augmented cementoplasties were performed for the remaining 31 lesions (15%), and included cannulated screws (n = 13, one study), bone puncture needles after removal of the tails and pinpoints (n = 6, one study) and 22 G stainless steel microneedles (n = 12, one study).

Authors	Main indication for PC	No of patients	No of lesions in the pelvic bone	No of lesions in the long bones	No of lesions in other locations	Additional treatment combined with PC	Needle diameter (G)	Mean volume of injected cement (mL)	Maximal volume of cement (mL)
Couraud et al.	Pain palliation	31	47	3	1	Balloon kyphoplasty – number not reported	11	N.R	N.R
Fares et al.	Pain palliation	30	20	10	–	RFA – 30 lesions	11 or 13	2.7	N.R
Tian et al.	Pain palliation	38	46	8	–	RFA – 54 lesions	11 or 13	6.6	28
Sun et al.	Pain palliation	51	53	5	–	–	11 or 13	N.R	N.R
Iannessi et al.	Pain palliation	20	13	7	..	.	11	4.3	10
Masala et al.	Pain palliation	39	17	22	–	–	13	3	4
Basile et al.	Pain palliation	13	6	6	1	–	11 or 13	3.5 (pelvic PC)	12 (pelvic PC)
Anselmetti et al.	Pain palliation	50	26	26	6	RFA – 7 lesions	10	5.9	15
Nierholzer et al.	Pain palliation	5	4	1	–	–	N.R	17.8	36
Kim et al.	Pain palliation	15	–	20	–	Insertion of flexible nails – 20 lesions	10	15.5	31
Cotten et al.	Pain palliation	11	12	.	..	.	10	15	23
Durfee et al.	Pain palliation	11	11	–	–	Balloon kyphoplasty – 1 lesion	N.R	N.R	N.R
Maccauro et al.	Pain palliation	25	30	.	.	–	10	N.R	N.R
Cazzato et al.	Pain palliation	51	.	66	.	–	11 or 13	N.R	N.R
Munk et al.	Pain palliation	12	13	1	–	RFA – 14 lesions	8, 11 or 13	8	16
Wedl et al.	Pain palliation	18	18	.	.	–	10	7.6	14
Kim et al.	Pain palliation	43	–	43	–	Intramedullary nailing – 43 lesions	11	19.1	37
Kelekis et al.	Pain palliation	12	–	12	–	Insertion of micromeshs – 12 lesions	8	N.R	N.R
Deschamps et al.	Fracture prevention	12	–	13	–	Screw fixation – 13 lesions	11	N.R	N.R
Hoffmann et al.	Pain palliation	8	6	3	–	RFA – 9 lesions	10 or 15	8	10
Moser et al.	Pain palliation	40	44	–	–	–	11 or 13	10.3	27
Kelekis et al.	Pain palliation	14	23	–	.	–	11	8	15
Wallace et al.	Pain palliation	12	12	–	–	Bipolar RFA – 12 lesions	N.R	12	30
Kurup et al.	Fracture prevention	7	7	–	–	Cryoablation and balloon kyphoplasty - 7 lesions	10	14	21
He et al.	Fracture prevention	6	–	6	–	Insertion of broken pins – 6 lesions	11 or 13	22.2	42
Toyota et al.	Pain palliation	12	12	3	2	RFA – 17 lesions	8 to 13	7	15
Wei et al.	Pain palliation	26	29	4	–	MWA – 33 lesions	13	8	14
Marcy et al.	Pain palliation	18	18	–	–	–	N.R	6	9
Colman et al.	Pain palliation	11	11	–	–	RFA – 3 lesions	N.R	N.R	N.R
Gupta et al.	Pain palliation	11	11	.	.	.	11 or 13	N.R	N.R

Table3: included studies and procedures details

1.3.2.2.2 Additional intervention

Detailed data were available for all studies but one (n_p = 29) that reported the use of balloon kyphoplasty for some pelvic lesions without further specifications. Cementoplasty was reported as a stand-alone procedure for 427 lesions (60.1%). Kyphoplasty was performed for 10 lesions (1.4%) (n_p = 2), all located in the acetabulum. For 186 lesions (26.2%), thermal ablation was combined to cementoplasty (n_p = 10): 134 lesions (72%) were ablated with monopolar radiofrequency ablation (RFA) (n_p = 7), 33 lesions (17.7%) with microwave (n_p = 1), 12 (6.5%) with bipolar RFA (n_p = 1) and 7 (3.8%) with cryoablation (n_p = 1). Localisation of the tumors that were ablated was the pelvis for 148 lesions (79.6%), the long bones for 34 lesions (18.3%) and other locations for 4 lesions (2.1%). Lesions that were cryoablated in the acetabulum all benefited from the combination of kyphoplasty and cementoplasty either the same day after cryoablation (2 patients) or the day after (5 patients) (n_p = 1). As priorly detailed, implant-augmented cementoplasty was performed for 94 lesions (12.3%) (n_p = 5), all located in the long bones.

1.3.2.2.3 Needle diameter

The needle diameter was reported in 25 articles representing 704 lesions (n_p = 25). Precise data could be extracted from 14 studies (379 lesions). The diameter of the needles in the remaining 11 studies (325 lesions) was variable, without the possibility of a case by case analysis. The needle diameter was 13-G for 72 lesions (10.2%) (n_p = 2),

11-G for 150 lesions (21.3%) (n_p = 5), 10-G for 145 lesions (20.6%) (n_p = 6), and 8-G for 12 lesions (1.7%) (n_p = 1). It ranged from 11- to 13 G for 285 lesions (40.5%) (n_p = 8) and from -8 to 15-G for 40 lesions (5.7%) (n_p = 3).

1.3.2.2.4 Volume of cement

The volume of injected cement was available in 20 studies, reported as a mean value in 11 articles and as case by case data in 9 articles. One study reported only the mean volume of cement for pelvic cementoplasties but not for lesions in the long bones. Nine studies did not report the amount of cement.

The mean volume of cement ranged from 2.7 ml to 32.2 ml across studies (n_p = 20) (Table3). Data from these 20 studies were extracted and used to calculate a mean volume using the overall weighted mean method. Hence, the mean volume was 8.8mL among the 485 lesions used for statistical evaluation (n_p = 20). More specifically, data for pelvic injections could be extracted from 13 studies: the mean volume calculated over 188 lesions (n_p = 13) was 9.1 ml (Table 4). The maximal reported volume for a pelvic osteoplasty was 36 mL For long bones, data from 8 studies were extracted: the mean volume was calculated over 84 lesions (n_p = 8) and was 16.9 mL (Table5). Maximal reported volume for a cementoplasty in a long bone was 42 ml. Detailed analysis of the 9 studies reporting case by case data showed that over 116 lesions, 50 were filled with more than 10 ml, 12 with more than 20 ml and 6 with more than 30 ml. Twenty-six of the 50 lesions filled with a volume greater than 10 ml were located in the pelvis (acetabulum was the most frequent location), and 24 in the long bones (femur was the most frequent location).

Authors	No of lesions	Mean volume(mL)	Lesion filling
Iannessi et al.	13	4.3	N.R
Basile et al.	6	3.5	N.R
Hierholzer et al.	4	17.75	N.R
Cotten et al.	12	15	N.R
Munk et al.	13	8.3	N.R
Weill et al.	18	7.8	N.R
Hoffmann et al.	6	8.7	N.R
Moser et al.	44	10.3	54.8%
Kelekis et al.	23	8	N.R
Wallace et al.	12	12	N.R
Kurup et al.	7	14	64%
Toyota et al.	12	7.5	N.R
Marcy et al.	18	6	N.R
	188	9.1	56.1%

Table4: Volume of injected cement for pelvic lesions.

Authors	No of lesions	Mean volume(mL)	Lesion filling
Iannessi et al.	7	4.3	N.R
Hierholzer et al.	1	18	N.R
Munk et al.	1	5	N.R
Kim et al.	20	15.5	N.R
Kim et al.	43	19.1	N.R
Hoffmann et al.	3	6.7	N.R
He et al.	6	32.2	N.R
Toyota et al.	3	6	N.R
	84	16.9	N.R

Table5: Volume of injected cement for long limbs lesions.

1.3.2.2.5 Technique of injection for volumes > 10 ml

Among the 17 studies that reported either a mean or a maximum volume superior to 10mL, 7 briefly stated how such injection was achieved. They all describe the use of additional needle(s) and cement(s) to complete the injection. The mean number of needles per site of injection was available for one of those 7 studies, with a mean value of 3.83. One study described precisely the technique used to inject more than 10mL of cement. In that article, the authors were injecting simultaneously different volumes of cement on 2 or 3 different bone trocars.

1.3.2.2.6 Lesion filling

Precise information (*i.e.*, not subjective) about the per- centage of filling by cement was available in 3 studies (62 lesions) focusing on pelvic osteoplasties. The percentage ranged from 54.8% to 64%, for a mean value of 56.8% using the overall weighted mean method. One other study reported the percentage of filling of the lesion as more than or less than 50%, with 70% of the lesions exhibiting a filling greater than 50% without further specification.

1.3.2.3 Outcomes

1.3.2.3.1 Pain palliation

Pain scores using a visual analogic scale (VAS) score could be extracted from 24 studies. Twenty-two of the 24 papers reported the VAS score as a 10 points scale; 2 studies used a 100 points scale which was turned into a 10 points scale for further evaluation. One study mentioned the VAS score but without the possibility to differentiate the extra-spinal cases from the spinal ones and was therefore not included for analysis. The 5 remaining studies did not report precisely the VAS score and only mentioned subjective evaluation of the pain. The preoperative VAS scores ranged between 3.2 and 9.5 ($n_p = 24$). For the postoperative pain scores, we used the last time point available for evaluation. This time point could be extracted from 21 papers and ranged from 24hours to one-year, with 14 articles reporting the last evaluation at one month or more (Table6), and 10 articles at 3 months or more. The number of patients completing the last follow-up could not be precisely numbered. Overall, postoperative

scores ranged from 0.4 to 5.6 (n_p = 24). Twenty-one papers over 24 reported a difference between the pre- and the post-interventional scores greater than two. Thirteen studies reported a reduction of 5 points or more.

Authors	Preoperative pain score	Postoperative pain score	Last time point for evaluation (Month)	Difference between pre-and post-operative pain scores	Statistically significant
Fares et al.	7.2	3.7	3	−3.5	Yes
Tian et al.	7.1	1.3	6	−5.8	Yes
Sun et al.	8.2	3	3	−5.2	Yes
Iannessi et al.	6.4	2	3	−4.1	Yes
Masala et al.	8.4	2.4	6	−6	Yes
Basile et al.	7.6	2.7	6	−4.9	Yes
Anselmetti et al.	9.1	2.4	12	−6.7	Yes
Kim et al.	7.2	2.8	1.5	−4.4	Yes
Maccauro et al.	8.6	5.1	12	−3.5	N.R
Munk et al.	7.9	3.6	1.5	−4.3	Yes
Deschamps et al.	6.1	1	1	−5.1	Yes
Wei et al.	7.4	1.2	6	−6.2	Yes
Marcy et al.	3.2	1.6	1	−1.6	N.R
Colman et al.	5.45	4	3	−1.45	N.R

Table6: Clinical outcomes in studies reporting a follow-up of minimum one month.

1.3.2.3.2 Symptomatic cement leakage

A total of 10 symptomatic leakages were numbered among the 761 lesions (n_p = 30), giving a rate of symptomatic leak- age of 1.3%. Nerve injury was the most frequent symptomatic leakage (*n* = 4; 0.6%).

1.3.2.3.3 Secondary fractures and secondary surgical procedures

Six studies did not clearly state if fracture assessment at the treated site was part of the follow-up. Hence, 24 articles (626 lesions) were analyzed. The length of follow-up was available for 22 of these 24 articles and ranged from 62 days to 26.4 months. A total of 14 fractures (2.2%) occurring at the treated site could be identified (n_p = 24), at an interval from the cementoplasty procedure ranging from 3 days to 7 months. Seven surgical interventions to fix the fracture were reported. Additionally, two surgical extractions of cement leakages and 7 delayed acetabular interventions following percutaneous cementoplasty of the acetabulum (interval from the procedure available for only 3 procedures, ranging from 10 to 39 months) were reported.

3.3 Discussion

Percutaneous cementoplasty is an effective tool to alleviate the pain associated with extra-spinal bone metastases. The technique has mostly been applied for acetabular lesions in the pelvis and in the femur for the long bones. The clinical benefit seems clear, as 21 over 24 studies reported a drop in pain score greater than 2 (which is considered as the thresh- old for significance), while the rate of symptomatic leakages was inferior to 2%. On the other hand, the review of the literature also demonstrates great heterogeneity in terms of clinical practice. Most of the procedures (84.2%) were performed by interventional radiologists, probably because of an easier access to computed tomography (CT) or cone bean CT that both offer high precision. Osteoplasty was performed as a stand-alone technique in the majority of lesions (60.1%), while in the remaining 40% it was combined with another

technique such as thermal ablation (26.2%), implant devices (12.3%) or balloon kyphoplasty (1.4%) prior to cement injection.

The exact benefit of combined ablation and cementoplasty vs. cementoplasty alone cannot be assessed, especially for lesion limited to bone without extension to the surrounding soft tissue [Kam 2017]. Thermal ablation certainly makes sense to alleviate the pain related to the invasion of the surrounding muscle in case of a large osteolytic metastasis [Coupal 2017]. This certainly explains that ablation was predominantly performed in association to cementoplasty for lesions located in the pelvic girdle, which frequently involve the surrounding soft tissue. Ablation prior to cement injection may also be indicated whenever local tumour control is indicated, as cementoplasty has little to no antitumoral effect and has been reported to transiently increase the level of the cancer circulating cells in the minutes following injection [Anselmetti 2009, Mohme 2017]. The predominance of monopolar RFA may seem strange in an era where bipolar RFA, cryoablation and even microwave ablation are more and more promoted for bone ablation. The most likely explanation comes with the year with which the papers were issued, when monopolar RFA was the main if not the single available modality [Goetz 2004].

The use of implant devices in association with cementoplasty for lesions located in the long bones but not in the acetabulum makes sense on a biomechanical point of view: the high resistance of cement to compression load is adapted to ensure bone consolidation in the acetabulum, while the poor resistance of cement to shear, bending and torsion stresses makes it unsuitable as a stand-alone intervention for metaphyseal/diaphyseal lesions with a high risk of impending fractures [Deschamps 2012, Cazzato 2019]. Interestingly, all the lesions localized in the long bones and that were treated by surgeons under- went nail fixation and cementoplasty, while only 15% of the procedures in the long bones performed by interventional radiologists were associated with other implant devices, for which little to no biomechanical validation exists. It is possible that the procedures performed by orthopedics were more driven towards a mechanical stabilization than the one performed by interventional radiologists where pain control was the major concern. As demonstrated in another review, stand-alone cementoplasty in the long bones is effective to achieve pain alleviation and to improve mechanical function but fracture is the most frequent complication [Cazzato 2015]. In any situations, mechanical stabilization should always be kept in mind when performing percutaneous cementoplasty in the long bones. In such area, the combination of fixation and cement can potentially improve the outcomes: nails/screws (depending on the location) stabilize the area while cement increases the anchorage of the device(s) and allows to optimize pain management related to the bony tumor infiltration [Lea 2019, Roux 2019].

The needle diameter used to perform cement injection ranged from 10- to 13-G in almost all procedures, which is similar to spinal cementoplasty [Tsoumakidou 2017]. However, one major difference with spine is the amount of cement that is injected. As shown in this review, the volume of cement is extremely variable. On average, the amount of injected cement was 8.8 ml, which is much higher than the mean value for a spinal vertebroplasty [Tsoumakidou 2017, Sun 2018]. This is most likely explained by the greater volume of extra-spinal tumors compared to spinal lesions. This review also outlines that a significant number of procedures, especially in the long bones, required a volume greater than 10 ml. Such volume exceeds the usual volume of cement available in most of the commercially available cement kits. Surprisingly, only one paper over the 30 included for that review described in detail the technical approach to deal with such large volume [Moser 2019]. Hence, in that paper

focusing on pelvic osteoplasty, the authors injected simultaneously in 2 trocars with the idea to provide a coalescence of the different cement streams while injecting as much as possible. In all other articles there was no or only brief description of the technique, which consisted in inserting an additional needle to inject more cement whenever required in most of procedures, but with- out further specification. Besides, filling of the lesions is rarely reported, and is inferior to 60% in the few papers publishing the data [Moser 2019, Colman 2015]. There is no standardized volume of cement for extra-spinal cementoplasties and most authors advocate to fill the lesion and the surrounding cancellous bone as much as possible to provide optimal bone consolidation [Sutter 2010, Kurup 2015]. The impact of the degree of lesion filling on the mechanical outcome is however unclear in clinical practice. Optimal filling has always to be balanced with the risk of leakage. Although it is rare, cement leakage can be symptomatic and potentially worsen the symptomatology of the patient. The risk is supposed to be increased if the bone cortex is disrupted. The use of ablation, balloon kyphoplasty and/or high-viscosity bone cement could potentially reduce the risk of leakage but evidences are still lacking for extra-spinal procedures [Wallace 2015].

In conclusion, percutaneous extra-spinal cementopasty is predominantly performed as a stand-alone procedure and for lesions in the bony pelvis. It appears to be an effective tool to manage pain associated with malignant bone tumours. There is however a lack of standardization of the technique among the different publications. The present study confirms that a large volume of cement was used in many studies.

1.4. Properties of PMMA bone cement and their relevance in interventional oncology

PMMA is by far the most frequent bone cement used in clinical practice. It is formed by the mixture of a polymeric powder and a monomeric liquid. It was developed by the chemical industry during the 19th century and was originally named acrylic acid due to the smell of the monomer [Webb 2007]. In 1936, PMMA became one of the first discovered biomaterials as the mixing of the polymer with a monomer lead to the production of a malleable dough [Webb 2007]. The use of Polymethylmetacrylate (PMMA) cement for medical purposes was first described in orthopaedic surgery in 1945 for the manufacturing of a femoral head prosthesis [Scales 1945]. It was then further used in the 60's by Charnley to secure the femoral and acetabular components during total hip arthroplasty [Charnley 1946]. Percutaneous image-guided injection of PMMA for the minimally invasive management of a spinal tumor was subsequently reported in 1987 to treat an aggressive C2 hemangioma which lead to the treatment of osteoporotic and pathologic compression fractures of the spine [Galibert 1987, Cotten 1998]. The most recent application of PMMA was the treatment of extra-spinal metastases, cementoplasty, which was reported to provide pain alleviation and/or bone consolidation, either as a stand-alone technique or in combination percutaneous screw fixation [Garnon 2019]. Concurrently over that past few decades, other types of cement, such as ceramic or composite bone cements, have been developed in an attempt to increase biocompatibility and long-term incorporation [He 2014]. However, these are more expensive and complex to handle than PMMA [Lieberman 2005]. Moreover, the theoretical advantage of biointegration and induction of new bone formation is of little significance for oncological cases, where the underlying bone is usually of poor quality and life expectancy somehow limited. Hence, PMMA is still the most widely used cement especially in interventional oncology [Lieberman 2005, Garnon 2019]. The present review therefore seeks to detail the properties of PMMA and discuss their potential relevance during percutaneous interventions in oncology.

1.4.1. Composition of PMMA

Acrylic bone cement is composed of a polymeric powder and a monomeric liquid [Nussbaum 2004, Lai 2013]. The polymeric powder is mostly composed of bead-shaped particles of pre-polymerized PMMA that comes in various compositions depending on the manufacturer [Kuehn 2005]. It also includes a radio-opacifier and an initiator that promotes polymerization at room temperature. The monomer liquid mainly contains the MMA monomers. In addition to MMA, the liquid also includes a co-initiator that activates the polymerization and a stabilizer which prevents premature polymerization during storage [Nussbaum 2004, Kuehn 2005, Lai 2013].

Manufacturers sometimes supplement their cement with additives, such as antibiotics to prevent infections or chlorophyll to make it clearly distinguishable in the surgical wound. Although those ingredients might be useful for some specific situations, they are associated with a modification of the properties of PMMA that might on the other hand be detrimental in the daily practice [Nussbaum 2004, Lai 2013, Sa 2018].

More specifically for oncological purposes, some authors developed a radioactive bone cement composed of a ceramic composite incorporating a radio-isotope beta emitter that was added to PMMA [Donanzam 2013]. To date, such cement has only been studied in-vitro. Another way to provide local radiation is to implant radioactive ^{125}I particles into the tumor prior to cement injection. This approach has been reported for the treatment of spinal metastases [Xie 2015]. However, it is not a direct propriety of the PMMA itself as the radioactive particles are delivered separately.

1.4.2. Polymerization of PMMA

Mixture of the polymeric powder and the monomeric liquid triggers two different processes. The dissolution of the powder into the liquid leads to a viscous fluid. Simultaneously, the polymerization begins and will ultimately transform the properties of the cement from an injectable pseudoplastic fluid to a viscoelastic solid [Kolmeder 2013, Landgraf 2015].

1.4.2.1. Chemical reaction

Once the monomer and the polymer are mixed, the polymerization process begins. The reaction is complex and involves many chemical reactions. The co-initiator contained in the liquid leads to the decomposition of the initiator of the powder, which in turn generates free radicals. At room temperature, the free radicals initiate an addition polymerization of the MMA monomer and PMMA polymer (fig.9) [Nussbaum 2004, Lai 2013].
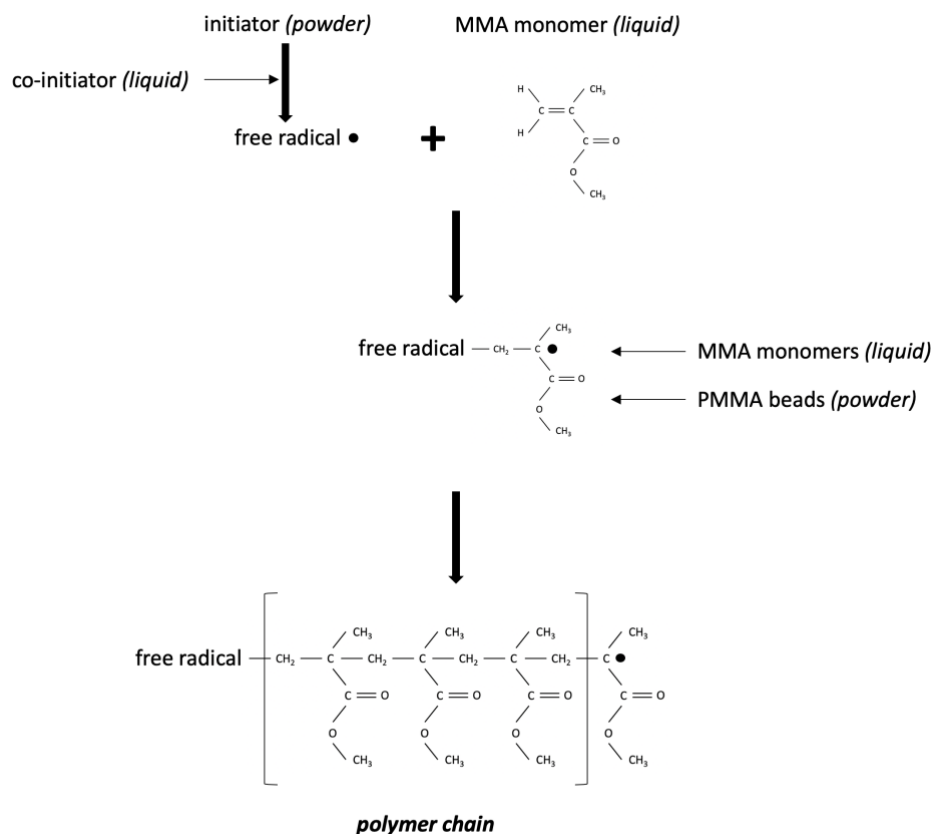
Fig.9: Representation of the reaction polymerization. The initiator and co-initiator lead to the release of free radicals that trigger the beginning of the chemical reaction. A radical is formed in an MMA monomer that can subsequently attack the C=C double bond of another MMA monomer. The polymer chain of PMMA is obtained by an addition mechanism.

As a result, a multitude of polymer chains grow up leading to a molecular weight ranging from 2.10^6 to 10^9 g/mol [Kuehn 2005]. The progress of the polymerization process is described by the evolution of a variable named degree of cure. It ranges between 0 at the beginning of the chemical reaction to theoretically 100% when monomers are fully polymerized [Borzacchiello 2018]. A 100% degree of cure is however impossible to achieve even under optimal experimental conditions [Kuehn 2005]. In clinical conditions, a small proportion of the monomer (around 2-3% of the original amount) is not included in the chemical reaction [Lai 2013]. The exact physiological and clinical consequences of this unreacted MMA residual monomer is not exactly known. It has been hypothesized that it may leak into the surrounding tissue and therefore negatively influence both the remodeling of bone and the properties of the nearby polymerized PMMA [Vallo 2002, Lai 2013]. Some papers also suggested that the toxicity of monomer could lead to cell necrosis but there is no clear evidence to support this [San Millan Ruiz 1999].

1.4.2.2. Phases of polymerization

Polymerization of PMMA progresses through 4 successive phases, referred as handling phases, that are characterized by the modifications of the cement viscosity [Lewis 1997, Lai 2013]:

- The mixing phase: typically lasts from 30 seconds to 1 minute depending on the manufacturer and the mixing tool. The powder and the liquid are mixed either manually using a bowl and a spatula or with help of a centrifugation or a vacuum mixing device, and eventually lead to a homogeneous dough composed by very mobile short polymer chains.
- The waiting (or liquid) phase: lasts around one minute (time can vary depending on the recommendations of the manufacturer) and is recommended to reach a non-sticky state. During this phase, there is a growing number of polymer chains leading to a slow increase of cement viscosity.
- The working (or application) phase: is the period in which cement can be injected inside the bone. Application of cement should be terminated by the end of this phase as viscosity is increasing gradually. Duration ranges between 10 to 20 minutes depending on the manufacturer.
- The hardening (or setting) phase: corresponds to cement hardening. At this point, cement cannot be injected anymore but the curing reaction goes on. The setting time of a given cement is defined by the ISO 5833:2002 standard as the time when the temperature in a 60 mm diameter x 6 mm height polymerizing cement cylinder is in the mid between ambient and maximum temperature inside the cement (measured with a thermosensor). In laboratory conditions, duration of the setting phase is about 8 to 13 min.

As the evolution of the polymerization process depends upon the temperature, the duration of each phase can be highly variable depending on the thermal conditions.

1.4.2.3. Exothermic reaction

The polymerization of PMMA bone cement is an exothermic reaction, i.e. the temperature of the cement is increasing during curing [Lewis 1997, Belkoff 2003]. During this phase, the increase of cement temperature is highly variable among manufacturers and testing conditions but temperatures as high as 100 degrees Celsius have been reported [Belkoff 2003, Lai 2013]. Ex-vivo studies confirmed that the local temperature in a cement-augmented vertebral body was increasing above 50 to 100 degrees Celsius for a few minutes during polymerization with large deviations of temperature values among the articles, the localization of the measures in the vertebral body and the cement brand [Eriksson 1984, Deramond 1999]. As protein denaturation and coagulation necrosis occur after a brief exposure (seconds) to temperatures higher than 60 degrees Celsius or even after a longer exposure (at least one minute) to temperatures higher than 50 degrees Celsius, the exothermic reaction of polymerization was reported as a potential source of bone necrosis (negative effect) but also destruction of the painful periosteal nociceptors (positive effect) [Eriksson 1984, Togawa 2003]. Some authors even hypothesized that cement had potentially an antitumor effect based on the retrospective study of patients suffering from spinal metastases from breast cancer [Roedel 2015]. On the contrary, several other studies suggest that the exothermic reaction comes with little clinical impact [Verlaan 2003, Urrutia 2008, Anselmetti 2009]. PMMA has a poor thermal conductivity and ex-vivo studies do not take into account the transfer of heat by convection (heat sink effect) due to blood perfusion [Webb 2007]. An animal study in goats failed to demonstrate any significant rise of local temperature at the limits of the vertebra or at the bone-cement interface (44 degrees Celsius at the bone-cement interface) [Verlaan 2003]. Another study in rabbits showed only focal areas of bone necrosis and no neural necrosis 24 hours after injection of PMMA in the spine [Urrutia 2008]. A clinical study in 22 patients showed that despite a great variability among cements, none of them were leading to a sufficient and durable increase of

temperature that could lead to extensive necrosis around the cement [Anselmetti 2009]. Finally, only focal areas of bone necrosis were seen on histopathological examination of 4 vertebral bodies extracted one-month to 2 years after kyphoplasty with PMMA [Togawa 2003]. Based on the available data, the injection of PMMA does not seem to lead to the destruction of the nociceptive fibers in-vivo. The mechanism of pain relief is most certainly related to mechanical stabilization [Verlaan 2003, Anselmetti 2009]. Furthermore, because of the limited in-vivo exothermic reaction, cementoplasty with PMMA should not be considered as an intervention that leads to tumor destruction. Additional thermal ablation and/or radiation are therefore indicated whenever local tumor control is indicated [Wallace 2015, Kurup 2018].

1.4.2.4. Shrinkage

During polymerization, the cement undergoes an increase of its density ultimately leading to a decrease of its volume (shrinkage) at the end of the curing reaction [Muller 2002, Kinzl 2012]. Reduction of the molecular distance between the free monomer molecules prior to polymerization and the bonded molecules at the end of polymerization explains this phenomenon. The theoretic amount of volume shrinkage is estimated to be around 6% to 7% [Lai 2013]. In reality, the shrinkage is lower (in the range of 2% to 5%) because of the air that is included in the cement dough during mixing. Hand-mixing is associated with a lower shrinkage rate than the vacuum mixing technique because of a greater inclusion of air [Lewis 1997, Muller 2002]. Preclinical studies showed that such percentage was associated with a reduction of almost 20% of the stiffness of the bone-cement composite compared to a model without shrinkage [Muller 2002, Kinzl 2012]. The clinical consequences of shrinkage are not completely elicited. Theoretically, it might negatively alter the bone-cement interface (see the bone-interface section) and therefore the stabilization by the cement. Greater shrinkage is usually associated with a lower porosity (see the porosity section) because of a lower inclusions of air particles [Lewis 1997, Muller 2002]. Shrinkage does not seem to have any real clinical implications.

1.4.3. Working properties of PMMA

1.4.3.1. Viscosity

Acrylic bone cements are characterized by their viscosity (also referred as dynamic viscosity η), which corresponds to the informal concept of fluidity, mobility or consistency of the material. For a given temperature, viscosity measures the resistance of the cement to flow at a given shear rate ($\dot{\gamma}$) and is given by the equation $\eta = \frac{\sigma}{\dot{\gamma}}$ where σ represents the shear stress of the material [Webb 2007]. In experimental conditions, it can be measured with a dynamic rheometer. Viscosity should be low enough ("liquid" enough) to flow through the delivery system, the bone needle and the bone. However, it should be high enough ("thick" enough) to prevent or minimize extravasation outside the bony structure [Lewis 1997].

Viscosity of PMMA varies among the different manufacturers because of the difference in composition. Low-viscosity bone cements are characterized by a low-viscosity that is rapidly increasing, with a working time ranging below 10 minutes. High-viscosity bone cements present a higher and more constant viscosity during the working phase, with a longer application time than low-viscosity cements [Zhang 2018]. A recent meta-analysis showed

that high-viscosity cements yielded the same clinical effect as low-viscosity cements with a reduced incidence of leakage in the veins and the disc space [Zhang 2018]. Due to these working properties, high-viscosity PMMA cements are theoretically more advantageous for oncological cases [Trumm 2013].

Viscosity for a given cement is a function of three variables: time, shear rate and temperature [Webb 2007]. Viscosity increases with time because of the polymerization process which is an irreversible reaction. Shear rate and temperature are parameters that can be used to impact on the duration of polymerization. Viscosity decreases with an increase in shear rate: forceful injection can theoretically reduce the viscosity [Dunne 1998]. However, it also exposes to the risk of leakages; shear rate is therefore no practicle in the clinical setting. Temperature has an exponential effect on the reaction of polymerization: lowering the temperature significantly decreases the viscosity thereby extending the duration of injectability of the cement [Nussbaum 2004, James 2006]. Hence, storing the components of PMMA in the refrigeration and/or immerging the mixture of polymer and monomer in an ice bath is an easy way to increase the duration of injection [Chavali 2003].

1.4.3.2. Porosity

Because of the inclusion of air particles during mixing and injection, PMMA bone cement contains voids once it is fully polymerized [Lewis 1997]. Voids > 1mm are defined as macropores, while those < 1mm are referred as micropores [Kurtz 2005]. The chemical formulation of PMMA and the mixing method (hand- vs vacuum- mixing) seem to influence the rate of porosity, which was estimated to range around 6% in a preclinical study [Kurtz 2005, Oonishi 2011]. Once curing of cement occurred, porosity does not seem to vary with time [Ries 2006]. Many pre-clinical studies suggest that pores are a potential source of crack initiation that can ultimately lead to fracture and fatigue failure of the cement in case of crack propagation [Kurtz 2005]. The size and distribution of pores seem to be an important factor, with larger and more coalescent pores initiating more and larger fatigue cracks (fig.10) [Hoey 2009]. Cracking can furthermore lead to the release of PMMA beads, which might subsequently trigger inflammation and osteolysis (foreign body reaction) [Ries 2006]. Micropores might however be beneficial as they contribute to impede shrinkage during polymerization and potentially blunt the propagation of cracks [Lewis 1997]. Whether porosity is clinically relevant is debated. Based on the long-term analysis of hip athroplasties, some authors believe that porosity is a major factor for the in-vivo mechanical properties and the fatigue failure of cement [Ries 2006]. There is almost no literature about the influence of porosity for percutaneous interventions using PMMA. Vertebroplasty is known to induce a mild foreign body reaction that is usually clinically irrelevant, and whether or not it is related to porosity remains unknown [Togawa 2006]. A single case of PMMA breakage with secondary bone collapse 2 years following vertebroplasty, for which the link with porosity cannot be assessed, has been reported [Huang 2019]. Overall, the consensus is that porosity (especially macroporosity) should be kept to a minimum. For that purpose, centrifugation or vacuum mixing seems superior to hand mixing [Lewis 1997].
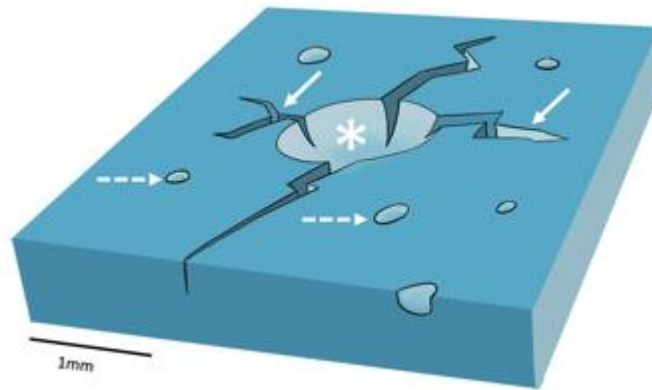
Fig.10: Porosity in PMMA. Macro- (asterisk) and micro- (dotted arrows) pores are incorporated in the cement and can be the source of cracks (arrows).

1.4.4. Interactions of PMMA

1.4.4.1. Interaction with bone

The interaction of PMMA with bone has mostly been studied in non-cancerous models. During injection, PMMA flows in between the trabeculae of the cancellous bone displacing the bone marrow. The depth of penetration depends upon two major factors: the bone structure and the cement viscosity [Bohner 2003]. A higher bone density reduces cement penetration whereas a higher viscosity seems to favor it [Silverman 2014]. Following injection, the embedded trabecular bone represents around 10% of the bone-cement composite [Race 2007]. Histological examinations have shown that there is no chemical bonding between bone and cement [Nussbaum 2004, Race 2007, Skripitz 1999]. Instead, gaps subsequently filled with fibrous tissue have been observed at the bone-cement interface in animals and post-mortem examinations, with focal areas of bone remodeling of the trabecular bone adjacent to the interface (fig.11) [Togawa 2006, Skripitz 1999, Fahlgren 2010].
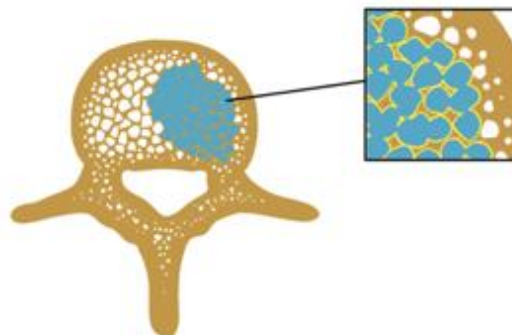
Fig.11: Bone-cement interface. PMMA (in blue) flows in the cancellous bone and interdigitates in between the trabeculae. PMMA does not bond to bone. Instead, a thin fibrous membrane (yellow) intervenes between the trabeculae and cement.

38

PMMA has no adhesive properties and acts more as a space filler than as a glue with adhesion and load transfer between PMMA and bone achieved through the intrusion of cement into the microstructure of the cancellous bone, also referred as mechanical interlocking [Bohner 2003, Skripitz 1999, Miller 2014]. A higher level of cement penetration therefore offers a greater mechanical interlock [Waanders 2010, Miller 2014]. Because balloon inflation compacts and displaces bone, kyphoplasty has been reported to decrease the quantity of cement interdigitation compared to vertebroplasty [Togawa 2003, Togawa 2006]. However, one animal study showed that peripheral compression of the cancellous bone following kyphoplasty could lead to an autografting of the vertebral body walls and endplates [Togawa 2003]. In-vivo, there is a trend towards resorption of the bone adjacent to the cement with time, that may ultimately lead to the loss of interlock and a decrease of interfacial strength [Goodheart 2017]. The phenomenon has mostly been studied in arthroplasties and seems multifactorial [Zhang 2016].

There is no specific literature on the interaction between cement and bone infiltrated by tumor. A clinical study has shown that the injection of PMMA into a metastatic vertebra leads to an increase of the level of circulating cancer cells, likely due to the displacement of cancer cells in the systemic circulation by the flow of cement within the tumor [Mohme 2017]. This could theoretically increase the risk of distant metastasis and may have implications in patients with low systemic disease burden. Tumor destruction prior to cement injection for patients with a long-life expectancy should therefore always be considered, especially in patients who are oligometastatic. The quality of mechanical interlocking in tumors seems obviously inferior to the one in porotic bone and dependent on the degree of osteolysis. Whenever possible, part of the cement should be interdigitated in some normal cancellous bone to increase the chance of creating a bone-cement interface [Lea 2019].

1.4.4.2. Interaction with hardware

The interaction between PMMA and hardware (such as a titanium screw for example) largely depends upon the surface and type of hardware [Vallittu 1995]. Bonding can only occur if cement is in contact with the hardware during the working phase. Mechanical bonding is secondary to the penetration of the cement into the macro- and micro-irregularities of the hardware [Brown 2013]. Chemical bonding between PMMA and hardware is more variable and can vary with the surface treatment of the hardware [Alaagel 2015]. The interfacial strength of the screw-cement interface is usually superior to the cement-bone interface [Liu 2016].

1.4.4.3. Mechanical properties

Assuming a linear elastic behavior, PMMA bone cement can be defined through the ensuing parameters Young's modulus and Poisson's ratio [Webb 2007]. Young's modulus of PMMA is around 2 GPa, which is three to fifteen times than that of cancellous bone and ten times lower than that of cortical bone [Turner 1999]. The mechanical properties differ from one cement to another. For PMMA bone cements, the highest strength values are obtained for compression loads [Webb 2007]. In a review reporting the properties of three major cement brands, the ultimate compressive strength ranged from 80 to 94 MPa, while the bending strength ranged from 67 to 72 MPa, the shear strength from 50 to 69 MPa and the ultimate tensile strength from 36 to 47 MPa [Webb 2007]. Hence, PMMA bone cement is mechanically more adapted to areas which are predominantly loaded with compression such as the vertebral bodies and the acetabulum (fig.12) [Wallace 2015, Kurup 2018]. Its use as a stand-alone technique in

locations predominantly loaded with tension, torsion or shear might expose to a risk failure of PMMA, with fractures occurring despite cement augmentation (fig.13) [Cazzato 2015].

Fig.12: cement injection in a spinal metastasis. (A) axial and (B) coronal CT-scan shows a lytic metastasis with pathological fracture. (C) sagittal and (D) coronal CBCT immediately after cement injection. In this location mostly loaded with compression, PMMA provides consolidation of the fracture.
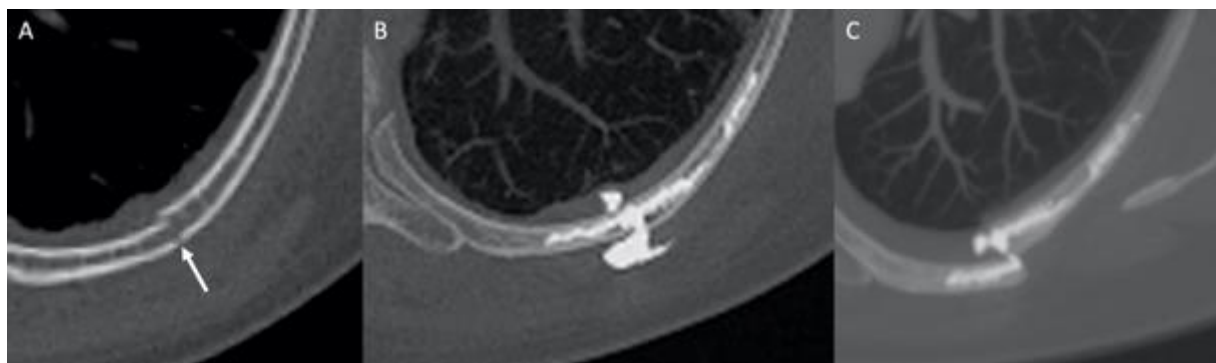
Fig.13: Failure of consolidation with cement. (A) pathologic rib fracture. (B) treatment with cementoplasty with leakage through the fracture lines. (C) One-month follow-up shows fracture of cement and secondary displacement of the fracture. The resistance of PMMA to shear does not allow effective consolidation in that location.

1.4.5. Clinical applications of PMMA: relevance in interventional oncology

The quality of bone in cancer patients may be impaired by the tumorous infiltration of the trabecular and/or cortical bone, the reduction of bone mineral density induced by systemic therapies (hormonotherapy, chemotherapy) or

radiation/ablation-induced bone necrosis. This can lead to pain, mechanical instability and/or pathological fractures that can occur even under physiologic loading. PMMA can be used to alleviate pain, provide bone consolidation in some locations and increase the anchorage of hardware (mostly screws) [Tschirhart 2006, Garnon 2019].

1.4.5.1. Pain management

PMMA injection has the potential to significantly decrease the level of pain related to bone metastasis, either as a stand-alone treatment or in combination with radiation or ablation. PMMA injection has mostly been applied to treat painful osteolytic metastases in the vertebral bodies, the bony pelvis and the long bones. Even though no relationship could be found between the percentage of cement fill and the decrease of pain, the major mechanism with which PMMA achieves pain alleviation is most likely mechanical reinforcement [Anselmetti 2009]. In addition to osseous metastases, cement injection can also be performed to treat painful insufficiency fractures in the spine and the sacral ala.

1.4.5.2. Bone augmentation

PMMA injection is increasingly being used as minimally invasive alternative to surgery to provide consolidation in cases of metastatic spinal compression fractures or impending fractures in various locations. Because of the mechanical properties of PMMA, consolidation can mostly be achieved in locations mostly stressed with compression (vertebral body, acetabular roof). In these areas, cement injection has the ability to restore strength, stiffness and load transfer [Molloy 2003, Tschirhart 2005, Li 2007]. Most of the publications studied on the effect of PMMA in the spine. In-vitro studies show that both the volume and distribution of cement is important to achieve stabilization [Molloy 2003, Tschirhart 2005, Li 2007]. Restoration of local stiffness requires a higher volume of cement than for the restoration of strength [Chevalier 2008, Luo 2009]. Moreover, the restoration of strength and load transfer seems to be of higher quality when the fragility area is filled from one end to the other [Tschirhart 2006]. On the other hand, excessive filling may lead to an increase of the stresses in the adjacent segments thereby theoretically increasing the risk of secondary adjacent fractures [Berton 2020]. This concern does not seem justified in a non-osteoporotic population. Based on preclinical studies, it therefore seems that complete filling of an osteolytic area should be the goal to avoid secondary collapse whenever the tumor is in a weight-bearing area. This is further supported by retrospective clinical studies which highlight that optimal cement distribution in acetabular and spinal metastases was associated with a better mechanical outcome [Delpla 2019, Hesler 2019]. Theoretically, when considering optimal filling, the reinforcement of local stiffness may also depend upon the presence and quality of the underlying bone. The mechanical properties of bulk cement have been reported to be higher than the ones of a bone-cement composite with bone of compromised quality (because of osteoporosis, tumor, ablation/radiation), as residual pathological trabeculae act as gaps within the cement [Race 2007]. Some authors suggested the use of balloon inflation following thermal ablation to increase the rate of filling with bulk cement [Kurup 2015]. Finally, achieving some kind of PMMA injection in the cancellous bone abutting an osteolytic area filled with cement is recommended by some authors (fig.14) [Lea 2019]. This would seem to increase the quality of load transfer through mechanical interlocking.
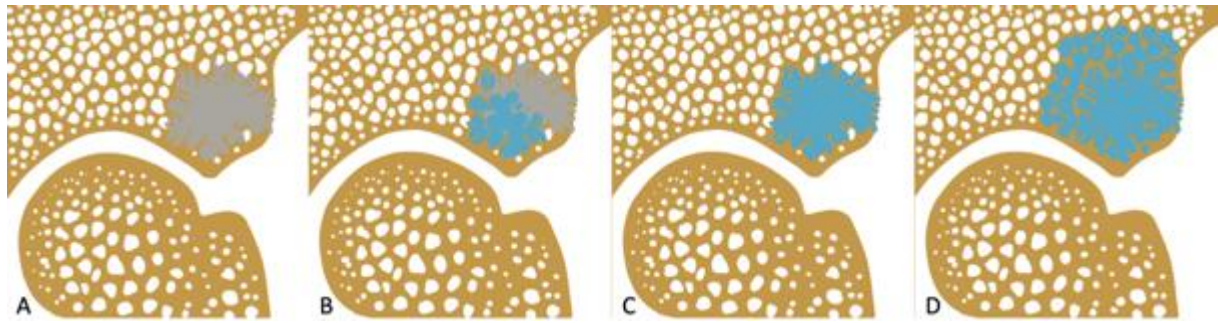
Fig.14: Consolidation with PMMA in a weight-bearing area (acetabular roof). (A) Destruction of bone by a metastasis (in grey) decreases the mechanical resistance of the area. (B) Partial filling with PMMA (in blue). Complete cement filling of the lesion without (C) and with (D) interdigitation of cement in the surrounding trabecular bone. (D) is theoretically the best option as it restores strength and should optimize load transfer to the surrounding bone through mechanical interlocking.

1.4.5.3. Anchorage of hardware

Percutaneous image-guided screw fixation is increasingly being used to consolidate pathological fractures in the bony pelvis and other locations such as the sternum or the shoulder [Roux 2019]. It allows to overcome the limitations of cement that cannot "glue" the osseous fragments together. Anchorage of both ends of the screw in cancellous bone of good quality is mandatory to achieve proper stable fixation: a bone with a normal trabecular density (i.e. a small distance between the trabeculae) offers an appropriate landing zone for the threaded part of the screw as there many are struts to engage with [Brown 2013]. However, the quality of cancellous bone is often compromised in cancer patients. In-vitro studies demonstrate that augmentation of the landing zone with PMMA is a way to increase screw stability [Liu 2013]. This leads to a dual interface: the screw-cement interface and the bone-cement-interface. The stability of the screw mostly depends on the strength of the cement-bone interface [Liu 2016]. PMMA is not gluing the screw in the bone but increases the purchase of the threaded part of the screw into the cancellous bone. Cement injection performed prior to screw insertion expands the contact surface to the surrounding trabecular structure through mechanical interlocking, thereby distributing the load over a larger number of trabeculae which in turn increase the load-bearing capacity of the landing zone (fig.15) [Schulze 2020]. The cement distribution seems equally important as the quantity, if not more (fig.16) [Elder 2015, Liu 2016]. An animal study showed that the screw-cement interface was stable 3 months following injection [Liu 2013]. The bone-cement interface remains the weak point of such a construct, unless the screw is inserted once cement has cured [Elder 2015]. In the latter scenario, failure is more likely to occur at the screw-cement interface. Many clinical studies report the efficacy of PMMA augmented screws [Lea 2019, Roux 2019]. Because of the underlying principles of hardware augmentation, the augmentation capacities of PMMA to increase screw anchorage in a complete osteolytic area may be limited as the cement-bone interface will be extremely weak.
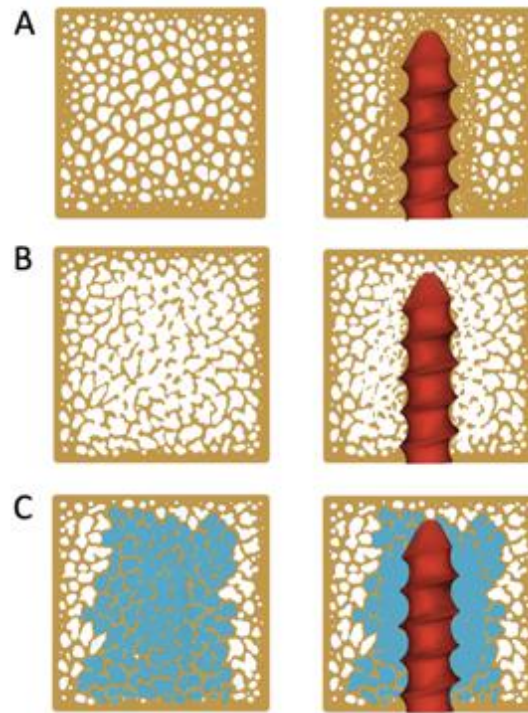
Fig.15: Screw augmentation with PMMA. (A) in a normal bone, the threads engage in trabeculae of normal density. (B) In a bone with decreased density, there is limited anchorage of the screw. (C) Injecting PMMA prior to screw insertion enables to increase the contact surface of the tip of the screw with the surround trabecular bone.
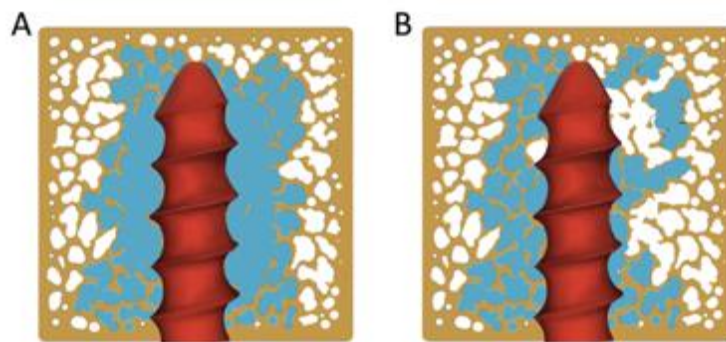
Fig.16: importance of adequate cement distribution to augment the screw. There is a higher risk of screw loosening in (B) compared to (A) as the load transfer will be more limited.

1.4.6. Discussion

PMMA bone cement has many potential applications in interventional oncology. Based on the review of the available literature, some theoretical recommendations can be made. Vacuum or centrifugation mixing should be favored over hand-mixing to reduce porosity, especially in patients with very long-life expectancy. The preferential use of high-viscosity cements is supposed to reduce the risk of leakage and increase the depth of cement penetration and therefore the quality of mechanical interlocking. Partial cement filling increases the strength of the augmented area while injection of a larger volume of cement can restore both strength and stiffness,

thereby limiting the risk of secondary collapse. Whenever consolidation is part of the treatment objective, filling as much as possible the osteolysis and injecting in the surrounding cancellous bone should be the goal in order to increase strength, stiffness and load transfer. PMMA has also the ability to increase the anchorage of screws in cancellous bone with reduced density. In this case, complete distribution of cement all around the threads of the screw should be the objective.

1.5. Biomechanics of the osseous pelvis and its implication for consolidative treatments in interventional oncology

The pelvis is the second most frequent site of osseous metastases after the spine. Alteration of bone integrity in the pelvic girdle may not only lead to pain but also to functional disability and pathological fractures, which in turn can greatly impair the patient's quality of life. Moreover, confinement to bed rest seriously exposes the patient to medical complications, such as thromboembolic and infectious adverse events. External beam radiation and stereotactic body radiation therapy are effective tools to alleviate the pain; however, they do not address the mechanical instability [Erler 2018]. A wide range of open surgical procedures have been developed to manage fractures and impending fractures of the pelvic girdle, mostly involving the acetabulum and the proximal femur [Wunder 2003, Spinelli 2016]. However, the ability to perform these potentially complex procedures depends on the general condition of the patient, as the morbidity is not negligible [Brown 2018]. Image-guided percutaneous minimally invasive procedures have emerged as a viable option for the treatment of pelvic bone metastases. Among the different tools, percutaneous cementoplasty and screw fixation can provide bone reinforcement and fracture fixation, as stand-alone or combined techniques [Mastier 2018, Roux 2019]. In addition to the patient's condition and clinical objective, the choice of approach and technique should be tailored to the location and features of the lesion. Clinical, anatomical and biomechanical considerations are of utmost importance when considering the different consolidative treatment options. The primary objective of this manuscript is to present a comprehensive review of the biomechanics of the osseous pelvis and its therapeutic implications for the interventional radiologist.

1.5.1. Osseous pelvis – generalities

The bony pelvis is formed by the pelvic (or coxal, hip or innomate) bones on each side and the sacrum in the midline. The pelvic bones are attached to each other at the level of the pubic symphysis anteriorly and are firmly joined to the sacrum via the sacro-iliac joints and ligaments posteriorly. Some authors also include the proximal femur as part of the bony pelvis [Dalstra 1995]. The proximal femur will not be included for the sake of this present review.

1.5.1.1. Biomechanics

The pelvic bone is mainly composed of low-density trabecular bone surrounded by a thin layer of high strength cortical bone which mimics the sandwich construction used in composite material, in which the majority of the weightbearing load is carried by a thin shell of a high-modulus material with a low-weight core material acting as a spacer [Dalstra 1993, Dalstra 1995]. In the pelvic girdle, the stresses are predominantly transferred through the

cortical bone, with a ratio of approximatively 50:1 compared to the underlying trabecular bone [Dalstra 1995]. The ligaments and cartilage of the sacro-iliac and hip joints increase the stability of the bony pelvis and the surrounding pelvic musculature help to maintain the stresses within the pelvic bone fairly constant during walking [Hammer 2013, Volinski 2018].

The pelvic bone is an almost immobile weight-bearing structure that transfers the gravitational and external loads from the spine to the lower limbs across the sacro-iliac and hip joints (fig.17) [Dalstra 1995]. Load transfer across the bony pelvis varies during gait (fig.18). The periacetabular area is the most important weight-bearing structure of the osseous pelvis whilst the sacro-iliac junction, the pubic region, the iliac wing and the ischium have less weightbearing function [Muller 2015]. These principles apply to the need of surgical reconstruction following partial pelvic resection. Most of the surgical series do not recommend reconstructions following resection of pelvic bone lesions except if the acetabulum is involved [Muller 2015, Brown 2018]. Reconstruction of the sacro-iliac joint is more controversial without a consensus [Wang 2019]. Lesions involving both the sacro-iliac joint and the acetabulum completely interrupt the transmission of stresses and require extensive and often complex reconstruction.

Fig.17: Representation of load transmission within the pelvis. (A) The loads are transmitted from the spine to the sacrum at the lumbosacral junction and then are transferred to the femur via the sacro-iliac joints and the hip joints. (B) Oblique sagittal CT-scan showing how the loads are transferred from the sacro-iliac joint to the acetabulum. (C) Same findings on an oblique coronal view.
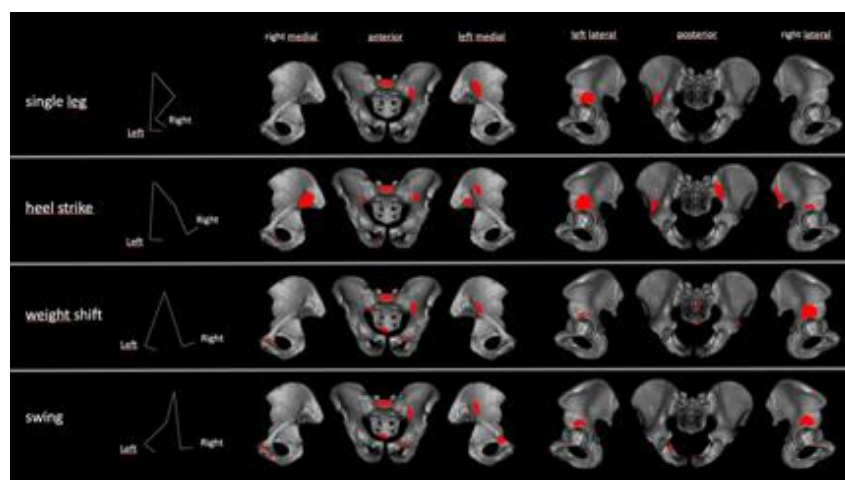
Fig.18: Simplified schematic of the peak stresses in the pelvis during the 4 phases of walking. The acetabular area is constantly stressed, while the sacro-iliac areas and to a lesser degree the upper pubic rami are occasionally stressed. Figure adapted from [Volinski 2018]

Stresses applied to the pelvis vary greatly depending on the location and include compression, tensile, bending and shear forces. Compression is the prevailing stress in the upper part of S1, the anterior part of the sacro-iliac joint and the acetabular roof [Vleeming 2012, Hammer 2013].

1.5.1.2. Implications for percutaneous treatment

Understanding the biomechanical load and distributions in the bony pelvis is critical. Contrary to the long bones of the limbs, there is currently no validated score to predict the risk of fracture within the bony pelvis [Muller 2015]. Indications and type of consolidation have to be tailored to each patient and result from several items such as clinical presentation (no symptoms vs mechanical pain), localisation/size/type of lesion, associated destruction of bony cortex, previous local treatments that could weaken the bone resistance (e.g. radiation therapy and thermal ablation), and presence of a pathological fracture (fig.19). Large osseous defects not only increase risk of local mechanical failure but also increase the risk of distant fractures due to the redistribution of the loads within the pelvis [Munro 2014].
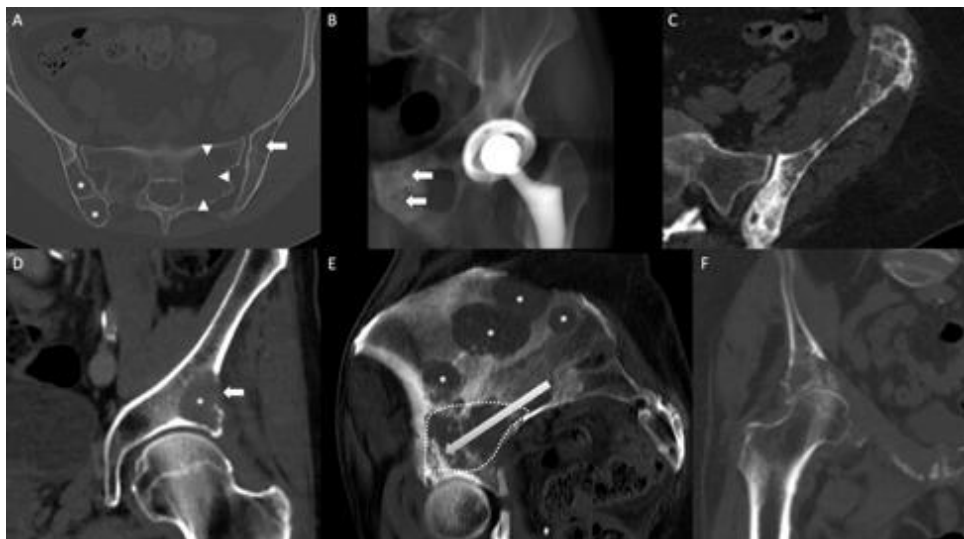
Fig.19: Pelvic lesions with different clinical and radiological presentations and risks of pathologic fracture. (A) 3 osteolytic lesions in the posterior right iliac bone (asterisks), the left sacral wing (arrowheads) and the left iliac bone (arrow). The lesions are not located in weight bearing areas and there is no cortical destruction: the risk of mechanical failure is minimal. (B) Mixed pubic metastasis (arrows): there is no bone defect and the stresses are limited in that area, the risk of mechanical failure is very low. (C) Mixed metastasis with some kind of cortical destruction in a complete non-weight bearing location (the iliac wing): the risk of pathological fracture might be increased but prophylactic consolidation is not indicated (no risk of mechanical failure). Should a fracture occur, percutaneous treatment is a possibility (see below). (D) Osteolysis with cortical destruction in a critical mechanical area (the acetabulum): consolidation should be considered even if the patient is not symptomatic. (E) Multiple osteolytic lesions in a right pelvic bone: the lesions in the iliac wing (asterisks) do not require consolidation, while the acetabular metastasis (dotted line) interrupts the transmission of loads and should imperatively be consolidated. (F) Diffuse acetabular osteolysis with cortical and articular involvement: the risk of mechanical failure is high.

Polymethylmethacrylate (PMMA) bone cement has excellent resistance to compressive forces and is indicated in all areas which are mostly submitted to compression stresses [Lewis 2011, Delpla 2019]. Whenever possible, cement should fill as much as possible the destructed area to restore the transmission of loads and avoid secondary fracture [Li 2007, Kurup 2015]. On the other hand, cement has limited resistance to other stresses than compression and act more as a grout than as a glue, which limits its use for the fixation of pelvic fractures [Lewis 2011]. To overcome these limitations, percutaneous screw fixation has been described more recently for the management of pathological fractures of the pelvis and the prophylactic stabilization of impending fracture of the proximal femur [Lewis 2019, Roux 2019]. Screws have also been used to provide additional support for cement packing and subsequently improve the transmission of loads through the bony pelvis with the analogy of the framework of a concrete construction [Lea 2019].

1.5.2. Sacral promontory

1.5.2.1. Biomechanics

The sacral promontory is key for load transmission as it connects the lumbar spine to the rest of the sacrum and subsequently the pelvic bone. Similar to other spinal levels, most of the load is sustained by the vertebral body [Sattar 2020]. Compared to the other sacral levels (S2 to S5), the body of S1 is permanently heavily stressed mostly with compression loads [Volinski 2018].

1.5.2.2 Implications for percutaneous treatment

Any bone destruction involving the sacral promontory is at risk of mechanical disability and fracture, even though there is no clear critical amount defined in the literature. Consolidation has to be considered in cases of extensive osteolysis, especially if the cortical bone is involved. Cementoplasty is feasible through a transpedicular or a trans-iliac approach and may allow to provide consolidation like for other spinal levels [Rohlmann 2010].

1.5.3. Sacro-iliac joints and sacral ala

1.5.3.1. Biomechanics

The design of the sacro-iliac joint can be assimilated to the one of a flat joint [Vleeming 2012]. Flat surfaces have the optimal design to transfer great moments of mechanical forces, especially compression which is the prevailing stress at the anterior and middle part of the sacro-iliac joint (fig.20A&20B) [Hammer 2013, Kiapour 2020]. Due to their anatomical design, the sacro-iliac joints act as a major stress transmitter and reliever within the bony pelvis. Tensile stresses are maximal in the dorsal and cranial part of the sacro-iliac joint (fig.20C&20D) [Hammer 2013, Kiapour 2020]. The stability of each sacro-iliac joint is therefore enhanced by a process described as "force closure": a perpendicular compressional reaction force to the sacro-iliac joint is generated through (1) a self-bracing mechanism that comes with the conformity and high friction coefficient of adjacent iliac and sacral articular surfaces and (2) the strong binding posterior sacro-iliac ligaments and muscles (piriformis, gluteus maximus). On the other hand, flat joints are particularly vulnerable to dislocation by shear stresses near the joint. However, the sacro-iliac joint can counteract shear stresses, provided that they are firmly pressed together via

force closure [Snijders 1993]. Each sacro-iliac joint has limited mobility, known as nutation. The sacro-iliac joint exhibit a greater range of motion in women than men, potentially explaining the higher rate of fractures of the sacral ala in the female population [Kiapour 2020].
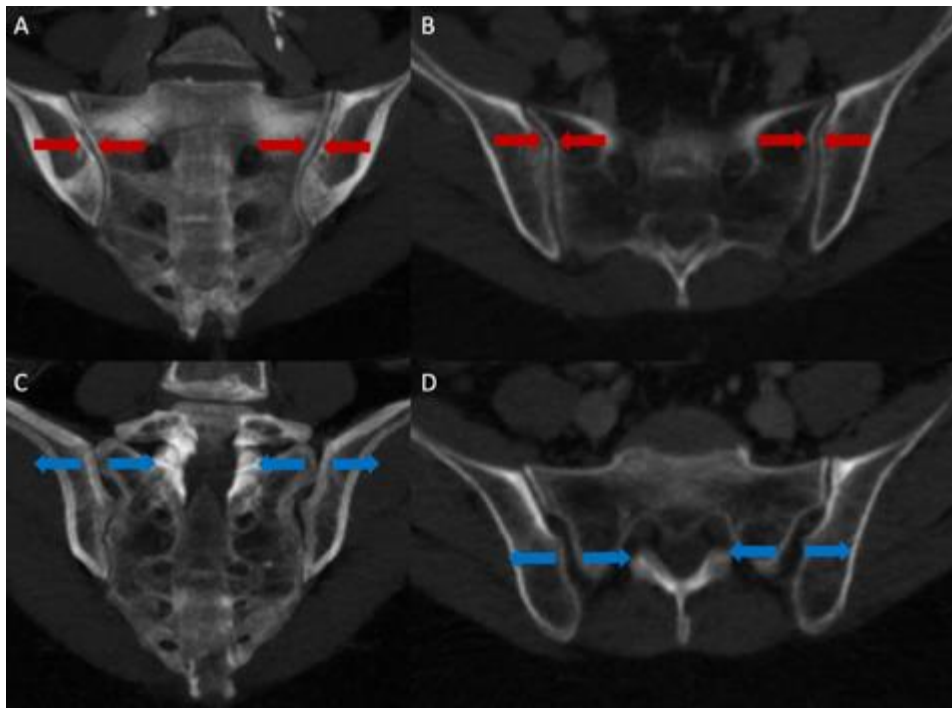
Fig.20: Sacro-iliac mechanical forces. Compression is the prevailing stress at the intermediate (A, coronal view) and anterior (B, axial view) part of the sacro-iliac joints. Tensile stresses predominate at the superior (C, coronal view) and posterior (D, axial view) part of the joints.

1.5.3.2. Implications for percutaneous treatment

The sacro-iliac junctions are mechanically important as they account for the transfer of great moments of compression from the trunk to the acetabular area in load-bearing conditions (sitting, standing). If resection without reconstruction is feasible, lumbopelvic instability can occur, and many advocate the need for post-operative reconstruction [Wang 2019]. In cancer patients with advanced disease, large open surgical procedures are typically not an option due to the morbidity and their invasiveness. Minimally invasive percutaneous interventions are therefore more and more offered as an alternative solution.

Fractures/osteolysis occurring in the anterior part of the sacral ala and associated with functional impairment can be treated with percutaneous cementoplasty (sacroplasty), as compression is the dominant stress in this location (fig.21A,21B,21C). Sacroplasty is superior to non-surgical management to restore patient mobility in case of sacral insufficiency fracture, a frequent condition in cancer patients. A recent meta-analysis involving more than 800 patients reported the effectiveness of sacroplasty to manage osteoporotic and malignant sacral fractures, with sustained benefits at 12 months [Chandra 2019]. Alternatively to cement injection, screw fixation of insufficiency/pathological fractures of the sacral ala has demonstrated good functional results requiring a trans-iliac approach in order to approach the fracture line perpendicularly [Roux 2019]. Based on cadaveric and finite

element models, the strongest fixation technique seems to be obtained with the insertion of two parallel screws (i.e that each screw goes through the right and left sacro-iliac joints), one in S1 and one in S2 [Hu 2017, Lee 2017]. Because of the underlying bone fragility, the authors usually recommend augmenting the anchorage of the tip of the screws with cement, in order to prevent screw loosening and dislodgement [Lea 2019]. There has been no study to date comparing screw fixation and sacroplasty for the management of nondisplaced fractures of the sacral ala. Osteolysis/fracture of the posterior and upper part of the sacro-iliac joint decreases the resistance to tension and shear leading to failure of the strong posterior ligamentous support increasing the risk of pelvic instability. In this situation, cementoplasty might not be sufficient due to poor resistance to shear forces and trans-sacroiliac screw fixation seems mandatory to prevent biomechanical failure, provided that the screws can be anchored in normal trabecular/cortical bone (fig.21D,21E,21F). Cement augmentation of the screws in the setting of advanced osteolysis may reduce failure of the fixation [Lea 2019, Roux 2019]. There is limited evidence to support prophylactic stabilization of asymptomatic sacro-iliac lesions, especially if there is no cortical disruption or involvement of the posterior and superior part of the sacro-iliac joint [Muller 2015].
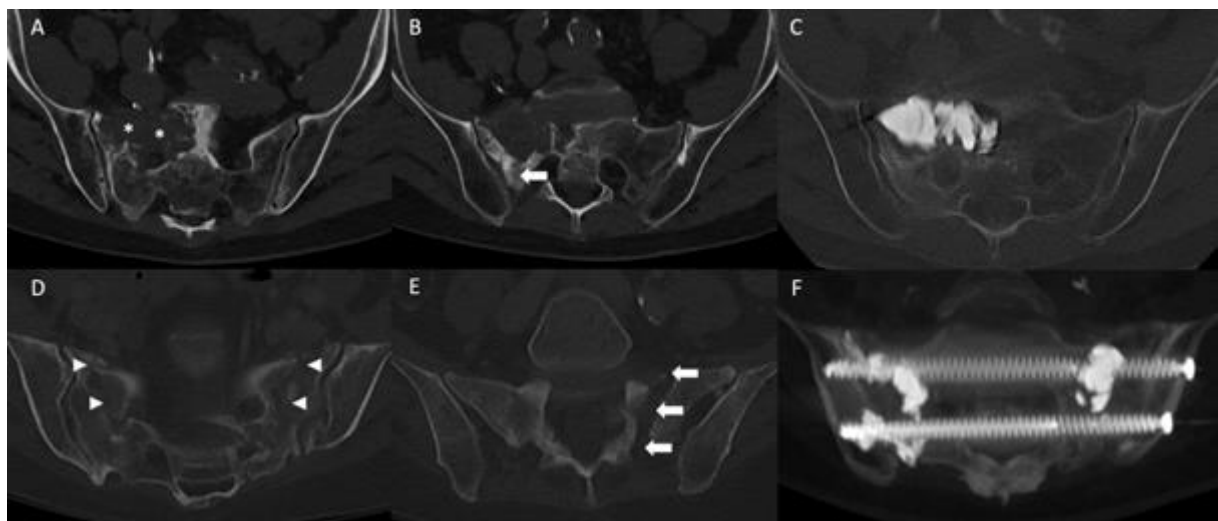
Fig.21: Consolidation of sacro-iliac lesions in patients with mechanical pain. (A) Axial CT-scan at the level of S1-S2 demonstrates an osteolytic lesion (asterisks) at the intermediate and anterior part of S1 and the right sacral ala. (B) CT at the L5-S1 level: there is no destruction of the superior and posterior part of the sacral ala. (C) The risk of fracture and failure to shear can be considered low: stand-alone cementoplasty was performed to provide resistance to compression. (D) Axial CT-scan at the S1-S2 level in another patient shows bilateral post-radiation fractures of the sacrum (arrowheads). (E) The fracture is extending cranially with complete disruption of the posterior and superior part of the sacral ala, exposing to shear forces. (F) The fractures were stabilized with two trans sacro-iliac screws (one in S1 and one in S2) with additional cement injection to improve the anchorage of the screws.

1.5.4. Acetabulum

1.5.4.1. Anatomy and biomechanics

The acetabulum is the most important structure of the pelvic bone for load transmission. The supra-acetabular area (i.e the superior and lateral part of the of the acetabulum, also called the acetabular roof) transmits most of the loads and therefore represents the main mechanical bearing part of the acetabulum, regardless the loading conditions (sitting, standing, walking) [Dalstra 1995, Hu 2017, Volinski 2018]. In particular, the transfer of the hip joint force to the sacro-iliac joint and to the pubic symphysis occurs predominantly through the lateral cortex located above the acetabulum (fig.22) [Ghosh 2015, Volinski 2018]. Consolidation should always be considered in case of an osteolysis in that region, even if the lesion is asymptomatic. The highest stresses distribution among the trabecular bone is located at the central part of the acetabulum, where the applied forces remain low compared to the supra-acetabular area [Dalstra 1995]. The stress concentration at the anterior part of the acetabulum mostly happens during the weight shift and swing phases of gait [Volinski 2018]. The posterior acetabulum is the weakest area in terms of load transmission [Hu 2017, Volinski 2018]. The acetabular cartilage contributes to the distribution of the loads more evenly over the acetabulum [Ghosh 2015]. The action of muscle and hip joint forces produce compressive and tensile stresses within the acetabulum. Overall, compressive stresses predominate on the lateral side and can be considered as high, while tensile stresses occur more on the medial side, the infero-posterior the supero-anterior quadrants of the acetabulum and appear to be much lower [Ghosh 2015].
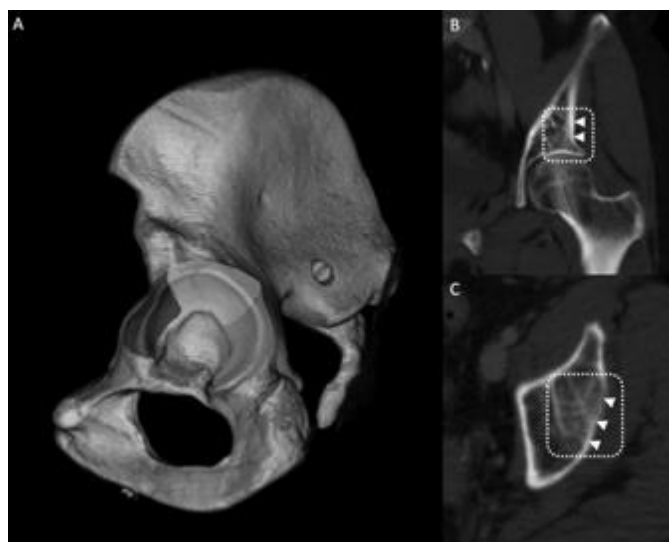
Fig.22: Acetabular loads. (A) The roof of the acetabulum (white area) is permanently stressed, while the anterior part (dark area) is typically only occasionally stressed and the posterior part (gray area) has a very limited role for load transmission. (B) Coronal and (C) axial CT-scan: the acetabular roof (dotted line) is key for the transfers of loads within the hip, with the lateral cortex (arrowheads) being the most important structure of the acetabulum.

1.5.4.2. Implications for percutaneous treatment

Cancer lesions located in the acetabulum have to be considered at high-risk of mechanical failure, as they may compromise the transmission of forces and lead to disastrous functional complications. Many different surgical options have been developed over the years to reconstruct the acetabulum related to primary/metastatic lesion(s) with or without pathologic fractures [Muller 2015]. Open surgery usually combines curettage of the tumor prior

to consolidation, followed by post-operative radiation. Lesions involving exclusively the acetabular roof can be surgically treated with cemented total hip arthroplasty [Muller 2015]. Lesions involving the medial wall will require the additional use of a reinforcement ring to avoid medial migration and lesions presenting with extensive cortical destruction are usually treated with total hip replacement reinforced by cement and acetabular reconstruction placing pins/screws from the acetabulum into an intact ilium to increase the strength of the anchorage [Charles 2017]. Even though the functional outcomes of open surgery are excellent, they can be very morbid and associated with a high rate of complications (especially for complex reconstructions) and is therefore often not feasible in frail patients or in those patients in which systemic therapy cannot be discontinued. Thus, percutaneous procedures provide a viable therapeutic option provided that they are adapted to the situation.

Percutaneous cementoplasty can provide efficient consolidation for lesions exclusively involving the acetabular roof ideally without disruption of the articular cortex (fig.23A&23B) [Spinelli 2016]. This would be analogous to the use of cement in cemented arthroplasty. A finite element analysis demonstrated that for this location complete filling of an acetabular defect, including those with involvement of the lateral cortices, with cement has the potential to restore the transmission of loads to a normal level [Li 2007]. The osteolysis should therefore always be filled with as much cement as possible to avoid secondary collapse [Kurup 2015, Delpla 2019]. Ablation prior to cement injection is technically feasible in that location and might also have a role for local tumor control in addition to bone consolidation and stabilization. It has been reported that complete tumor ablation was a predictive factor of pathologic acetabular fracture stabilization, most likely because it impedes the progression of the osseous destruction [Kurup 2018]. Another potential benefit of ablation is the creation of a cavity-like area that favour lesion filling while potentially reducing the risk of cement leakage. On the other hand, care should be taken not to overablate the surrounding normal bone/cartilage, as this might lead to post-ablation fracture and hip chondrolysis/osteonecrosis [Friedmann 2014]. Some authors advocate the additional use of balloon kyphoplasty following ablation and prior to cement injection in order to increase the chance of optimal acetabular roof filling and to prevent intra-articular leakage of cement (fig.23C-23G) [Kurup 2015]. This could be considered analogous to tumour curettage. The reinforcement of cement with pins/screws for lesions located in the acetabular roof is increasing being reported, even though there is no study demonstrating the superiority of additional hardware reinforcement versus cement alone for that specific indication [Lea 2019]. Keeping in mind that the contact between the hardware and cement should be as large as possible in order to effectively transmit the loads [Vielgut 2013]. In the case of a non-displaced acetabular pathological fracture, the use of screw fixation allows fixation of the fragments and theoretically improves the overall functional result over stand-alone cementoplasty [Roux 2019].
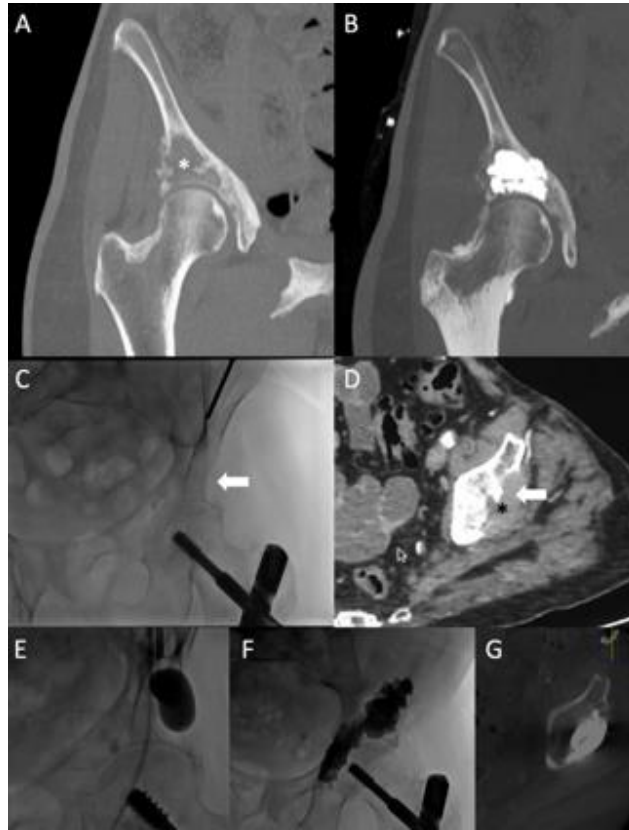
Fig.23: Acetabular roof cementoplasty for consolidation. (A) Coronal CT-scan demonstrates a lytic metastasis in the acetabular roof (asterisk) without destruction of the articular surface and limited involvement of the lateral cortex. (B) Cementoplasty provides immediate consolidation. (C) Anteroposterior fluoroscopic projection and (D) Axial CT-scan show a metastasis (black asterisk) with complete destruction of the lateral cortex (arrow) of the acetabulum resulting in high risk of mechanical failure. (E) Balloon kyphoplasty was used prior to cement injection to reduce the risk of leakage and the likehood of good filling (F) (G) Of osteolytic lesion and weightbearing portion of the supra-acetabular ilium.

For extensive osteolysis with or without fracture involving more than just the acetabular roof, percutaneous consolidative techniques will have limited results for consolidation (fig.24). In particular, lesions that destroy both the cortical bone of the roof and the medial wall of the acetabulum expose the patient to a very high risk of mechanical failure and protrusion of the femur inside the pelvis [Muller 2015, Charles 2017]. Surgery should therefore always be considered in those cases. If the patient is not a surgical candidate, percutaneous cementoplasty +/- screw fixation and thermal ablation might be used for palliation with reserved expectations for stabilization outcomes (fig.25).

Fig.24: Cementoplasty for extensive supra-acetabular osteolysis. (A) Axial CT- scan shows a large amount of osteolysis and destruction of the acetabular roof with minimal cortical integrity (asterisk). (B) Sagittal oblique view shows a diffuse extension of the lesion. The roof of the acetabulum (dotted line) is at high risk of mechanical failure, while the posterior part (black asterisk) has very limited weight-bearing function. (C) And (D) The roof was filled as much as possible with cement while the posterior part was left untreated. Small asymptomatic anterior leakage in the soft tissue. (E) Axial CT-scan in another patient demonstrating a large supra-acetabular osteolytic lesion (asterisk) with destruction of the lateral cortex (arrow). (F) Axial CT-scan more caudally shows that the medial wall of the acetabulum (asterisks) is also completely destroyed. (G) Large volume cementoplasty was performed as the patient was not a surgical candidate due to other comorbidities. (H) One-year follow-up shows recalcification under systemic treatment. However, there is a complete destruction of the hip joint due with acetabular protrusion.

Fig.25: Combined screw fixation and cementoplasty to consolidate a complex acetabular pathological fracture. (A) Coronal oblique and (B) Sagittal oblique CT-scan show a displaced pathological fracture of the acetabulum, in a patient not eligible for surgery. (C) AP fluoro projection and (D) Sagittal oblique CT-scan: Cementoplasty was performed to reinforce the acetabular roof (asterisk) in combination with one retrograde transpubic screw (black arrow) and two anterior trans-iliac screws (white arrow) for fracture fixation. Partial mechanical improvement was noted after the intervention.

1.5.5. The pubic area

1.5.5.1. Biomechanics

The ilio- and ischio-pubic rami and the pubic symphysis have limited weight-bearing function and participate to load transmission essentially during the weight shift and swing phases of walking [Volinski 2018]. At the pubic symphysis, tensile stress is found at the superior and anterior aspect of the pubic arch, while compressive stress occurs at the inferior and posterior aspect of the arch [Hammer 2015]. This results in bending moments in the intermediate region of the pubic symphysis. Because of their orientation and their support for multiple muscular insertions, the ischio- and ilio- pubic rami are submitted to complex stresses including bending and shear.

1.5.5.2. Implications for percutaneous treatment

The pubic rami have little participation in the transmission of mechanical loads within the pelvis and prophylactic stabilization in an asymptomatic patient suffering from a pubic bone osteolytic lesion or fracture is not mechanically necessary. In the traumatic and oncologic surgical literature, fixation/reconstruction of a unilateral pubic fracture/bone lesions are typically not performed [Muller 2015, Rommens 2020].

In the case of a mechanically symptomatic osteolysis, interventional radiology offers an effective minimally invasive solution [Mastier 2018]. Similarly to trauma, percutaneous screw fixation is an effective technique to achieve prompt stabilization, and is usually performed with a retrograde transpubic ascending access [Roux 2019, Rommens 2020]. Cement may be added to reinforce the anchorage of the hardware, but cementoplasty alone will not be as effective as screw fixation in terms of mechanical reinforcement due to its weak resistance to shear forces.

1.5.6. The iliac wing

1.5.6.1. Biomechanics

The iliac wing has very little bearing function and does not participate to the transmission of loads [Muller 2015, Volinski 2018]. However, it still sustains complex stresses during walking because of the insertions of various groups of muscles with strong functional activities.

1.5.6.2. Implications for percutaneous treatment

Osteolysis located in the iliac wing does not compromise the transmission of loads throughout the pelvis and prophylactic consolidation is usually not necessary [Muller 2015]. However, extensive cortical and cancellous bone loss in this area may increase the risk of fracture of the iliac wing similar to that seen following bone harvesting for orthopedic & spine surgeries. In particular, bone loss at the level of the anterior superior iliac spine seems to increase the risk of fracture [Schmitz 2018]. Cementoplasty is not effective to fix a pathological fracture of the iliac wing because of the complex involved stresses and the inability of cement to fix two bony fragments together. Percutaneous screw fixation is an excellent tool to consolidate a pathological/post-ablation iliac wing

fracture, allowing early mobilization of the patient (fig.26) [Tsoumakidou 2014]. Care should be taken to use long screws bridging the fracture line as perpendicular as possible with both extremities anchored in normal bone. The addition to cement might allow to increase the stability of the screw should the landing zone of one extremity of the screw be located in bone of poor underlying quality (e.g. osteopenia, post-radiation/ablation).
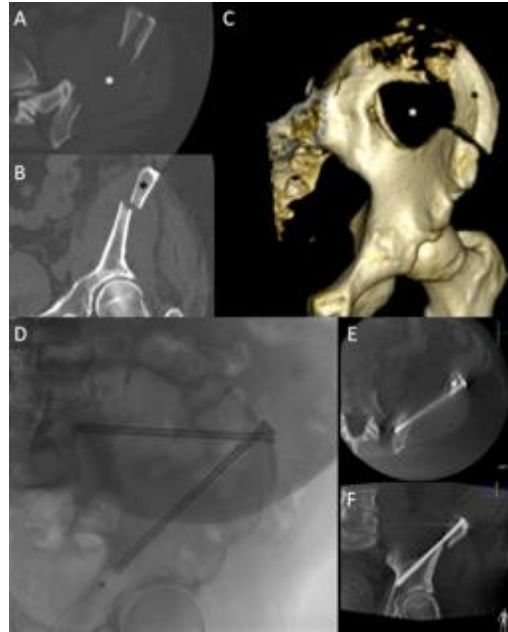
Fig.26: Screw fixation of a pathological iliac wing fracture. (A) Axial, (B) coronal and (C) VRT CT-scan show a large osteolytic metastasis with cortex destruction (white asterisk), responsible for a painful displaced fracture of the iliac wing with a mobile fragment (black asterisk). (D), (E), (F) Two screws were inserted perpendicular to the fracture line. Excellent immediate functional result.

1.5.7. Discussion

The sacral promontory and the acetabular roof are the most critical mechanical portions of the pelvis, mostly submitted to compressive stresses, and should always be carefully evaluated for consolidation. For all other localizations, the risk of mechanical failure can be considered as much lower, especially if the cortical bone is intact, within decreasing functional importance of the sacro-iliac, pubis, ischium and the iliac wing regions. The choice of optimal treatment should always be tailored to the clinical and radiological features of the tumor.

1.6. Conclusion

Cementoplasty with PMMA bone cement is increasingly being performed to treat painful extra-spinal metastases. Besides pain management, many papers underline the potential role of PMMA to provide consolidation in the bony pelvis either as a stand-alone technique or in combination with hardware such as titanium screws. In this perspective, the volume and the repartition of cement seems paramount even though there is only scarce preclinical data available. In the clinical practice, the injection of a volume greater than 10 ml (considered as "a large volume

of cement") is therefore very likely to be required. Such volume is hardly achieved with the devices designed for cementoplasty in the spine that do not offer the possibility to inject more than 10 ml for most of the manufacturers. Moreover, the injection of a large volume of cement comes with specific constraints of time to manage the polymerization of PMMA: a fast injection exposes to the risk of extravasation and leak, whereas a slow injection of the whole volume will be precluded by the increase of cement viscosity with time.

2ⁿᵈ Chapter – Evaluation of the clinical practice

The reviews of the literature highlight the lack of standardization and the limited descriptions on the technique to inject a large volume of bone cement. There are also limited results available about the rate of lesion filling following extra-spinal cementoplasty. Finally, if viscosity is a working property of PMMA that has been explored extensively, little is known about the potential consequence of porosity in extra-spinal cementoplasty. The present chapter therefore seeks to bring additional data through the evaluation of the clinical practice about the technique for the injection of a large volume of cement, the calculation of lesion filling and the analysis of fragmentation of the cement plug following cementoplasty.

2.1. Technique for the injection of a large volume of cement

The previous systematic reviews of the literature demonstrate that there is no clear description about how to inject a large volume of bone cement. Some authors advocate to evaluate the repartition of cement following the injection of an initial volume of 10 ml and eventually insert an additional needle to inject another volume of cement (sequential technique - fig.27), whilst some other recommend injecting simultaneously several kits of cement on several needles (simultaneous – several trocars technique - fig.28).
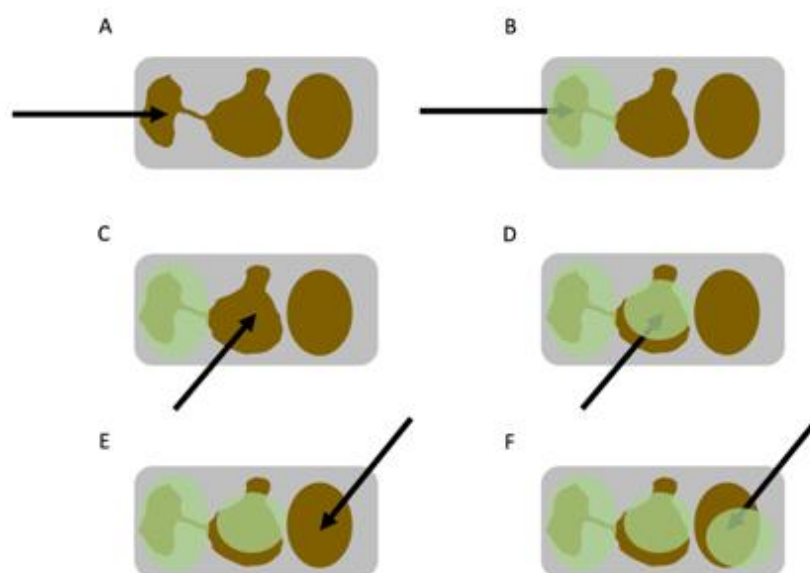
Fig.27: Sequential technique for the injection of a large volume of cement of 30 ml. In that example, a trocar (A) is inserted and a first volume of 10 ml of cement (green circle in B) is injected. A second trocar (C) is advanced in an area not filled with cement and a second volume is injected (D). The same procedure is repeated for the injection of a third volume.
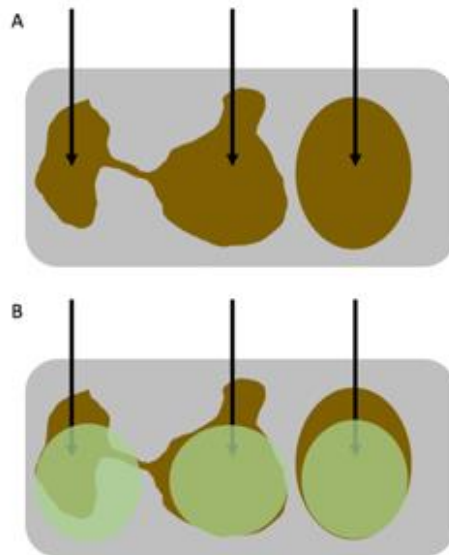
Fig.28: Simultaneous – several trocars technique for the injection of 30 ml. Same example as fig: 3 trocars are inserted inside the lesion (A) and 3 volumes of cement (green circle in B) are injected simultaneously inside the lesion

A third method may be applied in an attempt to achieve the most theoretical cohesive cement volume while limiting the number of needles (single trocar technique – fig.29).
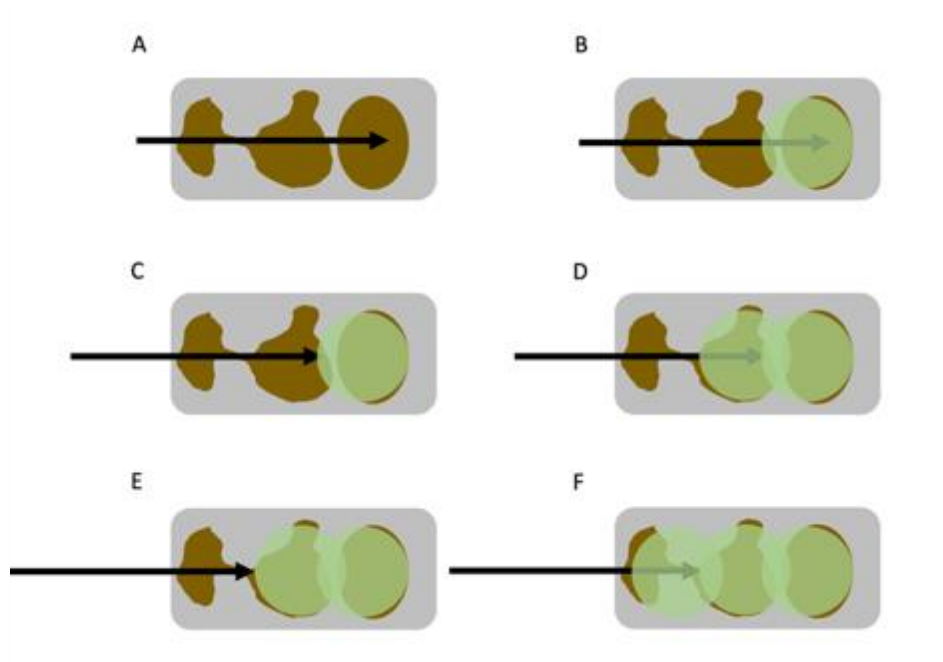
Fig.29: Single trocar – several volumes technique for the injection 30 ml of cement. A trocar (A) is advanced in the great axis of the lesion. 10 ml of cement is injected (B). The trocar is slightly withdrawn (C) and a second volume of cement is injected (D). Same procedure (E &F) for the injection of the third volume.

In this perspective, we retrospectively reviewed our experience whereby the injection of a large volume of cement was performed through a single puncture site, using a long trans-osseous access and continuous injection of different cement volumes that were sequentially prepared one after the other.

Over a 2-year period and out of 42 extra-spinal cementoplasties, 5 cancer patients were presenting with large osteolysis for which more than 10 ml of cement was likely to be injected. All 5 patients were treated using continuous injection of the contents of several (i.e. at least two) vertebroplasty cement kits through a single needle. The mean age of patients (3 women–2 men) was 69 years (range 29–89). Lesions were located in the acetabulum ($n = 4$) and the humerus ($n = 1$). Indication for cementoplasty was pain palliation and improvement in functional ability in all five cases. All 5 interventions were performed by one consultant interventional radiologist, under general anaesthesia in the supine position under combined CT and fluoroscopic guidance (Infinix-I 4DCT, Canon Medical System, Japan—Somatom definition AS & Arcadis Orbit, Siemens, Erlangen, Germany). The technique is presented in Fig.30.
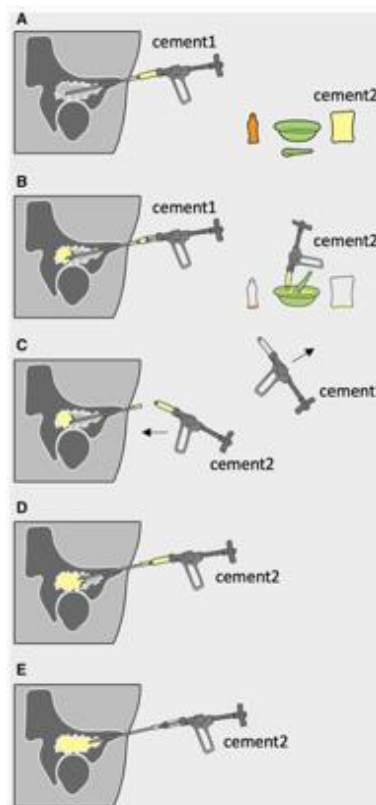
Fig.30: Schematic representation of the technique of injection of large volumes of cement through a single trocar needle. (A) Cement1 (10 ml of high-viscosity polymethyl methacrylate—Osteopal plus, Heraeus Medical, Wehrheim, Germany) is connected to a 15-cm–10G vertebroplasty needle (Gangi special set, Optimed, Erlingen, Germany) that has been introduced through the long axis of the tumour. The monomer and polymer of a second cement (cement2) kit are ready to be mixed. (B) After injection of 5 ml of the first volume (cement1) within the osteolytic tumour, cement2 is prepared and loaded in another device. (C) Once the first 10 ml has been injected, the device for cement1 is removed and the device for cement2 is immediately connected to the hub of the trocar (without emptying the cement inside the bone trocar with the stylet). The needle is slightly retrieved in the case of a leakage or if the cement would progress towards the proximal shaft of the bony trocar, and (D) cement2 is injected inside the tumour. (E) The vertebroplasty needle is progressively withdrawn to complete the filling of the lesion more proximally. If required, subsequent injections of further cement can be performed after the second volume using the same aforementioned technique.

The length of trans-osseous access was 11.3 cm on average (range 9–13). 2.8 (range 2–5) cement kits were prepared for a mean injected volume of 27.4 ml per needle (range 18–50) (Fig.31). In one case, a needle exchange was required, due to an episode of cement setting within the needle between cement preparation #2 and #3 (Fig.32). During injection, the bone trocar was pulled back from its initial position from 9 cm on average (range 7–12). The duration of injection was 21.2 minutes on average (range 15–31). Three patients experienced a reduction in VAS score greater than 2 at 1-month follow-up, whilst one patient had complete pain relief and one patient had no change to her symptoms. Functional improvement was noted in 4 out of 5 patients at 1-month follow-up.
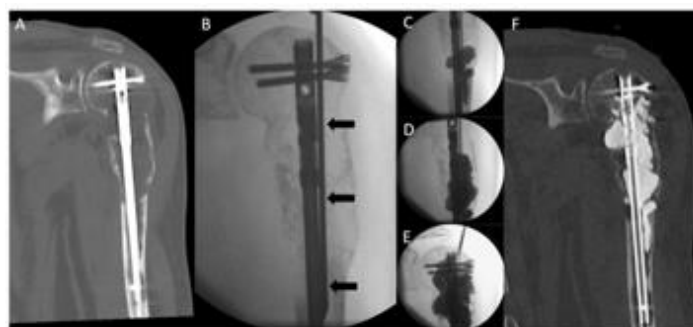
Fig.31: Cementoplasty of an osteolytic humeral metastasis from kidney cancer in a 71-year-old male patient. (A) Coronal CT-scan shows a large osteolytic lesion infiltrating the diaphysis and threatening the stability of the proximal insertion of the intramedullary nail. (B) A 10G vertebroplasty needle (black arrows) in inserted along the axis of the diaphysis under fluoroscopy. (C) Fluoroscopic view after injection of the first volume (10 cc) of cement. (D) Same view after partial withdrawal of the needle and further injection of 2 other volumes (30 cc in total). (E) Filling of the cranial part of the lesion after injection of 50 cc (i.e. 5 cement preparations in a row). (F) Final CT-control with coronal reconstruction demonstrating optimal cement integration.
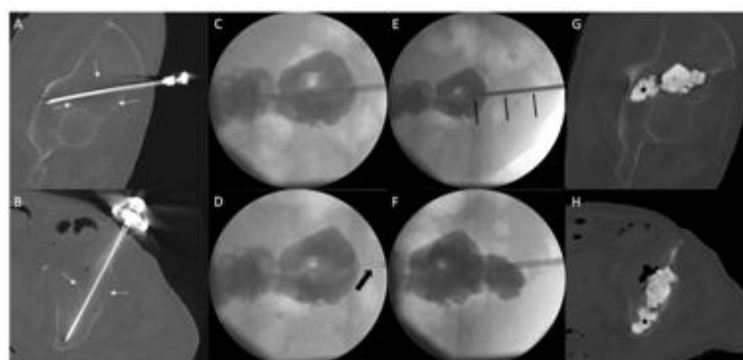
Fig.32: Cementoplasty of a left acetabular metastasis in an 89-year-old male patient (patient2). (A) Sagittal oblique and (B) axial oblique CT-scan shows the lesion (white arrows) and the vertebroplasty trocar inserted in the long axis of the acetabulum. (C) Oblique fluoroscopic projection: after injection of 2 cement kits in a row (20 cc), the third volume was not prepared in time and could afterwards not be injected because of cement hardening within the trocar. (D) The bone trocar (arrow) was withdrawn, and (E) a new needle (black arrows) was inserted with the same entry point. (F) An additional cement preparation was injected. (G) Sagittal oblique and (H) axial oblique CT-scan shows a volume of 30 cc of cement in the acetabular lesion but also in the distal cancellous bone (black star)

60

We were able to inject up to 50 ml of total cement through a single puncture site, whilst theoretically increasing the chance of forming one coalescent cement stream. The importance of optimal lesion filling to achieve long-standing consolidation in both spinal and acetabular osteolytic lesions has recently been underlined in two papers [Delpla 2019, Hesler 2019]. Even though it is not without limitations (need to approach the lesion in its long axis, need to manage simultaneously the pullback of the trocar and the countdown for next cement preparation), we believe that the approach herein described might be of help to manage large osteolytic lesions with the current available material.

2.2. Filling rate of acetabular osteolysis by bone cement

Most of the authors advocate injection of as much cement as possible, in order to restore the load transfer across the acetabulum. Proper estimation of the filling of the tumor following injection of cement may therefore be of utmost importance. In day to day practice, the evaluation of filling of a pelvic osteolytic lesion is usually performed cognitively by the operating physician, based on subjective analysis from an immediate post-operative CT-scan [Iannessi 2012]. Volumetric analysis of a structure using CT-scan images is feasible, precise and reproduceable, as demonstrated by the extensive experiences in liver volume calculation in oncology [Muller 2010]. The purpose of the present study is therefore to investigate the rate of lesion filling following cementoplasty of an acetabular osteolytic lesion, the interobserver agreement for the analysis and investigate how subjective analysis compares to volumetric analysis. The acetabulum was chosen as the region of interest as is at high risk of mechanical failure in case of bone destruction.

2.2.1. Materials and methods

The following section present the single centre retrospective study we performed. All patients gave informed written consent for the procedure. Institutional review board was waived.

2.2.1.1. Study population

Institutional electronic charts were reviewed to identify patients who benefited from pelvic percutaneous cementoplasty from January 2010 and December 2018. All images were then reviewed by a senior consultant in interventional radiology with 9 years of experience (JG) to identify acetabular lesions and exclude non acetabular locations. Further selection was made according to the appearance of the acetabular lesion: mixed and osteoblastic tumors were excluded. Finally, osteolytic lesions were selected using the Lodwick classification: geographic lesions (Lodwick grade I and II) were included while permeative lesions with poorly defined margins (Lodwick grade III) were excluded [Caracciolo 2016].

Lesion selection is demonstrated in Fig.33. A total of 21 acetabular osteolytic lesions in 21 patients were included for the present study.
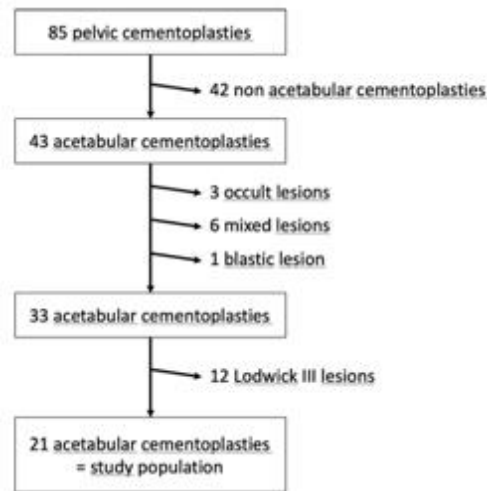
Fig.33: Lesion selection flowchart

All cases were then reviewed for subjective analysis by two senior interventional radiologists and one resident, who were not involved in the procedures, and for volumetric analysis by a third senior interventional radiologist.

2.2.1.2. Subjective analysis

Each radiologist (PA, RLC—senior interventional radiologists/TM—resident) reviewed retrospectively the planning and immediate post-cementoplasty CT-scans on a dedicated workstation (OsiriX—Pixmeo, Geneva, Switzerland). The readers were asked to examine MPR reconstructions (axial, coronal and sagittal planes) with side by side comparison of both pre and post-operative CT-scans with the following bone windowing settings: 300 WL 1500 WW for the planning CT and 1400 WL 4500 WW for the immediate post-cementoplasty control (in order to get rid of streak artifacts related to cement deposits).

Following image analysis, each reader had to define the cement filling ($F_{subjective}$) of the osteolytic lesion using the following 4 grade scale: $F \leq 25\%$, $25\% < F \leq 50\%$, $50\% < F \leq 75\%$ or $F > 75\%$. The radiologists were specifically asked to evaluate the osteolytic area and not the filling of the surrounding cancellous bone or the diffusion of cement beyond the bone structure, should a soft tissue leakage be present (Fig.34).
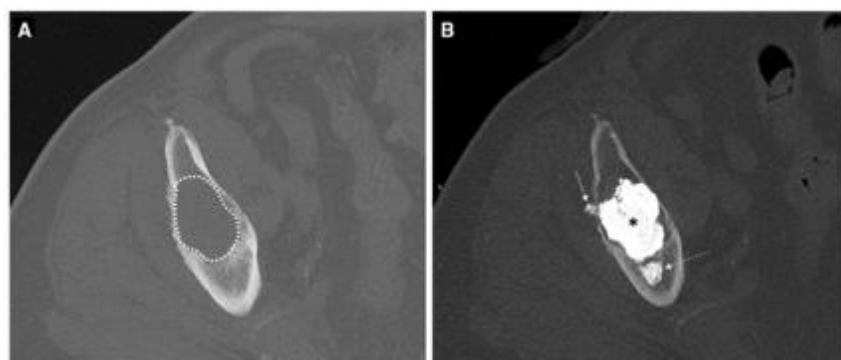
Fig.34: Subjective evaluation. The readers had to compare side by side the pre-operative (A) and post-operative (B) CT-scans. The lesion (dotted circle in A) corresponded to the osteolytic lesion. Cement within the lesion (black asterisk in B) had to be considered for filling evaluation, while filling of cancellous bone (dotted arrow in B) and soft tissue leakage (arrow in B) had to be excluded from analysis.

Maximum time to review the images was set to 5 minutes in order to reproduce as much as possible the quick intraprocedural evaluation required in daily clinical practice. The subjective analysis was made sequentially (each radiologist after the other and each reader being blind to the results of the two others).

2.2.1.3. Volumetric analysis

Volumetric analysis was performed separately by a third senior interventional radiologist, using dedicated medical processing software (OsiriX—Pixmeo, Geneva, Switzerland). The reader was software trained on 10 practise case sets (independent to those included in the study) prior to carrying out the final analysis.

Volumetric analysis was conducted in three steps (Fig.35):

(1) the osteolytic area was manually delineated with regions of interests (ROIs) on all axial planning CT-slices (1.5 mm thickness with the following settings: 300 WL 1500 WW) containing the tumor, excluding any soft tissue extension if present. The volume was then calculated using the compute volume function of the software. Results were rounded to the nearest figure.

(2) Cement within the osteolysis was contoured with ROIs on all axial post-operative CT-slices (1,5 mm thickness with the following settings: 1400 WL 4500 WW), without including any cement deposition in the normal cancellous bone and/or beyond the limits of the bone cortex. The volume was then calculated using the compute volume function of the software. Results were rounded to the nearest figure.

(3) Percentage filling of the lesion was calculated using the equation:

$$\frac{Volume\ of\ cement}{Volume\ of\ the\ lesion} \times 100$$

Results were rounded to the nearest figure. The filling of each lesion was further defined ($F_{volumetric}$) using the same 4 grade ($F \leq 25\%$, $25\% < F \leq 50\%$, $50\% < F \leq 75\%$ or $F > 75\%$) scale. Volumetric analysis was considered as the reference for further statistical evaluation.
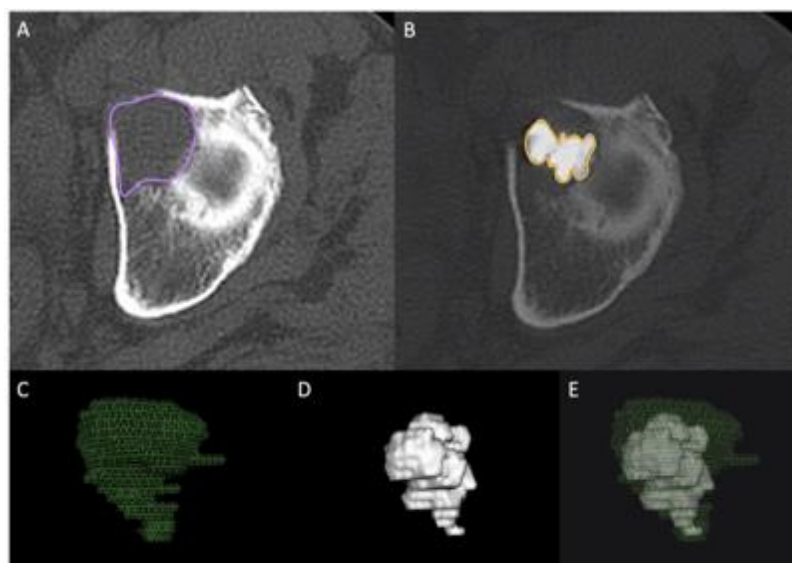
Fig.35: Volumetric analysis. The osteolytic lesion was segmented on each slice of the planning CT-scan (A). The contours of cement within the lesion was then drawn and segmented on each slice of the post-operative CT-scan (B). The volumes of the lesion (C) and of the cement within the osteolytic lesion (D) were then computed. The ratio between the two volumes (E) was then used to evaluate the filling of the lesion by the cement. In this case (patient 15), the filling of the lesion was 49% according to volumetric subtraction.

2.2.1.4. Statistical analysis

Statistical analysis was performed using R statistical software (v3.5.3).

The reliability of $F_{subjective}$ between the different readers (interobserver agreement) was evaluated using the Fleiss' Kappa test for the 4 grade scale, and subsequently for a simplified 2 grade scale ($F \leq 50\%$ and $F > 50\%$).

The performance of $F_{subjective}$ versus $F_{volumetric}$ (considered as the reference) was then evaluated for each reader using the calculation of accuracy and error to reference for the 4 grade scale (e.g. the probability of correctly classifying the percentage of filling cognitively compared to volumetric analysis) and accuracy, sensitivity, specificity, positive predictive value and negative predictive value for the 2 grade scale (e.g. the accuracy, sensitivity, specificity, positive predictive value and negative predictive of correctly classifying the filling in the $> 50\%$ group).

2.2.2. Results

2.2.2.1. Subjective and volumetric analysis

The results of $F_{subjective}$ for the 4 grade and 2 grade scales are presented in Table7. With the 2 grade scale classification, a $F_{subjective} > 50\%$ was given in 11/21 (52.4%) by all three readers.

	Accuracy	Se	Sp	PPV	NPV
Overall	60% (47–72)	83% (52–98)	55% (40–69)	30% (16–49)	93% (78–99)
Resident	57% (34–78)	75% (19–99)	53% (28–77)	27% (6–61)	90% (55–100)
Senior 1	67% (43–85)	100% (40–100)	59% (33–82)	36% (11–69)	100% (69–100)
Senior 2	57% (34–78)	75% (19–99)	53% (28–77)	27% (6–61)	90% (55–100)

Table7: Performance of subjective analysis to correctly classify a lesion in the $F > 50\%$ group

Mean filling of the osteolytic lesion, calculated with volumetric analysis was 35.3% (range 11–55). Detailed results of $F_{volumetric}$ are presented in table7. With the 2 grade scale classification, a $F_{volumetric} > 50\%$ was present in 4/21 (19%) of the cases.

2.2.2.2. Agreement between readers for subjective evaluation

p of the Fleiss kappa test were 0.01 and 0.04 for the 4 grade scale and 2 grade scale respectively, indicating statistically significant agreement and making both kappa tests interpretable. However, agreement was considered as very low (< 0.2) for the 4 grade scale analysis and as low (> 0.2 and < 0.4) for the 2 grade scale analysis with kappa factors of 0.196 [0.000; 0.443] and 0.36 [0.08; 0.68] respectively (Fig.36).
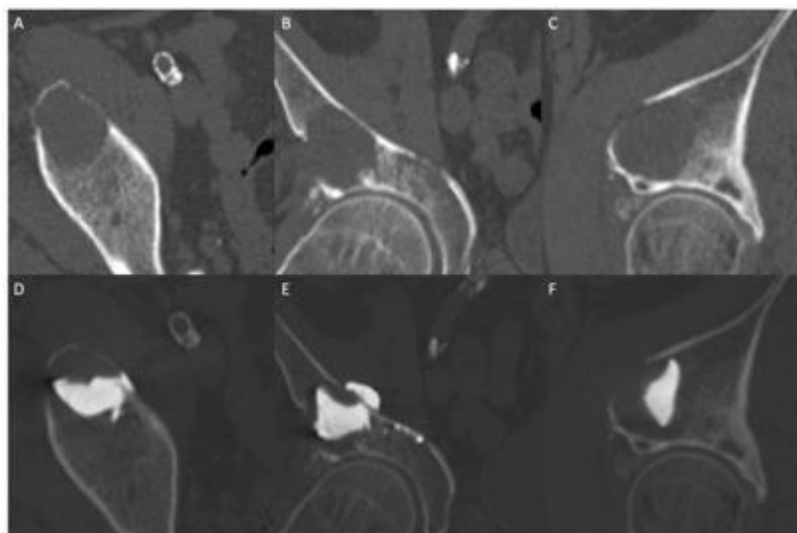
Fig.36: Subjective versus volumetric analysis (patient 1). Axial, coronal and sagittal images before and after cement injection (A–C and D–F respectively) show partial filling of the lesion. Using volumetric analysis, the filling of the lesion was 33%. Reader #2 and #3 (senior interventional radiologists) subjectively classified it in the $25\% < F \leq 50\%$ category, while the resident classified it in the $50\% < F \leq 75\%$ group.

2.2.2.3. Performance of subjective versus volumetric analysis

With the 4 grade scale, the overall, resident, senior 1 and senior 2 accuracy was 36.5% [24.7–49.6], 28.6% [11.3–52.2], 33.3% [14.6–57.0] and 47.6% [25.7–70.2] respectively. The resident overestimated the filling in 14 (67%) cases, senior 1 in 12 (57%) and senior 2 in 10 (48%). The mean error to gold standard for proper $F_{subjective}$ classification was + 0.67, + 0.76, + 0.57 and + 0.67 for all readers, resident, senior 1 and senior 2 respectively (Fig.37).
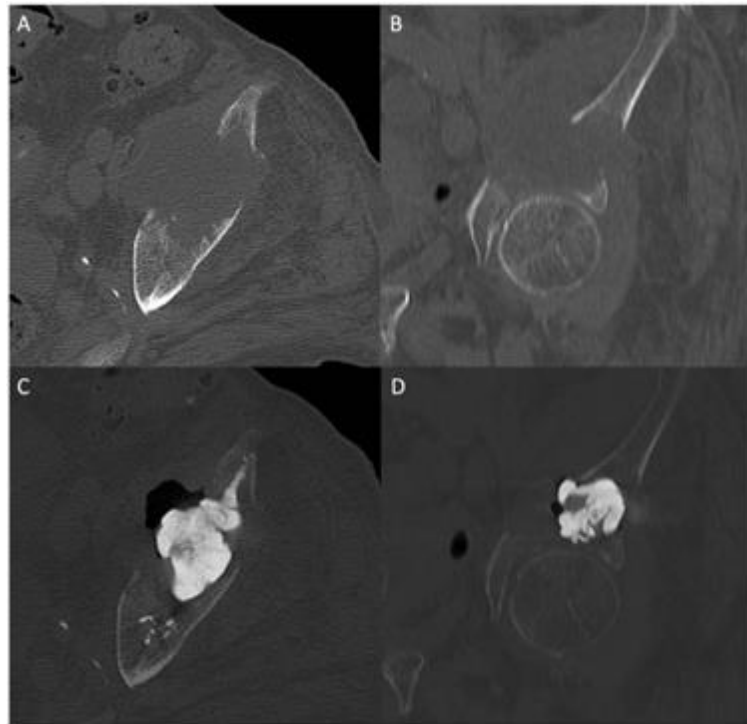
Fig.37: Subjective versus volumetric analysis (patient 20). Axial and coronal images before and after cement injection (A, B and C, D respectively) show partial filling of the lesion. Using volumetric analysis, the filling of the lesion was 34%. All three readers classified the filling as $50\% < F \leq 75\%$.

With the 2 grade scale, the overall accuracy, sensitivity, specificity, positive and negative predictive value to correctly classify a lesion in the $F > 50\%$ group were 60% [47–72], 83% [52–98], 55% [40–69], 30% [16–49] and 93% [78–99] respectively. Detailed results per reader are presented in Table7.

2.2.3. Discussion

Our study demonstrates that the subjective evaluation of the percentage of filling of an osteolytic acetabular lesion following percutaneous cementoplasty is not accurate, even if a simple 2 grade scale is used. The interobserver agreement is poor, and there is a general trend to overestimate the filling of a lesion. Statistical analysis demonstrated that the interventional radiologist usually correctly identifies the lesion filled with more than 50% of cement (83% of overall sensitivity to detect a filling > 50%) but fails to recognize when the filling is below 50%

66

(overall specificity of 55%). This is also reflected in the positive and negative predictive values: the probability that lesion filling is indeed greater than 50% if the radiologist thinks so is very low (30% positive predictive value), whilst on the other hand, it is highly likely that less than 50% of the lesion is filled with cement if the intervening operator subjectively says so (93% negative predictive value).

There is little clinical evidence supporting the fact that optimal lesion filling is associated with a better biomechanical outcome in cases of acetabular osteolysis [Garnon 2019]. A finite element analysis study has however shown that load transmission could be restored across the acetabulum following cementoplasty. The authors assumed in that paper that the filling of the osteolysis was complete [Li 2007]. Recently, Delpla et al. demonstrated that spinal metastases with suboptimal cement filling were associated with more pathological fractures, reinforcing the theory that the lesion should be filled as much as possible for optimal consolidation, especially in a weight bearing area such as the acetabulum [Kurup 2018, Delpla 2019]. Another recent study showed that the only predictive factor to reduce the occurrence or worsening of an acetabular fracture was cement filling (even if incomplete) of all of the sections of the acetabulum, thereby emphasizing the need for optimal filling of an osteolytic acetabular tumor [Hesler 2019]. In this respect, our study suggests that subjective evaluation of cement filling limits accurate evaluation of the quality of treatment. Interestingly, the percentage of lesion filling was quite low in our series (35.3%). A recent systematic review showed that the average lesion filling for pelvic cementoplasty was 56.1%, but with only 2 papers reporting that specific data [Garnon 2019]. The methodology was however not detailed and one may assume that an evaluation based on a simple calculation of the volume of a sphere is not adapted to bone, especially in an area with complex landmarks such as the acetabulum, and may have led to overestimation. Software volumetric calculation is easy, feasible, accurate, reproducible and has been reported in different locations, such as the liver or brain, to evaluate response to treatment [Winter 2018]. The algorithm is available in almost all workstations or modern picture archiving and communication system software, thus widely available and accessible in daily practice.

The major question that remains opened is the clinical feasibility of volumetric analysis. If the cement volume has been completely delivered within the lesion, the intervening physician has enough time to call for a volumetric analysis and decide whether or not he should inject another volume (most likely through the insertion of an additional bone trocar). We currently make such evaluation subjectively by quickly reviewing the post-operative CT-scan in all 3 planes immediately after the injection, but we feel to move to volumetric analysis for that specific purpose. On the other hand, volumetric analysis is very unlikely to be feasible in the mid of cement injection as it will not be time-compatible with the countdown for cement hardening. Ultimately, we believe that the calculation of the volume of the lesion before the procedure has probably the greatest interest, as it gives an idea of the required volume prior to injection especially for large lesions. In all cases optimal filling might however be precluded by the occurrence of cement leakage(s) that may lead to early termination of cement injection.

Our study has several limitations. First of all, volumetric analysis was only performed by one radiologist, and we therefore lack the evaluation of the interobserver agreement for the volumetric measurements. Time taken for volumetric analysis was also not measured. In our experience, it takes between 5 and 10 min to contour the lesion and the cement. This potentially limits the clinical utility of the technique as time is critical for decision making

during an intervention. The use of a simplified 4- and 2- grade scale can be criticized as it didn't offer the possibility for the readers to give a more precise estimation of the percentage of filling. We compared the results of 3 radiologists with only two of them being senior radiologists. Hence, it is possible that our results are not completely representative of the reality, as subjective evaluation is most certainly influenced by experience. We believe however that it is sufficient to demonstrate the heterogeneity of subjective analysis. Finally, due to the retrospective nature of the study, we were unable to collect robust clinical and imaging long-term follow-up data, which could have helped to demonstrate and support the notion that optimal filling improves mechanical stability.

In conclusion, osteolytic lesions are substantially underfilled in the clinical practice. Moreover, the subjective assessment of lesion filling following percutaneous cementoplasty of an acetabular osteolytic lesion is associated with poor interobserver agreement and overestimation of the percentage compared to volumetric analysis.

2.3. Fragmentation of PMMA bone cement

As seen in the reviews of the literature, cementoplasty has the ability to achieve consolidation of fractures and impending fractures in locations predominantly withstanding compression stresses. In the bony pelvis notably, cementoplasty has been indicated to stabilize insufficiency/pathological fractures of the sacral ala and impending fractures of the acetabulum. Once the cement has been deposited and has cured inside the bone, the plug of PMMA is not expected to undergo remodeling nor resorption over time [Oonishi 2011, He 2014]. However, in-vivo changes to the morphology of the cement volume may occur. Various potential causes of such findings have been reported in the experimental and clinical literature: infection, mechanical breakage, cracking, and foreign body reaction (FBR) [Deschamps 2012, Togawa 2016, Gibon 2017, Klopfeisch 2017, Liao 2018]. Most of the data on the causes and consequences of cement fragmentation come from the orthopedic literature, as loosening and failure of arthroplasties are relevant clinical issues [Goodmann 2005, Holt 2007]. There are only sporadic case reports of PMMA breakages in the spine following vertebroplasty [Liao 2018, Huang 2019]. Although it does not seem to be a frequent clinical problem, literature on cement fragmentation after percutaneous cementoplasty in the bony pelvis is still lacking. The purpose of the present study is therefore to report the rate of PMMA fragmentation following percutaneous cementoplasty in the bony pelvis (i.e pelvic bones or sacrum) and discuss the underlying mechanisms and consequences.

2.3.1 Materials and methods

This is a single centre retrospective observational study. Institutional review board approval was obtained for the retrospective evaluation of the radiological data. All patients gave informed consent to undergo the intervention.

2.3.1.1. Patient selection

Retrospective chart review of all cementoplasty procedures performed with PMMA in the sacrum or the pelvic bones between January 2010 and October 2019 was conducted. Patients who benefited from the combination of screw fixation and cementoplasty during the same intervention were excluded. In order to compare the radiological findings with the same modality, only the patients who were treated under combined CT-fluoroscopic guidance

(thus with an immediate post procedural CT-acquisition), and who were restaged (whatever the indication) with a thoraco-abdominopelvic, abdominopelvic or pelvic CT-scan during follow-up were included in the present study.

2.3.1.2. Procedures

All interventions were performed under combined CT and fluoroscopic guidance using a mobile C-arm prior to 2017 (Somatom Definition AS & Arcadis Orbit, Siemens, Erlangen, Germany) and an Angio-CT after 2017 (Alphenix 4DCT, Canon Medical, Japan). Cementoplasty was performed under conscious sedation, regional spinal anesthesia or general anesthesia, in the prone or supine position depending on the location and number of cement injection(s). PMMA was manually mixed (Osteopal V, Heraus medical) according to manufacturer's recommendations and injected through a 10 or 15cm 10G beveled vertebroplasty needle (Vertebroplasty special needle set, Optimed, Germany) using a dedicated injection device (Cemento MP, Optimed, Germany). Injection was performed under continuous fluoroscopic monitoring and intermittent CT-acquisitions. An immediate post-interventional volumetric CT-scan was systematically acquired to ensure optimal cement distribution and rule out any immediate complication.

2.3.1.3. Data collection and analysis

Pre and last-available post-operative CT-scans were reviewed side by side on a dedicated workstation (Osirix, Pixmeo, Switzerland) by two interventional radiologists with 4 and 10 years of experience in percutaneous cementoplasty on 1mm thickness axial, coronal, sagittal images and 15mm maximum intensity projection (MIP) axial, coronal and sagittal images, with a 3000 HU window level – 10000 HU window width setting (fig.38). Each radiologist reviewed the images independently. Differences were resolved by consensus.
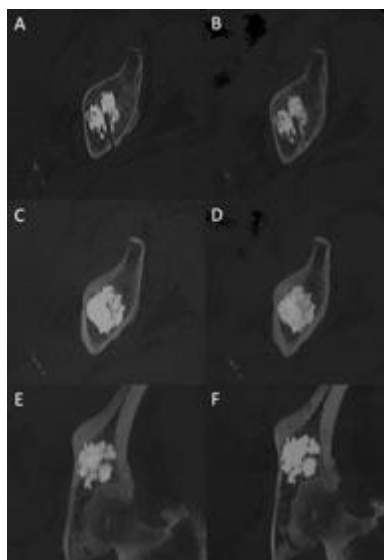
Fig.38: Side by side comparison. Immediate post-intervention axial 1mm thickness CT-scan (A) and 23 months follow-up 1mm thickness CT-scan (B). Immediate post-intervention axial (C) and coronal (E) 15mm MIP CT-scan and 23 months follow-up axial (C) and coronal (F) 15mm MIP CT-scan CT. Analysis was also performed in 1mm thickness coronal and sagittal and 15 mm MIP sagittal images (not shown).

The following features of the PMMA plug and surroundings were collected: 1) apparition of a fracture line inside the cement plug on 1mm thickness images; 2) modification of the shape of PMMA on MIP images; 3) identification of PMMA distant to the original cement volume on MIP images; 4) stability, consolidation, worsening or apparition of a bone fracture in the area of cementoplasty on 1mm thickness images; 5) stability, regression, increase or apparition of osteolysis around the cement on 1mm thickness images (fig.39).
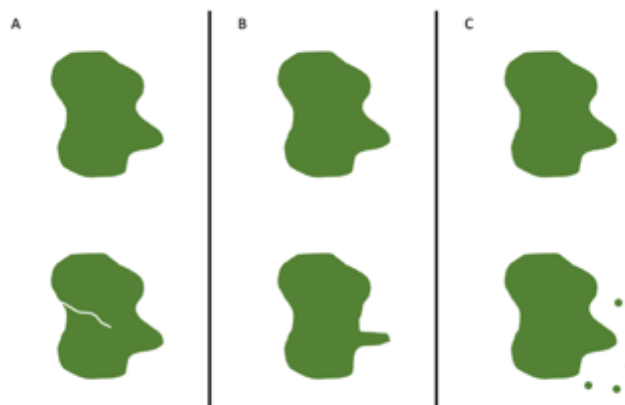
Fig.39: Patterns defining cement fragmentation in our study. (A) identification of a fracture line inside the cement plug. (B) modification of the shape of the cement volume. (C) identification of PMMA distant from the original cement plug.

According to descriptions in the literature, fragmentation of PMMA was recorded in case of an apparition of a fracture line inside the cement plug and/or if the shape of PMMA was modified and/or if PMMA was identified distant to the original volume [Yevich 2018, Huang 2019]. Should fragmentation be present, the entire patient's medical history was reviewed in order to look for signs of local infection and assess the pain level using the visual analogue score before the intervention and at the last clinical evaluation.

Descriptive statistics were used to present results. Categorical variables were expressed as absolute numbers and percentages. Continuous variables were expressed as means with standard deviations and ranges. Comparison of the length of follow-up and the rate of cement fragmentation between malignant lesions and benign insufficiency fractures was made using a t-test. A p-value<0.05 was considered statistically significant. Statistical analysis was performed by using R v3.6.3 (R Foundation for Statistical Computing, Vienna, Austria -*copyright mark*).

2.3.2. Results

One-hundred and eighty-nine patients were treated with percutaneous cementoplasty during the study period. After exclusion of patients treated with Cone-beam CT guidance and patients either lost to follow-up or without a restaging CT-scan, the final study population consisted of 56 patients (36 Men, 20 women) with a mean age of 68.4 +/- 15.4 (range 29 – 92), in which a total of 98 percutaneous target lesions/tumors were treated in 56 sessions (1.75 +/- 0.8 cementoplasty procedures per intervention; range 1 – 4). Indications for treatment were painful malignant tumors (42.9%; 42/98) and insufficiency fractures (57,1%; 56/98). Radiation therapy was performed

prior to the cementoplasty procedure in 19/42 (45.2%) and scheduled after the intervention in 11/42 (26.2%) malignant lesions. There was no systematic planification of radiation treatment for the remaining 12/42 (28.6%) lesions. Most frequent locations of cement injection were the sacral ala (60.2%; 59/98) and the acetabulum (21.4%; 21/98). Other cemented regions (18.4%; 18/98) included the iliac wing (n=13), the body of S1 (n=3) and the ischium (n=2). Cementoplasty of the sacral ala was predominantly performed for insufficiency fractures (83%; 49/59), whilst acetabuloplasty was mostly applied for malignant cases (91%; 19/21). A cortical fracture was noted in 39/56 (69.6%) of the insufficiency fractures (69.6%). For malignant cases, lesions were predominantly osteolytic (95%; 40/42). Cortical destruction and pathological fractures were present in 19/42 (45.2%) and 1/42 (2.4%) cases respectively. Percutaneous radiofrequency ablation was performed during the same procedure in 1/42 (2.4%) malignant cases. A flowchart of patient selection and lesions is presented in fig.40.
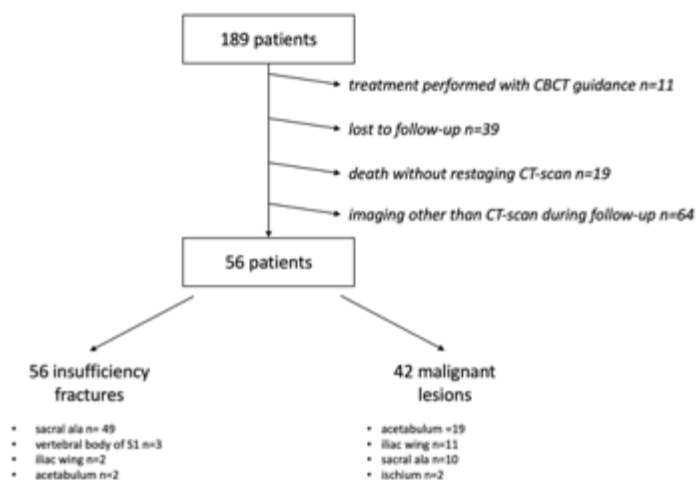
Fig40: flowchart of patient selection

Mean interval between the procedure and the last available CT-scan was 29.3 +/- 18.8 months (range 6 – 77). There was no significant difference in the length of follow-up of malignant lesions (27.6 +/- 15.1 months) vs insufficiency fractures (29 +/- 20.5 months) (p=0.69).

Analysis between the 2 readers was 100% concordant regarded the 5 collected items. A fracture with a modified PMMA shape was demonstrated in 2/98 (2%) cementoplasty procedures, both in malignant peri-acetabular lesions. PMMA distant to the initial cement volume (in the hip joint) was identified in one case. Hence, fragmentation was diagnosed in 2/98 (2%) cementoplasty procedures, all in the malignant lesions group (2/42 - 5%). The filling rate of the osteolysis by the cement was 36% and 49%. None of these two cases benefited from concomitant thermal ablation. Both lesions received additional external radiation therapy within the month following PMMA injection. The time intervals between the procedure and the first visualization of cement fragmentation were 6 and 24 months respectively. In one case, the last restaging CT-scan showed collapse of the hip joint and regression of the osteolysis around the cement (most likely secondary to systemic treatment and radiation therapy), while the other case was associated with an increase in osteolysis and apparition of a pathological fracture due tumor progression

71

(fig.41). There was no sign of infection in any of these 2 cases. Pre-intervention pain level scores were 9/10 and 6/10; corresponding pain scores at last available follow-up were 7/10 and 8/10 respectively.

For malignant cases, the osteolysis around the bone cement was classified as follow: stability in 15/42 (35.7%) cases, partial regression in 13/42 (31%), complete regression in 9/42 (21.4%) and progression in 5/42 (11.9%). For insufficiency fractures, radiological signs of consolidation were seen in 53 of the 56 (94.6%) PMMA injections at last available follow-up, more specifically in 36 of the 39 fractures (92.3%) with cortical disruption. There was no fragmentation of PMMA (0/56 - 0%), and no progressive osteolysis around the cement plug during follow-up of insufficiency fractures.

The difference in the rate of fragmentation between the malignant tumor and the benign insufficiency fracture groups did not reach significance (p=0.08).

Fig.41: Fragmentation of PMMA. (A) Coronal CT-scan prior to intervention shows an extensive osteolysis of the roof and medial wall of the acetabulum (arrowheads). (B) 14 months restaging CT-scan (coronal view with 15mm MIP reconstruction) shows a small fracture at the bottom part of the cement volume (arrow) and PMMA inside the joint distant to the initial plug (dotted arrows). Note the deformation of the hip joint with ascension of the femoral head. (C) Hip deformation was already visible 3 months after cementoplasty. This case was recorded as fragmentation due to mechanical breakage of PMMA.

2.3.3. Discussion

The present study proposes that fragmentation of the cement plug at mid-term follow-up (almost 3 years) is an uncommon finding following percutaneous injection of PMMA in the bony pelvis. It confirms the data of explanted arthroplasties showing that PMMA undergoes little change once injected in the bone [Oonishi 2011]. Based on imaging findings, the two cases of fragmentation likely to have occurred because of failure of the cement to resist complex mechanical stresses, due to extensive osteolysis at the time of treatment for one case and secondary to significant tumor progression with subsequent fracture in the other. The decreased resistance of cement to tension, bending and shear forces compared to compression most certainly accounts for the occurrence of fragmentation. Such a finding is a known limitation of percutaneous cementoplasty. It may explain why

fragmentation occurred only for malignant lesions, which were more likely to deteriorate the resistance of bone and expose PMMA to complex stresses. Hence, PMMA fragmentation in our series seems to be more of a consequence of the local mechanical environment than the cause of further bone collapse/fracture. Similar to radiological features, the lack of clinical improvement at last follow-up is likely due to the worsening of bone deformity and not to the minimal fragmentation of the PMMA plug. The relatively low rate of cement fragmentation in the present report might be explained by the additional use of screw fixation for complex/extensive pelvic metastases and/or fractures since 2013 in our institution, thereby reducing the risk of mechanical failure of stand-alone cementoplasty.

Whilst mechanical breakage is related to extrinsic stresses on the cement volume, the pathophysiology of cracking and FBR is more complex and seems to be linked to both extrinsic factors, such as loads and micromotions at the bone-cement interface, as well as the working properties of the cement itself such as porosity [Lewis 1997, Janssen 2005]. Porosity is an inevitable process related to the inclusion of air particles inside the PMMA during mixing and injection, leading to micro- (<1mm) and macro- (>1mm) pores inside the cement [Lewis 1997]. Although it should be interpreted with great caution, the present data potentially suggest that the porosity of bone cement has little clinical impact for percutaneous procedures at mid-term follow-up. Pre-clinical studies suggest that pores may be the origin of crack initiation that can ultimately lead to fracture and fatigue failure of cement should the cracks propagate [Ling 1998, Janssen 2005]. Moreover, pores and cracks are supposed to be a potential source for the release of PMMA beads which can subsequently trigger a FBR around the cement [Ries 2006]. Such reaction usually comes with an extensive osteolysis around the cement and a fragmentation of PMMA [Shardlow 2003]. There were no signs suggestive of cracking or FBR in our series. To a certain extent, this further supports that porosity is not clinically relevant, as reported in the orthopedic literature [Ling 1998, Sluttitel 2019].

The present study has many limitations. There was no follow-up imaging available for a majority of patients. In our institution, a systematic follow up CT-scan is not organized if the patient remains asymptomatic following cementoplasty. Moreover, many patients were in a palliative situation and died within weeks to months after treatment without restaging imaging. A certain number of patients were also referred from peripheral hospitals and were lost to follow-up following treatment. This might have led to an underestimation in the rate of PMMA fragmentation. Other causes of underestimation of PMMA fragmentation include the variability of the quality of imaging between baseline and restaging CT-scans in some cases. Hence, subtle modifications of the cement volume might have been missed. Finally, there was no histology in the two cases of PMMA fragmentation, in order to rule out formerly infection or FBR. However, the biological analysis and the absence of progressive osteolysis in these two cases were clearly not in favor of infection/FBR. The possibility of spontaneous cement cracking is also unlikely as both cases were associated with major mechanical stresses due to the underlying tumors.

In conclusion, fragmentation of the PMMA plug following percutaneous cementoplasty in the bony pelvis is a rare finding at mid-term follow-up. It happened only for cementoplasty performed in malignant lesions and seems to be more of a consequence of the local mechanical stresses than the cause of further bone collapse or fracture. This

tends to further confirm that porosity, contrary to viscosity, is not a relevant working property in the in the clinical practice of cementoplasty in the bony pelvis for oncological cases.

2.4. Conclusion

Different techniques to manage the injection of several volumes of cement have been described in the literature, without consensus nor standardization. This may explain why lesions are most of the time underfilled. Hence, if optimization of cement injection for extra-spinal cases seem of interest, two major questions remain unanswered: how much does the filling rate of a lesion influence the consolidation? Is there a difference in the final cement plug between the different techniques of injection of a large volume? Trying to answer those queries is the first step towards a better comprehension of the need and ways to assist the injection of a large volume of cement.

3rd Chapter – Influence of the volume of cement on the mechanical properties of bone

The risk of pathological fracture in the pelvic bone is theoretically increasing with the volume of bone destruction and the involvement of the cortical bone. As seen in the first part, the mean filling rate of osteolytic acetabular lesions after cementoplasty equaled to 35.3% in our clinical practice. Such value seems to range away from the concept of "filling as much as possible". On the other hand, it likely represents the real life and especially the technical limitations that may be faced during cement injection. There is no data that has so far evaluate the influence of the amount of cement on bone stiffness. Hence, the need for the injection of a large volume of cement still remains questionable. Moreover, there is no filling rate threshold that can be recommended in the clinical practice. An experimental study using pelvic custom models and a finite element analysis were therefore conducted to study this specific question in different scenarios.

3.1. Experimental study

The purpose of this study was to measure experimentally the influence of the filling rate of two different sizes of tumor models on local stiffness.

3.1.1. Materials and methods

3.1.1.1. Preparation of the pelvic models

Five pelvic solid foam radiopaque custom models (Pelvis Full Male, Sawbones Europe AB) were used for the present work. The model reproduces the real anatomy, with two iliac bones fused to each other anteriorly and to the sacrum posteriorly. The outer cortical walls have radiopaque properties (fig.42).
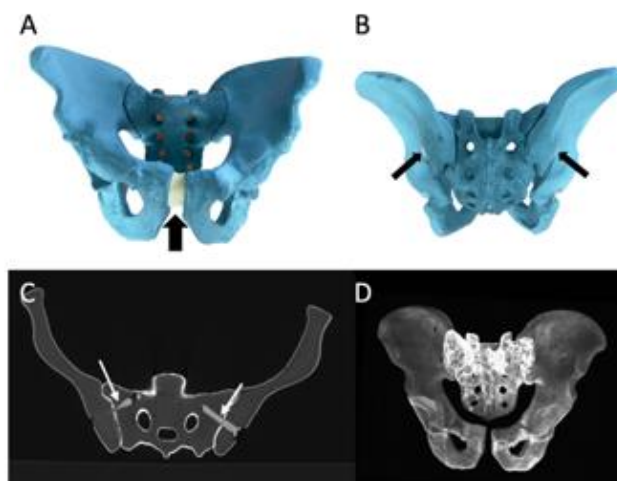
Fig.42: Foam radiopaque pelvic custom model. (A) Anterior view of the model with a mimic of the pubic symphysis (arrow) joining the two iliac bones. (B) Posterior view of the model showing the fixations (arrows) that joint the iliac bones to the sacrum. (C) Axial CT-scan view of the model. The outer shell is radiopaque. The fixations (arrows) between the iliac bones and the sacrum are also visible. (D) 3D CT-scan reconstruction of the model using MIP imaging.

One model was kept intact as a reference ("normal pelvic model"). In each of the remaining four custom models, two cavities (one on each side) were machined with a straight 5mm reamer in order to mimic a tumor at high risk of mechanical failure, i.e located in the acetabular roof with destruction of the lateral cortices ("metastatic pelvic model"). The target volume for the tumor model was 20 ml on the right side and 10 ml on the left side of each model. In this perspective, machining was made using external delineation of the cavity (fig.43).
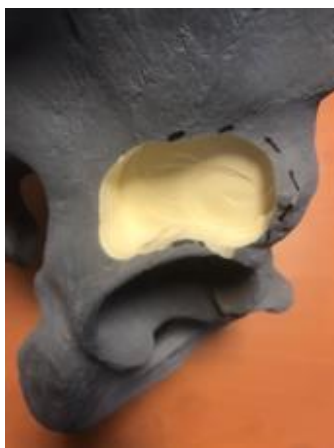
Fig.43: Tumor model creation. A cavity is machined within the foam of the model using the external delineation. In this case, the volume is supposed to approach 20 ml.

A CT-scan of the 4 metastatic pelvic models and the single normal pelvic model was acquired and reconstructed with a soft tissue algorithm and the following parameters: 0.5mm thickness – 0.3 mm intervals. The exact volume of each tumor model (2 per metastatic pelvic model / 8 in total) was calculated using manual delineation of the contour of each cavity on a dedicated post-treatment software (OsiriX—Pixmeo, Geneva, Switzerland). More specifically, delineation was performed manually every 5 mm using the closed polygon function, starting from the very cranial part of the cavity. For the intervals, delineation was calculated automatically using the generate missing ROIs function. The whole contour of the cavity was then reviewed in the axial plane and final adjustments were made should the automatic creation of ROIs do not completely fit to the cavity. Calculation of the volume was then performed using the compute volume function (fig.44).
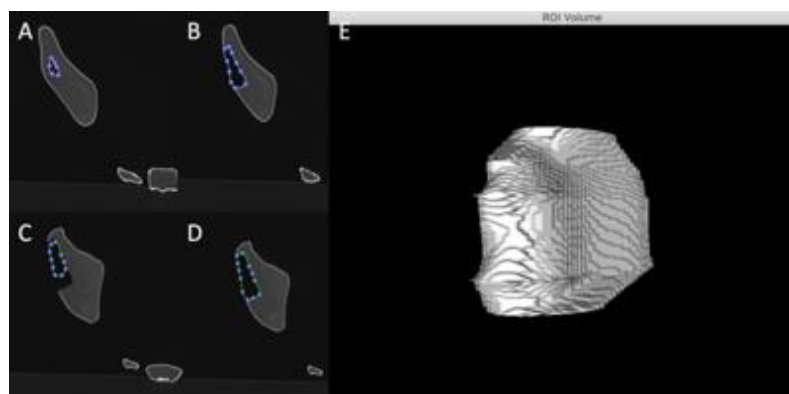
Fig.44: Calculation of the volume of the cavity on CT imaging. (A) Manual delineation of the limits of the cavity at its cranial part. (B) Same procedure 5mm below. (C) Automatic segmentation of the intervals. (D) in that case, manual adjustment of the contour. (E) calculation of the volume using all ROIs.

76

Each metastatic pelvic model was then assigned a certain rate of cement filling. One was used as a "non-cemented metastatic pelvic model" i.e that both cavities were left empty without deposition of PMMA bone cement. Both cavities of the remaining 3 metastatic pelvic models were filled with PMMA bone cement ("cemented metastatic pelvic models"). Three threshold rates of filling (one per model) were then defined: 20%, 60% and 100%. To calculate the amount of required cement for each cavity, the volume of the tumor model was multiplied by the target filling rate (table8).

Pelvic model	lesion	(a): Volume of the cavity (ml)	(b): Target filling rate (%)	(aXb): Volume of PMMA (ml)
normal	-	-	-	-
non-cemented metastatic	large	17.2	0	0
	small	8.2	0	0
cemented metastatic#1	large	18.1	20	3.6
	small	8.9	20	1.8
cemented metastatic#2	large	16.3	60	9.8
	small	9.5	60	5.7
cemented metastatic#3	large	17.6	100	17.6
	small	10.5	100	10.5

Table8: calculation of the volume of PMMA to achieve 3 different rates of filling for each size of tumor model

PMMA bone cement (Osteopal V, Heraeus Medical, Germany) was prepared using hand mixing and applicated directly within each cavity using a 20 ml syringe filled with the previously calculated volume of cement (fig.45). Each pelvic model was then kept immobile for 45 min to avoid any mobilization of the bone cement during the hardening phase and was subsequently imaged with CT-scan using the same aforementioned protocol. Fig.46 presents the CT-scans of the 4 different metastatic models.

Fig.45: Filling of the cavity with PMMA bone cement: example of a 20% filling of a large lesion (cemented metastatic#1 pelvic model). (A) Lateral and (B) anterior oblique view shows the PMMA bone cement (asterisks) partially filling the cavity.
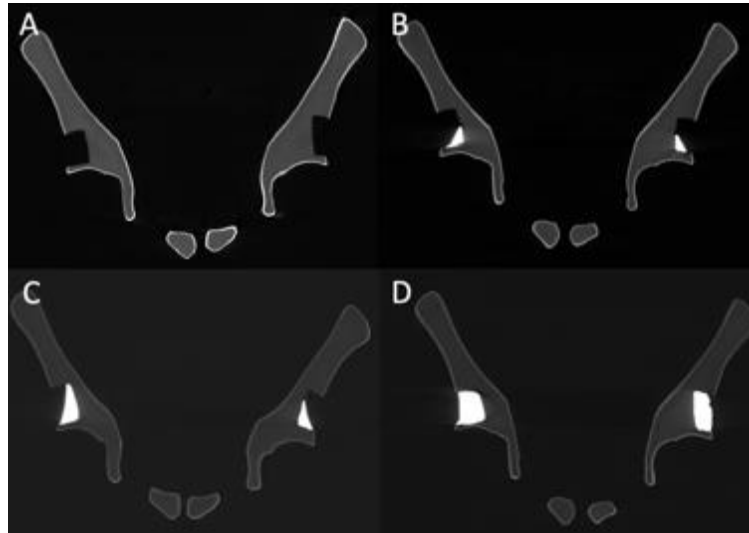
Fig.46: CT-scan of the 4 metastatic models. (A) Non-cemented metastatic. (B) Cemented metastatic#1 (20%). (C) Cemented metastatic#2 (60%). (D) Cemented metastatic#3 (100%).

3.1.1.2 Experimental measures

Each pelvic model (one normal pelvic model, one non-cemented metastatic pelvic model and three cemented metastatic pelvic models with 3 different filling rates) were tested with a simulation of a compression load on the acetabulum. The pelvic model was maintained in position at the level of the iliac crests thanks to two supports designed by additive manufacturing. The load was applied vertically on each acetabulum sequentially (right first then left) using a traction testing machine (Zwick Roell, 2005) (fig.47&48) with a 1mm/min speed. Preload was set to 1N.

Fig.47: Set-up for the compressive test. (A) Overview of the installation. (B) Magnified picture showing the normal pelvic model with both iliac crests fixed in their corresponding support. The one on the side of the test is fixed. Compression load is applied vertically on the acetabular roof.

Fig.48: Test for the large tumor model filled with 20% of cement. The lateral view demonstrates the axis of the applied load.

3.1.1.3. Data collection and analysis

For each side of each model, force and displacement were recorded continuously until loss of resistance. The stiffness of each tumor model and each filling rate was then extracted using the equation:

$$\frac{(Force2-Force1)}{(Displacement2-displacement1)}$$

Results of the metastatic pelvic models were then graphically presented for the large and the small cavities and compared to those of the normal pelvic model.

3.1.2. Results

All the results are presented in table 9. An example of the results of one compressive test is given in fig.49. Graphical representation of the results for the small and large volumes lesions is shown in fig.50&51.

pelvic model	lesion	filling rate (%)	stiffness (N/mm)
normal	-	-	-
non-cemented metastatic	large	0	59
	small	0	114
cemented metastatic#1	large	20	70
	small	20	127
cemented metastatic#2	large	60	81
	small	60	141
cemented metastatic#3	large	100	Test failure
	small	100	168

Table9: Stiffness of all pelvic models
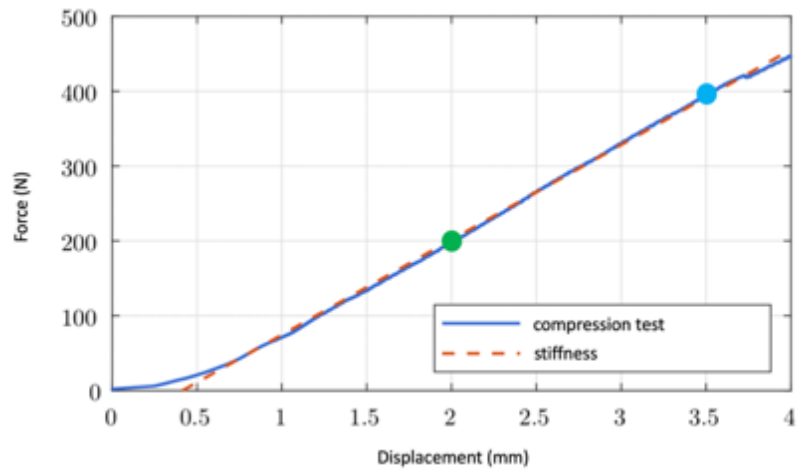
Fig.49: Compressive test for the small volume lesion of the 20% cemented pelvic model. Stiffness was calculated using the values of force and displacement at two different points (blue and green) of the curve
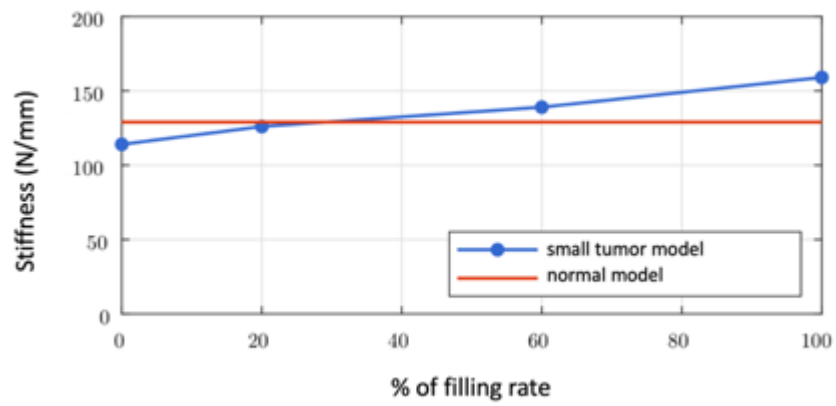
Fig.50: Representation of the stiffness for small volume lesions depending on the filling rate. ([Marche 2019])
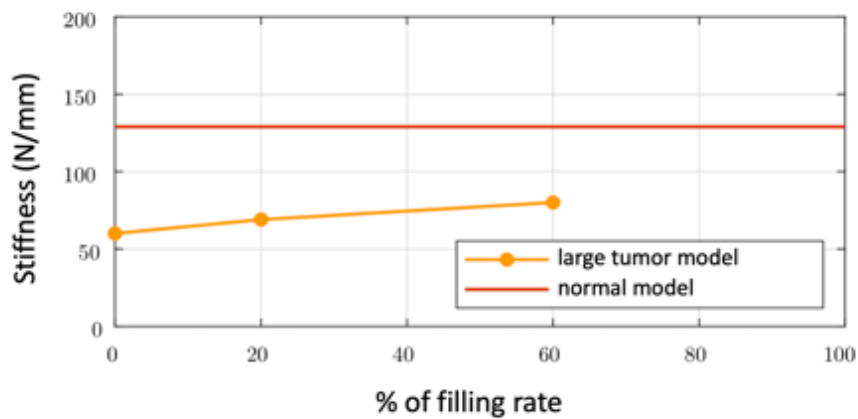
Fig.51: Representation of the stiffness for large volume lesions depending on the filling rate. No value was obtained for the 100% test. ([Marche 2019])

3.1.3. Discussion

The present experiment tends to confirm that the filling rate of an acetabular lesion may impact the biomechanical results. For the small tumor model, the injection of PMMA bone cement restored the stiffness to the value of a non-tumorous model for a filling rate of 35% on the extrapolations from the original data. Based on the evaluation of the clinical experience, such value is achievable and does not require a large volume of cement. For the large tumor model, the injection of PMMA did restore part of the stiffness but not to the level of a normal model even for a filling of 60%. Unfortunately, the experiment during the 100% filling rate compressive test failed, thereby limiting the conclusion for higher rates of filling. The restoration of stiffness seems nevertheless quasi linear for both volumes of tumor models: if normalization of the stiffness would have therefore been unlikely to occur even for a 100% filling rate, the data suggest that a 20 ml tumor should indeed be filled as much as possible. Such volume of lesion is a frequent condition in case of a metastasis in the periacetabular area. Hence, the injection of a large volume of cement should be considered as clinically relevant as it may impact the mechanical result.

The present observation suffers from numerous limitations that limit its significance. The properties (Young modulus, Poisson coefficient) of a foam model differ from the ones of a human bone that includes two components (cortical and cancellous bone). The repartition of the cement plug in the three cemented metastatic pelvic models was homogenously packed within the cavity, contrary to the clinical experience in which cement diffusion is highly unpredictable and variable amongst patients and lesions. Furthermore, the volumes of the small and the large cavities were not completely equal from one model to another. Finally, the compressive test did not reflect the physiology. The compressive loads were applied on the acetabular roof directly and vertically whilst the physiological compressive loads exhibit a slightly more oblique sagittal and frontal axis. Moreover, the fixation at the level of the iliac crest is not realistic as it appears to happen at the level of the sacral promontory in the clinical biomechanics.

In conclusion, this study suggests that restoration of local stiffness in case of bone destruction is influenced by the rate of cement filling especially for large volume lesions. The injection of a large volume of cement may therefore be a need during extra-spinal cementoplasty in the acetabular area.

3.2. Finite element analysis

The principle of finite element analysis (FEA) is to simulate a physical phenomenon using numerical mathematic techniques by discretizing into small elements. FEA has ideally to be confirmed by the confrontation to the experiment in order to confirm its validity. One of the critical features of FEA is how realistic the numerical model is. We therefore had to develop a strategy allowing to reproduce the complex anatomy of the pelvic bone before proceeding to numerical analysis of the influence of lesion filling by the bone cement.

3.2.1. Methodology for the computer assisted design (CAD) of bone structures

FEA is performed on a numerical model of a geometrical structure. For the purpose of the present simulation, the geometrical structure had to correspond to the geometry of bone. The CAD of bone structures was prepared using the following methodology, which corresponded to the best compromise between image quality and ease of use:

1) CT-scan of the bone structure was acquired in soft tissue filtering with a 0.5 mm thickness X 0.3 mm overlap reconstruction algorithm.

2) DICOM (digital imaging and communication in medicine) images from the CT-scan were uploaded in the ITKsnap software to generate a stereolithographic (STL) file representing the 3D segmentation of the bone structure (fig.52).
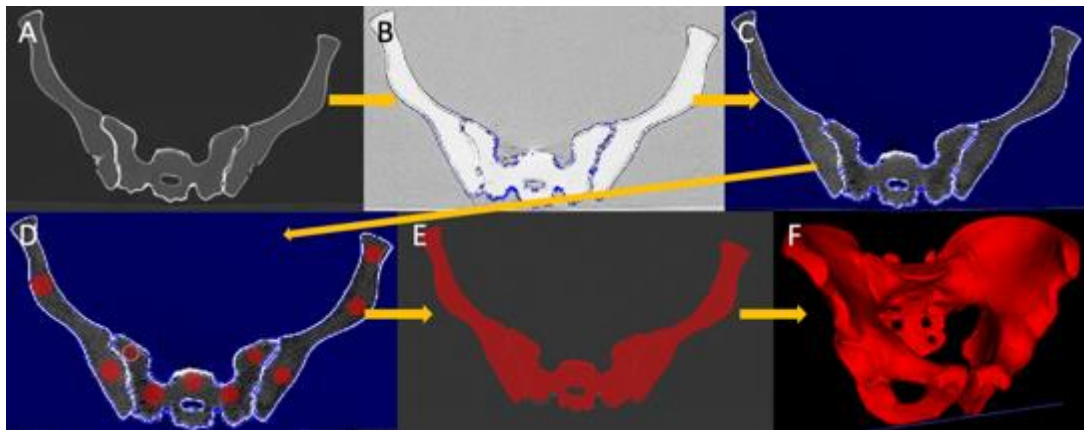
Fig.52: Methodology for the creation of the STL file in ITKsnap. ([Harrer 2020]) (A) DICOM images are uploaded. (B) The bone structure within the CT-images is extracted using the segmentation tool (C) while modulating the upper and lower thresholds of grayscale to remove all surrounding non-osseous structures. (D) Delimitation of the geometry of bone using regions of interest positioned at various locations (E) allowing to encompass the whole volume with automatic growth (F) and finally leading to the extraction of the 3D geometry of the bony structure.

3) the external surface of the generated STL file is composed by multiple meshes that need to be smoothed before proceeding to solidification of the geometry. This was done with Geomagic Studio using the mesh doctor, remove spikes, reduce noise and defeature functions. Final aspect of the 3D geometry is represented in fig.53
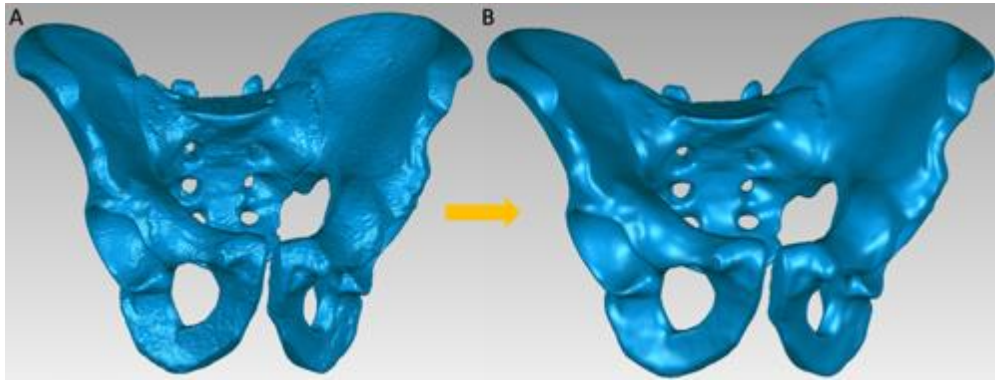
Fig.53: 3D geometry of the pelvic bone (A) before and (B) after smoothing of the meshwork ([Harrer 2020]).

4) the reconstruction of the surface and the solidification of the geometry of the bone from the meshwork of the STL file can be performed with two different softwares (fig.54). With Geomagic the autosurface function allows to approximate the external surface of an organic structure (such as bone) using NURBS (non-uniform rational basis splines) surfaces. With Creo, NURBS surfaces and polygones are used and the whole process is performed using the reconstruction from facets, solidify and decimate functions.

Fig.54: Creation of a solid version of the bone structure from the meshwork of the STL file using two different softwares ([Harrer 2020]).

5) the solid geometry is performed for the FEA. Simulations on geometries that have been solidified with Geomagic are performed on Altair Inspire. Simulations on geometries that have been solidified with Creo are performed on the Simulate module of Creo.

3.2.2. Parameters of bone and bone cement for FEA

Bone has cortical and trabecular components that have anisotropic and non-linear properties. Moreover, the thickness of the cortical bone is variable. Although it would be ideal to consider these complex properties for simulation, a simplified characterization of the parameters of bone and bone cement was used in the present model. These parameters of normal and osteoporotic bones were extracted from the literature and are detailed in table 10

and 11 [Turner 1999, Harper 2000, Phillips 2007, Zaharie 2019]. The properties of cartilage, ligaments and muscles were not considered for the present simulations.

	Young modulus	Poison's ratio	Simplified properties
Trabecular bone	150 MPa	0.2	Homogenous & isotropic
Cortical bone	17.7 GPa	0.3	Homogenous & isotropic Constant thickness
PMMA bone cement	2 GPa	0.4	Homogenous & isotropic

Table10: parameters of trabecular bone, cortical bone and PMMA bone cement for the simulation in a normal bone

	Young modulus	Poison's ratio	Simplified properties
Trabecular bone	80 MPa	0.2	Homogenous & isotropic
Cortical bone	16 GPa	0.3	Homogenous & isotropic Constant thickness
PMMA bone cement	2 GPa	0.4	Homogenous & isotropic

Table11: parameters of trabecular bone, cortical bone and PMMA bone cement for the simulation in an osteoporotic bone

3.2.3. Validation of the method

The method of FEA was validated by confronting the results of simulation to the available experimental data from a cadaveric cemented humerus that was performed in a prior study [Garnon 2020].

The geometry of the bone and the bone cement was extracted from DICOM images of the cemented humerus using the aforementioned method, with Geomagic to generate the final 3D geometry (fig.55).
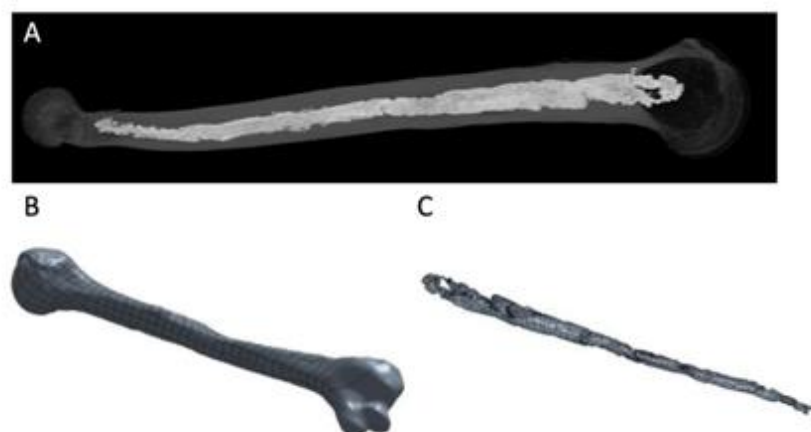
Fig.55: Extraction of the geometry of the humerus. (A) DICOM images from the cemented humerus (PMMA appears as the high central density). From these images the 3D solid geometry of (B) the humerus and (C) the PMMA bone cement is generated.

In order to separate the trabecular and the cortical bone from the solid geometry of the humerus, the scale of the solid structure was reduced from a 10% factor and assembled within the original geometry, thereby providing a smaller central humerus geometry (representing the trabecular bone) within the original geometry (representing the cortical shell). Bone cement was finally added inside the trabecular area (fig.56)
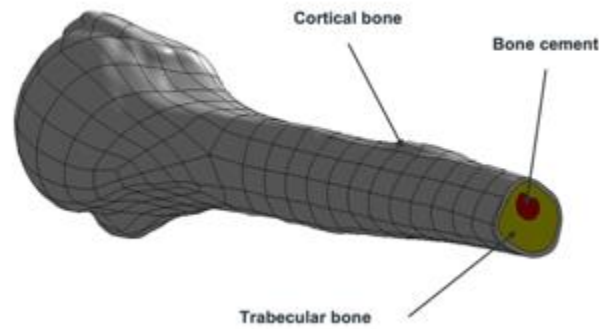
Fig.56: Final model for simulation. ([Harrer 2020])

The simulation was performed on Altair Inspire using the parameters of an osteoporotic bone as the humerus came from a donation of a 90 years old body to the institute of Anatomy. The simulation reproduced the 3 points flexural test of the experiment that was conducted on the traction testing machine (Zwick Roell, 2005) (fig.57).
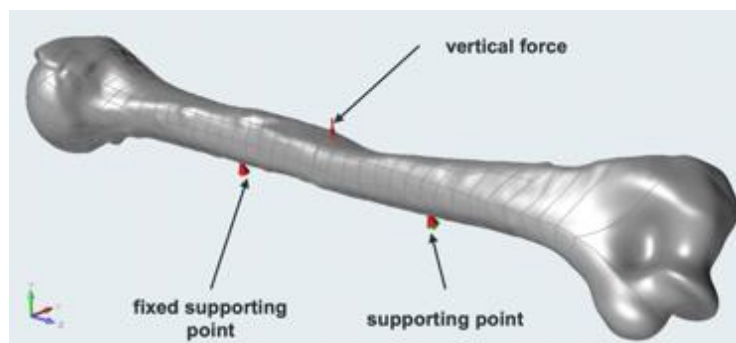
Fig.57: Numerical reproduction of the experimental 3 points flexural test. the length of the humerus was 330 mm and the gap between the integrated and the supporting points was 103 mm ([Harrer 2020]).

The simulated force was increased from 500 N to 3000 N with 500N steps. Stiffness was calculated and compared to the results of the experiment. Results are presented in fig.58
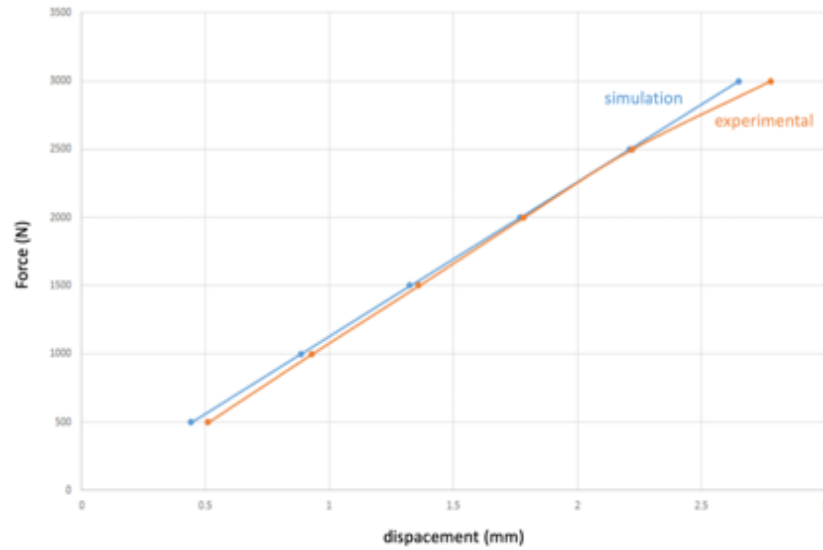
Fig.58: Results of simulation vs experiment.

The comparison of simulation and experimental data demonstrates good correlation of the stiffness with both models. The same method of FEA was therefore used for the simulation in the pelvic bone.

3.2.4. FEA of the influence of lesion filling in the pelvic bone

3.2.4.1. Creation of the numerical pelvic bone model

The geometry of the bone was extracted from CT-scan images of a foam model of the pelvic bone (Pelvis Full Male, Sawbones Europe AB) using Creo to generate the final 3D geometry. To generate the cortical and trabecular components, the shell function of the software was used to generate an external shell of 2 mm thickness representing the cortical bone. The rest of the geometry was considered as the cancellous bone (fig.59).

Fig.59: Numerical model of the pelvic bone for the FEA ([Harrer 2020]).

3.2.4.2. Protocols and results of simulation

FEA was conducted to simulate a single leg stance position. Force was applied at the center of the acetabulum with a direction mimicking the axis of the proximal femur [Ravera 2018, Volinski 2018]. Using the weighted link function, the force was then propagated to the whole surface of the acetabulum (fig.60). The Young modulus and the Poison's ratio for the simulations were those of a normal bone.
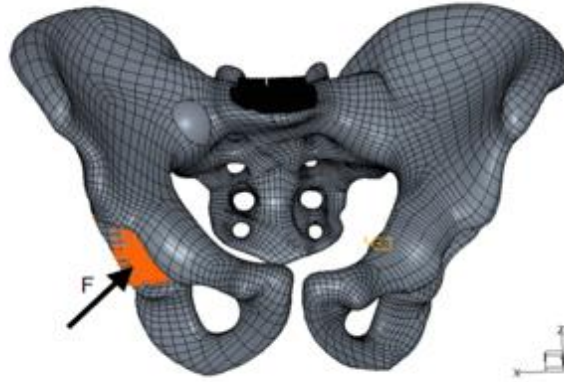
Fig.60: Simulation of the single leg stance. The Force (F) is applied at the center of the acetabulum and its transmission to the whole articular surface is mediated through a weighted link ([Harrer 2020]).

3.2.4.2.1 Simulation1

A weighted link was defined at the upper surface of the sacral promontory and considered as a fixed point (black structure in fig.60). 5 increasing forces were applied: 500N, 1000N, 1500N, 2000N and 2500N. Von Mises stresses and displacement were collected. Fig.61 presents the results of von Mises stresses with a force of 2500N.
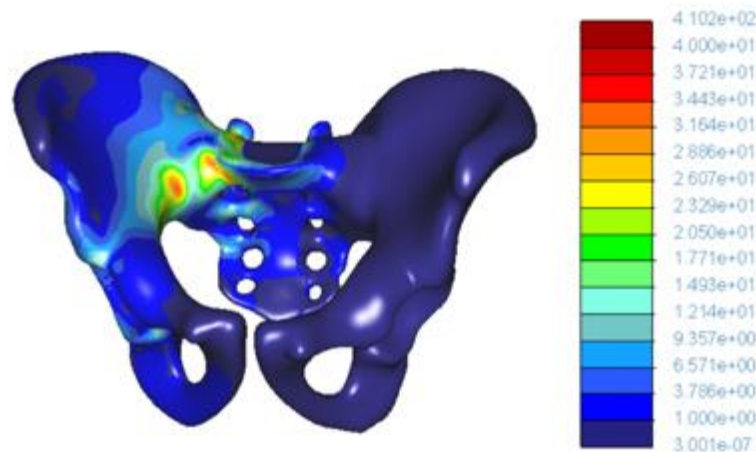
Fig.61: Von Misses stresses (MPa) of the normal pelvic bone model with a Force of 2500N (simulation1) ([Harrer 2020]).

A 20 ml empty sphere was then positioned to simulate an osteolytic tumor at the posterior part of the iliac bone at the level of the sacro-iliac junction as it was the area of maximal stresses after calculation in the normal pelvic model. Two scenarios were considered: one for which the sphere encompassed the cortical shell, thereby simulating a tumor with cortical destruction, and one without modification of the shell, which mimics a tumor without involvement of the cortical bone. For each scenario, 8 degrees of cement filling were considered: 0%, 30%, 50%, 65%, 75%, 85%, 90% and 100% (fig.62). Calculations were made with the same fixation point and applied forces (500 to 2500N) as for the pelvic bone without tumor model. Displacement were collected for each simulation and used to calculate stiffness.
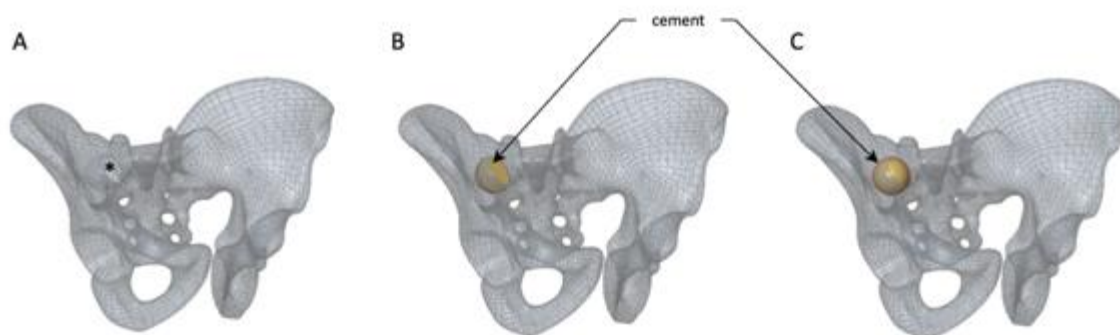
Fig.62: Tumor model. (A) A 20 ml empty sphere is created (asterisk). (B) 50% and (C) 100% filling of the sphere by bone cement. ([Harrer 2020])

The results of stiffness of the tumor model with cortical destruction and of the tumor model without cortical destruction are presented in fig.63 and fig.64 respectively and compared to the results of the model without tumor.
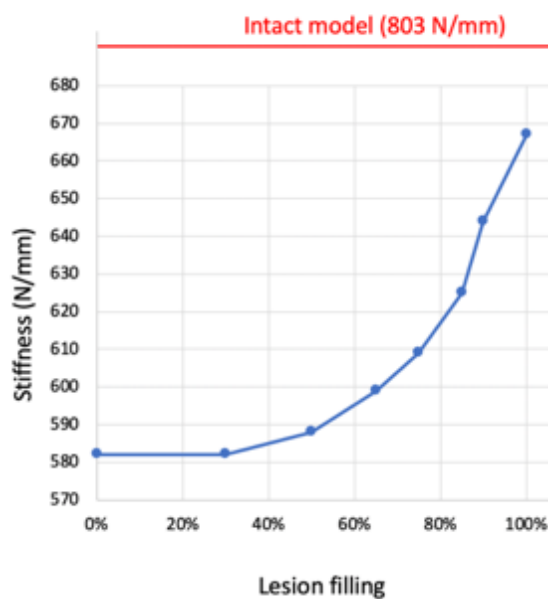
Fig.63: Stiffness as a function of lesion filling of the tumor model with cortical destruction. The red line represents the stiffness of normal bone.
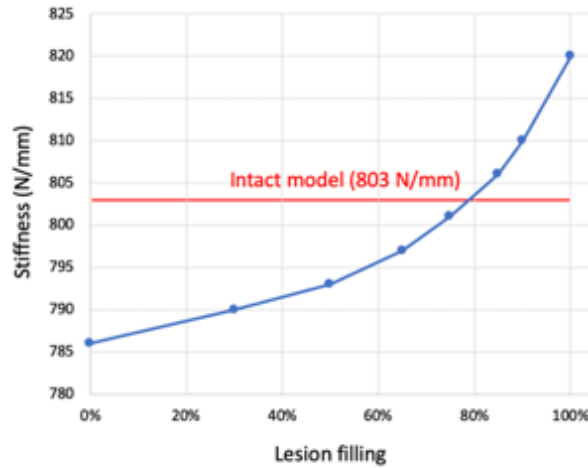
Fig.64: Stiffness as a function of lesion filling of the tumor model without cortical destruction. The red line represents the stiffness of normal bone.

There is a correlation between the rate of lesion filling and the increase of the stiffness of the tumor pelvic model with cortical destruction essentially above 50% of filling. Below the 50% filling rate, there is almost no restoration of stiffness. However, the stiffness is not restored to the level of the intact model even if complete filling is considered.

For the tumor model without cortical destruction, there is also a correlation between the filling rate and the restoration of stiffness that is already visible for the lower rates of filling. The stiffness returns to its original level with an 80% filling rate.

3.2.4.2.2. Simulation2

This simulation was performed to integrate the partial mobility of the L5-S1 intervertebral disk that connects the spine to the sacral promontory. In this perspective, a force was applied vertically at the center of the sacral promontory. The parameters of acetabular force and filling rate were simplified after review of simulation1. The application of the force on the acetabulum was similar to simulation1. For the tumor model, a 20 ml empty sphere encompassing the cortical shell was positioned at the same location as for simulation1. A model without cortical interruption was not considered for simulation2. Calculations with 6 different rates of filling: 30%, 50%, 65%, 75%, 85% and 100% were performed with an acetabular and sacral promontory force of 500N and 1000N, as it was deemed sufficient compared to a physiological stress, for a normal pelvic bone model and for the tumor model

Figure 65 show the von Misses stresses with forces of 500N and for different rates of filling. Stiffness of the normal bone was 826 N/mm whilst the one of the tumor model filled with 100% was 701.5 N/mm (table12)
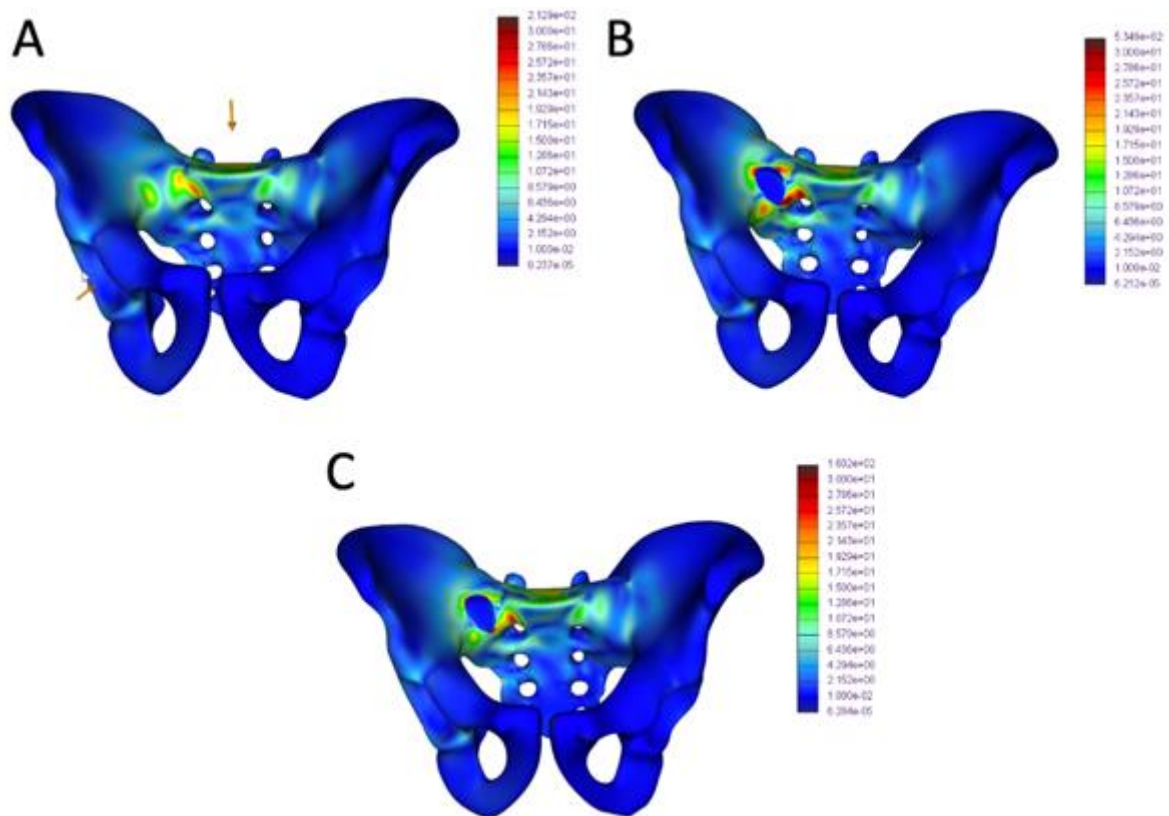
Fig.65: Von Misses stresses (MPa) with a Force of 500N (simulation2). (A) Normal pelvic bone (B) Tumor model with 30% filling rate (C) tumor model with 100% filling rate.

		Intact model	Tumor model					
			30% filling	50% filling	65% filling	75% filling	85% filling	100% filling
displacement	500N	0,605	0,798	0,789	0,778	0,766	0,749	0,713
	1000N	1,21	1,596	1,578	1,556	1,532	1,497	1,425
stiffness		626	633	642	652	667	701	826

Table12: results of displacement (mm) and stiffness (N/mm) according to force for simulation2

Maximum von Mises stress and stiffness as a function of lesion filling are presented in fig.66
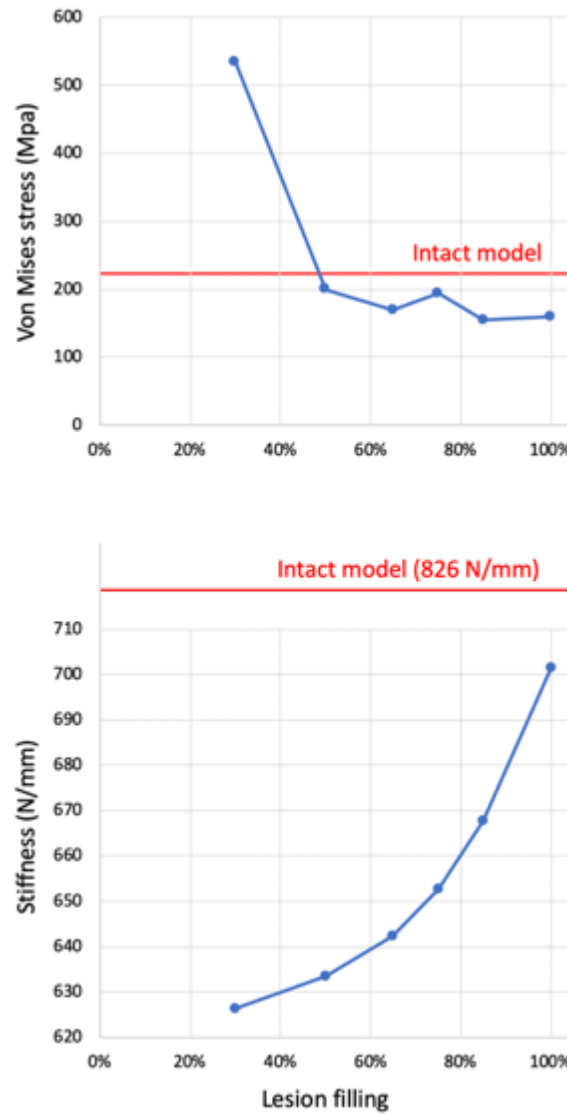
Fig.66: Evolution of stresses and stiffness depending on lesion filling.

Note that the maximum values of the von Mises stress are important. Indeed, peaks stresses are locally observed. However, von Mises stress is below 30 or 40 MPa for all the analyses performed.

Simulation2 demonstrates an exponential increase in stiffness with the augmentation of lesion filling, yet it does not reach the value of the intact model. On the other hand, the study of the peak stresses shows that a 50% filling is sufficient to restore to the baseline level.

3.2.3. Discussion

FEA tend to confirm that PMMA bone cement has the potential to restore the stiffness, partially in case of cortical destruction and completely in case of cortical preservation. It also demonstrates that the reduction of stiffness is limited when the bone cortex is intact, which makes sense as most of the loads are transferred through the cortex. Consequently, the mechanical benefit of cementoplasty seems limited in case of a lesion preserving the cortex. On the other hand, the present data confirms that the volume of bone cement may strongly influence the quality of

consolidation should the cortical bone be destroyed. For a 20 ml tumor with cortical disruption, partial restoration of stiffness occurred for filling rates greater than the threshold of 50%, with a subsequent exponential increase of stiffness with the rate of filling. Theoretically, a complete filling should therefore always be attempted to decrease the risk of local deformation. On the other hand, the study of peak stresses shows that a 50% filling is sufficient to reduce the distribution of maximal stresses to a normal level. The 50% threshold therefore seems the very minimal filling rate when treating pelvic tumors with cortical destruction, in an attempt to restore strength among the pelvic girdle. These findings are similar to the studies focusing on spine [Chevalier 2008, Luo 2009]. It also confirms the data of Li et al, which measured a normalization of the peak stresses following complete filling of a 15ml pelvic lesion with cortex destruction, both experimentally and numerically [Li 2007]. Considering the average volume of pelvic osteolysis, a volume greater 10ml may frequently be required in the clinical practice even when considering a 50% filling rate.

The results of the impact of lesion filling on stiffness are almost equivalent between the two simulations, which suggest that the influence of the mobility of the lumbo-sacral junction on pelvic displacement is limited. This should however be moderated in view of the simplified model used for the present simulations. FEA was validated on another bone and the pelvic simulations were not directly confronted to the experiment. The properties of bone and PMMA have been simplified and many anatomical structures, such as the hip joint, the cartilage, the ligaments and the muscles, have not been considered. These structures are known to reduce substantially the loads and stresses over the bone and may explain the discrepancies of values of pelvic displacement, stress and stiffness between our data and other paper from the literature, which were however not studying specifically cement injection [Ravera 2018, Volinski 2018]. The repartition of cement in our model was considered as completely homogenous, which differs from the clinical practice where PMMA bone cement distribution always present a more heterogenous pattern. However, we still believe that these results contribute to promote an optimized approach towards the injection of a large volume of bone cement.

3.3. Conclusion

The analysis of the mechanisms of interaction of PMMA with bone and the preclinical studies in the spine suggested that the volume of cement may impact the restoration of strength and the transmission of loads. The present preclinical data do support the relation between lesion filling and mechanical resistance and therefore the need for the injection of a large volume of cement in the pelvic area. In this perspective, technical considerations have to be taken in account.

4th Chapter – Comparison of the different techniques to inject a large volume of bone cement

Three different ways to achieve the injection of a large volume of bone cement with current delivery systems have been identified and described in the first chapter of this thesis. Besides the anatomical considerations, the lack of cohesion between the cement plugs has been hypothesized as a potential concern with the multiple needles approach, while the difficulties to handle cement viscosity is an issue with the single trocar approach. In order to further explore the advantages and drawbacks of each technique, numerical simulations and experiments on phantoms were performed.

4.1. Numerical simulation

The simulation of the flow of the acrylic bone cement inside a bony structure is complex as the state of PMMA changes from liquid to solid during the polymerization process. Besides external factors such as the local degree of bone loss, viscosity if the key working property of PMMA that may influence the distribution of bone cement. Different mathematical models integrating the Ostwald law for their simulations have been proposed to predict the behavior of bone cement [Krause 1982, Rusu 2009, Landgraf 2015, Lepoutre 2019]. All these models are however limited to take simultaneously in account all overlapping parameters (time, temperature and shear) that influence the viscosity of the bone cement. An alternative way to simulate the evolution of cement viscosity is to integrate a Cross rheology equation into the Castro-Macosko viscosity model [Cross 1965, Castro 1982]. This approach has the advantage to consider shear, temperature and time for the modelling of viscosity. A software using the later model was therefore used for the numerical simulation. The goal was to study the polymerization of the PMMA bone cement into different geometrical and realistic anatomical parts, with the final intent to simulate specifically the injection of a large volume of cement

4.1.1. Materials and methods

The simulation was performed with a plastic injection and compression molding simulation software (Moldflow, USA)

4.1.1.1. Theoretical considerations

Moldflow integrates different parameters that allow to reproduce as accurately as possible the complex process of polymerization

4.1.1.1.1. Kinetic parameters

The autocatalytic equation of Kamal is used to model the cure reaction kinetics of a thermoset polymer [Kamal 1973]:

$$\frac{d\alpha}{dt} = (K_1 + K_2\alpha^m)(1 - \alpha)^n$$

In this equation, the K_i coefficients follow the Arrhenius law:

$$K_i = A_i \exp\left(-\frac{E_i}{RT}\right)$$

with the α the degree of polymerization,

T the temperature (°K),

t the time (seconds),

E_i the activation energies (J/mol),

R the gas constant (8.314 J/(mol.K)) and

m,n & A_i material constants.

4.1.1.1.2. Viscosity parameters

The Castro-Macosko viscosity equation describes the variation of viscosity of a polymer during the pre-gel stage as a function of the degree of cure:

$$\eta(\alpha, T) = A \exp\left(\frac{E}{RT}\right)\left(\frac{\alpha_g}{\alpha_g - \alpha}\right)^{(C_1 + C_2\alpha)}$$

In this equation, α is given by equation of Kamal,

α_g represents the degree of polymerization at the gel point,

C_1 and C_2 correspond to constants of the material.

The Castro-Macosko model does not however consider the influence of shear on viscosity.

The Cross model expresses dynamic viscosity η depending on shear rate:

$$\eta = \frac{\eta_0}{1 + \left(\frac{\eta_0 \cdot \dot{\gamma}}{\tau^*}\right)^{1-n}}$$

with $\dot{\gamma}$ the shear rate (1/s),

τ^* the critical stress level at the transition to shear thinning (Pa),

n the power law in the high shear rate regime.

The zero-shear viscosity η_0 follows the temperature dependence Arrhenius law:

$$\eta_0(T) = B \exp\left(-\frac{T_b}{T}\right)$$

with T the temperature (K),

and B & T_b a material constant

Integration of the Cross equation into the Castro-Macosko model allows to represent the dependence of viscosity to temperature (through the Arrhenius law and the degree of polymerization), time (through the Kamal equation) and shear (through the Cross equation):

$$\eta(\alpha, T, \dot{\gamma}) = \frac{\eta_0(T)}{1 + \left(\frac{\eta_0(T)\dot{\gamma}}{\tau^*}\right)^{1-n}} \left(\frac{\alpha_g}{\alpha_g - \alpha}\right)^{(C_1 + C_2 \alpha)}$$

4.1.1.2. Configuration of the simulation

4.1.1.2.1. Parameters of the material

The parameters of PMMA bone cement had to be implemented as they are not included in the Moldflow database. Bakelite is a polyepoxide resin which is part of the database. It is very similar to PMMA in terms of properties of viscosity and was therefore used as a basis for the creation of a model of PMMA in the software. The different kinetic parameters of PMMA were retrieved from the literature and presented in table13 [Kolmeder 2011]. The viscosity parameters of PMMA required for the Castro-Macosko and Cross models are not available in the literature as most of the authors used the Ostwald law for their simulations. As the viscosity behavior of the Bakelite is quite similar to the one of PMMA, the viscosity parameters of the polyepoxide were initally not modified for the simulations but some characteristics of PMMA were ultimately included (table14).

Parameter	Value
m	2.05
n	0.95
A_1	1.792×10^{10}
A_2	3.234×10^6
E_1	7.964×10^4 (J/mol)
E_2	4.571×10^4 (J/mol)

Table13: kinetic parameters of PMMA

Parameter	Value
n	0.8294
n	0.95
B	1.23×10^{-9}
T_b	7893 (°K)
C_1	4.09
C_2	1.55×10^{-5}

Table14: viscosity parameters

4.1.1.2.2. Conditions of injection

Different conditions have to be given to proceed to the simulations:

- The location of the injection point(s), which should simulate the position of the tip of the bone trocar
- The diameter of the injection point(s), set to 2.69 mm as it corresponds to the inner diameter of the 10G bone trocar used in the clinical practice
- The temperature of the material at the beginning of injection, was set to 25°
- The temperature of the surface of the geometry part, set to 37° to simulate the thermal condition of a patient
- The injection rate of the material, which defines the speed of injection of PMMA
- The length of the curing time, which defines the length of the simulation following the filling of the mold by the material

4.1.1.3. Simulations

The simulations were performed using three different parts of growing size and complex geometry.

4.1.1.3.1. Sphere

A sphere with a volume of 3.05 ml was used initially. Meshing of the sphere included 637993 tetrahedrons. The injection point was positioned at the entrance of the sphere and the injection rate was set to 0.037 ml/s.

4.1.1.3.2. Vertebra

The DICOM images from a CT-scan acquired after a vertebroplasty procedure in a 72 years old woman were retrieved from the PACS imaging system of our institution. The geometry of the bone cement was solidified and extracted as a STL file using the ITK-snap software. The file was subsequently imported in Moldflow to create a part of the injected cemented, thereby simulating the result of an injection from the clinical practice (fig.67). The mesh of the part included 1915030 tetrahedrons for a total volume of 6.97ml. The injection point was positioned at the level of the tip of the bone trocar, which could be identified as a void area within the cement on CT-imaging. The injection rate was set to 0.075 ml/s, which is the approximate speed of injection during a real intervention.

CT-scan   computer-aided design software   flow simulation of bone cement
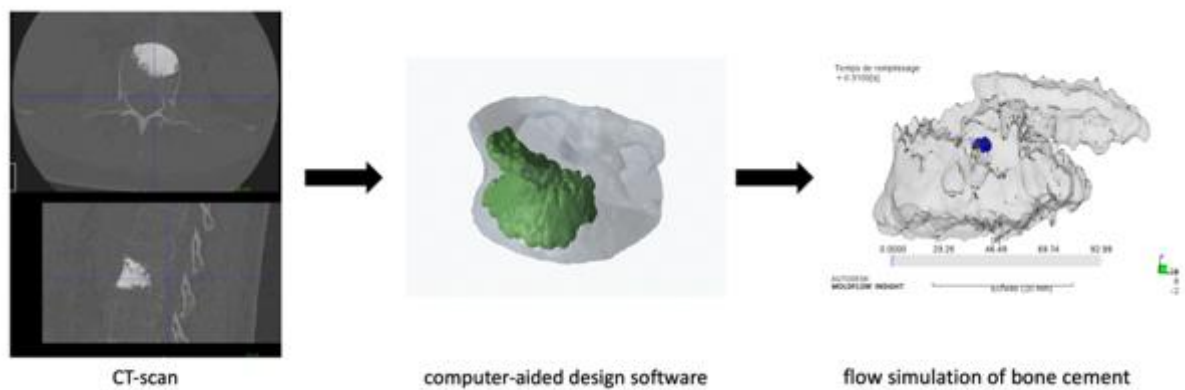
Fig.67: Protocol to create the flow simulation of the bone cement ([Anselmini 2020]).

4.1.1.3.3. Humerus

The DICOM images of the CT-scans of two cadaveric humerus filled with PMMA bone cement during a previous study were retrieved [Garnon 2020]. Both humerus had been filled with a large volume of cement using the sequential technique (several trocars used sequentially, see 6.1) by the time of the experiment (fig.68). The CAD models of both cementoplasty areas were created as previously aforementioned. Two different scenarios were then created to simulate the single trocar technique in humerus1 and the simultaneous – several trocars technique in humerus2.
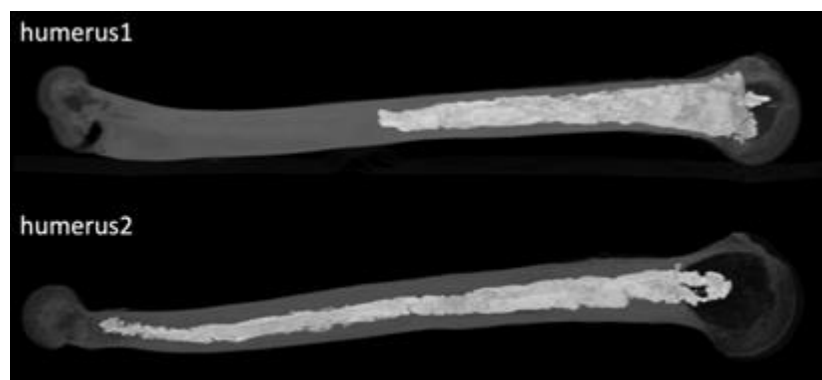
Fig.68: CT-scans of the two humerus filled with cement

Meshing of the bone cement of humerus1 included 1106245 tetrahedrons. A single injection point was defined inside the cement, corresponding to the tip of the first trocar. To mimic the single trocar – several volumes technique for the injection of a large volume of cement, the simulation included the injection of two 10 ml volumes of bone cement at a rate of 0.075 ml/s, with a one-minute interval between the two injections in order to reproduce the pause that is required to exchange the delivery systems with this technique (fig.69).
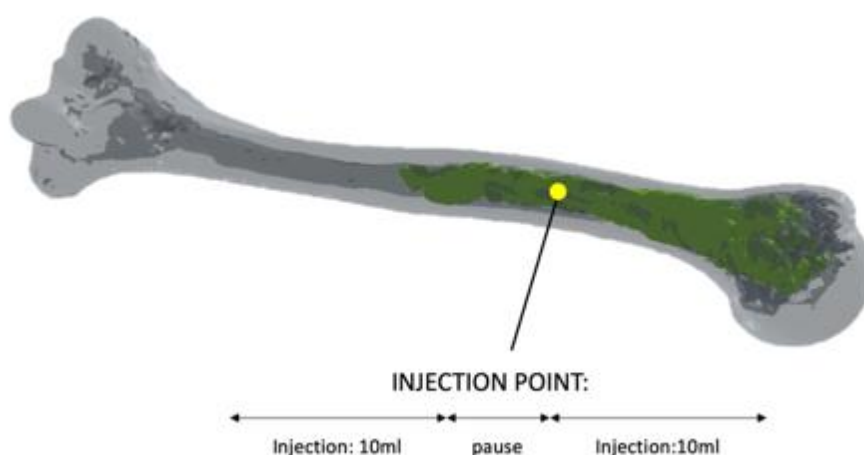
Fig.69: simulation of injection in humerus1: single trocar technique. The green geometry represents the mold of the bone cement, the gray geometry corresponds to the humerus. ([Anselmini 2020])

Meshing of the bone cement of humerus2 included 1542646 tetrahedrons. Two injection points were defined, one at each extremity of the bone cement. To mimic the simultaneous – several trocars technique for the injection of a large volume of cement, the simultaneous injection of 10 ml of bone cement was simulated at each injection point with a rate of 0.075 ml/s (fig.70&71).
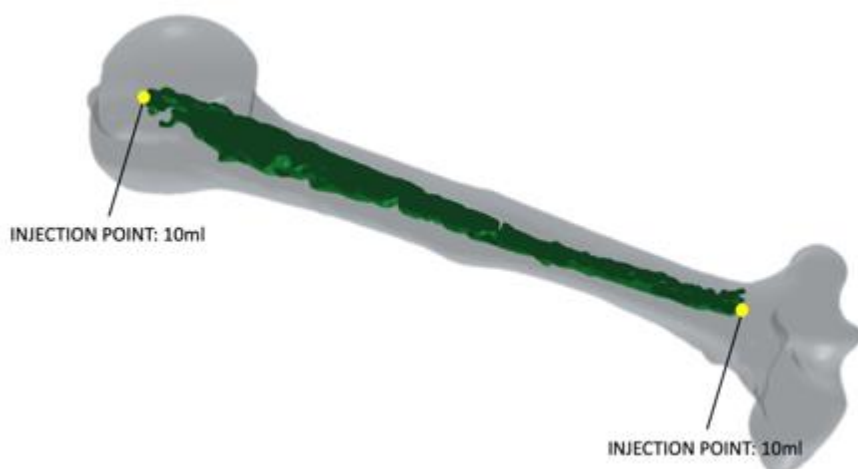
Fig.70: simulation of injection in humerus2: simultaneous – several trocars technique. The green geometry represents the mold of the bone cement, the gray geometry corresponds to the humerus. ([Anselmini 2020])

Fig.71: progressive filling of the mold by cement (in blue) from both injection points (humerus2).

([Anselmini 2020])

4.1.1.4. Data collection and analysis

For each model of simulation, four parameters of the material were recorded: temperature (°C), shear rate (1/s), viscosity (Pa.s) and conversion at node that reflects the polymerization of the material through its actual cure. Results are presented for the sphere (at t=18s, 80s and 240s), the vertebra (at t=33s,93s and 334s) and humerus1 (at t=55s, 132s, 286s and 587s). Results of viscosity and conversion at node are focused at the front between the two bone cement volumes for humerus2 (at t=220s, 225s, 301s and 383s)

4.1.2. Results

4.1.2.1. Sphere

The increase of cement viscosity goes from the periphery to the center due to the higher temperature of the boundaries.. Shear rate is neglectable throughout the entire injection (fig.72).
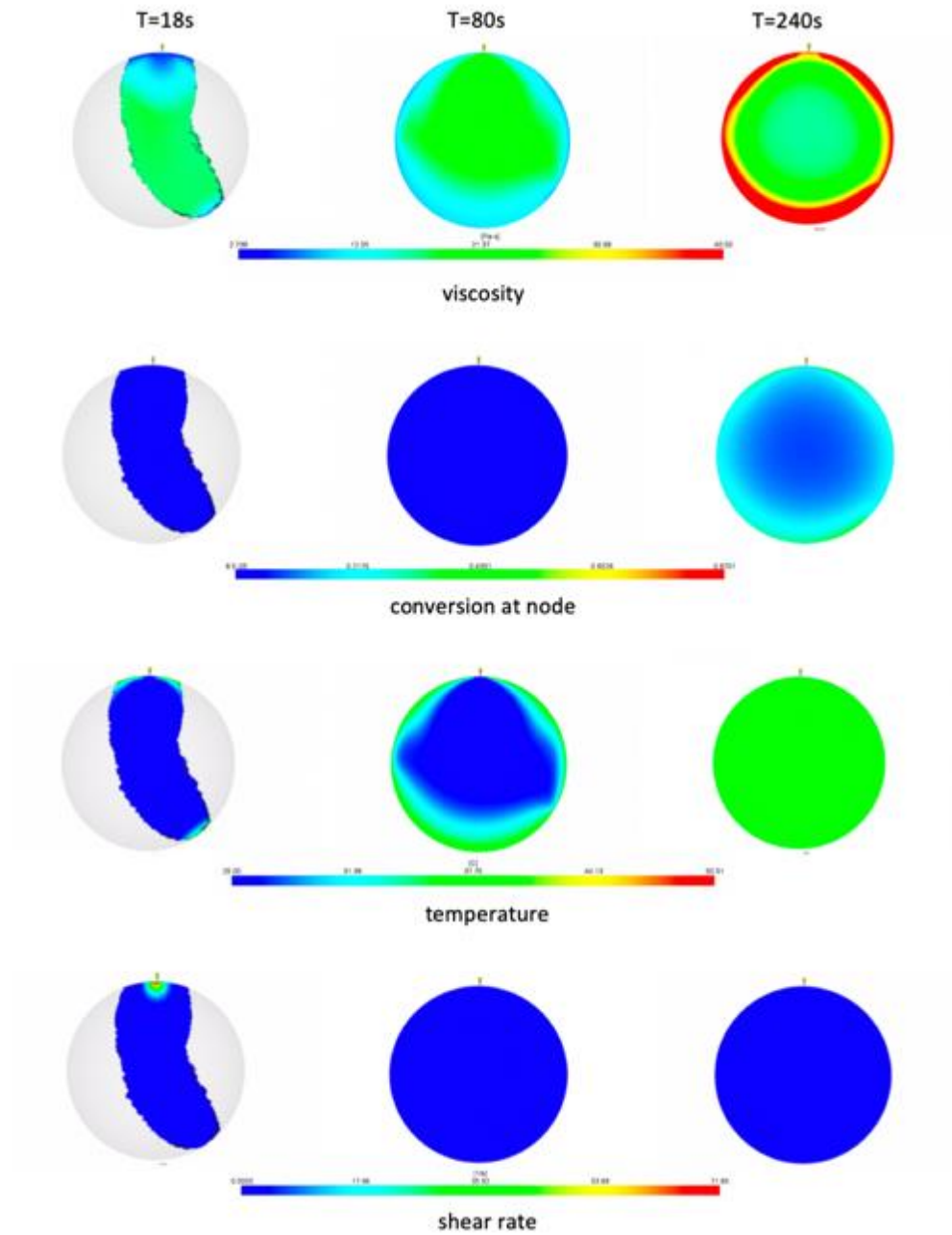
Fig.72: Results of the simulation for a sphere. ([Anselmini 2020])

4.1.2.2. Vertebra

Same findings as in the sphere regarding progression of cement viscosity and shear rate are noticed in the vertebral model (fig.73).

T=33s T=93s T=334s

viscosity

conversion at node

temperature

shear rate
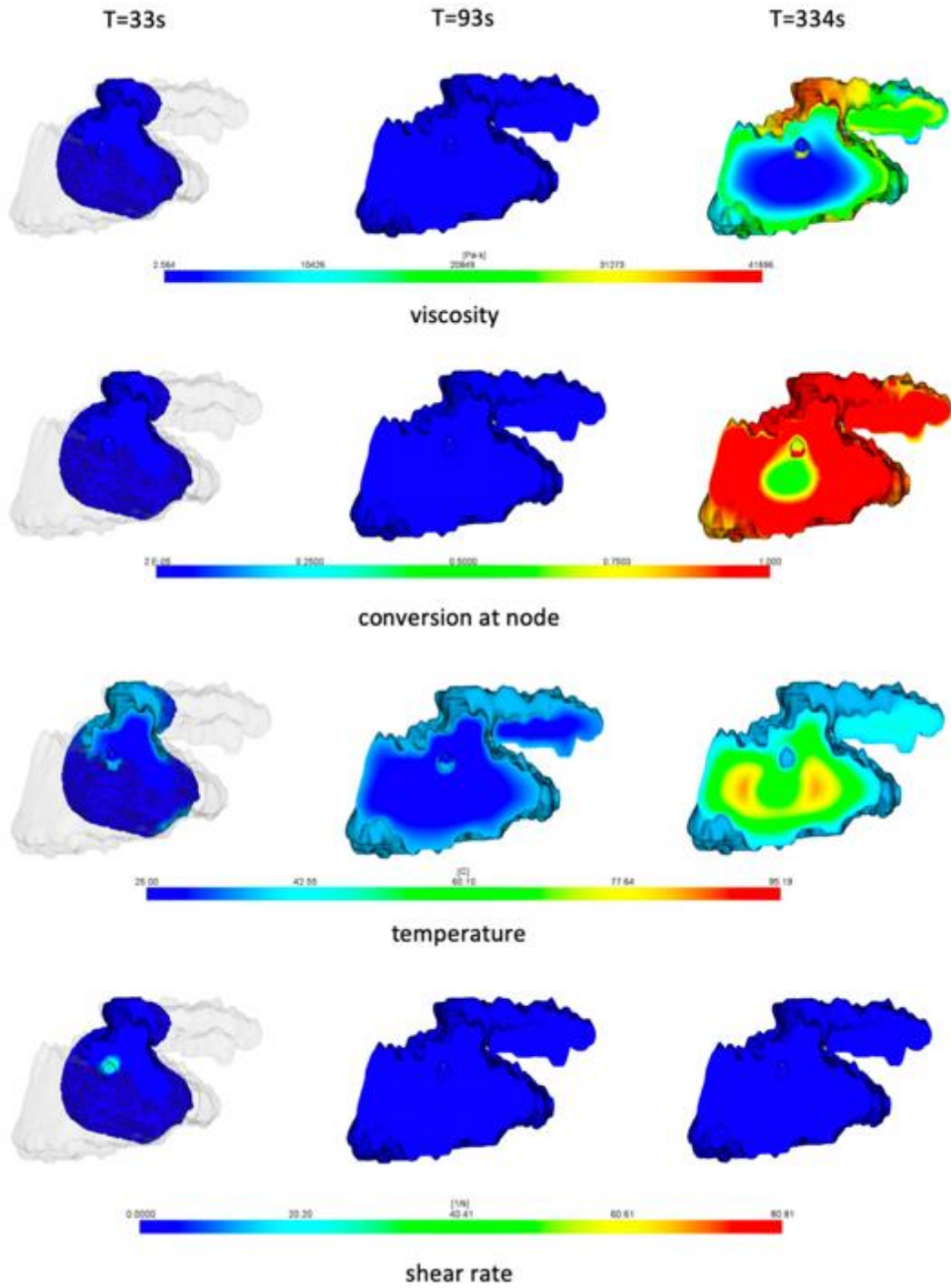
Fig.73: Results of the simulation for the vertebral mold. ([Anselmini 2020])

4.1.2.3. Humerus

In humerus1, the evolution of viscosity is different than in the simple low volume model. Before completion of the whole injection, there is an increase of viscosity and conversion at node around the injection point (fig.74).
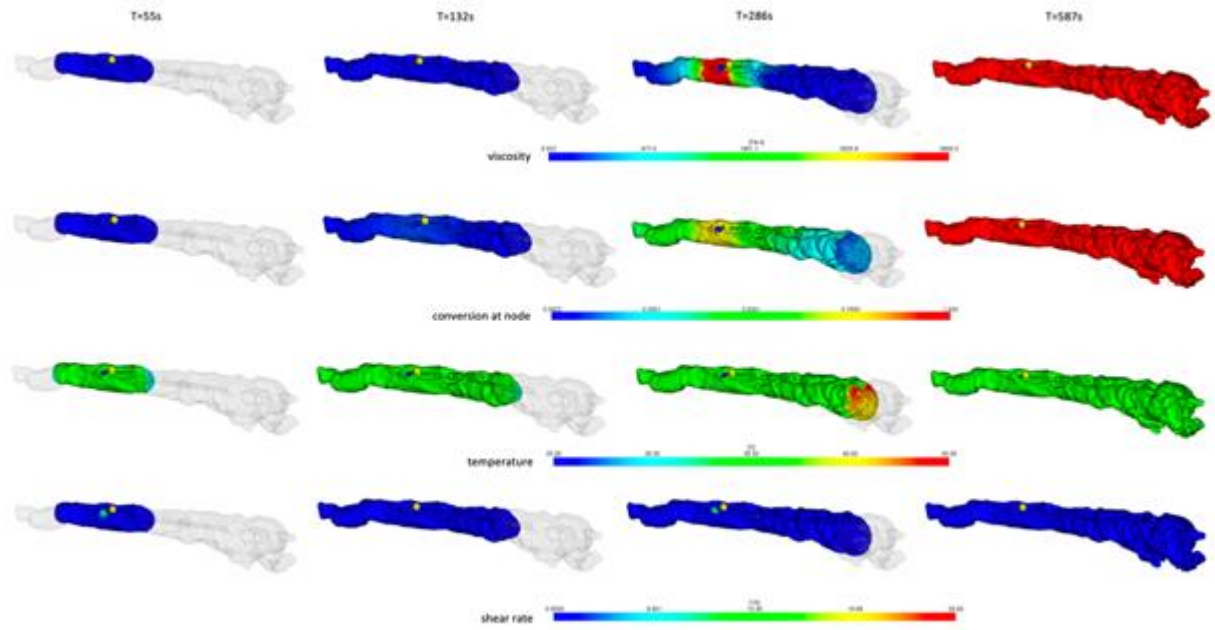
Fig.74: Results of the simulation for humerus1. ([Anselmini 2020])

In humerus2, there is a time difference in viscosity augmentation at the interface of the two volumes of bone cement (fig.75)
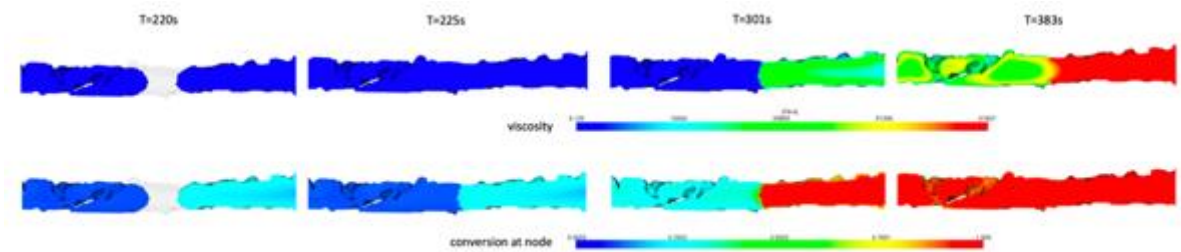
Fig.75: Results of the simulation focusing on the front of the two volumes of cement for humerus2.
([Anselmini 2020])

4.1.3. Discussion

The simulations of injection within the sphere and the spinal cement mold were performed to assess the feasibility and the quality of the prediction. These models demonstrate that the conversion at node, i.e polymerization, increases from the periphery to the center during injection and that temperature increases significantly during curing. These findings seem corresponds to the reality thereby supporting the potential information given by the simulation.

Regarding the simulations of the injection of a large volume of cement in the two humerus, the results bring some insights on the potential limitations of the two tested techniques. In humerus1, which tested the single trocar technique, there is a clear increase of viscosity and polymerization around the injection point before completion of the injection of the two volumes of cement. Although the injection was pursued in the simulation, this suggests that such reticulation of the material may translate in the clinical practice to blockage of the injection at tip of the needle by the hardened cement, ultimately leading to the impossibility to complete the injection. In clinics, it is also very much likely that the pause between the delivery of the two cement volumes may favor the polymerization of the injected bone cement around the tip or inside the trocar itself because of the decrease in shear rate. This parameter is hardly explored by the simulation as shear turned out to be extremely low throughout the different calculations. Moreover, the conversion at node only began once the material was injected in the simulation, while polymerization starts immediately following cement mixing in the real practice. Hence, the increase of polymerization may be more deleterious when performing the single trocar – several volumes technique during an extraspinal cementoplasty: if cement cannot be delivered through the same cannula, another needle has to be inserted in the pathologic area. This comes in the line with our practical experience presented in the first part. In humerus2 where the simultaneous – several trocars technique was simulated, the results demonstrate that there was a different timeline for the polymerization of the two volumes of cement, which may explain the absence of mixing at the front of the two materials. Although direct translation to the clinical practice cannot be made, the simulation suggests that the simultaneous – several trocars technique may not lead to a single cohesive bone cement plug but more to different appended volumes of PMMA which polymerized asynchronously. We have presented in [Garnon 2020] that the mechanical resistance of the injected humerus on either side was altered by the presence of weld surfaces.

The present simulation has numerous limitations that may lead to significant differences with real injections. The simulation was not compared to a similar experimental model or to other simulation models (such as the Ostwald law). The parameters of the material were not completely those of PMMA, as part of them were from a polyepoxyde. The injection was simulated in a closed geometry with a continuous and stable rate of injection, which differs from the clinical practice where the injection is frequently paused to perform imaging or avoid cement leakage because of the absence of delimited boundaries. Hence, the duration of injection and the shear rate certainly vary much more in clinics.

Despite several limitations, the numerical simulation confirms that the single trocar – several volumes technique present a risk of complete reticulation of the PMMA at the injection site before completion of the injection of all cement volumes, and that the simultaneous – several trocars technique may lead to non-cohesive cement plugs

4.2. Experimental comparison

To further study the potential differences amongst the techniques of injection of a large volume of cement, a comparison was made on a pre-clinical model. We hypothesized that the use of a single large volume of cement through one bone trocar was the most effective technique to create a single cohesive cement plug.

4.2.1. Material & methods

4.2.1.1. Techniques of injection

The three techniques to achieve a large volume of bone cement are described in detail in the 1st part of the present thesis. It includes the sequential technique, the simultaneous several trocars technique and the single trocar – several volumes technique. All three techniques were considered in the present evaluation. The sequential and the simultaneous several trocars techniques were not modified for the present experiment. For the single trocar technique, the clinical experience and the numerical simulation demonstrate that the sequential use of several delivery systems is associated with a risk of early cement polymerization thereby precluding the effectiveness of the technique. For the present study, we therefore used the hand-mixing of several bone cement kits in a single cup to create a large volume of bone cement that was delivered thanks to a single large containing syringe (see the experiment set- up section further below for technical description).

4.2.1.2. Development of a specific model for the experiment

4.2.1.2.1. Rationale

Several models were successively considered to perform the experiments. First, full models of the osseous pelvis (Pelvis Full Male, foam cortical shell, Sawbones Europe AB) were prepared. Unfortunately, the density of the inner foam was too high to inject PMMA bone cement in it. A second series of injections were attempted on a different foam model with inner cancellous material (Hemipelvis, Sawbones Europe AB). Although it was supposed to reproduce the consistence of the trabecular bone, the density still precluded the feasibility of a realistic injection (fig.76) Same was the case on a final series of experiments conducted on dry pelvic bones coming from the institute of Anatomy. Given the lack of realistic models, it was decided to design a pelvic model suitable for the injection of bone cement using additive fabrication.
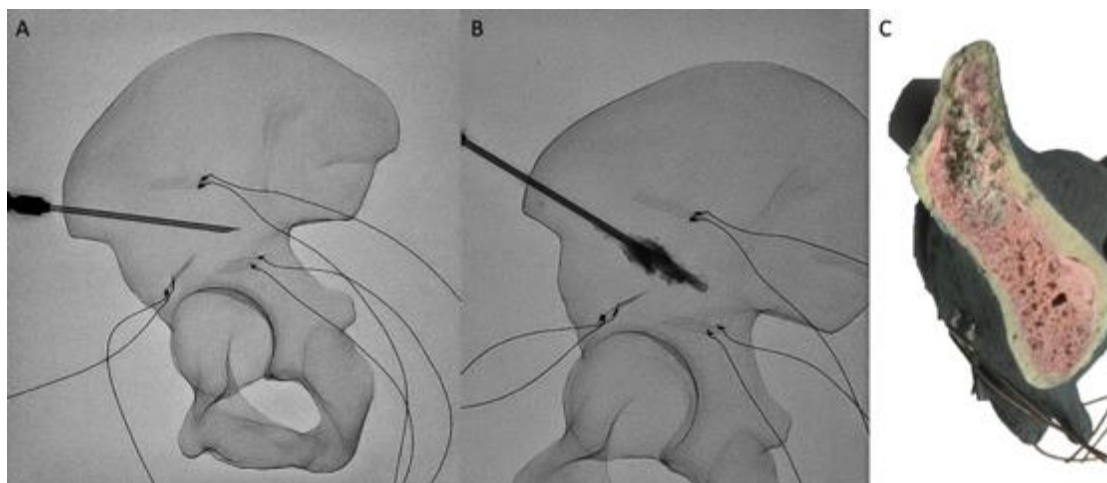
Fig.76: Failure of the experiment on a hemipelvis model. (A) The needle is in position above the acetabular roof. (B) Injection of a few drops of PMMA turned out to be extremely difficult and early polymerization occurred inside the trocar. (C) Cutting of the model shows that the inner foam is extremely dense with little space for the bone cement to spread.

The idea behind additive fabrication was to create a pelvic model with the following characteristics: visual resemblance with a real pelvic bone, possibility to inject at least 30 ml of bone cement and similarities with a real cementoplasty procedure regarding sensation during insertion of the bone trocar, resistance to cement injection and diffusion of the PMMA bone cement from the injection point. Bone is constituted by cortical and cancellous parts that have different densities, architectures and mechanical resistances. If cortical bone can be seen as a completely dense structure, the creation of a realistic trabecular bone model is more complex. Imaging of the cancellous architecture is feasible with micro-CT and may be used to create CAD models of the trabecular bone [Joffre 2017, Sabet 2018]. However, the size of these models is usually limited to a few millimeters or less [Bevill 2009, Werner 2019]. Lattices structures, also called cellular materials, are structures made of strips of a material which crosse over each other leaving holes in between [Gibson 1982]. As this kind of geometry mimics the architecture of the trabecular bone, it may be used to create synthetic bone [Barba 2019]. They were therefore used for the creation of our model.

4.2.1.2.2. Considerations of different lattice structures for the model

Among the different possible geometries, triple periodical minimal surfaces (TPMS) based skeleton type lattices have been reported to be the most advantageous for bone applications [Yan 2015, Barba 2019]. They are defined mathematically and are increasingly being used for the conception of bone implants. Three different types of TPMS lattice structures were considered in the present work: gyroid, primitive and diamond (table15).
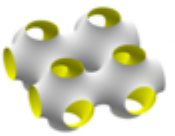
basis structural unit	author	definition	representation
giroid	Schoen Allan	$\sin(x)\cos(y)$ $+ \sin(y)\cos(z)$ $+ \sin(z)\cos(x) = 0$	
primitive	Schwarz Herrmann	$\cos(x) + \cos(y) + \cos(z) = 0$	
diamond	Schwarz Herrmann	$\sin(x)\sin(y)\sin(z)$ $+ \sin(x)\cos(y)\cos(z)$ $+ \cos(x)\sin(y)\cos(z)$ $+ \cos(x)\cos(y)\sin(z) = 0$	

Table15: Types of TPMS structures considered in the present work.

Another type of lattice structure, the regular beam-based structure, can be used to generate synthetic bone structure [Zadpoor 2019]. This model is based on the assembly of beams in different orientations (fig.77).

Fig.77: Representation of a regular beam-based lattice structure.

Each lattice structure is defined by three parameters: the size of basic structural unit, the volume of the strip of material and the material itself.

The size of the basic structural unit and the thickness of the solid fraction considered for our model are represented in table16.

scale	Size of the basic structural (mm)	Thickness (mm)
2	20	2
1.5	15	1.5
1	10	1
0.5	5	0.5
0.25	2.5	0.25
0.15	1.5	0.15

Table16: Correlation between the scale ant the dimensions of a basic structural unit.

4.2.1.2.3. Additive fabrication of the pelvic model

Numerical development

The models were computed with the three types of TPMS and the regular beam lattice structures using the lattice function of the Creo 6.0 software. Due to an excessive size of the files computed for a cubic structure of 512 ml with scales ranging from 0.15 to 0.5, the next versions were designed with scales between 0.5 and 2 and with a volume of the total structure measuring less than 100 ml.

The CAD of the osseous pelvis developed for the finite element analysis described in the previous section was used to generate the shape of the whole model. A geometric area located at the supra-acetabular area was contoured and extracted from the CAD of the pelvic bone. The idea was to machine different geometric areas with different lattices structures while keeping the remaining pelvic bone as a basis for insertion (fig.78) The advantage of this

approach was to limit the volume generated with lattice structures and the quantity of material needed for additive fabrication.
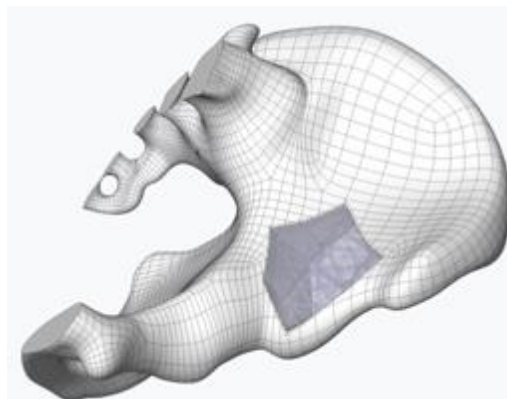
Fig.78: Principle of additive fabrication of our model: lattice structures were only used in the geometric area defined in the supra-acetabular area (blue) ([Poursillie 2020]).

Three types of pelvic bone were computed: version1 with a cavity of 36 ml, version2 with a cavity of 92 ml and version3 with a cavity extending in the acetabulum thereby allowing simulation of lesion with cortical destruction (fig.79).
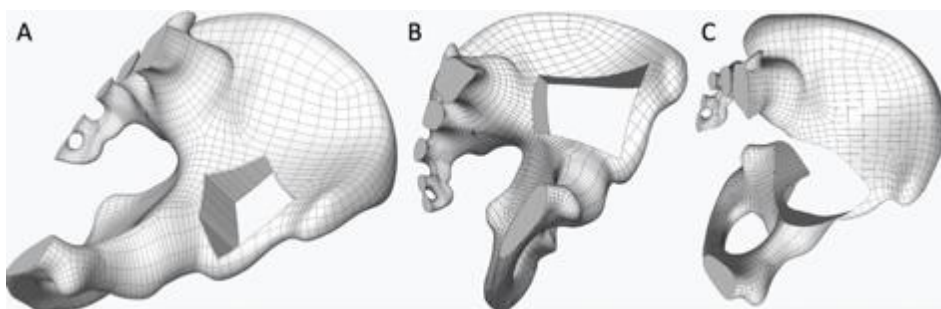
Fig.79: The three types of pelvic bone models: (A) version1 (B) version2 (C) version3 ([Poursillie 2020])

The corresponding geometrical areas were computed using a volumic method (fig.80). Each geometry was created with different lattice structures simulating the trabecular bone and with a 0.6 mm thickness shell simulating the cortical bone. For the pelvic bone version2, geometries with two different porosities (i.e two scales of lattice structures) were created to simulate the trabecular bone and a lesion. For pelvic bone version3, there was no shell developed around the lattice structure because of the geometrical complexity. Table presents all the geometrical areas that were numerically developed for the different pelvic versions.
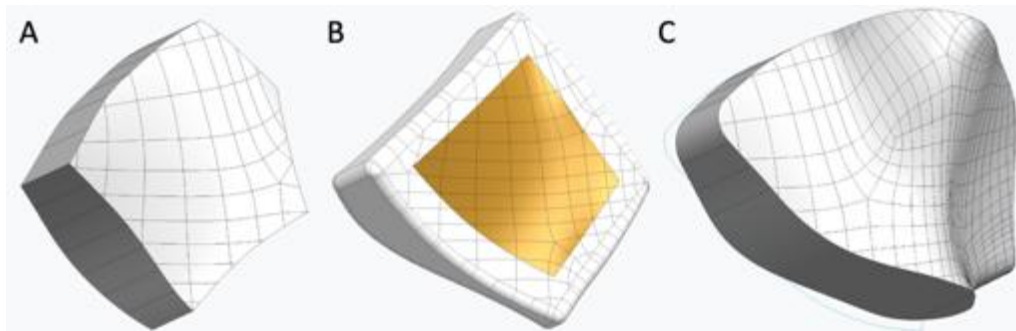
Fig.80: The three types of geometrical areas: (A) version1 (B) version2 (C) version3 ([Poursillie 2020])

3D printing

3 different printers were used: the Stratasys Connex2 350 (polyjet technology), the BCN3D Sigma R19 (fdm technology) and the Prusa I3Mk3 (fdm technology). Different polymers were used for additive fabrication: polylactic acid (PLA) and polyethylene terephthalate (PETG) for the items printed with fdm technology and VeroWhite for the items printed with polyjet technology. The fdm technology was preferentially used for large items because of its limited precision whilst polyjet was preferred in case of small size items with thin thickness. As a result, the pelvic bones and the geometrical areas for pelvic version1 and 2 were printed with fdm technology. Table17 present all the fabricated items that were evaluated experimentally. Fig.81 presents the fabricated pelvic models and fig.82 provides examples of geometrical areas for the pelvic bone.

Fig.81: Pictures of the fabricated pelvic model (A) Version1 (B) Version2 (C) Version3 ([Poursillie 2020])

pelvic bone	
item name	*printing technology*
Version1	fdm
Version2	fdm
Version3	fdm

geometrical areas for the pelvic bone				
item name	*printing technology*	**Designed for pelvic version**	*Lattice structure*	*scale*	*Reference for the evaluation*
---	---	---	---	---	---
bi_lesion_primitive	fdm	2	TPMS – primitive	2 (center) & 1 (periphery)	B
back_bi_lesion_merged_v1	fdm	1	beam – triangular	1	C
back_bi_lesion_merged_v2	fdm	2	beam – triangular	2 (center) & 1 (periphery)	D
truss_lattice_mono_lesion	fdm	1	beam – triangular	1	E
bi_lesion_v3_truss_v1_0_5	polyjet	3	beam – triangular	0.5	F
bi_lesion_v3_stochastic_lattice	polyjet	3	beam – stochastic	1.5	G
diamond_mono_lesion_scale_1_5	fdm	1	TPMS – diamond	1.5	H
giroid_mono_lesion_scale_1_5	fdm	1	TPMS – giroid	1.5	I
primitive_mono_lesion_scale_1_5	fdm	1	TPMS – primitive	1.5	J

cube			
item name	*printing technology*	*Lattice structure*	*scale*	*Reference for the evaluation*
---	---	---	---	---
primitive_open_cube_scale_1	fdm	TPMS – primitive	1	A

Table17: List of fabricated items.
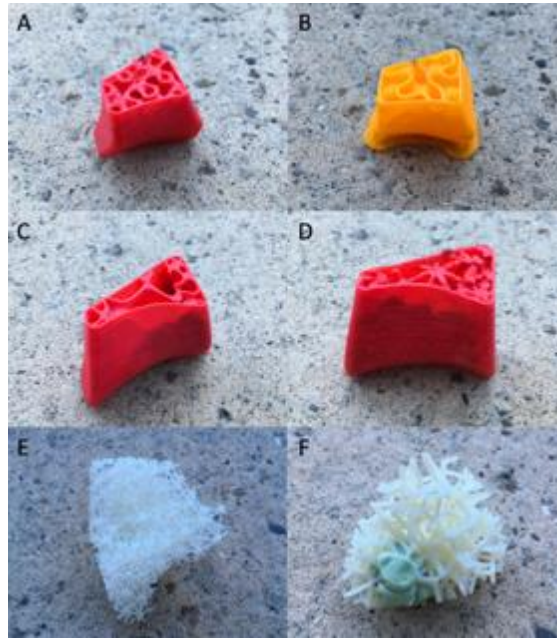
Fig.82: Different geometrical areas. (A) TMPS diamond lattice structure for pelvic bone version1 (ref H); (B) TMPS giroid lattice structure for pelvic bone version1 (ref I); (C) TPMS primitive lattice structure with 2 porosities for pelvic bone version2 (ref B); (D) triangular beam lattice structure with 2 porosities for pelvic bone version2 (ref D); (E) beam triangular lattice structure with scale 0.5 for pelvic bone version3 (ref F); (F) beam stochastic lattice structure for pelvic bone version3 (ref G) ([Poursillie 2020])

4.2.1.2.4. Evaluation of the different versions of geometrical areas

An experimental evaluation of all the fabricated cubic and geometrical items was conducted. The experiments were performed in the Cone-beam CT interventional suite of the department of interventional radiology. Following manual insertion of a 10G bone trocar (Gangi special needle, Optimed, Germany) in each of the items, PMMA bone cement (Osteopal V, Heraeus Medical, Germany) was mixed manually and deposited in the dedicated delivery system (Gangi Cemento-RE Kit, Optimed). Injection of one cement kit per item was performed by the interventional radiologist under intermittent fluoroscopic guidance. Each of the following parameters was quoted from 0 (poor) to 5 (excellent) by the radiologist compared to a real vertebroplasty procedure: visual resemblance with a bone structure, sensation during needle insertion, modification of needle positioning, modification of the position of the bevel, resistance during injection and geometry of cement repartition within the structure (fig.83). A target score was assigned to each parameter. A global score was given to each geometrical item by calculating the summation of deviation from the target scores.
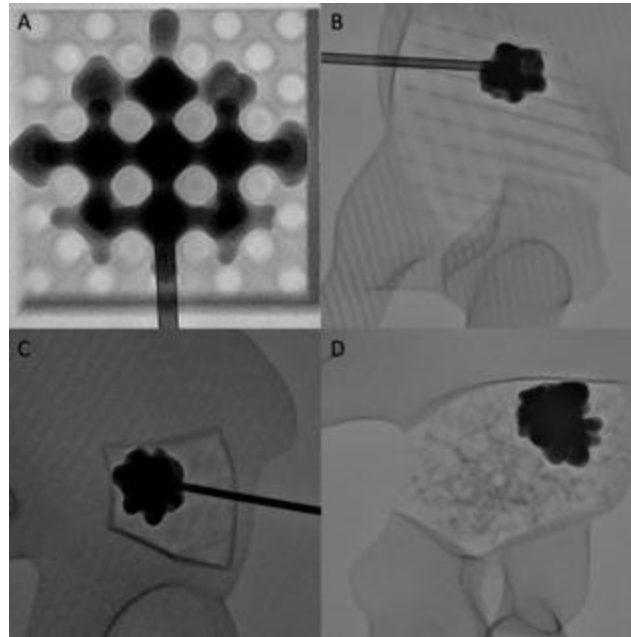
Fig.83: Different examples of cement distribution. (A) TPMS – primitive lattice structure with a scale of 1 in a cube (B) Beam – triangular lattice structure with a 0.5 scale in a geometrical area for pelvic version3 (C) Beam – triangular lattice structure with a scale of 1 in a geometrical area for pelvic version1 (D) Beam – stochastic lattice structure with a scale of 1.5 in a geometrical area for pelvic version3.

Based on the global score, the top three representative geometrical items were 1/Ref F: beam – triangular lattice structure with a scale of 0.5, 2/Ref E: beam – triangular lattice structure with a scale of 1, and 3/Ref D: beam – triangular lattice structure with a dual scale. Detailed results of each parameter and of the global score are given in table18.

Geometrical item	Visual resemblance (target score 5)	sensation during needle insertion (target score 3)	modification of needle positioning (target score 3)	modification of the position of the bevel (target score 3)	resistance during injection (target score 3)	geometry of cement repartition (target score 5)	Global score (summation of deviation from target scores)
A	2	4	4	4.5	3.5	3.5	8.5
B	3	3.5	4	5	3	3.5	7
C	3	3.5	3.5	4	2.5	4	6.5
D	3.5	2.5	3.5	3.5	3	4	4
E	3.5	2.5	3	3.5	2.5	4	3.5
F	4.5	3	3	3	3	5	0.5
G	4	4.5	3.5	4	3	4.5	4.5
H	2	5	4.5	5	4.5	2	13
I	2	4.5	4	4.5	4.5	2	11.5
J	2	4.5	4	4.5	4	3.5	9.5

Table18: detailed results of the tests

Based on the evaluation, the regular beam lattice structures offer the best option to create a realistic cement plug and were evaluated as the best to mimic the trabecular bone. Moreover, the flow of cement seems even more realistic with a smaller scale of the lattice structure which confirms the data from the literature [Barba 2019]. The stochastic repartition of the beam structures could certainly contribute to build a better model of bone but would require a deeper evaluation (only one item was tested in the present experiment). TMPS lattice structures were not judged as the most representative. One explanation may be the strong influence of the geometry of these structures in all 3 dimensions, thereby limiting the variation of cement deposition. The primitive TPMS lattice structure was however subjectively evaluated as an interesting model to simulate an osteolytic tumor. Same was the case for the structures with a dual scale as the lower scale may simulate the lower porosity related to tumor infiltration within the trabecular bone.

Based on these evaluations and after considering the limitations of additive fabrication for some items, the choice of the optimal pelvic model for the comparison of the different techniques of injection was pelvic model version2 with a dual scale beam – triangular lattice structure (ref D)

4.2.1.3. Experiments

Experiments were conducted in a Cone-beam CT interventional suite (Allura XperFD20, Philips, the Netherlands) with one pelvic model (version2) and 6 interchangeable dual scale beam – triangular lattice structure items that were printed for that study. Four access holes to the geometrical items were drilled at the anterior part of the pelvic model in order to different access channels for the insertion of the needles (fig.84)
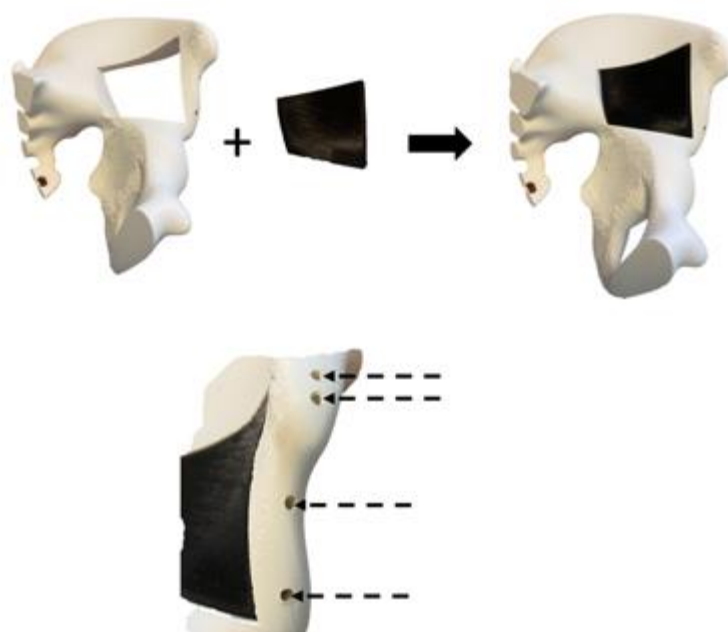
Fig.84: Models for the experiments. Pelvic version2 and the geometrical item. Four holes (dotted arrows) were drilled to create the access for the bone needles.

11G end-hole needle(s) were used for cement injection. PMMA Cement kits (Osteopal V, Heraeus Medical), similar to the ones used in clinical practice, were taken out from the fridge where they are stored at 4°C (same low temperature as for the clinical use, to increase the time of application). Hand-mixing of the PMMA was performed for 45 seconds and a waiting time of 1 minute (according to the recommendation of the manufacturer to increase cement homogeneity) was respected before depositing PMMA into the syringe of the delivery cement. For the injection of a maximum volume of 10 ml through one needle, the 10 ml syringe and injector device for vertebroplasty (Gangi Cemento-RE Kit, Optimed) were used. For injection over one needle of a volume greater than 10 ml, several kits were simultaneously mixed in a single cup and the desired volume of PMMA (20 or 30ml, see further) was poured in a 30ml syringe (30 ml, Ardes) prior to its manual injection by pushing on the piston. Intermittent fluoroscopic images were acquired (typically every 10 s) to assess the repartition of cement (fig.85).

Fig.85: Set-up for the experiment. (A) Overview of the IR suite (B) Injection device for vertebroplasty (10 ml) (C) Syringe for manual injection of up to 30 ml of bone cement.

The comparison was performed with 2 different target volumes of bone cement: 20 and 30 ml. Details about the different techniques of injection are presented in table19

Technique	nb of needles	description	delivery device
injection of 20 ml of bone cement			
sequential several trocars	2	1) Insertion of a needle 2) Injection of 10 ml 3) Insertion of 2nd needle 4) Injection of 10 ml	delivery system for vertebroplasty
simultaneous several trocars	2	1) Insertion of 2 needles 2) Simultaneous injection of 10 ml on each needle	delivery system for vertebroplasty
single trocar	1	1) Insertion of 1 needle 2) Injection of 20 ml on the needle	30 ml syringe
injection of 30 ml of bone cement			
sequential several trocars	3	1) Insertion of a needle 2) Injection of 10 ml 3) Insertion of 2nd needle 4) Injection of 10 ml 5) Insertion of 3rd needle 6) Injection of 10 ml	delivery system for vertebroplasty
simultaneous several trocars	3	1) Insertion of 3 needles 2) Simultaneous injection of 10 ml on each needle	delivery system for vertebroplasty
single trocar	1	1) Insertion of 1 needle 2) Injection of 30 ml on the needle	30 ml syringe

Table19: Technical details of the techniques of injection.

For each injection, the confidence of the radiologist in the identification of cement dispersion and the force required to perform the injection were subjectively quoted using a 3 levels scale: well adapted, poorly adapted and not adapted for the clinical practice. The height/width ratio of the final cement plug was calculated on fluoroscopic images. A CT-scan of all cemented items was performed in order to look for any void within the cement plug and subsequently quote the cement plug as completely cohesive, partially cohesive or non-cohesive (fig.86).
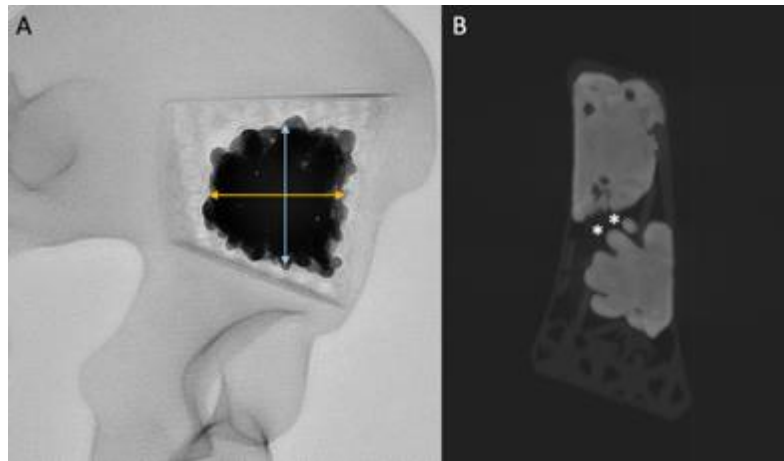
Fig.86: Radiological analysis. (A) The height (blue arrow) to width (orange arrow) ratio is determined on fluoroscopic images. (B) CT-scan of the cemented item. In that was there is an area of non-cohesion (asterisks) inside the final cement plug.

Each item was weighted and then tested with a traction testing machine (Zwick Roell, 2005) with a 1mm/s compression (fig.87). Preload was set to 5N. Measures were performed with a 5000N sensor. Compression tests were terminated at the threshold level of 4700N. Stiffness was calculated for each item

Fig.87: Compression test. A 3D printed item (asterisk) was fabricated to enable compressive of the pelvic geometrical item with the traction machine.

4.2.2. Results

All injections were technically successful (fig.88). Results about the subjective evaluation during injection and radiological results are provided in table20.
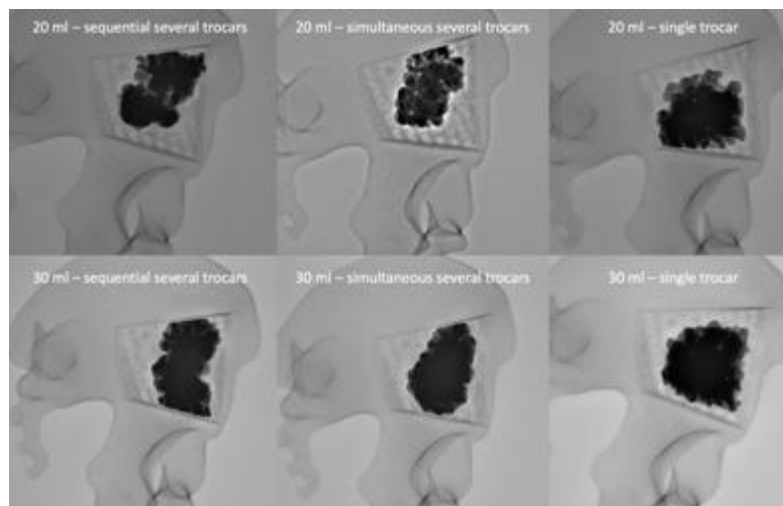
Fig.88: fluoroscopic aspect of the bone cement following the different injections

technique	confidence of the radiologist in the identification of cement dispersion	force required to perform the injection	height/width ratio	CT aspect of the cement plugs
injection of 20 ml of bone cement				
sequential several trocars	well adapted for clinical practice	well adapted for clinical practice	1.2	partially cohesive
simultaneous several trocars	Poorly adapted for clinical practice	well adapted for clinical practice	1	Completely cohesive
single trocar	well adapted for clinical practice	Poorly adapted for clinical practice	0.9	Completely cohesive
injection of 30 ml of bone cement				
sequential several trocars	well adapted for clinical practice	well adapted for clinical practice	1.5	Completely cohesive
simultaneous several trocars	Not adapted for clinical practice	well adapted for clinical practice	1.3	Completely cohesive
single trocar	well adapted for clinical practice	Not adapted for clinical practice	0.9	Completely cohesive

Table20: Fluoroscopic aspect of the bone cement following the different injections.

The sequential several trocars and the single trocar techniques offered good confidence for the evaluation of cement repartition in both situations (20 and 30ml), whilst this was a limitation of the simultaneous several trocars technique. There was no issue to inject 10ml of bone cement using the dedicated delivery device. The manual injection of a large volume of cement with the single trocar technique required forceful injection by the radiologist,

which did not appear to be adapted to the clinical practice. The height/width ratio was quite similar after the injection of 20ml; for a 30ml volume, the single trocar technique offered the most homogenous shape of cement plug. The final cement plug was completely cohesive except for the sequential several trocars technique to inject 20 ml. Fig.89, 90 and 91 present three examples of injection.
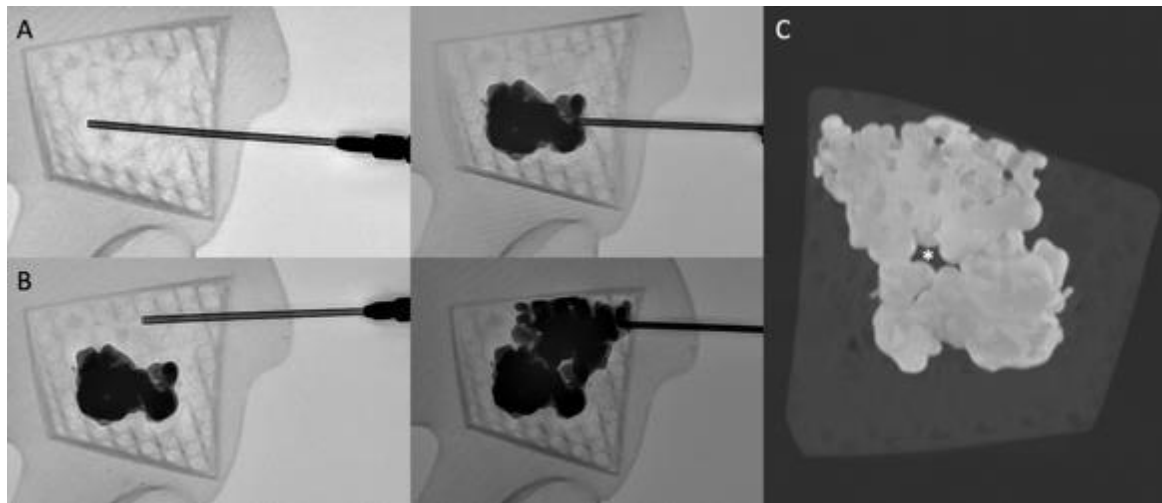
Fig.89: Sequential several trocars technique for the injection of 20ml. (A) A first neelde is inserted and 10ml of PMMA bone cement is injected. (B) A second needle is inserted above the first plug of cement and 10ml are additionally injected (C) CT-scan of the item demonstrating the final cement plug with an area of non-cohesion (asterisk).
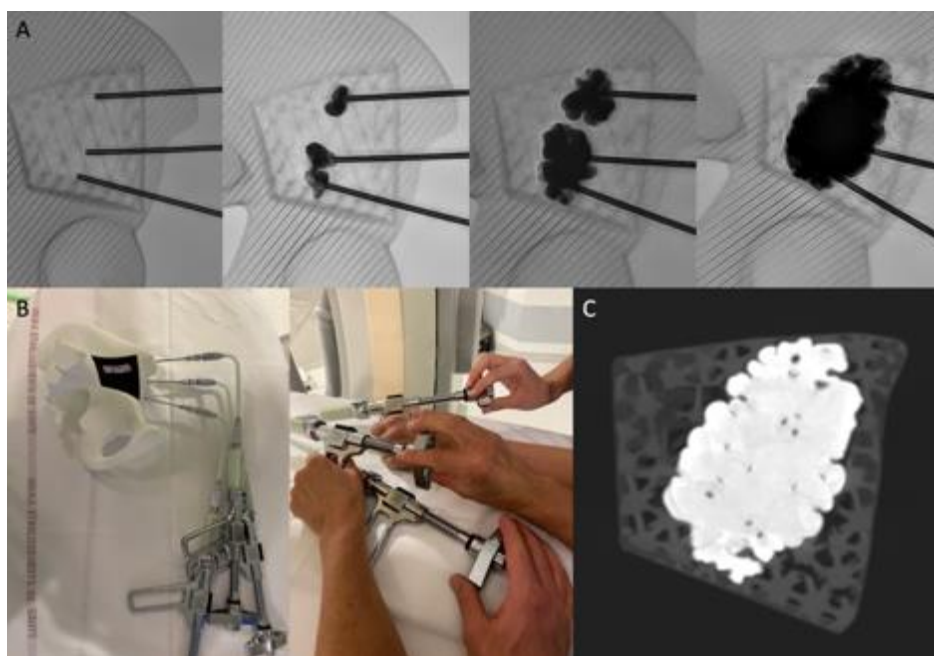
Fig.90: Simultaneous several trocars technique for the injection of 30ml. (A) 3 needles are inserted and 10ml of PMMA is injected on each needle simultaneously leading to a final cement plug. (B) Overview of the set-up for the technique. Three physicians are needed for the injection. (C) CT-scan showing a final cohesive cement plug
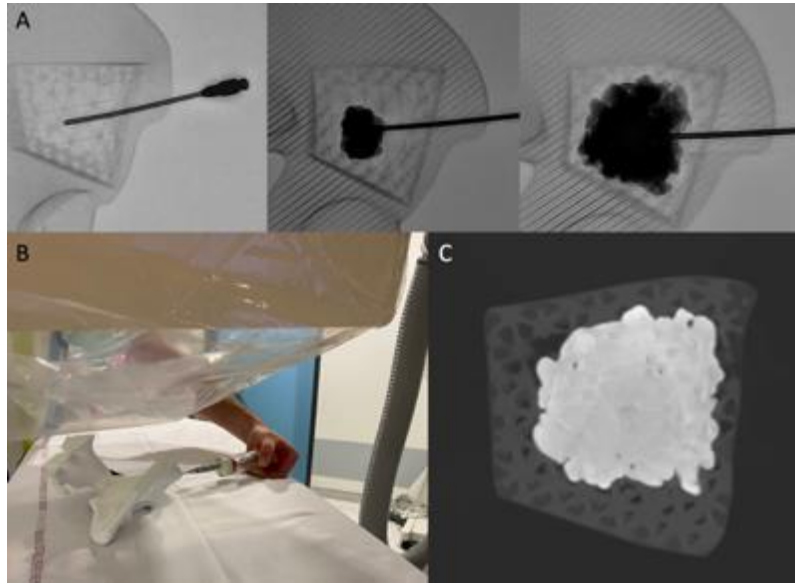
Fig.91: Single trocar technique for the injection of 30ml. (A) The 30ml volume is injected on a single needle. (B) Overview of the manual injection using a 30ml syringe. (C) CT-scan showing a cohesive cement plug

4.2.3. Discussion

The present experiment confirms that the 3 different techniques to achieve the injection of a large volume of bone cement are feasible. If the interpretation of the results should be balanced by the limited number of experiments, some trends may be highlighted. Although the several simultaneous trocars technique seems to offer interesting radiological results, it is probably the least transposable technique to the clinical practice. Monitoring of cement diffusion, a critical parameter to avoid any potentially symptomatic extra-osseous leakage, is difficult especially as the radiologist has to examine all the injection points simultaneously. Moreover, this approach requires one intervening physician per cement delivery device, which becomes problematic in case of a triple (or more) simultaneous injection. Finally, it is hard to prefigure where to exactly introduce all the trocars as cement diffusion is hard to predict in a real pathological bone. Hence, the sequential several trocars and the single trocar seem to be more adapted for the injection of a large volume of cement. The single trocar technique appears as the best potential solution as there is a greater chance to obtain a completely cohesive and homogenous cement plug (as shown by the height/width ratio). The major issue with the single trocar technique is the lack of dedicated device. Manual injection of such a large volume using a 30ml syringe required a forceful pressure on the piston. The development of a device to inject a large volume of bone cement may however help to overcome this current limitation.

The present experiment failed to demonstrate that the non-cohesion of bone cement may be a systematic issue as suggested by some clinical cases and the numerical simulation. As analysis was based on the CT-scan examination, it is however impossible to rule out that any interface ocurred between different flows of PMMA at a microscopic level with the several trocars techniques. Still, partial non-cohesion was noticed at the front of the two cement volumes with the sequential several trocars technique to inject 20ml. The compressive tests demonstrated some differences in term of stiffness between the 3 techniques, which was not in favor of the single trocar technique. However, the real significance is relative as cement volume was slightly differing amongst the techniques as shown by the different weights of the tested items.

4.3. Conclusion

The data from the numerical simulation and from the experiments on phantoms suggest that the easiest way to achieve the injection of a large cohesive and homogenous cement plug is to use the single trocar technique. However, the management of polymerization of a large volume of cement is challenging especially with manual syringes that are not adapted to the clinical practice. Moreover, the insertion of the trocar needs to be performed with a different anatomical approach.

5th Chapter – Assistance for the injection of a large volume of cement through a single puncture site

The filling rate of an osteolytic lesion seem to strongly influence the restoration of bone stiffness, particularly in case of destruction of the bone cortex. Should a large volume of cement be required, the injection through a single access site seems to be the ideal solution to deposit a single cohesive cement plug with maximum control. However, there is currently no dedicated delivery system to deal with large volume of cement. In the bony pelvis, the injection with a single needle requires an optimized access to approach the destroyed area in its greater axis thereby increasing the chance to inject cement all along the pathway of the trocar. As reported in the first chapter of this manuscript, the viscosity of the cement during injection may also affect its distribution within the normal and pathological bone. Monitoring of viscosity during injection and prolongation of the duration of cement injection should therefore theoretically help to improve delivering a large volume of cement. In this part, two different accesses to the periacetabular area are first evaluated. Then in-situ analysis of cement viscosity is evaluated. Finally, a robotic solution is presented for the assistance to the injection of a large volume of bone cement.

5.1. Standardized single needle anatomical access to the peri-acetabular area

For the pelvic bone, the retrograde trans-pubic and ascending trans-ischial approaches have been described to access the anterior and posterior acetabulum respectively along their long axis [Yevich 2018]. In an attempt to fill the osteolytic space involving both the acetabular roof and the posterior acetabulum with a single anterior puncture, an alternative double oblique anterior trans-iliac approach may be used but has not been so far standardized in the literature. The purpose of the present section is to present the technique implementing a double oblique anterior approach to the acetabulum based on standardized anatomical landmarks, as well as evaluate its feasibility and safety.

5.1.1. Double oblique anterior approach to the acetabulum

In an attempt to fill the osteolytic space involving both the acetabular roof and the posterior acetabulum with a single anterior puncture, an alternative double oblique anterior trans-iliac approach may be used but has not been so far standardized in the literature. The present section seeks to present the technique implementing a double oblique anterior approach to the acetabulum based on standardized anatomical landmarks, as well as evaluate its feasibility and safety.

5.1.1.1. Materials and methods

5.1.1.1.1. Technique of the double oblique anterior approach

The principle of the approach is to enter into the iliac bone at a point situated 1cm above the anterosuperior iliac spine (ASIS). The bone trocar (Special vertebroplasty needle, Optimed, Germany) is then advanced through the iliac wing whilst applying craniocaudal and lateromedial angulation above the roof of the acetabulum, until the tip

of the needle reaches the posterior acetabulum at the most superior part of the ischial spine. The typical trajectory for the anterior double oblique percutaneous approach is presented on a pelvic model in Fig.92. A clinical example for acetabular cementoplasty is shown in Fig.93.

Fig.92: Double oblique anterior approach to the acetabulum. (A) VRT (right lateral view) and (B) &(C) axial CT-scan illustrating the double oblique approach in a phantom. The needle enters the iliac wing (arrow in A & B) just above the ASIS and is advanced medially and caudally to the superior part of the posterior acetabulum (arrowhead in A & C).
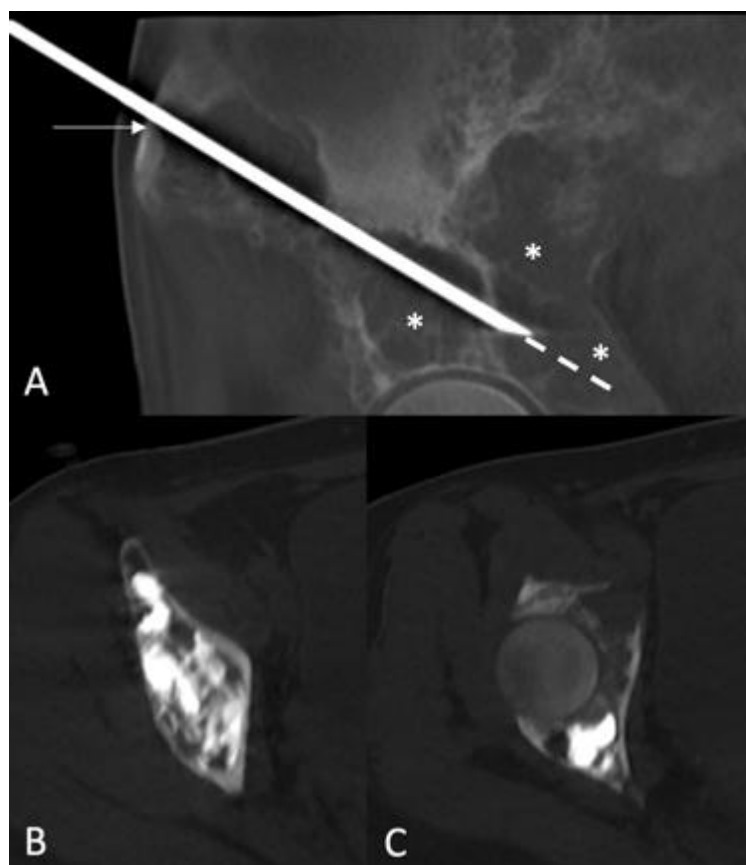
Fig.93: Double oblique anterior approach to the acetabulum. (A) VRT (right lateral view) and (B) &(C) axial CT-scan illustrating the double oblique approach in a phantom. The needle enters the iliac wing (arrow in A & B) just above the ASIS and is advanced medially and caudally to the superior part of the posterior acetabulum (arrowhead in A & C).

The approach can be performed with stand-alone fluoroscopic guidance and is presented in detail in Fig.94. The same access can be performed with CBCT or CT guidance with a needle trajectory software using the same aforementioned landmarks (Fig.95). Under CBCT guidance, the needle is then advanced using both the entry point and progression views [Tselikas 2015] to check the for the correct trajectory. Utilizing CT-guidance, the application of quick volumetric acquisition with postprocessing multiplanar reconstructions (MPR) is a precise way to assess correct needle advancement [Sato 2017].
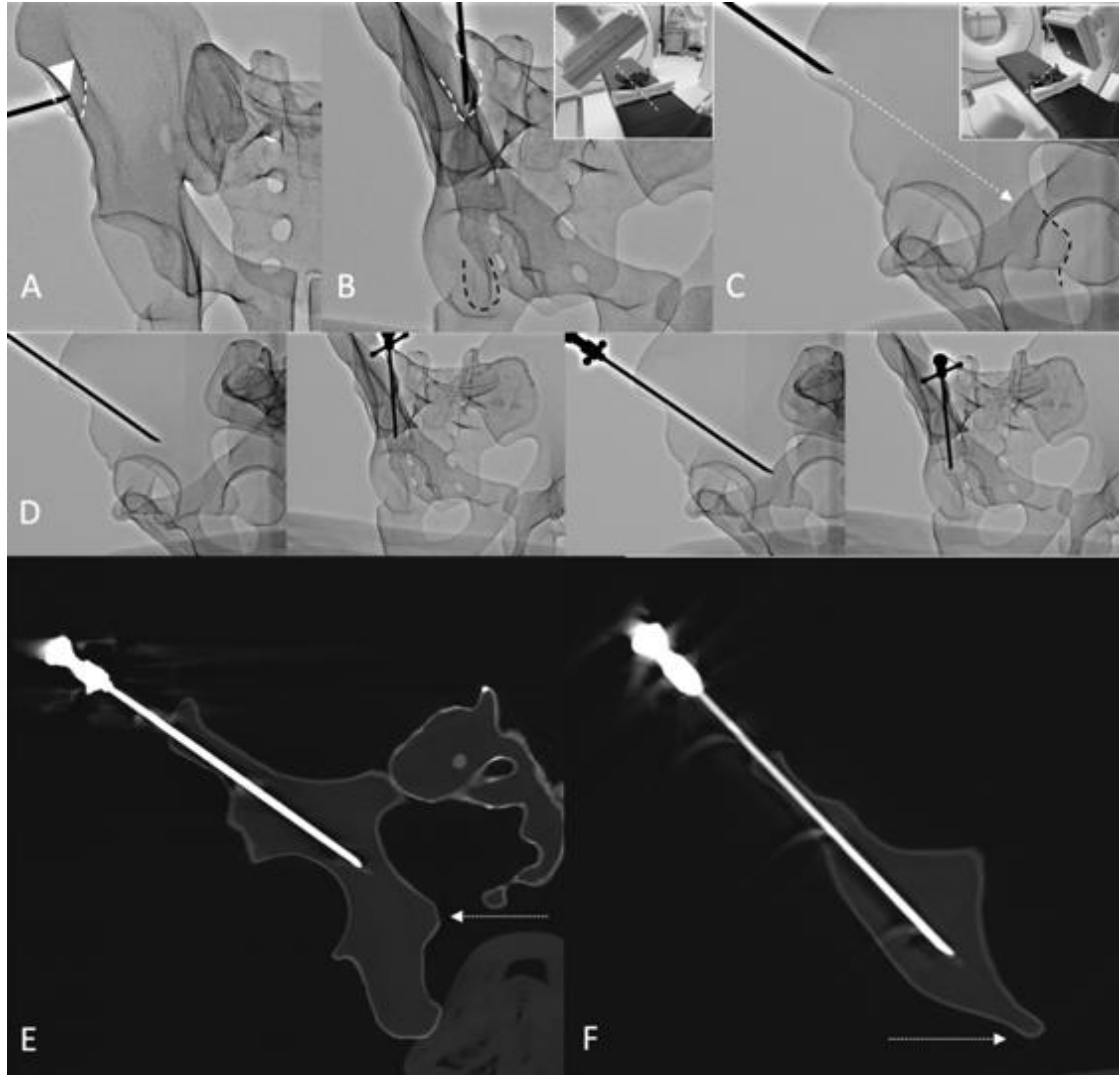
Fig.94: Approach with fluoroscopic guidance. (A) Anteroposterior projection: the middle part of the iliac crest (arrowhead) just above the ASIS (dotted line) is located. The C-arm is rotated (B) to align with the needle inserted in the mid-point of the iliac crest (white dotted line) with the ischial spine (black dotted line). The C-arm is rotated perpendicular to the oblique view (C), which displays the optimal projection to reach the posterior acetabulum without transgressing the joint (dotted arrow). The ischial spine is also visible (black dotted line). The needle is advanced under alternative perpendicular oblique views (D) to ensure that the tip targets the ischial spine on the entry point view and the caudocranial angulation is appropriate in the progression view. Note that this approach enables reaching the roof of the acetabulum and the posterior acetabulum depending on the depth of the needle. Corresponding (E) sagittal oblique and (F) axial oblique CT-scans illustrating the intraosseous trajectory of the double oblique approach with the ischial spine as the target landmark (dotted line).
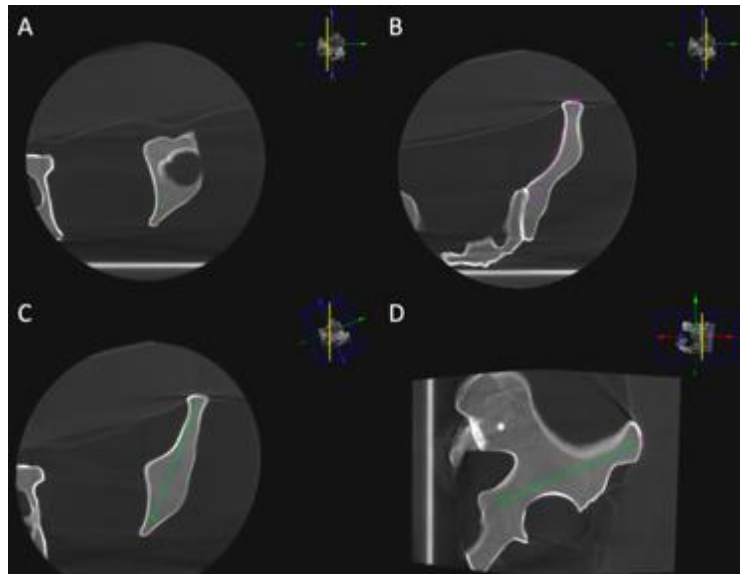
Fig.95: Approach with CBCT guidance and needle trajectory. (A) The target point is marked in the posterior acetabulum at the level of the upper part of the ischial spine. (B) The entry point is defined 1 cm above the ASIS. (C) Planned needle trajectory. (D) Progression view

5.1.1.1.2. Evaluation of the feasibility and safety of the approach

To analyze the feasibility of the double oblique approach, the pelvic CT scans of 60 patients (30 male – 30 female) were randomly retrieved from the PACS of our institution. DICOM images were analyzed on the bone window presets by an interventional radiologist with 10 years of experience in MSK interventions. A virtual trajectory was defined on axial CT-images using the aforementioned technique: the entry point was marked 1cm above the ASIS and the endpoint was defined just above the level of the ischial spine in the mid of the posterior acetabulum (Fig.96A-96C).

5.1.1.1.3. Data collection and analysis

The following items were recorded (Fig.96D-96E): (a) patient age; (b) sagittal oblique angulation; (c) axial oblique angulation; (d) length of intraosseous trajectory, (e) breach of the hip joint; (f) disruption of the cortices (medial, lateral or both) of the iliac bone, (g) any intervening structure(s) between the skin and the bone entry points. For each patient both hemipelvices were analyzed making a total of 120 analyses.

Descriptive statistics were used to present results. Categorical variables were expressed as absolute numbers and percentages. Continuous variables were expressed as means with standard deviations and ranges. Difference attributed to age, length or pelvic angles between genders were assessed using a t-test. A p-value<0.05 was considered statistically significant. Statistical analysis was performed by using R v3.6.3 (R Foundation for Statistical Computing, Vienna, Austria -copyright mark).
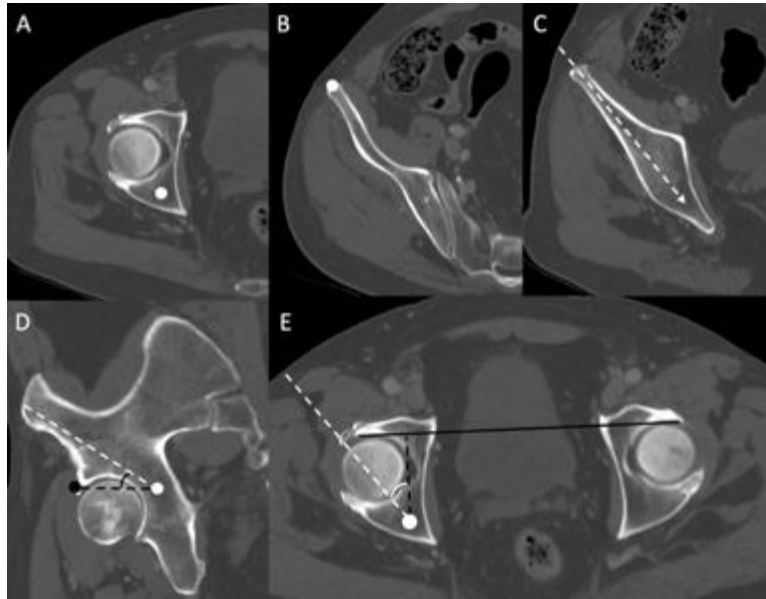
Fig.96: Imaging study. (A) Target point (circle) marked just above the level of the ischial spine in the mid-point of the posterior acetabulum. (B) Entry point (circle) marked 1cm above the ASIS in the mid-point of the anterior iliac wing. (C) Virtual planned trajectory (dotted arrow): no intervening structure, no transgression of the iliac cortex. (D) Sagittal oblique view: the virtual trajectory (dotted line) does not transfix the joint until it reaches the target point (white circle). The sagittal angulation is measured between the virtual trajectory and the line (black dotted line) joining the target point and the anterior part of the acetabulum (black circle). (E) The axial angulation is measured on an axial view between the virtual trajectory and the sagittal axis of the bony pelvis.

5.1.1.2 Results

Mean patient age was 62.6 ± 13.2 (range $22 - 86$). There was no significant difference of age between men (62.7 ± 12.0) and women (62.4 ± 14.5) (p=0.92). Mean sagittal and axial oblique angulations were 34.2 ± 4.5 (range $24 - 46$) and 31.5 ± 6.7 (range $15 - 48$) degrees respectively. Mean length of the intraosseous trajectory was 11.8 ± 0.9 cm (range $9.5 - 14$). The axial oblique angle and length of trajectory were significantly lower in the female than male population: 29.6 ± 7.5 vs 33.4 ± 5.3 degrees (p=0.002) and 11.4 ± 0.8 vs 12.1 ± 0.9 cm (p<0.001) respectively. There was no significant difference between the two populations for the sagittal oblique angle.
None of the virtual trajectories crossed the hip joint. In 112/120 trajectories (93.3%), there was no transgression of the cortex of the iliac bone. In 2 female patients, the virtual trajectory intersected the medial iliac cortex on both sides (4/120 - 3.3%). In 2 other female patients, the virtual trajectory intersected the medial iliac cortex and the iliac muscle on both sides (4/120 – 3.3%) (Fig.97). Intervening structures between the skin and the iliac bone included abdominal wall muscles in 17/120 trajectories (14.2%) and abdominal wall muscles plus digestive structure(s) in 3/120 trajectories (2.5%). All soft tissue structures were deemed easily manually displaceable. In the remaining 100 trajectories, subcutaneous fat was the only structure interposed between the skin and the bone entry points.

124
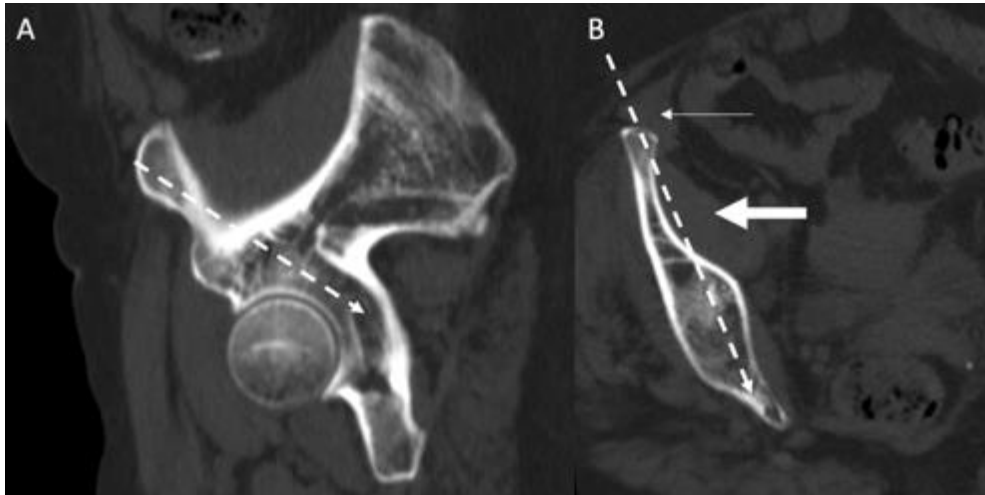
Fig.97: imaging study: case of a failed virtual approach using the anatomical landmarks. (A) sagittal oblique showing the virtual trajectory (dotted arrow). (B) axial oblique in the axis of the planned trajectory: the access transfixes the abdominal muscle (thin arrow, easily removable by displacing the abdominal apron), the medial cortex and the iliac muscle.

5.1.1.3. Discussion

The present study describes the anatomical landmarks for the double oblique intraosseous approach to the acetabulum. It allows rapid and consistent identification of the entry point -and the target point when using needle trajectory software. Knowledge of the respective fluoroscopy landmarks is also noteworthy as appropriate angulation is immediately estimated without the need to repeat multiple 3D acquisitions during needle advancement in case of doubt. Finally, access can be performed with stand-alone fluoroscopic guidance should the important obliquity preclude the use of a planned trajectory as encountered several times in the clinical experience.

Based on this imaging study, the double oblique approach seems feasible in almost all cases. Imaging findings demonstrate that the access defined purely on two anatomical landmarks still carries a low risk of breach of the medial iliac cortex in women. Routine careful review of the diagnostic CT-scan or of the planned trajectory prior to needle insertion is required in order to adjust the access whenever necessary to mitigate against any cortical transgression during advancement of the needle. Regarding safety, the major theoretical concern may be the risk of injury to the abdominal muscles or to the abdominal viscus in obese patients. In our clinical practice using this approach, the abdominal muscles and the digestive structures are however easily avoidable by physically displacing the abdominal apron towards the contralateral side. Hence, the access does not traverse any muscles before entering the iliac bone, thereby theoretically reducing the risk of hematoma formation [Huang 2014]. Additionally, this approach stays away from the emergence of the lateral cutaneous nerve of the thigh that courses in the subcutaneous fat below the level of the ASIS. The intraosseous trajectory is relatively long but remains feasible in clinical practice.

We believe that this approach can be valuable when performing cementoplasty in patients with extensive disease. In our clinical experience, we were able to fill the posterior acetabulum whilst still gaining access to the acetabular roof through a single access point simply by withdrawing the bone trocar during cement injection. It is advantageous compared to a pure axial anterior access, for which diffusion of cement to the posterior column is

unpredictable and most of the time limited as the tip of the needle lies away from the ischial spine. This is noteworthy as cement repartition in the different osteolytic areas of the acetabulum has been identified as a prognostic factor for reducing the incidence or worsening of a pathological fracture [Hesler 2019]. It may also avoid for the need of patient repositioning to access specifically the posterior acetabulum through a lateral or posterior approach. Finally, the double oblique approach might decrease the risk of soft tissue cement leakage along the needle tract because of the long-intraosseous tunnel which allows better control of cement backflow. It is however difficult to scientifically prove the superiority of the aforementioned described access over a direct approach for these specific purposes without a dedicated randomized controlled trial.

The double oblique approach undoubtedly presents limitations. As for all double oblique approaches, it is certainly more technically challenging than using pure axial accesses. It might be difficult to perform in cases of extensive cortical destruction rendering the anatomical bony landmarks (most importantly the hip joint and the ischial spine) less discernible. Finally, the very anterior part of the acetabulum is not easily covered by this approach. In such a case, an additional anterior needle might be required to optimize the filling of the supra-acetabular region.

5.1.2. Anterior and posterior trans-iliac accesses for the restoration of load transmission in the metastatic bony pelvis: a CT-based anatomical evaluation

Many authors seek to use a long trans-iliac route to inject cement and/or insert hardware (mostly screws) along the weight-bearing axis of the pelvic bone, i.e. along the acetabular roof and the posterior part of the arcuate line, should an osteolysis compromising the integrity of the area. In this perspective, both ascending anterior and posterior descending accesses have been described in the literature [Lea 2019]. However, there is no standardized anatomical landmark used for these approaches. In most cases, planning and guidance are done with cone-beam CT and needle guidance software. Although it offers optimal precision, such guidance also comes with limitations that can make needle placement challenging. The bull's eye perspective (entry point view) may not be reachable by the C-arm because of excessive steepness, and any misregistration of augmented fluoroscopy can lead to trocar malposition. Furthermore, needle guidance software is not very intuitive in case of double obliquity. The purpose of the present section is therefore to propose a pathway based on anatomical landmarks and evaluate its feasibility and safety with both anterior and posterior approaches.

5.1.2.1. Materials and methods

This is a single center observational study. Institutional review board approval was not required for the retrospective evaluation of the patient radiological data and postprocessing.

5.1.2.1.1. Anatomical landmarks

Load transfer across the pelvic bone passes most predominantly across the anterior and intermediate part of the iliac surface of the sacro-iliac joint (at the S1-S2 level), the medial cortex of the posterior part of the arcuate line, the acetabular roof and the lateral cortex of the acetabulum. We hypothesized that the antero-inferior iliac spine (AIIS) and the postero-superior iliac spine (PSIS) may be used as reliable anatomical landmarks to plan a trans-

iliac route that would follow exactly the one of load transfer. This approach may be feasible with an anterior access or a posterior access.

5.1.2.1.2. Imaging analysis of the approach

To analyze the feasibility and safety of the proposed landmarks, the pelvic CT scans of 20 patients acquired in supine position were randomly retrieved from the PACS of our hospital and analyzed bilaterally. Following upload of DICOM data into the same 3D workstation with the same planning software as the one used in clinical practice (Xperguide, Philips, the Netherlands), imaging analysis was independently performed by a resident radiologist. For each patient and each side, two virtual trajectories were defined: one with an anterior access and one with a posterior access. In both situations, the goal was to define a trajectory that would extend from the sacro-iliac joint to the acetabular roof. For both trajectories, the AIIS and the PSIS were used as anatomical landmarks as defined in fig.98.
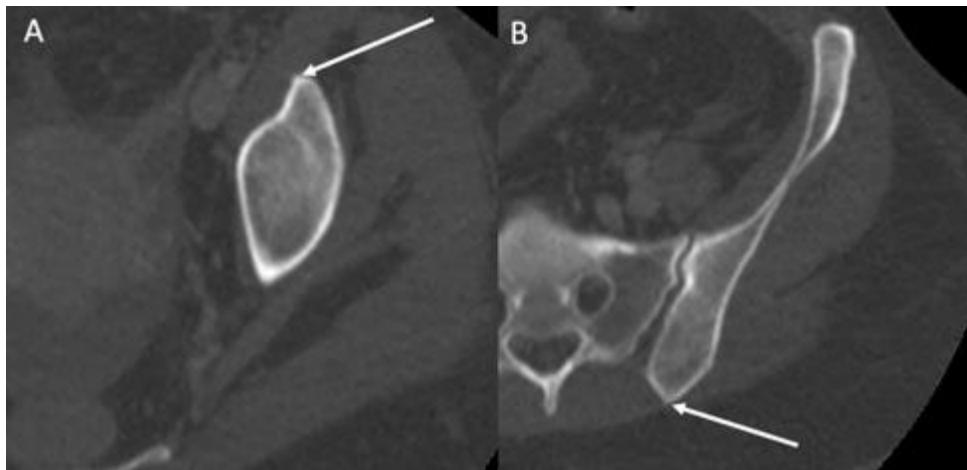
Fig.98: Imaging identification of the mid of the AIIS (A, arrow) and the mid of the PSIS (B, arrow). Both structures were spotted in axial plane while scrolling the images from caudal to cranial.

For both routes, the AIIS was spotted as the entry point on axial images and the PSIS was subsequently used as the initial target point on axial images (fig.99).
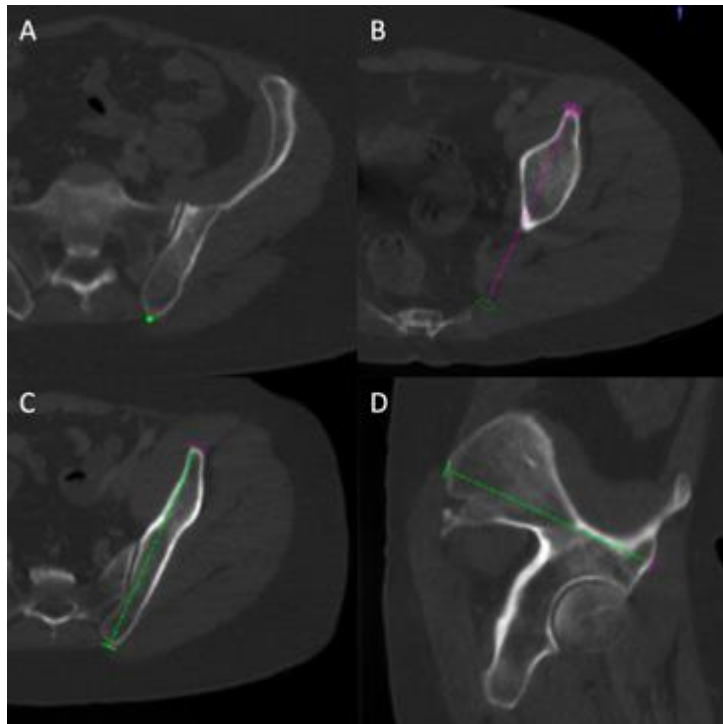
Fig.99: Definition of the virtual route. (A) The PIIS is spotted on axial images. (B) The AIIS is spotted on axial images. (C) Planning view and (D) progression view of the needle pathway based on anatomical landmarks.

For the anterior route, the length of the virtual trajectory was then adjusted in the planned trajectory without any modification of the angulation, in a way that the final target point would be located at the level of the posterior part of the sacro-iliac joint (fig.100). For the posterior virtual route, the length of the virtual trajectory was then adjusted to locate the final target point at the center of the acetabular roof (fig.101).

Fig.100: Anterior virtual route. The target point (green circle) is positioned at the posterior level of the sacro-iliac joint. (A) Planification view and (B) progression view
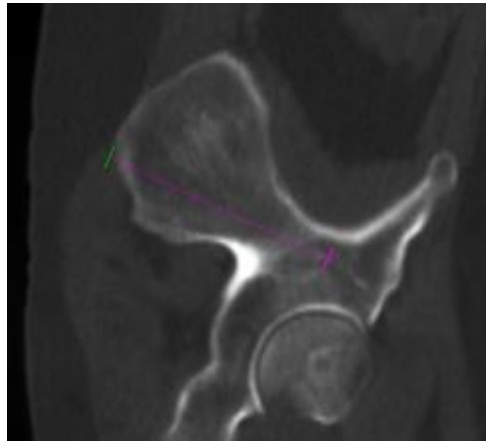
Fig.101: Posterior virtual route. The target point (purple circle) is positioned at the same anteroposterior level of the center of the femoral head.

5.1.2.1.3. Data collection and analysis

For each trajectory, the following items were recorded by each reader for both anterior and posterior approaches: a) confidence of the radiologist in the identification of the 2 anatomical points using a simple 2 grades scale: 0-low confidence / 1-high confidence; b) intervening structure(s) other than fat between the skin and the bone entry point; c) length of the virtual trajectory; d) cortical breach along the virtual trajectory; e) distance of the virtual trajectory with respect to the acetabular roof as defined in fig.102.
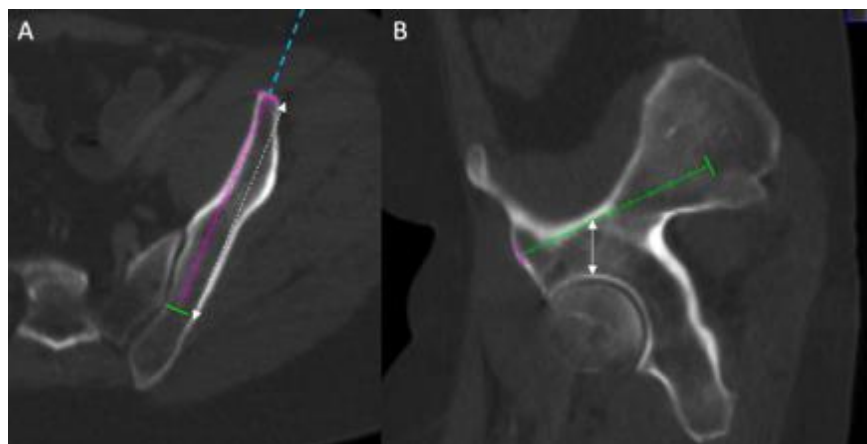
Fig.102: Evaluation of the virtual route. The length of the route is measured (dotted double arrow in A) as well as the distance from the acetabular roof (double arrow in B). Any intervening structure along the virtual access between the skin and the bone (blue dotted line) is recorded, as well as any transgression of the cortical bone.

Descriptive statistics were used to present results. Categorical variables were expressed as absolute numbers and percentages. Continuous variables were expressed as means with standard deviations and ranges. Comparison of the results between the anterior and posterior trajectories was made using a t-test. A p-value<0.05 was considered statistically significant. Statistical analysis was performed by using R v3.6.3 (R Foundation for Statistical Computing, Vienna, Austria -*copyright mark*).

5.1.2.2. Results

The AIIS and the PIIS were identified with confidence in 36/40 (90%) and 38 /40 (95%) of the cases respectively. The intervening structure between the skin and the bone entry point was muscle in all 40 anterior virtual routes while there was no intervening structure for all 40 posterior virtual routes.

The mean length of the trajectory was 101 +/- 11 mm (range 90 - 131) for the anterior route and 108.5 +/- 8.5 mm (range 95 - 125) for the posterior route (no statistically significant difference, p=0.05578). The virtual anterior route was transfixing the cortical bone in 11/40 (27.5%) cases, tangent to the cortical bone in 4/40 (10%) cases and purely intra-osseous in 35/40 (62.5%) cases. The virtual posterior route was transfixing the cortical bone in 3/40 (7.5%) cases, tangent to the cortical bone in 8/40 (20%) cases and purely intra-osseous in 29/40 (72.5%) cases (fig.103).

Mean distances from the acetabular roof were 20.5 +/- 4.5 mm (range 12 – 39) and 20 +/- 5 mm (range 14 – 34) with the anterior and the posterior route respectively. The difference between the anterior and the posterior routes was not significant (p=0.74358).
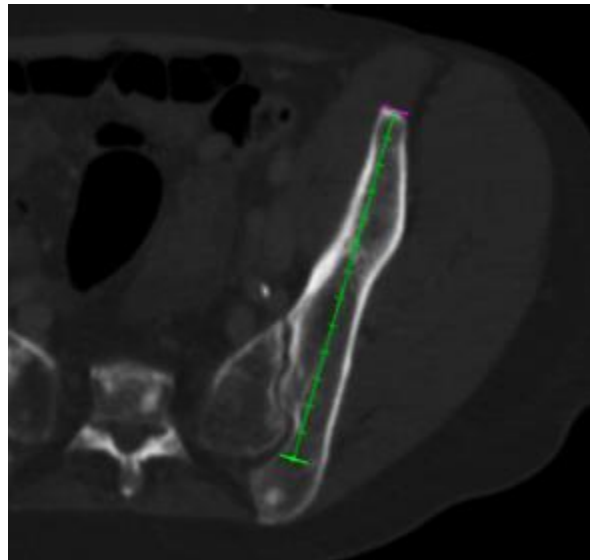
Fig.103: Example of an anterior virtual route. The virtual access has a pure intra-osseous location and does not transfix the cortical bone.

5.1.2.3 Discussion

The present study evaluated the reliability of selected anatomical landmarks to standardize the planification of percutaneous consolidative treatments in the periacetabular and sacro-iliac areas. Based on the retrospective analysis of clinical cases from our institution, the AIIS and PSIS were judged as potential targets for the planification of the needle pathway. In the present study, the AIIS and PSIS were confidently spotted in almost all cases by a junior radiologist, suggesting that these landmarks could be considered as reliable and reproducible. The anatomical analysis confirmed that a virtual route joining the AIIS and the PSIS was going along both the acetabular roof and the sacro-iliac junction near the S1-S2 level, thereby providing access to the weight-bearing axis of the pelvic bone through a single trajectory. However, the virtual pathway that was defined by the center of the AIIS and PSIS was transgressing the cortex of the iliac bone in a significant percentage of cases, especially

with the anterior approach. Such issue was easily overcome by displacing the entry point (for the anterior route) or the target point (for the posterior route) at the lateral edge of the AIIS (5 mm lateral to the midpoint of the AIIS). In any case, slight modification to the planned trajectory (defined thanks to the two anatomical landmarks) can be performed on the planning software to precisely adjust the approach.

Based on the present anatomical evaluation, the posterior trans-iliac route may seem safer as it is not transgressing any muscular structure. This should be associated with a theoretical lower risk of bleeding which, although rare, is a possible complication of percutaneous bone interventions. Hence, if consolidation is to be performed solely along the weight-bearing axis, prone positioning may be preferred [Yevich 2018]. In this position, the herein discussed trans-iliac access can also be combined with an ascending trans-ischiatic approach for complex cases [Lea 2019]. The anterior route may still be used and be of particular interest in case of a combined ascending retrograde trans-pubic approach [Bauones 2015].

The present study is not without limitations. The number of trajectories that was analyzed is still rather small and may not be representative of all anatomical variations of the pelvic bone. The virtual trajectories were determined on diagnostic CT-scans that were all acquired in supine position. Hence, there may be some discrepancies compared to the position at the time of an intervention, especially in case of prone positioning. Finally, only one virtual trajectory was defined per side and position. This is therefore not representative of the situation where two ipsilateral accesses are required, notably if 2 screws are to be inserted. We believe however that the AIIS and the PSIS mays help to improve the standardization of planification on axial images and do not preclude further adjustments. Moreover, these anatomical landmarks can still be used with stand-alone fluoroscopic guidance should the needle trajectory software be inaccessible due to excessive angulation.

5.2. In-situ monitoring of cement viscosity

Viscosity is a key working property of PMMA during injection: it is the only major parameter influencing cement distribution that is not related to the bone structure [Bohner 2003, Loeffel 2008, Lai 2013]. It should be low enough to flow through the delivery system, the bone needle and the bone. On the other hand, it should be high enough not to leak outside the bony structure and promote the distribution of PMMA within the trabecular bone [Lewis 1997, Breusch 2002, Waanders 2010]. The polymerization reaction is a dynamic process that leads to an increase of bone cement viscosity during injection. Hence, knowing the value of viscosity at any time may be helpful for the performing physician to adapt the timing and speed of injection. It is possible to measure the viscosity ex-vivo with a rotational rheometer, or to calculate dynamic viscosity thanks to the Hagen-Poiseuille law provided that the diameter and the length of cannula, the volumetric flow rate and the injection pressure are known [Loeffel 2008, Lepoutre 2019]. Information on flow rate and injection pressure are however not accessible in the clinical practice where the injection is performed manually either with syringes or dedicated injecting devices. Continuous measurement of the viscosity of PMMA inside the bony structure would therefore be an ideal solution.

Dielectric analysis (DEA) monitors the physical properties of a polar material by measuring its conductance and capacitance [Vassilikou-Dova 2008, Chu 2019]. These parameters can then be used to calculate the material characteristics of permittivity, conductivity and resistivity, which are fundamental material properties that do not

depend on the quantity of the tested material. DEA is based on the electric response of a dielectric material to an alternating current at a given frequency, which depends on the orientation of molecules and movements of ions [Zhu 2019]. DEA of composites used in dentistry has already been reported in the literature to determine ion viscosity [Steinhaus 2014, Steinhaus 2016]. The purpose of the present study is to determine whether or not DEA could successfully be used to monitor the viscosity of the PMMA cement inside the bone.

5.2.1. Theoretical model

Our goal is first is to explain how DEA can be used to calculate the dynamic viscosity of PMMA. The polarization of a polymer submitted to an alternating electrical current comes from the ionic polarization and the dipolar polarization [Vassilikou-Dova 2008]. Hence, mathematical evaluation of the DEA of a PMMA sample needs to consider the contribution of both the charged particles (ions) and the molecules (dipoles) (fig.104).
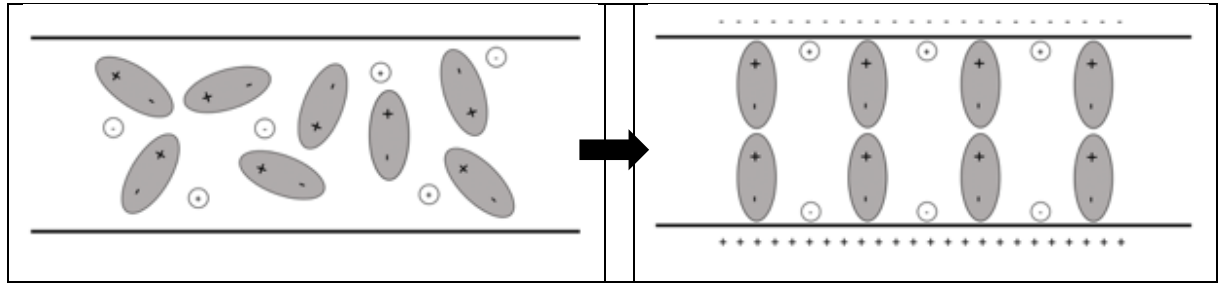
Fig.104: Application of an electric field to a sample of a dielectric material leads to the orientation of molecules and movement of atoms, providing the basis for DEA.

5.2.1.1. Definitions

Permittivity − Permittivity (ε) is related to energy storage in a material [Vassilikou-Dova 2008, Chu 2019] . The complex permittivity (ε^*) function of a material tested with an angular frequency (ω) has a real (ε') and an imaginary (ε'') part:

$$\varepsilon^*(\omega) = \varepsilon'(\omega) - i\varepsilon''(\omega) \qquad (1)$$

The real part of permittivity (or relative permittivity) (ε') is related to the ability of a dielectric material to store energy and comes from the contributions of vacuum and the real part of the susceptibility of the material medium itself. It is composed by the unrelaxed permittivity (ε_u), which is the baseline of dielectric permittivity without the contributions of dipoles and charged particles and is not frequency dependent, and by a factor (ε_d') that represents the permittivity due to the polarization of the dipoles and is frequency dependent:

$$\varepsilon'(\omega) = \varepsilon_u + \varepsilon_d'(\omega) \qquad (2)$$

The imaginary part of permittivity (ε''), also known as loss factor, describes the energy losses both from the dipoles (ε_d'') and the charged particles (ε_c''):

$$\varepsilon''(\omega) = \varepsilon_d''(\omega) + \varepsilon_c''(\omega) \qquad (3)$$

According to the model of DeBye, losses are predominantly related to the dissipation of charged particles, at least for low frequencies. Hence, loss factor mostly represents losses arising from the movements of ions. As shown in

(1), the complex permittivity of a dielectric material depends upon the orientation of the dipoles (measured by the real part of permittivity) and the movements of charges particles (measured by the imaginary part of permittivity).

Capacitance − Capacitance (C) is the ability of a system to store an electric charge [Vassilikou-Dova 2008, Lee 2017]. For a sample of material tested with an alternating electric current of angular frequency (ω), capacitance is defined by:

$$C(\omega) = \varepsilon_0 \varepsilon'(\omega) \frac{S}{d} \quad (4)$$

Conductivity and conductance, resistivity and resistance − Conductivity (σ) is an intrinsic property, related to the ability of a material to conduct an electric current. It has frequency independent (σ_{DC}) and frequency dependent (σ_{AC}) components:

$$\sigma = \sigma_{DC} + \sigma_{AC} \quad (5)$$

Conductivity and permittivity are linked through the following equation:

$$\sigma = \varepsilon_0 \omega \varepsilon'' \quad (6)$$

where ε_0 is representing the permittivity of vacuum ($\varepsilon_0 = 8.85\ X\ 10^{-14}$ F/cm).

Conductance (G) is an extrinsic property. Related to the material conductivity, it is however specific to a given object or sample, for which it indicates how it conducts electricity. It is defined by:

$$G(\omega) = \varepsilon_0 \omega \varepsilon''(\omega) \frac{S}{d} \quad (7)$$

with *S* defined by the sample's cross-sectional area and *d* the sample thickness.

Resistivity (ρ) is the inverse of conductivity, and resistance is the inverse of conductance. Resistivity has frequency independent (ρ_{DC}) and frequency dependent (ρ_{AC}) components:

$$\rho = \frac{1}{\sigma} = \rho_{DC} + \rho_{AC} \quad (8)$$

Calculation of the conductance, capacitance, permittivity and resistivity using DEA − The amplitude of the current and the phase shift θ provide the measures to calculate the conductance and capacitance of the tested material using the following equations:

$$G_{material} = \frac{I_{res}}{V_{exc}} \sin \theta \quad (9)$$

$$C_{material} = \frac{I_{res}}{V_{exc}} \cos \theta \quad (10)$$

with I_{res} the alternating current through the material under test (Amperes)

and V_{exc} the alternating current voltage across the material under test (Volts)

Knowing the electrode area *A* and the distance *d* between the electrodes, the material properties of relative permittivity ε' and conductivity σ can then be extracted from equations (5) to (8):

$$\sigma_{material} = \frac{G_{material}}{\left(\varepsilon_0 \frac{A}{d}\right)} \quad (11)$$

$$\varepsilon'_{material} = \frac{C_{material}}{\left(\varepsilon_0 \frac{A}{d}\right)} \quad (12)$$

5.2.1.2. Ions and dipoles in PMMA

PMMA contains a certain amount of ions, which might be positively (Cu2+) or negatively (Cl-) charged and correspond to impurities that do not participate to the curing reaction [Lepoutre 2019]. The concentration of ions is therefore likely to stay stable during the different handling phases of the bone cement. On the other hand, dipoles are constituted by the asymmetrical repartition of charges in the molecules of MMA. At the beginning of the polymerization reaction, there is a certain number of molecules of MMA, whose mobility is inversely proportional to viscosity. As the curing reaction goes on, the molecules of MMA bond to each other, thereby progressively reducing the number of dipoles (fig.105).
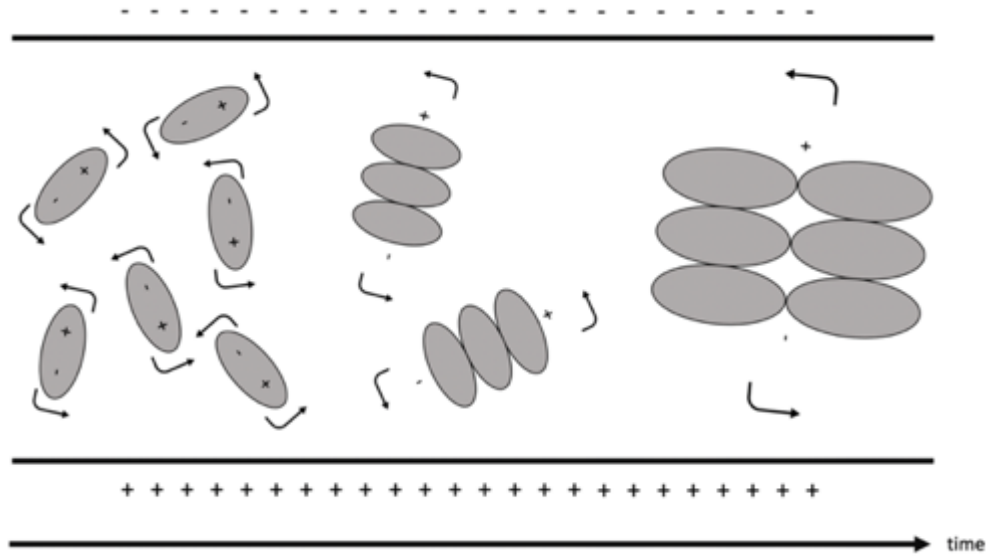
Fig.105: Evolution of the number of dipoles with time in PMMA.

5.2.1.3. Resistivity of ions: ion viscosity

The polarization of ions, also called ion viscosity, occurs almost instantaneously. It equals to the frequency-independent part ρ_{DC} of resistivity and is given by the following equation [Aziz 2017, Lee 2017]:

$$\rho_{DC} = \frac{1}{q\mu n} \quad (13)$$

where q is the electric charge [C],

μ the free ion mobility ([Cs/kg]),

and n the free ion concentration [m^{-3}].

The mobility of the free ions is given by the Einstein's relationship:

$$\mu = \frac{qD}{kT} \quad (14)$$

where D is the diffusion coefficient [m^2/s],

k the Boltzman's constant,

and T the temperature [K].

The diffusion coefficient D is temperature dependent [Lee 2017, Aziz 2019]:

$$D = D_0 e^{-\frac{Q}{kT}} \quad (15)$$

with D_0 the maximum value of diffusion coefficient,

and Q the activation energy [eV].

D_0 is constant with temperature but decreases with the advancement of the polymerization reaction.

Combining (13), (14) and (15) gives the following equation for ion viscosity:

$$\rho_{DC} = \frac{kT}{q^2 n D_0} e^{\frac{Q}{kT}} \quad (16)$$

Hence, ion viscosity depends on the mobility of the ions under the influence of the electrical current, and on the temperature at the time of measurement.

5.2.1.4. Resistivity of dipoles

Contrary to ion viscosity, the movement of MMA molecules is not instantaneous and depends not only on viscosity but also on the advancement of the curing reaction, which determines the number of MMA molecules available. Hence, the conductance of the dipoles G_d depends on the time required for dipoles alignment [Jossinet 2018]:

$$G_d = C_d \frac{\omega^2 \tau}{1 - \omega \tau^2} \quad (17)$$

where τ [s] is the dipole time constant.

Combining (6), (11), (12) and (17) gives the resistivity of dipoles ρ_d, as:

$$\rho_d = \frac{1}{\frac{C_d}{\left(\varepsilon_0 \frac{A}{d}\right)} \frac{\omega^2 \tau}{1 - \omega \tau^2}} \quad (18)$$

The resistivity of the dipoles is frequency dependent during DEA and corresponds to ρ_{AC} in equation (6) [Vassilikou-Dova 2008, Lee 2017].

5.2.1.5. Mathematical relationship between ion and dynamic viscosity

In the limit of low Reynold's numbers, the diffusion coefficient D car be calculated by the Stokes-Einstein's relation if ions are modeled as spheres [Coglitore 2017]:

$$D = \frac{kT}{6\pi\eta r} \quad (19)$$

where η is the mechanical viscosity [Pa. s] and r the sphere radius [m]. Combining (13), (14) and (19) leads to:

$$\rho_{DC} = \frac{6\pi\eta r}{q^2 n} \quad (20)$$

Hence ion viscosity ρ_{DC} is proportional to the dynamic viscosity η. As PMMA turns more and more viscous (increase of dynamic viscosity), the mobility of the free ions is decreasing and ρ_{DC} is increasing [Steinhaus 2016].

5.2.2. Experimental model

5.2.2.1. DEA of a PMMA sample

A sample of PMMA (Osteopal V, Heraeus Medical, Germany) was applied on an interdigitated DEA electrode with a surface of analysis of 33 mm^2 (Mini-IDEX, Netzsch). DEA was subsequently conducted at 4 frequencies of analysis (1, 10, 100, 1000 Hz) during 20 minutes using a DEA generator (DEA 288 Ionic, Netzsch). Experiment was performed with a room temperature of 21° C.

5.2.2.2. Synchronous evaluation of dynamic and ion viscosity of PMMA

A dynamic rheometer with parallel plates geometry (Haake Mars, Thermofisher Scientific) was paired to a DEA generator (DEA 288 Ionic, Netzsch). A DEA electrode and a thermosensor were placed over the plate of the rheometer. Following mixture of the mono- and polymer, a sample of PMMA (Osteopal V, Heraeus Medical) was analyzed synchronously both dynamically with a shear rate of and dielectrically at 1, 10, 100, 1000, 10000 and 100000 Hz. The same experiment was conducted during 60 minutes with 3 different none cement temperatures: 17, 20 and 23°C.

5.2.2.3. Measurement of the PMMA ion viscosity on a phantom model

A spinal custom model including spinal vertebral bodies articulated with anterior and posterior intervertebral latex ligaments as well as flexible intervertebral discs (Sawbones Europe AB) was used. In the model, each vertebral body is composed of a foam radio opaque cortical shell filled with inner cancellous material, which is designed to simulate a lumbar osteoporotic vertebral body (fig.106).
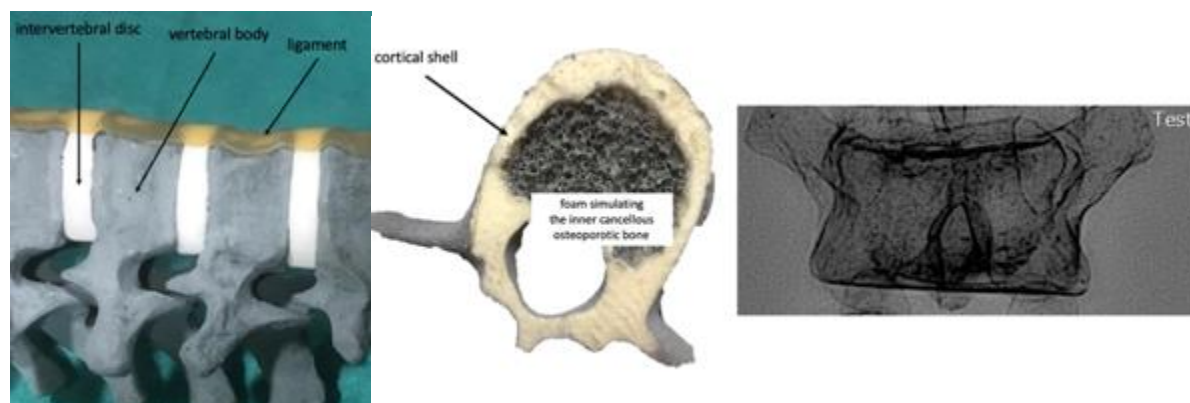
Fig.106: Spinal custom model. aspect of the foam inside the vertebral body. The model is radiopaque.

Five vertebral levels were prepared to allow in-situ DEA. The set-up for DEA measurements is presented in fig107.
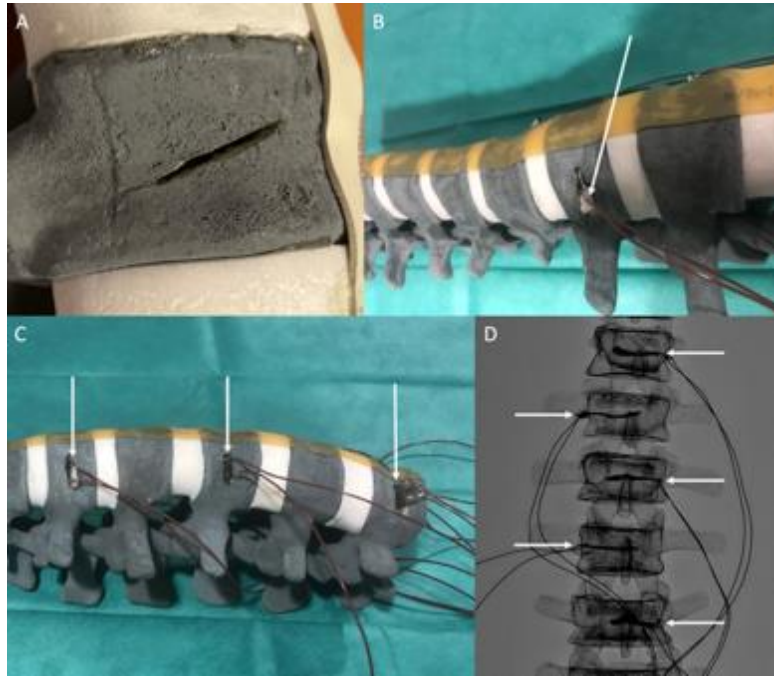
Fig.107: Preparation of the spinal custom model for DEA. (A) An incision was made on the lateral side of the vertebral body. The width of the cut was equal to the one of the DEA electrode while the height measured 1.5mm and the depth 2cm. (B) A compress soaked with contrast media (Visipaque 270, GE) (arrow) was taped up at the bottom part of the interdigitated electrode (Mini-IDEX, Netzsch) in order to increase the visualization of the electrode under fluoroscopic imaging. The electrode was then positioned inside the vertebral body through the incision. (C) Model after insertion of one electrode (arrows) per level. (D) Corresponding anteroposterior fluoroscopic projection showing all electrodes (arrows) in position. Visualization is enhanced by the contrasted compress.

Experiments were conducted in a Cone-beam Computed Tomography (CBCT) interventional suite (Philips Allura FD20), which is used to perform vertebroplasties in clinical practice (fig.108).

Fig.108: Overview of the experiment. The spinal custom model is positioned in the X-ray beam of a CBCT suite. The DEA generator is positioned on the examination table.

137

The room temperature was set to 20°C. A 10G vertebroplasty needle (Gangi vertebroplasty needle, Optimed, Germany) was manually inserted just above the DEA electrode through the lateral cortex (fig.109). In addition, a thermosensor was inserted in two vertebral levels through a 14G bone trocar (Ostycut, Bard,USA).
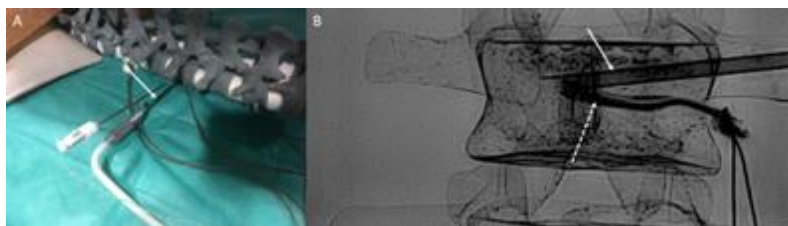
Fig.109: Insertion of the vertebroplasty needle. (A) The trocar (arrow) is inserted into the vertebral body with a lateral approach. (B) Same view on anteroposterior projection: the trocar (arrow) lies above the DEA electrode (dotted arrow).

Lateral and anteroposterior fluoroscopic projections were acquired prior to cement injection to confirm the proper position of the electrode and vertebroplasty needle within the vertebral body. The electrode was connected to the generator (DEA 288 Ionic, Netzsch). A cement kit (Osteopal V, Heraeus Medical), similar to the ones used in clinical practice and previous experiments, was taken out from the fridge where they are stored at 4°C (same low temperature as for the clinical use, to increase the time of application). Hand-mixing of the PMMA was performed for each volume for 45 seconds. After a waiting time of 1 minute (according to the recommendation of the manufacturer to increase cement homogeneity), the cement was poured into the syringe that was subsequently connected to the injector device (Gangi Cemento-RE Kit, Optimed). The injector device was connected to the vertebroplasty trocar and DEA analysis was started at 1 Hz, 10 Hz, 100 Hz and 1 kHz. Cement was injected by manually turning clockwise the injector device, with an approximate speed of injection of 0,075-0.1. Intermittent fluoroscopic images were acquired (typically every 10 s) to assess the proper repartition of cement within the vertebral body and on the surface of the interdigitated electrode (fig.110).
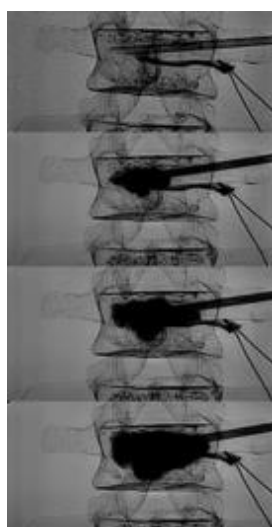
Fig.110: Cement injection and DEA. Intermittent fluoroscopic monitoring shows PMMA bone cement progressively infiltrating the vertebral body and coming in contact with the DEA electrode.

Once the whole volume of PMMA had been injected, the injector device was disconnected from the hub of the needle and the inner lumen of the trocar was cleared with the stylet, like for a standard vertebroplasty procedure. Overall, DEA was performed for 17 minutes following the beginning of recording. One cement volume (10 ml) was used per level. The same experiment was conducted over 5 spinal levels. Following completion of the experiments, the different spinal levels were cut in order to assess visually the repartition of PMMA on the DEA electrode.

5.2.3. Experimental results

5.2.3.1. DEA of a PMMA sample

Ion viscosity is slowly increasing during the initial phase of polymerization without significant differences between the frequencies of analysis. This is due to the exclusive contribution of the free ions to the DEA signal. The sudden increase of the values of ion viscosity corresponds to the reticulation and curing reaction of the PMMA bone cement (fig.111). This is associated with a contribution of the signal of the dipoles thereby leading to a variation of the values of ion viscosity depending on the frequency of analysis.
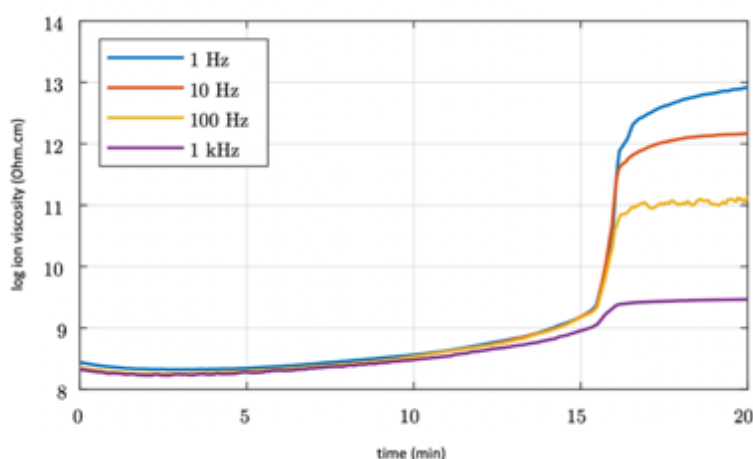
Fig.111: Logarithmic representation of ion viscosity of PMMA as a function of time.

5.2.3.2. Synchronous evaluation of dynamic and ion viscosity of PMMA

The correlation between dynamic and ion viscosity is presented in fig.112. There is good temporal concordance between the two analyses that both show the slow initial increase of the bone cement viscosity as well as the process of reticulation that comes with a peak augmentation of the viscosity. The influence of the temperature on viscosity is also depicted with ion viscosity: the application phase is longer with a colder bone cement, which is similar to the experimental findings. Table21 presents the value of ion viscosity and dynamic viscosity at several time points to give an approximation between the values of dynamic viscosity and those of ion viscosity.
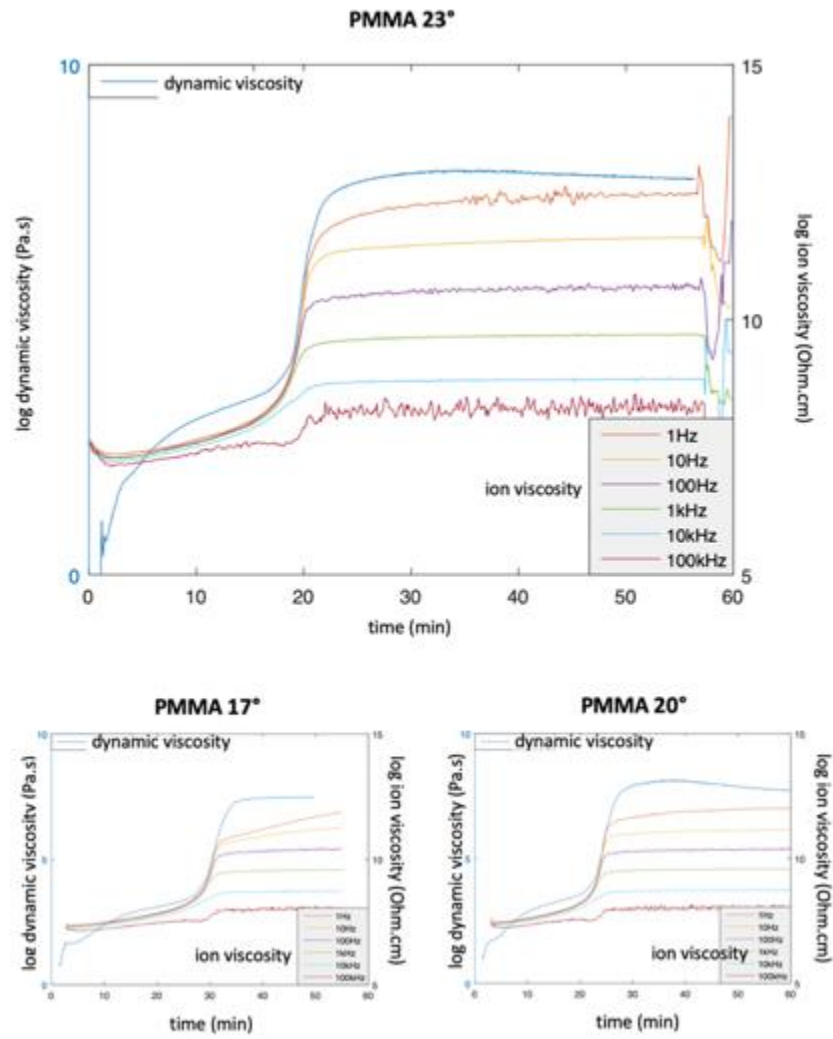
Fig.112: Logarithmic representation of dynamic viscosity and ion viscosity for different temperatures of PMMA.

Time (min)	dynamic viscosity (Pa.s)	log ion viscosity (Ohm.cm)
0	0	7,65071
1	0,334879	7,42358
2	9,955503	7,36285
3	54,931087	7,36728
4	96,905266	7,38924
5	171,551834	7,41539
6	301,607727	7,45053
7	466,987366	7,49098
8	654,053894	7,53325
9	873,039551	7,59131
10	1106,795898	7,65198
11	1361,7146	7,70876
12	1649,629639	7,76395
13	1976,686523	7,83105
14	2343,894287	7,92081
15	2787,559326	8,00933
16	3402,553711	8,13299
17	4535,559082	8,31401
18	7653,462891	8,61099
19	20364,89844	9,20166
20	697261	10,59688
25	49458340	12,03922
30	75072200	12,24685
35	80942520	12,39171
40	77696432	12,28944
45	74933344	12,24509
50	63394156	12,44923

Table21: corresponding values of dynamic and log ion viscosity (1Hz analysis) at 23°

5.2.3.3. DEA of PMMA on the spinal custom model

Measurements of ion viscosity were feasible for all 5 levels without technical failure. Graphical representations of ion viscosity of vertebra2 and of the 4 other vertebrae are presented in fig113. The graphics demonstrate that the in-situ results of the DEA signal of PMMA is similar to the one of a sample of PMMA. The main difference with in-situ DEA comes with respect to the initial part of the curve: in the spinal custom model, ion viscosity is initially higher as there is no PMMA on the electrode. As soon as the bone cement reaches the surface of the electrode, its ion viscosity starts to be recorded, which is associated to the inflection of the curve. Full coverage of the electrode is necessary to have a representative evaluation of the bone cement viscosity. The progressive increase of ion viscosity then represents the slow increase of cement viscosity during polymerization. It is followed by a sudden and significant increase of ion viscosity that represents the curing phase of PMMA. Fig.114 explicits the different phases of DEA during in-situ analysis
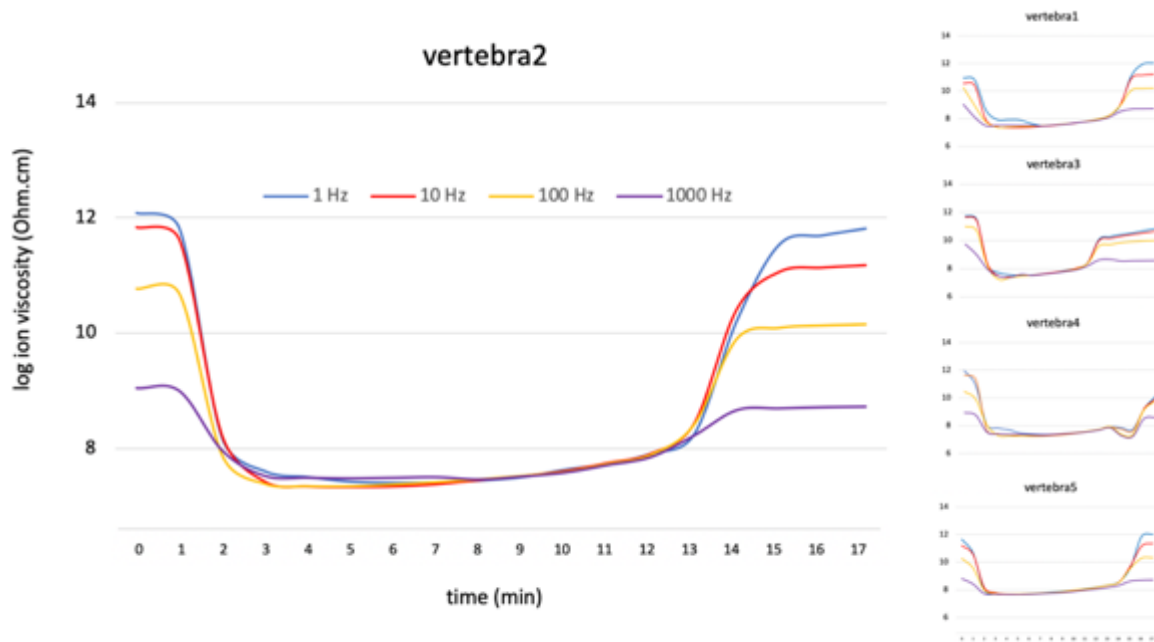
Fig113: Left: DEA of vertebra2; ion viscosity at the 4 frequencies of analysis is represented. Right: DEA of vertebra 1, 3, 4 and 5.
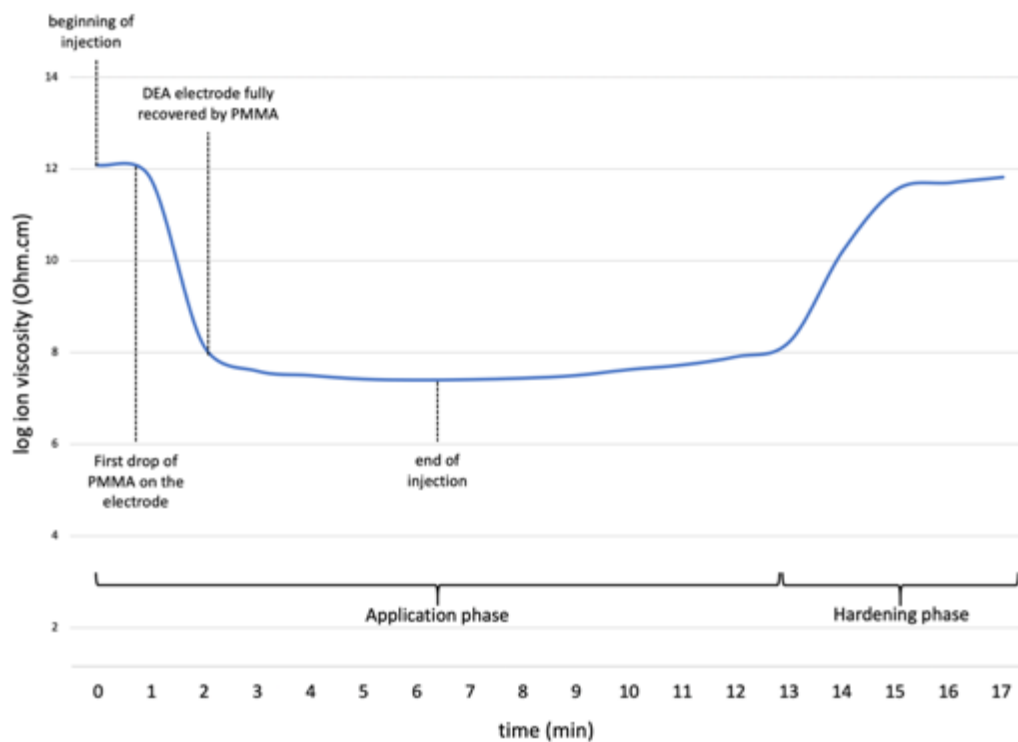
Fig.114: interpretation of ion viscosity during in-situ DEA

The ability of ion viscosity to detect the reticulation process is further confirmed by the synchronous measurement of the temperature (fig.115), which shows that the peak temperature during curing of PMMA corresponds to the increase of ion viscosity.

142
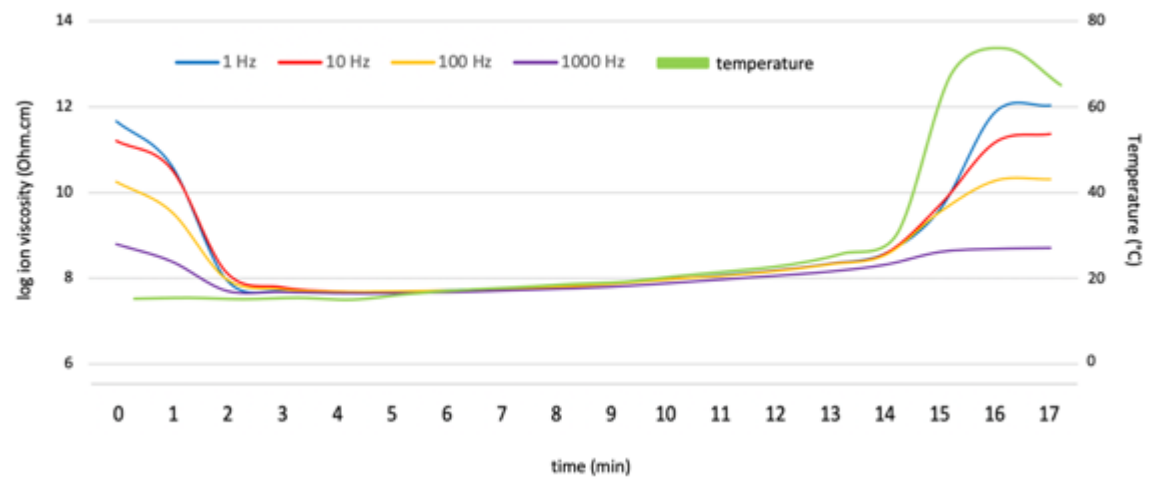
Fig.115: Temperature and ion viscosity (vertebra5).

DEA of all levels at each frequency is shown in fig116. An earlier curing phase for level 3 and a delayed curing phase for level 4 were detected in-situ. These discrepancies may be explained by slight differences in the testing conditions (temperature, rate of injection).
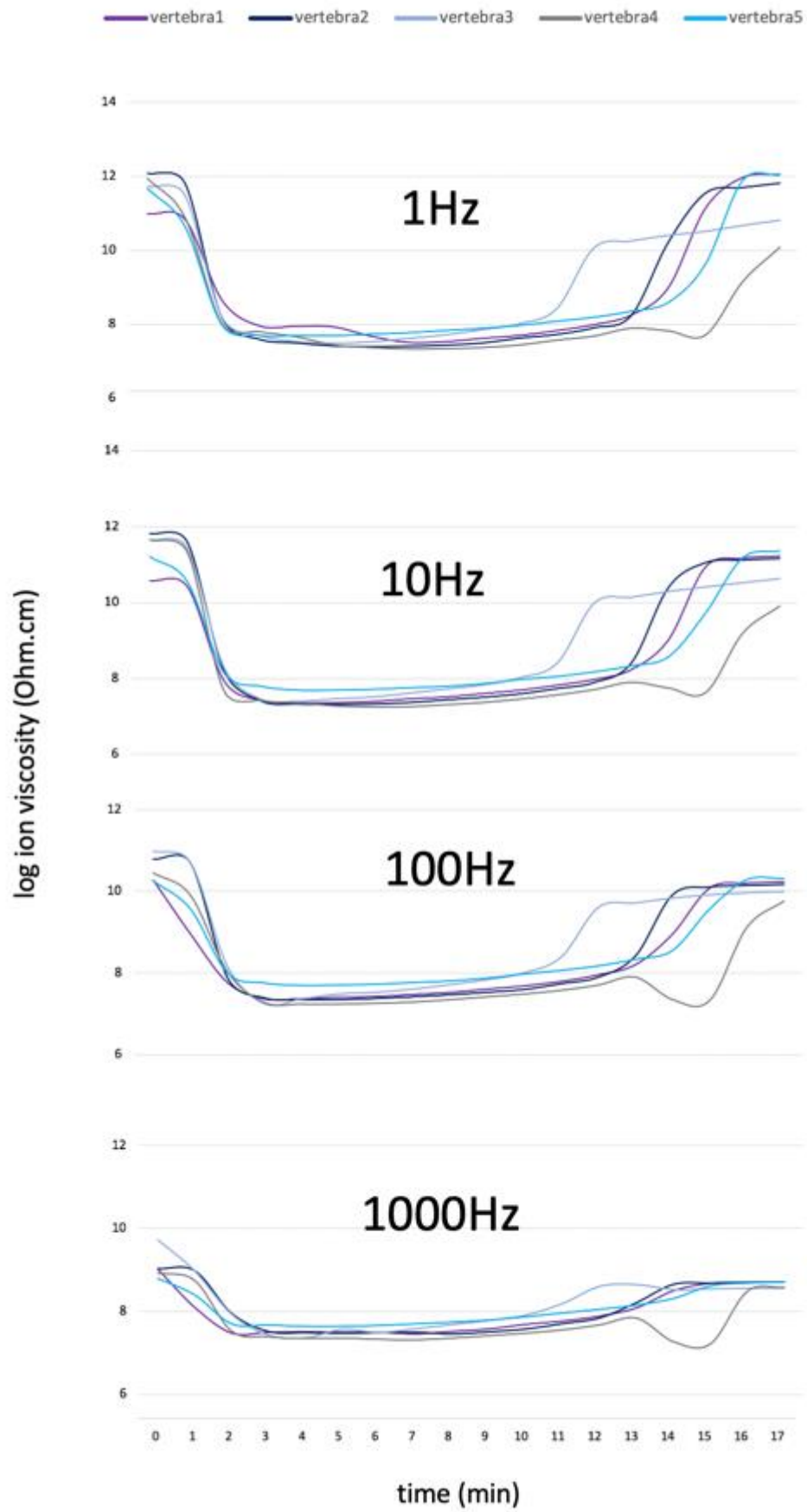
Fig.116: Values of DEA for all levels depending on the frequency of analysis, for all the vertebra.

Macroscopic evaluation of the inner structure of the spinal model confirmed that all DEA electrodes were completely covered by PMMA bone cement (fig.117).
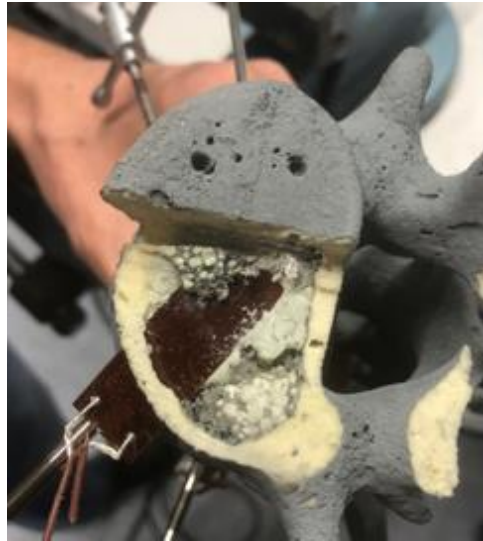
Fig.117: Post-experimental evaluation of the spinal model. The PMMA bone cement in green is in contact with the active face of the DEA electrode.

5.2.4. Discussion

The previous results confirm the feasibility of DEA to monitor the evolution of bone cement viscosity. It was not only effective for a sample of PMMA, but also for in-situ measurements during the simulation of vertebroplasty procedures. In the present study, the theoretical correlation between ion viscosity and dynamic viscosity was confirmed experimentally: ion viscosity correlates with dynamic viscosity independently from the temperature. Hence, ion viscosity has the potential to monitor the modification of PMMA from a liquid to a solid state. The experiments also assess the mathematical description of DEA that started this chapter, in particular with respect to the frequency dependent and frequency independent components of viscosity. As it can be observed from fig. 17, before the curing phase, the signal arises from the alignment of ions that is frequency independent. Once the bone cement starts to harden, the values of ion viscosity begin to differ depending on the frequency of analysis. This is due to the progressive contribution of the MMA molecules (i.e. dipoles) in the DEA signal. The curing phase therefore represents the limit of the domain of validity of ion viscosity (fig.118). On the other hand, ion viscosity still is proportional to dynamic viscosity.
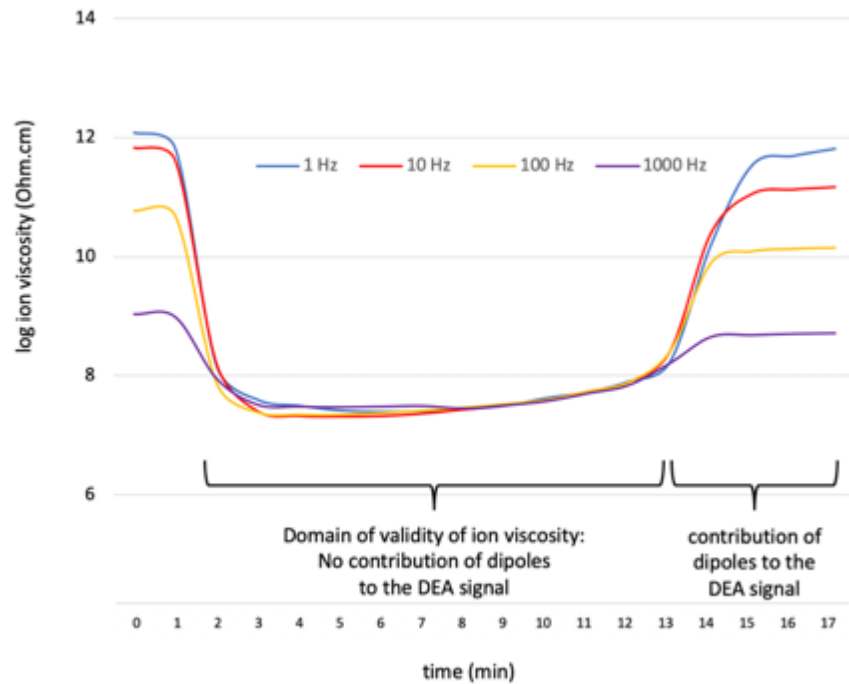
Fig.118: Domains of validity of ion viscosity (vertebra2).

The choice of the optimal frequency of analysis does not seem to be critical, as there is no significant difference between the 4 tested frequencies (1Hz, 10Hz, 100Hz and 1000Hz) during the first ten minutes, before curing of bone cement.

The major potential interest of the presented results for clinical practice is to provide real-time evaluation of the bone cement viscosity inside the bone, as only limited knowledge and literature is available. Viscosity has been shown to be a predictive factor to improve distribution of PMMA within the bone and avoid leakages. Based on the literature, the optimal viscosity interval for injection ranges between 200 and 2000 Pa.s [Bohner 2003, Lepoutre 2019]. Unfortunately, the intervening physician is blinded to those values by the time of injection. Some authors have advocated for the use of a dynamic rheometer to calculate the dynamic viscosity of a sample of PMMA prior to injection [Bohner 2003]. However, this approach is not compatible with the practice in the clinical routine. Moreover, it does not allow to evaluate the thermal impact on cement viscosity, as the local temperature inside the bone differs from the in-room temperature. In this perspective, DEA could be of valuable interest. Based on the present results, the ideal window for injection using log of ion viscosity at 1 Hz ranges between 7.4 and 7.8 Ohm.cm, which corresponds to a dynamic viscosity ranging from 200 to 2000 Pa.s. Vertebra4 was the only level where the minimal value of log ion viscosity was below the lower threshold: it was equal to 7.34 Ohm.cm 7 minutes after the beginning of injection, which corresponds to a dynamic viscosity less than 100 Pa.s. This suggests that bone cement was certainly too fluid by the time of injection in that case. Not surprisingly, delayed onset of the hardening phase happened. This further suggests the good correlation between DEA and the thermosetting reaction of PMMA. Current limitations for an extension to a clinical testing include the size of the DEA electrodes

146

and the need for an additional access inside the bone that preclude the human feasibility. One theoretical approach could be the integration of a DEA electrode at the tip of the bone trocar, thereby allowing real monitoring at the injection site.

5.3. Robotic assistance to the injection of a large volume of bone cement

The delivery of a large volume of bone cement through a single bone trocar appears as the best solution. The application phase of the bone cement therefore needs to be extended as much as possible to offer the possibility to deliver the cement slowly, to avoid leakages, and without being in a hurry because of the fear of an early polymerization. High viscosity bone cements have been designed for such purpose. However, their working time rarely exceeds 20 minutes in the clinical practice. Moreover, there is no delivery system on the market adapted for the injection of a large volume of cement. During the evaluation of the different techniques in section 2.2., the simultaneous mixing of several bone cement kits and the use of a simple 30 ml syringe allowed us to deliver a volume of up to 30 ml through a single bone trocar without the need for any exchange of the delivery system. The injection speed however had to be high to avoid early polymerization, which makes it unsuitable for the clinical practice. Robotic devices for the injection of bone cement have been developed by different groups. The S-tronic robot, developed in our research group, is a remotely controlled injection device designed for vertebroplasty that allows to extend the injection time of bone cement while regulating the viscosity [Lepoutre 2019]. The purpose of the present section is to present the modifications applied to the S-tronic in order to allow the single injection of up to 30 ml of PMMA bone cement.

5.3.1. The S-tronic robot

The components of the S-tronic robot are presented in fig.119
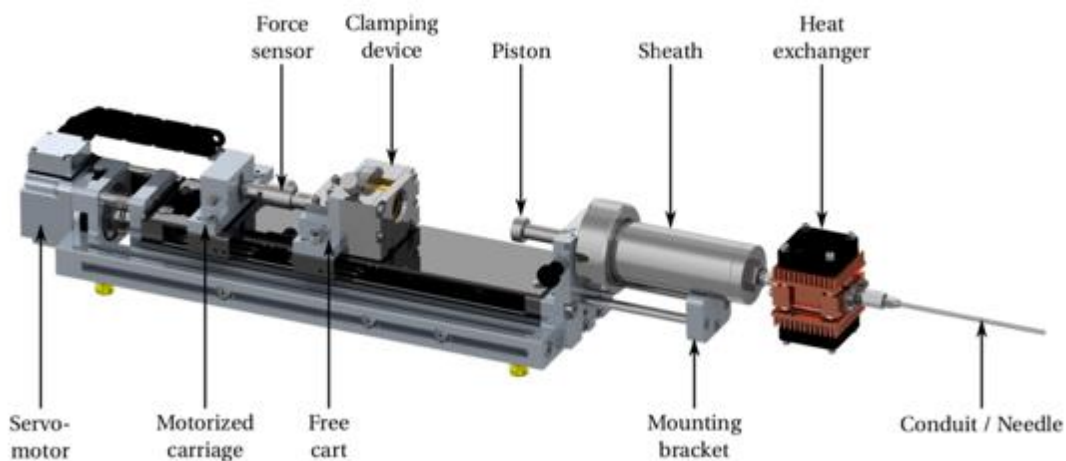
Fig.119: components of the S-tronic robot

The injection device is based on a ball screw linear axis, which transforms the rotation of a high-torque motor into a linear translation, in order to push the piston of the cement-filled syringe with pressures up to 140 bar. The linear axis combines a linear guide and a ball screw, with a pitch of 5 mm, a dynamic load of 1830 N and a static load of 2390 N. A manual clamping device with a limit switch is placed on the free cart to grip the syringe piston. The

motorized carriage is coupled to the free one through a 2 kN uniaxial tension-compression force sensor in order to measure the injection force applied to the piston. At the end of the guide, a mounting bracket allows to easily plug and remove the sheath holding the syringe filled beforehand with bone cement. The sheath is machined out of stainless steel in order to provide a high resistance both to pressure and to various chemical products. Passive cooling of the bone cement is carried out by filling cavities inside the sheath with eutectic gel. The sheath offers a fixation on its back that can interface with the mounting bracket. Thanks to a screw and nut assembly, the disposable syringe can easily be introduced and removed. Finally, at the outlet of the syringe, a heat exchanger, and a conduit are connected one after another. With the additional cover that has been designed to protect the internal elements, the overall dimension of the system reaches 54 cm×12 cm×10 cm for a mass of approximately 10 kg. The robot is remotely controlled which enables the intervening physician to move away from the source of X-ray thereby reducing scattered radiations to the medical staff.

5.3.2. Adaptation of the robot for the injection of a large volume of bone cement

The modification of the delivery system of the robot was a step by step procedure from the choice of a 30 ml syringe, its reinforcement by a dedicated sheath and the cooling of the syringe-sheath set.

5.3.2.1. 30 ml syringe

The syringe chosen to contain a large volume of bone cement is a polypropylene reusable syringe commercialized by Ardes and supposed to resist to all pharmaceutical products. It has a 30 ml capacity (fig.120). The tip is luer-lock made of stainless steel. The device is sterilizable in the autoclave.

Fig.120: 30 ml syringe

5.3.2.2. Sheath

The aluminum sheath is designed to hold the syringe, connect it to the robot via the piston and reinforce the syringe externally to avoid deformation and breakage.

5.3.2.2.1 Determination of the maximal threshold pressure with the current delivery system

148

The syringe that comes with the delivery system used in the clinical practice (Cemento mini-set, Optimed, Germany) is made of polycarbonate. The mechanical properties of polycarbonate can be approached through its Young modulus $E = 2$ GPa and elastic limit $\sigma_e = 80$ MPa. Using Creo Parametric, a computer assisted design of a quarter of the syringe was created. The simulation revealed that the elastic limit was reached for a force of 17 MPa inside the syringe (fig.121)
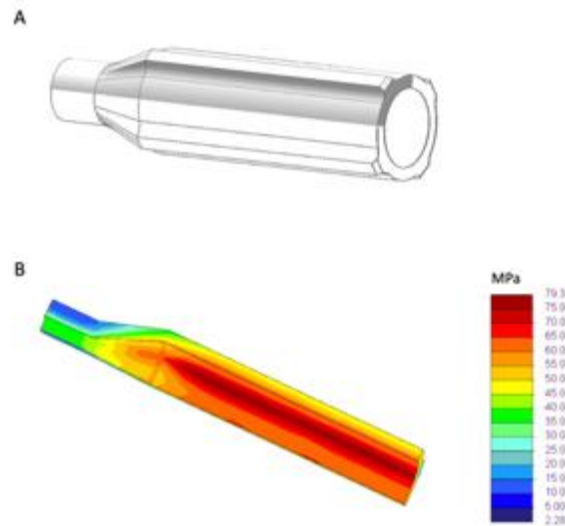
Fig.121: Finite element analysis. (A) Computer assisted design of the syringe of the Cemento mini-set. (B) Finite element analysis with a 17 MPa pressure inside the syringe ([Marche 2019])

The simulation was confronted to an experiment conducted with the traction testing machine (Zwick Roell, 2005). The pressure when the syringe breaks is around 16 MPa, demonstrating a good correlation with the numerical simulation (fig.122). This corresponds approximatively to a force of 3200N applied on the handle of the delivery system
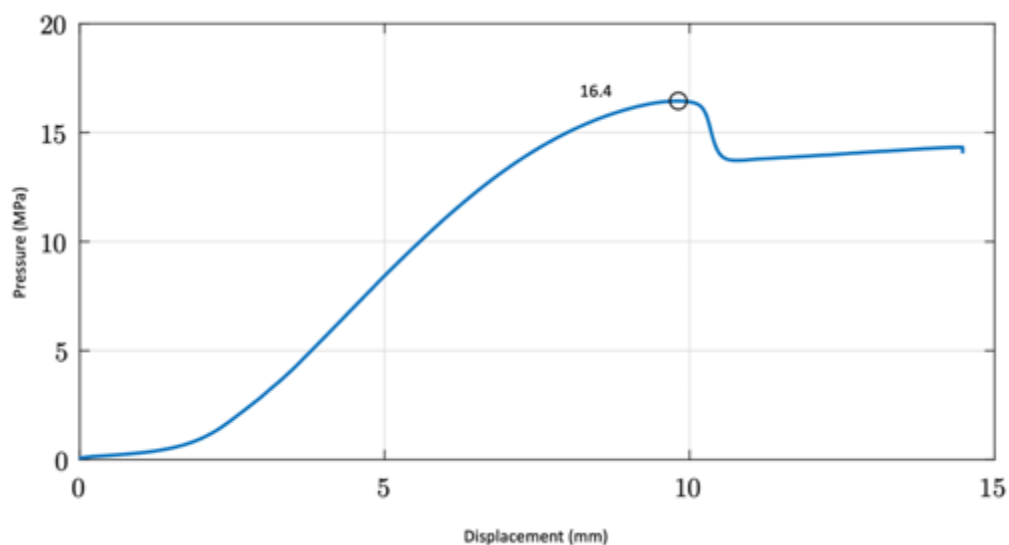
Fig.122: Results of the experiment: the syringe fails for a force of 16.4 MPa.

5.3.2.2.2. Design of the sheath for the 30 ml syringe

Given the good correlation between the CAD and the experiment, a finite element analysis was conducted. The goal was to determine the acceptable play between the inner surface of the aluminum sheath and the outer surface of the 30 ml syringe that would lead to a resistance to an internal pressure of 17 MPA as calculated previously. The elastic limit of the syringe was set as the one of the polypropylene σ_e = 50 MPa. With a 0.1 mm play and an internal stress of 17 MPa, the calculated pressure was beyond the elastic limit of the polypropylene (fig.123)
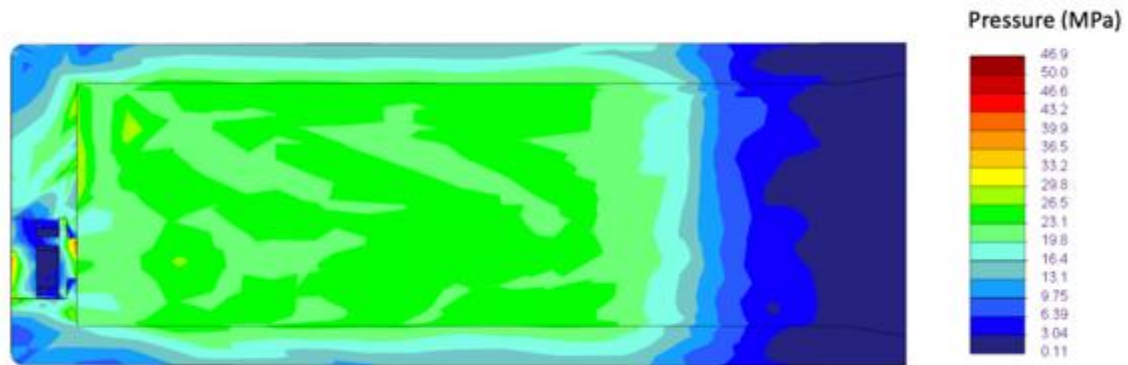
Fig.123: Stress inside the syringe simulated with a 0.1mm play and a 17 MPa pressure ([Marche 2019])

5.3.2.2.3. Fabrication of the sheath for the 30 ml syringe

The sheath was manufactured with 7075 aluminum alloy. It was designed to have a maximal 0.1 mm play with the outer surface of the syringe and to connect with the cap of the S-tronic Robot (fig.124)
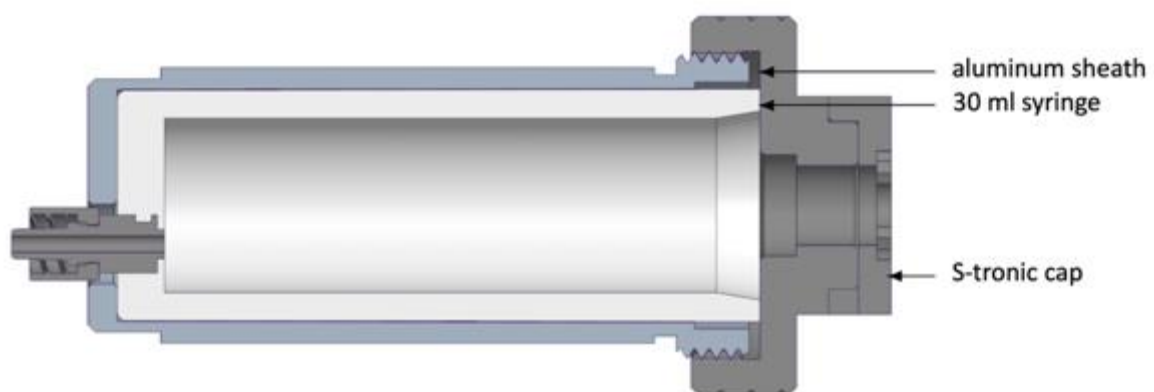
Fig.124: Design of the sheath for the 30 ml syringe ([Marche 2019])

5.3.2.3. Cooling of the syringe-sheath set

The continuous monitoring of the temperature inside a 30 ml syringe filled with 30 ml of PMMA bone cement (Osteopal V, Heraeus Medical) demonstrated that the application phase was lasting for 16 minutes, which does not differ from a 10 ml volume of bone cement (fig.125).
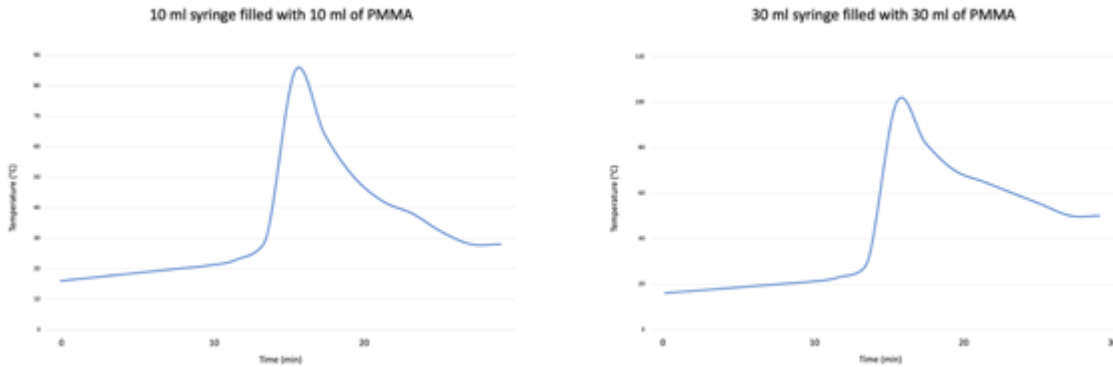
Fig.125: Temporal evolution of the temperature inside 10- and 30- syringes filled with PMMA. The peak temperature occurs at the same time. The 30 ml volume of bone cement cures at a higher level than the 10 ml volume.

As the experiment was conducted at room temperature, one could even expect a shorter working time in the clinical conditions where the bone cement is deposited at a higher temperature. As seen in the first chapter of the thesis, temperature has an (exponential) influence on the reaction of polymerization: lowering the temperature significantly extends the duration of injectability of the cement as it lowers the viscosity [Nussbaum 2004, James 2006]. Same principle is applied for the robot injection with passive cooling of the bone cement thanks to the sheath that can be stored in the fridge. On a cadaver study, this set-up allowed to extend the application phase of a low-viscosity bone cement from 10 minutes to around 30 minutes [Lepoutre 2019]. Such a working time would be perfectly adapted to the injection of a large volume of bone cement. Hence, the sheath should not only reinforce the resistance of the syringe but also ensure cooling and isolation of the bone cement. In this perspective, an additional external sheath was machined using additive fabrication and filled with an eutectic gel (Cryomed gel, Medicold) (fig.126).

Fig.126: Design of the PLA case filled with eutectic gel to ensure cooling of the aluminum sheath

The eutectic gel has a high thermal capacity that makes it theoretically suitable to ensure prolonged cooling. A 30 ml syringe filled with 30 ml of PMMA bone cement (Osteopal V, Heraeus Medical) was positioned inside the PLA case – eutectic gel – aluminum sheath that was stored in the fridge at 6°C for 2 hours prior to its use. Temperature monitoring inside the syringe demonstrated that the hardening phase was now occurring 34 minutes after end of cement preparation (fig.127). The cooled syringe – sheath set effectively allowed to double the application phase experimentally thereby achieving the prerequisite for the injection of a large volume of bone cement.
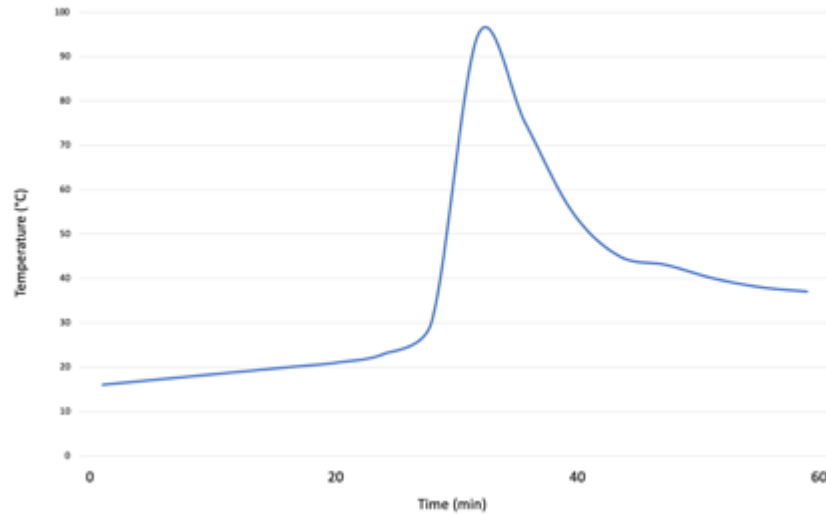
Fig.127: Temporal evolution of the local temperature inside a 30 ml syringe positioned in the aluminum sheath surrounded by the PLA case and its eutectic gel cooled in the fridge at 6°C for 2 hours. The peak temperature occurs at 34 min.

5.3.3. Robotic injection of PMMA bone cement with the large volume sheath

The compatibility of the new sheath with the S-tronic robot was confirmed experimentally. The back of the sheath was plugged to the piston similarly to the 10 ml sheath designed for vertebroplasty. The heat exchanger, which was originally designed to control thermally cement viscosity at the exit of the sheath, was not used in combination with the large volume sheath. As there was no pelvic phantom available at the time of the tests, the experiment was conducted on a spinal foam osteoporotic model (Sawbones Europe AB). Three cement kits (Osteopal V, Heraeus Medical, Germany) were hand-mixed manually all together and subsequently deposited in the 30 ml syringe positioned in the aluminum sheath (as shown in fig.126). The sheath was introduced in the PAL case with the cooled eutectic gel and plugged to the robot. The luer lock of the syringe was connected to the bone needle via the dedicated extension kit (fig.128). The injection was robotically controlled with an injection rate of 1ml/min. A total of 30 ml was injected inside 3 consecutive vertebrae (10 ml per vertebral level) using a single syringe, thereby confirming the long-lasting application phase achieved with the device. The injection force applied to the piston was below 1800N during the entire injection.

Fig.128: Robotic injection of a large volume of cement. (A) Installation of the robot and the computer in the CBCT suite. (B) Remote control of the robot. (C) Overview of the robot. The sheath surrounded by the eutectic gel is plugged to the piston on one side and to the bone trocar on the other side

5.3.4. Discussion

The S-tronic robot was originally designed to assist cement injection in the spine. The cooled sheath allowed to increase the injection time above half an hour while the heat exchanger was designed to increase cement viscosity before it entered the bone trocar [Lepoutre 2019]. The goal was to perform the injection with a predictable and stable viscosity. For the injection of a large volume of bone cement, the lengthening of the application phase is mandatory. It allows to proceed with an injection rate compatible with the radiological control of proper cement repartition. For that specific purpose, the passive cooling of the sheath seems sufficient without the need for a heat exchanger, keeping in mind that the application phase may be shorter in a patient than in a custom model due to the higher temperature. Two advantages of robotic assistance seem paramount when considering the injection of one large volume of cement through a single needle. First, the applied force is greater than the one of a manual injection which allows to actually take advantage of the increase of the application phase. Hence, it allows to get rid of the major concern about the required force for injection identified with the single trocar technique during the experiment on phantoms. Second, the remote control allows the radiologist to take some distance from the radiation source. As cement injection is performed under continuous fluoroscopic monitoring, it is the main source of scattered radiation during a cementoplasty procedure. Robotic assistance offers the ability to completely get away from the X-ray source. One major current limitation of the S-tronic robot is the size of the device, which makes it hardly compatible with the clinical practice.

154

5.4. Conclusion

Some solutions to the different problematics related to the injection of a large volume of bone cement have been proposed and evaluated. For the pelvic bones, it is possible to approach the most important weight-bearing areas in their longer axis. It is also possible to monitor the cement viscosity inside a bone structure through the measure of ion viscosity. Finally, the use of passive cooling and remote control of injection can increase the application phase of a large volume of PMMA bone cement. The combination of all three parameters could be beneficial to assist the injection of a large volume of cement with maximum efficacy and safety.

Conclusion and perspectives

Percutaneous extra-spinal cementoplasty is a percutaneous image-guided procedure which consists to inject bone cement within a pathological bone. It is derived from spinal cementoplasty, also known as vertebroplasty, whereby treatment of painful of osteoporotic or malignant fractures of the vertebral body is provided. Extra-spinal cement injection was initially most exclusively being indicated for the management of painful bone metastases refractory to radiation therapy. With the increase of survival in oncological patients, a growing field of application of cementoplasty is bone consolidation in addition to pain palliation. The intervention is essentially performed with Polymethylmetacrylate (PMMA) acrylic bone cement, which offers a good efficacy/safety/cost ratio.

Although the principle of extra-spinal cementoplasty is very similar to the one of vertebroplasty, there are some practical differences notably regarding the volume of PMMA. If pain alleviation does not seem to be related to the amount of bone cement, bone consolidation may be affected by the quantity of PMMA. As mechanical reinforcement is an increasing indication of extra-spinal cementoplasty in patients suffering from cancer, the volume of bone cement may become a subject of concern. Most of the cement delivery devices are designed for injection in the spine. As a result, the volume of PMMA that can be injected with one device barely exceeds 10 ml, which is not always adapted for extra-spinal cases. 10 ml of PMMA can therefore be seen as a threshold above which it can be considered as a large volume of cement. The use of several needles to deliver several small volumes of bone cement in the same area may be a solution to achieve the injection of a final large volume. However, this approach may present some drawbacks, such as difficulties to monitor cement injection and lack of cohesion of the final cement plug, that have not been addressed in the literature. The injection of a large volume through a single needle may be seen as an attractive solution yet there is no specific device for this purpose. Besides simple quantitative considerations, the injection of a unique large volume of cement needs to solve anatomical and polymerization constraints before it can be offered as a viable solution.

In the first chapter of the thesis, a review of the literature about extra-spinal cementoplasty is presented. It outlines notably that the pelvic bone is the most frequent treated bone with variable volumes of cement and lack of description/standardization of the technique to achieve the injection of a large volume of bone cement. A narrative review on the properties of PMMA is then conducted to identify the most important working properties and mechanical effects of acrylic bone cement. Of note, viscosity is a key parameter for cement dispersion within bone and strength and stiffness seem to depend on the volume of PMMA. As the pelvic girdle is the most frequent site of extra-spinal cementoplasty, a review of the biomechanics of the osseous pelvis is performed. It identifies the supra-acetabular area as the most important weight-bearing zone for which PMMA reinforcement seems well adapted as it is mostly loaded with compression. An evaluation of the clinical practice is then presented. The technique to injection a large volume of cement through a single needle with multiple vertebroplasty delivery systems is described. A retrospective study of the filling of acetabular osteolysis by PMMA is performed and demonstrates that the filling rate in the clinical practice stands below 50%. Finally, the analysis of delayed fragmentation of the cement plug is presented. It shows that it is an uncommon finding and that porosity consequently appears as a non-relevant working property of PMMA contrary to viscosity.

In the second chapter, the mechanical influence of the volume of PMMA is analyzed through experimental and numerical studies. A tumor model with two different volumes of acetabular lesions with cortex destruction is created on foam pelvic bone models. Biomechanical testing is performed with a traction machine on models with different rates of filling with PMMA. The results show a linear relation between the amount of cement and the restoration of stiffness. A finite element analysis if then presented. The step by step method to compute the numerical models of bone is described. The comparison of experimental data and numerical simulation using cemented humerus validates the method. Simulation on different pelvic tumor models are conducted. For a 20 ml tumor model with cortical destruction, it demonstrates that cement injection has the potential to restore completely stresses above a 50% filling rate and to partially restore stiffness with an exponential relation between the quantity of cement and the level of stiffness. The results of this chapter confirm the mechanical need for the injection of a large volume of bone cement in the pelvic bone.

In the third chapter, the different techniques to achieve the injection of a large volume of cement are compared. First, a numerical simulation of injection is proposed. After describing the theory, the results of the simulation of the flow of PMMA in a sphere, a vertebral mold and a humeral geometry are presented. It notably shows that the increase of viscosity around the injection point happens in case of a dual injection on a single needle. For the simultaneous injection on two different injection points, the progression of the polymerization of cement is not completely synchronous, suggesting that it can lead to non-cohesive plugs of cement. An experimental comparison is then performed with dedicated pelvic phantoms. The method to fabricate pelvic phantoms with lattice structures is described in detail. Two volumes of cement (20 ml and 30 ml) are then injected in the models with 3 different approaches: simultaneous injection on several trocars (10 ml per trocar), sequential injection on several trocars (10 ml per trocar) and single injection of a large volume on one needle (30 ml per trocar). The subjective appreciation, radiological and mechanical results are presented. The single injection appears to be the ideal solution after considerations of all ratings. However, major issues with this approach are the need for specific anatomical access and the lack of device able to deal with viscosity and force to injection.

In the last chapter, some solutions to provide the assistance to the injection of a large volume of bone cement are proposed. Two anatomical approaches to the supra-acetabular are proposed and validated through the retrospective analysis of pelvic CT-scans. As viscosity has been identified as critical parameter of cement diffusion during injection, a method to monitor viscosity inside a bone structure is proposed and analyzed on a phantom spinal model. Dielectrical analysis can explore the parameters of material trough the study of the polymerization of ions and dipoles. For a polymer like PMMA, the free ions correspond to impurities and the dipoles to the molecules of MMA. Mathematically, there is a link between the dynamic viscosity and ion viscosity. This was verified experimentally. The experimental study in the phantom model demonstrates that ion viscosity is representative of the progression of polymerization and allows to evaluate dynamic viscosity. It could therefore be used to perform the injection in the optimal ranges of viscosity. This could be particularly helpful for the injection of a large volume of bone cement. Finally, the adaptation of the S-tronic robot originally designed for vertebroplasty is detailed. It includes the design of a specific sheath to increase the application phase of PMMA via passive cooling. Thanks to the newly designed injection device, the injection can be increased up to half an hour. This allows to deliver a large amount of cement with maximum safety thanks to the slow progression of the cement flow.

Many experiments conducted during the present thesis would benefit for further explorations. The numerical models used for the finite element analysis of the influence of cement volume and the simulation of cement flow included simplified parameters of bone and PMMA. Inclusion of more detailed characteristics of bone and cement as well as other structures such as ligaments and muscles would allow to increase the precision of these simulations. The experimental biomechanical study on pelvic phantoms with a tumor model used also a simplified and not completely physiological load on the acetabulum. These limitations are inherent to all preclinical models but there is a way to make these models more realistic. Same is the case with the pelvic phantoms as additive fabrication of items with smaller scales of lattice structures would certainly represent a more physiologic model. Nevertheless, the injection of a large volume of bone cement appears as a need and may be facilitated by specific devices.

The present work opens some perspectives. Besides improvement of the models, the different simulations presented in the thesis may also be used to explore more than just PMMA. Percutaneous screw fixation is more and more proposed in combination with bone cement but with little preclinical investigations. It may be studied with the different models presented in the thesis. The design of a dedicated delivery system for a large volume of bone cement has been proposed. The next step is to adapt it for the clinical practice. Miniaturization, optimization of the connections and interface have to be made. The measure of ion viscosity also has to be transposed to the real practice; this could be done through the integration of the technology in dedicated bone trocars. The ultimate goal would be to design devices (needles, cement delivery system, PMMA kit) adapted for the specificities of extra-spinal cementoplasty.

References

Alageel O, Abdallah MN, Luo ZY, et al. Bonding metals to poly(methyl methacrylate) using aryldiazonium salts. Dent Mater. 2015 Feb;31(2):105-14. doi: 10.1016/j.dental.2014.11.002.

Anselmetti GC, Manca A, Ortega C, et al. Treatment of extraspinal painful bone metastases with percutaneous cementoplasty: a prospective study of 50 patients. Cardiovasc Intervent Radiol 2008;31:1165—73.

Anselmetti GC, Manca A, Kanika K, et al. Temperature measurement during polymerization of bone cement in percutaneous vertebroplasty: an in vivo study in humans. Cardiovasc Intervent Radiol. 2009 May;32(3):491-8. doi: 10.1007/s00270-009-9509-7.

Anselmini R. *Simulation de l'écoulement du ciment orthopédique en cimentoplastie*. Mémoire de diplôme d'ingénieur et de Master. Institut National des Sciences Appliquées de Strasbourg. Faculté de Physique et Ingénierie de l'Université de Strasbourg. 2020.

Aziz SB, Abdullah RM, Rasheed MA, et al. Role of Ion Dissociation on DC Conductivity and Silver Nanoparticle Formation in PVA:AgNt Based Polymer Electrolytes: Deep Insights to Ion Transport Mechanism. Polymers (Basel). 2017 Aug 4;9(8):338. doi: 10.3390/polym9080338. PMID: 30971015; PMCID: PMC6418533.

Aziz SB, Karim WO, Brza MA, et al. Ion Transport Study in CS: POZ Based Polymer Membrane Electrolytes Using Trukhan Model. Int J Mol Sci. 2019 Oct 23;20(21):5265. doi: 10.3390/ijms20215265. PMID: 31652832; PMCID: PMC6862139.

Barba D, Alabort E, Reed RC. Synthetic bone: Design by additive manufacturing. Acta Biomater. 2019 Oct 1;97:637-656. doi: 10.1016/j.actbio.2019.07.049. Epub 2019 Aug 5. PMID: 31394295.

Basile A, Giuliano G, Scuderi V, et al. Cementoplasty in the management of painful extraspinal bone metastases: our experience. Radiol Med 2008;113:1018—28.

Bauones S, Freire V, Moser TP. Retrograde Transpubic Approach for Percutaneous Radiofrequency Ablation and Cementoplasty of Acetabular Metastasis. Case Rep Radiol. 2015;2015:146963. doi:10.1155/2015/146963

Belkoff SM, Molloy S. Temperature measurement during polymerization of polymethylmethacrylate cement used for vertebroplasty. Spine (Phila Pa 1976). 2003 Jul 15;28(14):1555-9.

Berton A, Salvatore G, Giambini H, et al. A 3D finite element model of prophylactic vertebroplasty in the metastatic spine: Vertebral stability and stress distribution on adjacent vertebrae. J Spinal Cord Med. 2020 Jan;43(1):39-45. doi:10.1080/10790268.2018.1432309.

Bevill G, Keaveny TM. Trabecular bone strength predictions using finite element analysis of micro-scale images at limited spatial resolution. Bone. 2009 Apr;44(4):579-84. doi: 10.1016/j.bone.2008.11.020. Epub 2008 Dec 14. PMID: 19135184.

Bohner M, Gasser B, Baroud G, et al. Theoretical and experimental model to describe the injection of a polymethylmethacrylate cement into a porous structure. Biomaterials. 2003 Jul;24(16):2721-30.

Borzacchiello A, Ambrosio L, Nicolais L, et al. Comparison between the polymerization behavior of a new bone cement and a commercial one: modeling and in vitro analysis. J Mater Sci Mater Med. 1998 Dec;9(12):835-8.

Breusch S, Heisel C, Müller J, et al. Influence of cement viscosity on cement interdigitation and venous fat content under in vivo conditions: a bilateral study of 13 sheep. Acta Orthop Scand. 2002;73(4):409–415. doi:10.1080/00016470216320

Brown CJ, Sinclair RA, Day A, et al. An approximate model for cancellous bone screw fixation. Comput Methods Biomech Biomed Engin. 2013 Apr;16(4):443-50. doi: 10.1080/10255842.2011.624516.

Brown TS, Salib CG, Rose PS, et al. Reconstruction of the hip after resection of periacetabular oncological lesions: a systematic review. Bone Joint J. 2018;100-B(1 supply A):22–30. https://doi.org/10.1302/0301-620X.100B1.BJJ-2017-0548.R1.

Caracciolo JT, Temple HT, Letson GD, et al. A modified Lodwick-Madewell grading system for the evaluation of lytic bone lesions. AJR Am J Roentgenol. 2016;207(1):150–6. https://doi.org/10.2214/ajr.15.14368.

Castro JM, Macosko CW. "Studies of mold filling and curing in the reaction injection molding process". In : AIChE Journal 28.2 (mar. 1982), p. 250-260. issn : 0001-1541, 1547-5905. doi : 10.1002/aic.690280213.

Cazzato RL, Buy X, Eker O, et al. Percutaneous long bone cementoplasty of the limbs: experience with fifty- one non-surgical patients. Eur Radiol 2014;24:3059—68.

Cazzato RL, Palussière J, Buy X, et al. Percutaneous Long Bone Cementoplasty for Palliation of Malignant Lesions of the Limbs: A Systematic Review. Cardiovasc Intervent Radiol. 2015 Dec;38(6):1563-72. doi:10.1007/s00270-015-1082-7.

Cazzato RL, Garnon J, Shaygi B, et al. Percutaneous consolidation of bone metastases: strategies and techniques. Insights Imaging 2019;10:14.

Chandra V, Wajswol E, Shukla P, et al. Safety and efficacy of sacroplasty for sacral fractures: a systematic review and meta-analysis. J Vasc Interv Radiol. 2019;30(11):1845–54. https://doi.org/10.1016/j.jvir.2019.06.013.

Charles T, Ameye L, Gebhart M. Surgical treatment for periac- etabular metastatic lesions. Eur J Surg Oncol. 2017;43(9):1727–32. https://doi.org/10.1016/j.ejso.2017.03.018.

Charnley J. The bonding of prostheses to bone by cement. J Bone Joint Surg Br 1964;46:518–29.

Chavali R, Resijek R, Knight S, et al. Extending polymerization time of polymethylmethacrylate cement in percutaneous vertebroplasty with ice bath cooling. Am J Neuroradiol 2003;24:545-6.

Chevalier Y, Pahr D, Charlebois M, et al. Cement distribution, volume, and compliance in vertebroplasty: some answers from an anatomy-based nonlinear finite element study. Spine (Phila Pa 1976). 2008 Jul 15;33(16):1722-30. doi: 10.1097/BRS.0b013e31817c750b.

Chu Y, Nie S, Liu S, et al. Complex dielectric permittivity of metal and polymer modified montmorillonite. J Hazard Mater. 2019 Jul 15;374:382-391.doi: 10.1016/j.jhazmat.2019.04.066.

Coglitore D, Edwardson SP, Macko P, et al. Transition from fractional to classical Stokes-Einstein behaviour in simple fluids. R Soc Open Sci. 2017 Dec 13;4(12):170507. doi: 10.1098/rsos.170507. eCollection 2017 Dec.PubMed PMID: 29308217

Colman MW, Karim SM, Hirsch JA, et al. Percutaneous acetabuloplasty compared with open reconstruction for extensive periacetabular carcinoma metas- tases. J Arthroplasty 2015;30:1586—91.

Cotten A, Deprez X, Migaud H, et al. Malignant acetabular osteolyses: percutaneous injection of acrylic bone cement. Radiology 1995;197:307—10.

Cotten A, Boutry N, Cortet B, et al. Percutaneous vertebroplasty: state of the art. Radiographics. 1998 Mar-Apr;18(2):311-20

Cross, M. M. (1965). Rheoogy of non-Newtonian fluids: A new flow equation for pseudoplastic systems. *Journal of Colloid Science*, 20(5), 417–437. doi: 10.1016/0095-8522(65)90022-X

Coupal TM, Pennycooke K, Mallinson PI, et al. The hopeless case? Palliative cryoabla- tion and cementoplasty procedures for palliation of large pelvic bone metastases. Pain Physician 2017;20:E1053—61.

Couraud G, André-Pierre G, Titien T, et al. Evaluation of short-term efficacy of extraspinal cementoplasty for bone metastasis: a monocenter study of 31 patients. J Bone Oncol 2018;13:136—42.

Dalstra M, Huiskes R, Odgaard A, et al. Mechanical and textural properties of pelvic trabecular bone. J Biomech. 1993;26(4–5):523–35.

Dalstra M, Huiskes R. Load transfer across the pelvic bone. 29. J Biomech. 1995;28(6):715–24.

Delpla A, Tselikas L, De Baere T, et al. Preventive Vertebroplasty for Long-Term Consolidation of Vertebral Metastases. Cardiovasc Intervent Radiol. 2019 Dec;42(12):1726-1737. doi: 10.1007/s00270-019-02314-6.

Deramond H, Wright NT, Belkoff SM. Temperature elevation caused by bone cement polymerization during vertebroplasty. Bone. 1999 Aug;25(2 Suppl):17S-21S.

Deschamps F, Farouil G, Hakime A, et al. Cementoplasty of metastases of the proximal femur: is it a safe palliative option?. J Vasc Interv Radiol 2012;23:1311-1316.

Deschamps F, Farouil G, Hakime A, et al. Percutaneous stabilization of impending pathological fracture of the proximal femur. Cardiovasc Intervent Radiol 2012;35:1428—32.

Donanzam BA, Campos TP, Dalmázio I, et al. Synthesis and characterization of calcium phosphate loaded with Ho-166 and Sm-153: a novel biomaterial for treatment of spine metastases. J Mater Sci Mater Med. 2013;24(12):2873–2880. doi:10.1007/s10856-013-5024-0.

Dunne NJ, Orr JF. Flow characteristics of curing polymethyl methacrylate bone cement. Proc Inst Mech Eng H. 1998;212(3):199-207.

Durfee RA, Sabo SA, Letson GD, et ak. Percutaneous acetabuloplasty for metastatic lesions to the pelvis. Orthopedics 2017;40:e170—5.

Elder BD, Lo SF, Holmes C, et al. The biomechanics of pedicle screw augmentation with cement. Spine J. 2015;15(6):1432–1445. doi:10.1016/j.spinee.2015.03.016

Eriksson RA, Albrektsson T, Magnusson B. Assessment of bone viability after heat trauma. A histological, histochemical and vital microscopic study in the rabbit. Scand J Plast Reconstr Surg. 1984;18(3):261-8.

Erler D, Brotherston D, Sahgal A, et al. Local control and fracture risk following stereotactic body radiation therapy for non-spine bone metastases. Radiother Oncol. 2018;127(2):304–9. https://doi.org/10.1016/j.radonc.2018.03.030.

Fahlgren A, Bostrom MP, Yang X, et al. Fluid pressure and flow as a cause of bone resorption. Acta Orthop. 2010 Aug;81(4):508-16. doi: 10.3109/17453674.2010.504610.

Fares A, Shaaban MH, Reyad RM, et al. Combined percutaneous radiofrequency ablation and cementoplasty for the treatment of extraspinal painful bone metastases: a prospective study. J Egypt Natl Canc Inst 2018;30:117—22.

Friedman MV, Hillen TJ, Wessell DE, et al. Hip chondrolysis and femoral head osteonecrosis: a com- plication of periacetabular cryoablation. J Vasc Interv Radiol. 2014;25(10):1580–8. https://doi.org/10.1016/j.jvir.2014.06.016.

Garnon J, Meylheuc L, Bayle B. Injection Device for Percutaneous Osteoplasty. Seventh International Workshop on Medical and Service Robots" (MESROB2020)

Garnon J, Meylheuc L, Cazzato RL, et al. Percutaneous extra-spinal cementoplasty in patients with cancer: A systematic review of procedural details and clinical outcomes. Diagn Interv Imaging. 2019 Dec;100(12):743-752. doi: 10.1016/j.diii.2019.07.005.

Ghosh R, Pal B, Ghosh D, et al. Finite element analysis of a hemi-pelvis: the effect of inclusion of cartilage layer on acetabular stresses and strain. Comput Methods Biomech Biomed Eng. 2015;18(7):697–710. https://doi.org/10.1080/10255842.2013.843674.

Gibon E, Córdova LA, Lu L, et al. The biological response to orthopedic implants for joint replacement. II: Polyethylene, ceramics, PMMA, and the foreign body reaction. J Biomed Mater Res B Appl Biomater 2017 Aug;105:1685-1691.

Gibson IJ, Ashby MF. "The mechanics of three-dimensional cel- lular materials". In : Proceedings of the Royal Society of London. A. Mathematical and Physical Sciences 382.1782 (juil. 1982), p. 43-59. doi : 10.1098/rspa.1982. 0088. url : https://doi.org/10.1098/rspa.1982.0088.

Goetz MP, Callstrom MR, Charboneau JW, et al. Percutaneous image-guided radiofrequency ablation of painful metastases involving bone: a multicenter study. J Clin Oncol 2004;22:300—6.

Goodheart JR, Miller MA, Oest ME, et al. Trabecular resorption patterns of cement-bone interlock regions in total knee replacements. J Orthop Res. 2017 Dec;35(12):2773-2780. doi: 10.1002/jor.23586.

Goodman S. Wear particulate and osteolysis. Orthop Clin North Am 2005 Jan;36:41-8, vi.

Gupta AC, Hirsch JA, Chaudhry ZA, et al. Evaluating the safety and effectiveness of percutaneous acetabuloplasty. J Neurointerv Surg 2012;4:134—8.

Hammer N, Steinke H, Lingslebe U, et al. Ligamentous influence in pelvic load distribution. Spine J. 32. 2013;13(10):1321–30.https://doi.org/10.1016/j.spinee.2013.03.050.

Harper EJ, Bonfield W. Tensile characteristics of ten commercial acrylic bone cements. J Biomed Mater Res. 2000 Sep;53(5):605-16. doi: 10.1002/1097-4636(200009)53:5<605::aid-jbm22>3.0.co;2-5. Erratum in: J Biomed Mater Res 2001;58(2):216. PMID: 10984711.

Harrer L, Husser M. *Conception d'un modèle de simulation de bassins et humérus*. Mémoire de Projet de Recherche et Technologique. Institut National des Sciences Appliquées de Strasbourg. 2020.

He Z, Zhai Q, Hu M, et al. Bone cements for percutaneous vertebroplasty and balloon kyphoplasty: Current status and future developments. J Orthop Translat. 2014 Dec 12;3(1):1-11. doi: 10.1016/j.jot.2014.11.002.

He C, Tian Q, Wu CG, et al. Feasibility of percutaneous cementoplasty combined with interventional internal fixation for impending pathologic fracture of the proximal femur. J Vasc Interv Radiol 2014;25:1112—7.

Hesler MC, Buy X, Catena V, et al. Assessment of risk factors for occurrence or worsening of acetabular fracture following percutaneous cementoplasty of acetabulum malignancies. Eur J Radiol. 2019 Nov;120:108694. doi: 10.1016/j.ejrad.2019.108694.

Hierholzer J, Anselmetti G, Fuchs H, et al. Percutaneous osteoplasty as a treatment for painful malignant bone lesions of the pelvis and femur. J Vasc Interv Radiol 2003;14:773—7.

Hoey DA, Taylor D. Statistical distribution of the fatigue strength of porous bone cement. Biomaterials. 2009 Oct;30(31):6309-17. doi:10.1016/j.biomaterials.2009.07.053.

Hoffmann RT, Jakobs TF, Trumm C, et al. Radiofrequency ablation in combination with osteo- plasty in the treatment of painful metastatic bone disease. J Vasc Interv Radiol 2008;19:419—25.

Holt G, Murnaghan C, Reilly J, et al. The biology of aseptic osteolysis. Clin Orthop Relat Res 2007 Jul;460:240-52.

Hu P, Wu T, Wang HZ, et al. Influence of different boundary conditions in finite element analysis on pelvic biome-chanical load transmission. Orthop Surg. 2017;9(1):115–22. https://doi.org/10.1111/os.12315Epub 2017 Mar 16.

Huang AJ, Halpern EF, Rosenthal DI. Incidence of delayed complications following percutaneous CT-guided biopsy of bone and soft tissue lesions of the spine and extremities: a 2-year prospective study and analysis of risk factors. Skeletal Radiol. 2013 Jan;42(1):61-8. doi: 10.1007/s00256-012-1433-2.

Huang A, Fang S, Wang L, et al. Vertebral collapse and polymethylmethacrylate breakage after vertebroplasty: A case report. Medicine (Baltimore). 2019 Aug;98(34):e16831. doi: 10.1097/MD.0000000000016831.

Iannessi A, Amoretti N, Marcy PY, et al. Percutaneous cementoplasty for the treatment of extraspinal painful bone lesion, a prospective study. Diagn Interv Imaging. 2012;93(11):859–70.

James SL, Connell DA. The effect of temperature reduction on cement working time in percutaneous vertebroplasty. Clin Radiol. 2006 Sep;61(9):797-9.

Janssen D, Aquarius R, Stolk J, et al. The contradictory effects of pores on fatigue cracking of bone cement. J Biomed Mater Res B Appl Biomater 2005;74:747-753.

Joffre T, Isaksson P, Procter P, et al. Trabecular deformations during screw pull-out: a micro-CT study of lapine bone. Biomech Model Mechanobiol. 2017 Aug;16(4):1349-1359. doi: 10.1007/s10237-017-0891-9. Epub 2017 Mar 6. PMID: 28265781; PMCID: PMC5511599.

Jossinet J. Elementary electrodynamics. Technol Health Care. 2008;16(6):465-74. PMID: 19212042.

Kam NM, Maingard J, Kok HK, et al. Combined vertebral augmentation and radiofrequency ablation in the management of spinal metastases: an update. Curr Treat Options Oncol 2017; 18:74.

Kamal MR, Sourour S. Kinetic and thermal characterization of thermoset cure. Polym Eng Sci 1973;13(1):59-64

Kelekis A, Lovblad KO, Mehdizade A, et al. Pelvic osteoplasty in osteolytic metastases: tech- nical approach under fluoroscopic guidance and early clinical results. J Vasc Interv Radiol 2005;16:81—8.

Kelekis A, Filippiadis D, Anselmetti G, et al. Percutaneous augmented peripheral osteoplasty in long bones of oncologic patients for pain reduction and prevention of impending pathologic frac- ture: the rebar concept. Cardiovasc Intervent Radiol 2016;39: 90—6.

Kiapour A, Joukar A, Elgafy H, et al. Biomechanics of the sacroiliac joint: anatomy, function, biomechanics, sexual dimorphism, and causes of pain. Int J Spine Surg. 2020;14(Suppl 1):3–13. https://doi.org/10.14444/6077.

Kim YI, Kang HG, Kim TS, et al. Palliative percutaneous stabilization of lower extremity for bone metastasis using flexible nails and bone cement. Surg Oncol 2014;23:192—8.

Kim YI, Kang HG, Kim JH, et al. Closed intramedullary nailing with percutaneous cement augmentation for long bone metastases. Bone Joint J 2016;98: 703—9.

Kinzl M, Boger A, Zysset PK, et al. The mechanical behavior of PMMA/bone specimens extracted from augmented vertebrae: a numerical study of interface properties, PMMA shrinkage and trabecular bone damage. J Biomech. 2012 May 11;45(8):1478-84. doi: 10.1016/j.jbiomech.2012.02.012.

Klopfleisch R, Jung F. The pathology of the foreign body reaction against biomaterials. J Biomed Mater Res A. 2017;105:927–940.

Kolmeder S et al. "Thermophysical properties and material modelling of acrylic bone cements used in vertebroplasty". In : Journal of Thermal Analysis and Calorimetry 105.2 (août 2011), p. 705-718. issn : 1388-6150, 1572-8943. doi : 10. 1007/s10973-011-1508-7.

Kolmeder S, Lion A. Characterisation and modelling rheological properties of acrylic bone cement during application. Mech Res Commun. 2013;48:93-99. doi:10.1016/j.mechrescom.2012.12.010

Krause WR, Miller J, Ng P. The viscosity of acrylic bone cements. J Biomed Mater Res. 1982 May;16(3):219-43. doi: 10.1002/jbm.820160305. PMID: 7085686.

Kuehn K-D, Ege W, Gopp U. Acrylic bone cements: composition and properties. Orthop Clin North Am. 2005;36(1):17-28. doi:10.1016/j.ocl.2004.06.010

Kurtz SM, Villarraga ML, Zhao K, et al. Static and fatigue mechanical behavior of bone cement with elevated barium sulfate content for treatment of vertebral compression fractures. Biomaterials. 2005 Jun;26(17):3699-712.

Kurup AN, Morris JM, Schmit GD, et al. Balloon-assisted osteoplasty of periacetabular tumors following percutaneous cryoablation. J Vasc Interv Radiol. 2015 Apr;26(4):588-94. doi:10.1016/j.jvir.2014.11.023.

Kurup AN, Schmit GD, Atwell TD, et al. Palliative Percutaneous Cryoablation and Cementoplasty of Acetabular Metastases: Factors Affecting Pain Control and Fracture Risk. Cardiovasc Intervent Radiol. 2018 Nov;41(11):1735-1742. doi: 10.1007/s00270-018-1998-9.

Lai PL, Chen LH, Chen WJ, et al. Chemical and physical properties of bone cement for vertebroplasty. Biomed J. 2013 Jul-Aug;36(4):162-7. doi: 10.4103/2319-4170.112750.

Landgraf R, Ihlemann J, Kolmeder S, et al. Modelling and simulation of acrylic bone cement injection and curing within the framework of vertebroplasty. ZAMM - J Appl Math Mech Z Für Angew Math Mech. 2015;95(12):1530-1547. doi:10.1002/zamm.201400064

Lea WB, Neilson JC, King DM, et al. Minimally Invasive Stabilization Using Screws and Cement for Pelvic Metastases: Technical Considerations for the Pelvic "Screw and Glue" Technique. Semin Intervent Radiol. 2019 Aug;36(3):229-240.

Lee CH, Hsu CC, Huang PY. Biomechanical study of different fixation techniques for the treatment of sacroiliac joint injuries using finite element analyses and biomechanical tests. Comput Biol Med. 2017;1(87):250–7. https://doi.org/10.1016/j. compbiomed.2017.06.007.10.1055/s-0039-1693982.

Lee HL, The Handbook of Dielectric Analysis and Cure Monitoring. 2017.

Lepoutre N, Meylheuc L, Bara GI, et al. Bone cement modeling for percutaneous vertebroplasty. J Biomed Mater Res B Appl Biomater. 2019 Jul;107(5):1504-1515. doi: 10.1002/jbm.b.34242. Epub 2018 Sep 29. PMID: 30267639.

Lewis G. Properties of acrylic bone cement: state of the art review. J Biomed Mater Res. 1997 Summer;38(2):155-82.

Lewis G. Viscoelastic properties of injectable bone cements for orthopaedic applications: state-of-the-art review. J Biomed Mater Res B Appl Biomater. 2011;98(1):171–91. https://doi.org/10. 1002/jbm.b.31835Epub 2011 Apr 18.

Li Z, Butala NB, Etheridge BS, et al. A biomechanical study of periacetabular defects and cement filling. J Biomech Eng. 2007 Apr;129(2):129-36.

Liao JC, Lai PL, Chen LH, et al. Surgical outcomes of infectious spondylitis after vertebroplasty, and comparisons between pyogenic and tuberculosis. BMC Infect Dis 2018;18:555.

Lieberman IH, Togawa D, Kayanja MM. Vertebroplasty and kyphoplasty: filler materials. Spine J. 2005 Nov-Dec;5(6 Suppl):305S-316S.

Ling RS, Lee AJ. Porosity reduction in acrylic cement is clinically irrelevant. Clin Orthop Relat Res 1998 Oct:249-53.

Liu D, Zhang Y, Zhang B, et al. Comparison of expansive pedicle screw and polymethylmethacrylate-augmented pedicle screw in osteoporotic sheep lumbar vertebrae: biomechanical and interfacial evaluations. PLoS One. 2013 Sep 23;8(9):e74827. doi:10.1371/journal.pone.0074827.

Liu Y, Xu J, Sun D, et al. Biomechanical and finite element analyses of bone cement-Injectable cannulated pedicle screw fixation in osteoporotic bone. J Biomed Mater Res B Appl Biomater. 2016 Jul;104(5):960-7.doi: 10.1002/jbm.b.33424.

Loeffel M, Ferguson SJ, Nolte LP, et al. Vertebroplasty: experimental characterization of polymethylmethacrylate bone cement spreading as a function of viscosity, bone porosity, and flow rate. *Spine (Phila Pa 1976)*. 2008;33(12):1352–1359. doi:10.1097/BRS.0b013e3181732aa9.

Luo J, Daines L, Charalambous A, et al. Vertebroplasty: only small cement volumes are required to normalize stress distributions on the vertebral bodies. Spine (Phila Pa 1976). 2009 Dec 15;34(26):2865-73. doi: 10.1097/BRS.0b013e3181b4ea1e.

Maccauro G, Liuzza F, Scaramuzzo L, et al. Percutaneous acetabuloplasty for metastatic acetab- ular lesions. BMC Musculoskelet Disord 2008;9:66.

Marche C. *Etude de l'injection et de la tenue mécanique de gros volumes de PMMA pour la cimentoplastie*. Mémoire diplôme d'ingénieur. Institut National des Sciences Appliquées de Strasbourg. 2019.

Marcy PY, Palussière J, Descamps B, et al. Percutaneous cementoplasty for pelvic bone metasta- sis. Support Care Cancer 2000;8:500—3.

Miller MA, Terbush MJ, Goodheart JR, et al. Increased initial cement-bone interlock correlates with reduced total knee arthroplasty micro-motion following in vivo service. J Biomech. 2014 Jul 18;47(10):2460-6. doi: 10.1016/j.jbiomech.2014.04.016.

Masala S, Volpi T, Fucci FP, et al. Percutaneus osteoplasty in the treatment of extraspinal painful multiple myeloma lesions. Support Care Cancer 2011;19:957—62.

Mastier C, Gjorgjievska A, Thivolet A, et al. Musculoskeletal metastases management: the interventional radiologist's toolbox. Semin Interv Radiol. 2018;35(4):281–9. https://doi.org/10.1055/s-0038-1673420.

Mohme M, Riethdorf S, Dreimann M, et al. Circulating Tumour Cell Release after Cement Augmentation of Vertebral Metastases. Sci Rep. 2017 Aug 3;7(1):7196. doi: 10.1038/s41598-017-07649-z.

Molloy S, Mathis JM, Belkoff SM. The effect of vertebral body percentage fill on mechanical behavior during percutaneous vertebroplasty. Spine (Phila Pa 1976).2003 Jul 15;28(14):1549-54.

Moser TP, Onate M, Achour K, et al. Cementoplasty of pelvic bone metastases: systematic assessment of lesion filling and other factors that could affect the clinical outcomes. Skeletal Radiol 2019;48:1345—55.

Muller SD, Green SM, McCaskie AW. The dynamic volume changes of polymerizing polymethyl methacrylate bone cement. Acta Orthop Scand. 2002 Dec;73(6):684-7.

Müller SA, Bläuer K, Kremer M, et al. Exact CT-based liver volume calculation including nonmetabolic liver tissue in three-dimensional liver reconstruction. J Surg Res. 2010;160(2):236–43.

Muller DA, Capanna R. The surgical treatment of pelvic bone metastases. Adv Orthop. 2015. https://doi.org/10.1155/2015/ 525363.

Munk PL, Rashid F, Heran MK, et al. Combined cementoplasty and radiofrequency ablation in the treatment of painful neoplastic lesions of bone. J Vasc Interv Radiol 2009;20:903—11.

Munro JT, Fernandez JW, et al. Altered load transfer in the pelvis in the presence of periprosthetic osteolysis. J Biomech Eng. 2014. https://doi.org/10.1115/1.4028522.

Nussbaum DA, Gailloud P, Murphy K. The chemistry of acrylic bone cements and implications for clinical use in image-guided therapy. J Vasc Interv Radiol. 2004 Feb;15(2 Pt 1):121-6.

Oñate Miranda M, Moser TP. A practical guide for planning pelvic bone percutaneous interventions (biopsy, tumour ablation and cementoplasty). Insights Imaging. 2018 Jun;9(3):275-285. doi: 10.1007/s13244-018-0600-y.

Oonishi H, Akiyama H, Takemoto M, et al. The long-term in vivo behavior of polymethyl methacrylate bone cement in total hip arthroplasty. Acta Orthop. 2011 Oct;82(5):553-8. doi:10.3109/17453674.2011.625538.

Phillips AT, Pankaj P, Howie CR, et al. Finite element modelling of the pelvis: inclusion of muscular and ligamentous boundary conditions. Med Eng Phys. 2007 Sep;29(7):739-48. doi: 10.1016/j.medengphy.2006.08.010. Epub 2006 Oct 10. PMID: 17035063.

168

Poursillie E. *Génération de phantom de bassin pour la cimentoplastie*. Mémoire de diplôme d'ingénieur et de Master. Institut National des Sciences Appliquées de Strasbourg. Faculté de Physique et Ingénierie de l'Université de Strasbourg. 2020.

Race A, Mann KA, Edidin AA. Mechanics of bone/PMMA composite structures: an in vitro study of human vertebrae. J Biomech. 2007;40(5):1002-10.

Ravera EP, Crespo MJ, Catalfamo Formento PA. A subject-specific integrative biomechanical framework of the pelvis for gait analysis. Proc Inst Mech Eng H. 2018 Nov;232(11):1083-1097. doi: 10.1177/0954411918803125. Epub 2018 Oct 3. PMID: 30280643.

Roedel B, Clarençon F, Touraine S, et al. Has the percutaneous vertebroplasty a role to prevent progression or local recurrence in spinal metastases of breast cancer? J Neuroradiol. 2015 Jul;42(4):222-8. doi: 10.1016/j.neurad.2014.02.004.

Ries MD, Young E, Al-Marashi L, et al. In vivo behavior of acrylic bone cement in total hip arthroplasty. Biomaterials. 2006 Jan;27(2):256-61.

Rohlmann A, Boustani HN, Bergmann G, et al. A probabilistic finite element analysis of the stresses in the augmented vertebral body after vertebroplasty. Eur Spine J. 2010 Sep;19(9):1585-95. doi: 10.1007/s00586-010-1386-x. Epub 2010 Apr 2. PMID: 20361339; PMCID: PMC2989288.

Rommens PM, Graafen M, Arand C, et al. Minimal- invasive stabilization of anterior pelvic ring fractures with ret- rograde transpubic screws. Injury. 2020;51(2):340–6. https://doi.org/10.1016/j.injury.2019.12.018.

Roux C, Tselikas L, Yevich S, et al. Fluoroscopy and Cone-Beam CT-guided Fixation by Internal Cemented Screw for Pathologic Pelvic Fractures. Radiology. 2019 Feb;290(2):418-425. doi: 10.1148/radiol.2018181105.

Rusu MC, Ichim IC, Popa M, et al. New radiopaque acrylic bone cement. II. Acrylic bone cement with bromine-containing monomer. J Mater Sci Mater Med. 2008 Jul;19(7):2609-17. doi: 10.1007/s10856-007-3357-2. Epub 2008 Jan 16. PMID: 18197369.

Sa Y, Yang F, Wang Y, et al. Modifications of Poly(Methyl Methacrylate) Cement for Application in Orthopedic Surgery. Adv Exp Med Biol.2018;1078:119-134. doi: 10.1007/978-981-13-0950-2_7.

Sabet FA, Jin O, Koric S, et al. Nonlinear micro-CT based FE modeling of trabecular bone-Sensitivity of apparent response to tissue constitutive law and bone volume fraction. Int J Numer Method Biomed Eng. 2018 Apr;34(4):e2941. doi: 10.1002/cnm.2941. Epub 2017 Dec 21. PMID: 29168345.

San Millán Ruíz D, Burkhardt K, Jean B, et al. Pathology findings with acrylic implants. Bone. 1999 Aug;25(2 Suppl):85S-90S.

Sato R, Aramaki T, Yoza K, et al. "Direct MPR": A Useful Tool for Oblique CT Fluoroscopy-Assisted Puncture. Cardiovasc Intervent Radiol. 2017 Aug;40(8):1261-1266. doi:10.1007/s00270-017-1642-0.

Sattar MH, Guthrie ST. Anatomy, back, sacral vertebrae. In: StatPearls [Internet]. Treasure Island (FL): StatPearls Publishing; 2020. https://www.ncbi.nlm.nih.gov/books/NBK551653/

Scales JF, Herschell W. Perspex (methylemthacrylate) in orthopaedics. Br Med J 1945:245-9.

Shardlow DL, Stone MH, Ingham E, et al. Cement particles containing radio-opacifiers stimulate pro-osteolytic cytokine production from a human monocytic cell line. J Bone Joint Surg Br 2003 Aug;85:900-5.

Schmitz P, Cornelius Neumann C, Neumann C, et al. Biomechanical analysis of iliac crest loading following cortico-cancellous bone harvesting. J Orthop Surg Res. 2018;13(1):108. https://doi.org/10.1186/s13018-018-0822-1.

Silverman EJ, Landy DC, Massel DH, et al. The effect of viscosity on cement penetration in total knee arthroplasty, an application of the squeeze film effect. J Arthroplasty. 2014 Oct;29(10):2039-42. doi: 10.1016/j.arth.2014.05.010.

Schulze M, Riesenbeck O, Vordemvenne T, et al. Complex biomechanical properties of non-augmented and augmented pedicle screws in human vertebrae with reduced bone density. BMC Musculoskelet Disord. 2020 Mar 6;21(1):151. doi: 10.1186/s12891-020-3158-z.

Skripitz R, Aspenberg P. Attachment of PMMA cement to bone: force measurements in rats. Biomaterials. 1999 Feb;20(4):351-6.

Slullitel PAI, Brandariz R, Oñativia JI, et al. Aggressive granulomatosis of the hip: a forgotten mode of aseptic failure. Int Orthop 2019 Jun;43:1321-1328.

Snijders CJ, Vleeming A, Stoeckart R. Transfer of lumbosacral load to iliac bones and legs part 1: biomechanics of self-bracing of the sacroiliac joints and its significance for treatment and exercise. Clin Biomech (Bristol, Avon). 1993;8(6):285–94. https://doi.org/10.1016/0268-0033(93)90002-Y.

Spinelli MS, Ziranu A, Piccioli A, et al. Surgical treatment of acetabular metastasis. Eur Rev Med Pharmacol Sci. 2016;20(14):3005–100.

Steinhaus J, Moeginger B, Grossgarten M, et al. Dielectric analysis of depth dependent curing behavior of dental resin composites. Dent Mater. 2014 Jun;30(6):679-87. doi: 10.1016/j.dental.2014.03.002.Epub 2014 Apr 14. PubMed PMID: 24731684.

Steinhaus J, Hausnerova B, Haenel T, et al. Correlation of shear and dielectric ion viscosity of dental resins - Influence of composition, temperature and filler content. Dent Mater. 2016 Jul;32(7):899-907.doi: 10.1016/j.dental.2016.03.015.

Sun G, Jin P, Liu XW, et al. Cementoplasty for managing painful bone metastases outside the spine. Eur Radiol 2014;24:731—7.

Sun HB, Jing XS, Liu YZ, et al. The optimal volume fraction in percutaneous vertebroplasty evaluated by pain relief, cement dispersion, and cement leakage: a prospec- tive cohort study of 130 patients with painful osteoporotic vertebral compression fracture in the thoracolumbar vertebra. World Neurosurg 2018;114:e677—88.

Sutter EG, Mears SC, Belkoff SM. A biomechanical evaluation of femoroplasty under simulated fall conditions. J Orthop Trauma 2010;24:95—9.

Tian QH, Wu CG, Gu YF, et al. Combination radiofrequency ablation and percutaneous osteoplasty for palliative treatment of painful extraspinal bone metas- tasis: a single-center experience. J Vasc Interv Radiol 2014;25:1094—100.

Togawa D, Bauer TW, Lieberman IH, et al. Histologic evaluation of human vertebral bodies after vertebral augmentation with polymethyl methacrylate. Spine (Phila Pa 1976). 2003 Jul 15;28(14):1521-7.

Togawa D, Kovacic JJ, Bauer TW, et al. Radiographic and histologic findings of vertebral augmentation using polymethylmethacrylate in the primate spine: percutaneous vertebroplasty versus kyphoplasty. Spine (Phila Pa 1976). 2006 Jan 1;31(1):E4-10.

Toyota N, Naito A, Kakizawa H, et al. Radiofrequency ablation therapy combined with cementoplasty for painful bone metastases: initial experience. Cardiovasc Intervent Radiol 2005;28:578—83.

Trumm CG, Jakobs TF, Stahl R, et al. CT fluoroscopy-guided vertebral augmentation with a radiofrequency-induced, high-viscosity bone cement (StabiliT(®)): technical results and polymethylmethacrylate leakages in 25 patients. Skeletal Radiol. 2013 Jan;42(1):113-20. doi: 10.1007/s00256-012-1386-5.

Tschirhart CE, Roth SE, Whyne CM. Biomechanical assessment of stability in the metastatic spine following percutaneous vertebroplasty: effects of cement distribution patterns and volume. J Biomech. 2005 Aug;38(8):1582-90.

Tschirhart CE, Finkelstein JA, Whyne CM. Optimization of tumor volume reduction and cement augmentation in percutaneous vertebroplasty for prophylactic treatment of spinal metastases. J Spinal Disord Tech. 2006 Dec;19(8):584-90.

Tselikas L, Joskin J, Roquet F, et al. Percutaneous bone biopsies: comparison between flat-panel cone-beam CT and CT-scan guidance. Cardiovasc Intervent Radiol. 2015 Feb;38(1):167-76. doi: 10.1007/s00270-014-0870-9.

Tsoumakidou G, Borensztein M, Zini C, et al. Postablation insufficiency fracture of the iliac crest: management by percutaneous screw fixation. Cardiovasc Interv Radiol. 2014;37(4):1126–8. https://doi.org/10.1007/s00270-013-0781-1.

Tsoumakidou G, Too CW, Koch G, et al. CIRSE Guidelines on percutaneous vertebral augmentation. Cardiovasc Intervent Radiol 2017;40:331—42.

Turner CH, Rho J, Takano Y, et al. The elastic properties of trabecular and cortical bone tissues are similar: results from two microscopic measurement techniques. J Biomech. 1999 Apr;32(4):437-41. doi: 10.1016/s0021 9290(98)00177-8. PMID: 10213035.

Urrutia J, Bono CM, Mery P, et al. Early histologic changes following polymethylmethacrylate injection (vertebroplasty) in rabbit lumbar vertebrae. Spine (Phila Pa 1976). 2008 Apr 15;33(8):877-82. doi:10.1097/BRS.0b013e31816b46a5.

Vallittu PK. A review of methods used to reinforce polymethyl methacrylate resin. J Prosthodont. 1995 Sep;4(3):183-7.

Vallo CI. Theoretical prediction and experimental determination of the effect of mold characteristics on temperature and monomer conversion fraction profiles during polymerization of a PMMA-based bone cement. J Biomed Mater Res.2002;63(5):627-42.

Vassilikou-Dova A, Kalogeris IM. Dielectric analysis (DEA). In book: Thermal Analysis of Polymers: Fundamentals and Applications, Edition: 1st, Chapter: 6, Publisher: Wiley, pp.497 – 613 DOI: 10.1002/9780470423837.ch6

Verlaan JJ, Oner FC, Verbout AJ, et al. Temperature elevation after vertebroplasty with polymethylmethacrylate in the goat spine. J Biomed Mater Res B Appl Biomater. 2003 Oct 15;67(1):581-5.

Vleeming A, Schuenke MD, Masi AT, et al. The sacroiliac joint: an overview of its anatomy, function and potential clinical implications. J Anat. 2012;221(6):537–67. 37. https://doi.org/10.1111/j.1469-7580.2012.01564.x.

Vielgut I, Sadoghi P, Gregori M, et al. The modified Harrington procedure for metastatic peri-acetabular bone destruction. Int Orthop. 2013;37(10):1981–5. https://doi.org/10. 1007/s00264-013-1940-3Epub 2013 Jun 12.

Volinski B, Kalra A, Yang K. Evaluation of full pelvic ring stresses using a bilateral static gait-phase finite element modeling 33. method. J Mech Behav Biomed Mater. 2018;78:175–87. https:// doi.org/10.1016/j.jmbbm.2017.11.006.

Waanders D, Janssen D, Mann KA, et al. The mechanical effects of different levels of cement penetration at the cement-bone interface. J Biomech. 2010 Apr 19;43(6):1167-75. doi: 10.1016/j.jbiomech.2009.11.033.

Wallace AN, Robinson CG, Meyer J, et al. The Metastatic Spine Disease Multidisciplinary Working Group Algorithms. Oncologist. 2015 Oct;20(10):1205-15. doi: 10.1634/theoncologist.2015-0085.

Wallace AN, Huang AJ, Vaswani D, et al. Combination acetabular radiofrequency ablation and cemen- toplasty using a navigational radiofrequency ablation device and ultrahigh viscosity cement: technical note. Skeletal Radiol 2016;45:401—5.

Wang B, Zou C, Hu X, et al. Reconstruction with a novel combined hemipelvic endoprosthesis after resection of periacetabular tumors involving the sacroiliac joint: a report of 25 35. consecutive cases. BMC Cancer. 2019;19(1):861. https://doi.org/ 10.1186/s12885-019-6049-7.

Webb JC, Spencer RF. The role of polymethylmethacrylate bone cement in modern orthopaedic surgery. J Bone Joint Surg Br. 2007 Jul;89(7):851-7.

Werner B, Ovesy M, Zysset PK. An explicit micro-FE approach to investigate the post-yield behaviour of trabecular bone under large deformations. Int J Numer Method Biomed Eng. 2019 May;35(5):e3188. doi: 10.1002/cnm.3188. Epub 2019 Mar 13. PMID: 30786166.

Webb JC, Spencer RF. The role of polymethylmethacrylate bone cement in modern orthopaedic surgery. J Bone Joint Surg Br. 2007 Jul;89(7):851-7.

Wei Z, Zhang K, Ye X, et al. Com- puted tomography-guided percutaneous microwave ablation combined with osteoplasty for palliative treatment of painful extraspinal bone metastases from lung cancer. Skeletal Radiol 2015;44:1485—90.

Weill A, Kobaiter H, Chiras J. Acetabulum malignancies: tech- nique and impact on pain of percutaneous injection of acrylic surgical cement. Eur Radiol 1998;8:123—9.

Wells G, Shea B, O'connell D, et al. The Newcastle- Ottawa Scale (NOS) for assessing the quality of non-randomised studies in meta-analyses. [Available from: http://www. evidencebasedpublichealth.de/download/Newcastle Ottowa Scale Pope Bruce.pdf].

Winter KS, Hofmann FO, Thierfelder KM, et al. Towards volumetric thresholds in RECIST 1.1: therapeutic response assessment in hepatic metastases. Eur Radiol. 2018;28(11):4839–48. https://doi.org/10.1007/s00330-018-5424-0.

Wunder JS, Ferguson PC, Griffin AM, et al. Acetabular metastases: planning for reconstruction and review of results. Clin Orthop Relat Res. 2003;415 Suppl:187–97.

Xie L, Chen Y, Zhang Y, et al. Status and prospects of percutaneous vertebroplasty combined with ^{125}I seed implantation for the treatment of spinal metastases. World J Surg Oncol. 2015;13:119. Published 2015 Mar 25. doi:10.1186/s12957-015-0484-y

Yan C, Hao L, Hussein A, et al. Ti-6Al-4V triply periodic minimal surface structures for bone implants fabricated via selective laser melting. J Mech Behav Biomed Mater. 2015 Nov;51:61-73. doi: 10.1016/j.jmbbm.2015.06.024. Epub 2015 Jul 9. PMID: 26210549.

Yevich S, Tselikas L, Gravel G, et al. Percutaneous Cement Injection for the Palliative Treatment of Osseous Metastases: A Technical Review. Semin Intervent Radiol 2018 Oct;35:268-280.

Zadpoor AA. Mechanical performance of additively manufactured meta-biomaterials. Acta Biomater. 2019 Feb;85:41-59. doi: 10.1016/j.actbio.2018.12.038. Epub 2018 Dec 24. PMID: 30590181.

Zaharie DT, Phillips ATM. Pelvic Construct Prediction of Trabecular and Cortical Bone Structural Architecture. J Biomech Eng. 2018 Sep 1;140(9). doi: 10.1115/1.4039894. PMID: 29801165.

Zhang QH, Cossey A, Tong J. Stress shielding in bone of a bone-cement interface. Med Eng Phys. 2016 Apr;38(4):423-6. doi: 10.1016/j.medengphy.2016.01.009.

Zhang ZF, Huang H, Chen S, et al. Comparison of high- and low-viscosity cement in the treatment of vertebral compression fractures: A systematic review and meta-analysis. Medicine (Baltimore). 2018 Mar;97(12):e0184. doi: 10.1097/MD.0000000000010184.

Zhu HT, Chen Y, Xiong YF, et al. A Flexible Wireless Dielectric Sensor for Noninvasive Fluid Monitoring. Sensors (Basel). 2019 Dec 27;20(1). pii: E174. doi: 10.3390/s20010174. PubMed PMID: 31892240.

RESUME EN FRANCAIS

Introduction

La cimentoplastie percutanée est une intervention mini-invasive qui consiste à injecter du ciment orthopédique dans un os fragilisé par l'ostéoporose ou une tumeur. L'imagerie est utilisée pour guider l'insertion du trocart osseux et pour visualiser la répartition du ciment dans l'os lors de l'injection. La cimentoplastie a d'abord été développée pour des applications dans le rachis (on parle alors de vertébroplastie) puis a ensuite été utilisée pour traiter des tumeurs extra-rachidiennes douloureuses. Si le principe général du geste est similaire, la cimentoplastie extra-rachidienne diffère de la vertébroplastie par certains aspects comme l'abord anatomique et le volume de ciment injecté. Si un faible volume de ciment orthopédique semble suffisant pour traiter la douleur, peu de données existent sur l'influence de la quantité de ciment sur la consolidation osseuse. Par ailleurs, il n'existe à l'heure actuelle pas de système spécifique permettant une injection supérieure à 10 ml. Le but de cette thèse est d'étudier l'influence mécanique du volume de ciment et de proposer et évaluer des solutions potentielles pour l'injection d'un volume de ciment supérieur à 10 ml (large volume de ciment) qui s'accompagne de contraintes spécifiques notamment concernant la viscosité

Revue de la littérature

Dans un premier temps une revue de la littérature a été réalisée. La revue systématique des articles sur la cimentoplastie extra-rachidienne a permis d'inclure 761 lésions traitées chez 652 patients. Le ciment orthopédique utilisé était toujours du polymethylmetacrylate (PMMA). La majorité des lésions traitées se situaient au niveau du bassin (489/761). Le volume moyen de ciment injecté variait entre 2,7 et 32,2 ml selon les études. Seuls 7 articles sur 30 décrivaient brièvement comment injecter plus de 10 ml avec les systèmes de vertébroplastie, sans qu'il y ait de standardisation dans la technique. Cela nécessitait toujours la mise en plus de plusieurs aiguilles, soit simultanément soit séquentiellement.

La revue portant sur le PMMA a montré l'importance de la viscosité dans la diffusion du ciment au sein d'une structure osseuse. Une fois dans l'os le ciment agit principalement par interaction mécanique, et non par interaction chimique, avec les trabécules osseuses. Le PMMA présente une meilleure résistance en compression qu'en tension ou cisaillement. L'analyse des études biomécaniques au niveau du rachis montrent qu'un remplissage partiel d'une vertèbre permet de restaurer les transmissions de force alors qu'un remplissage plus important est nécessaire pour restaurer la rigidité.

Enfin, une revue de la littérature sur la biomécanique du bassin a été réalisée afin de mieux comprendre l'intérêt potentiel de la cimentoplastie à visée de consolidation. La région acétabulaire, et plus particulièrement le toit du cotyle, est soumise à d'importantes contraintes de compression et représente donc une localisation préférentielle pour l'injection de ciment.

Evaluation des pratiques cliniques

Dans un premier temps, les techniques d'injection d'un large volume de PMMA sont détaillées. La première technique consiste à insérer un premier trocart et injecter 10 ml puis insérer une deuxième aiguille et ainsi de suite (technique séquentielle à plusieurs trocarts). Une deuxième technique consiste à insérer d'emblée plusieurs aiguilles puis à injecter simultanément plusieurs volumes de 10 ml de ciment sur chacune des aiguilles (technique simultanée à plusieurs trocarts). Enfin, une troisième possibilité est décrite sur la base de 3 cas réalisés en clinique : un seul trocart est positionné dans le grand axe de la lésion et plusieurs volumes de ciment de 10 ml sont injectés successivement les uns après les autres à travers ce seul trocart (technique à un seul trocar). La principale limite de cette dernière technique est de gérer la viscosité des ciments successifs afin que la polymérisation n'intervienne pas avant l'injection.

Une analyse rétrospective des cimentoplasties du cotyle réalisées entre Janvier 2010 et Décembre 2018 a été réalisée pour déterminer le taux de remplissage moyen d'une lésion ostéolytique en pratique clinique. Cette étude a porté sur 21 lésions. Le taux moyen de remplissage en analyse volumétrique était de 35,3%. Par ailleurs, l'analyse subjective par l'opérateur (sans calcul volumétrique) tendait à surestimer le remplissage de manière constante.

Enfin, une étude sur la fragmentation secondaire du PMMA après cimentoplastie pelvienne chez 56 patients a été menée. Sur 98 zones de cimentoplastie, seules 2 ont présenté des signes de fragmentation lors d'un suivi moyen de 29,3 mois. Les deux cas sont survenus sur des métastases et semblaient liés à des contraintes mécaniques et non à un défaut de la qualité du ciment. Il en a été conclu que la porosité, autre propriété de travail du PMMA avec la viscosité, n'avait pas d'influence en cimentoplastie extra-rachidienne.

Influence du volume de ciment sur les propriétés mécaniques de l'os

Les différentes analyses de la littérature et des pratiques cliniques ont montré l'absence de données robustes sur l'influence mécanique du volume de ciment. Dans cette partie, une analyse expérimentale et une analyse par éléments finis ont été réalisées.

Analyse expérimentale

5 modèles de bassin en mousse solide (Pelvis Full Male, Sawbones Europe AB) ont été utilisés. Un modèle était laissé intact pour servir de référence. Les 4 autres modèles ont été préparés en usinant une cavité au-dessus du cotyle afin de simuler une tumeur d'environ 10 ml d'un côté et d'environ 20 ml de l'autre. L'ensemble des bassins ont été passés au scanner afin de calculer le volume exact des cavités et définir le volume nécessaire de ciment pour 4 niveaux de remplissage (0%, 20%, 60%, 100%). Après remplissage avec le volume prédéfini de PMMA, les bassins ont été testés sur une machine de traction à la vitesse de 1 mm/min avec une précharge de 1N en appliquant la force sur le cotyle et en maintenant la crête iliaque homolatérale fixe. La rigidité a ensuite été calculée pour chaque volume de cavité et de remplissage. Les résultats pour la cavité de 10 ml sont représentés en figure1 et ceux pour la cavité de 20 ml en figure2. Les mesures expérimentales montrent une relation nette entre le taux

de remplissage de la cavité et la rigidité. Pour une cavité de petit volume, le remplissage complet permet une restauration de la rigidité, alors que cela ne semble pas être le cas pour une cavité de plus grand volume. Ces résultats tendent à confirmer que le remplissage maximal d'une lésion doit être la règle.
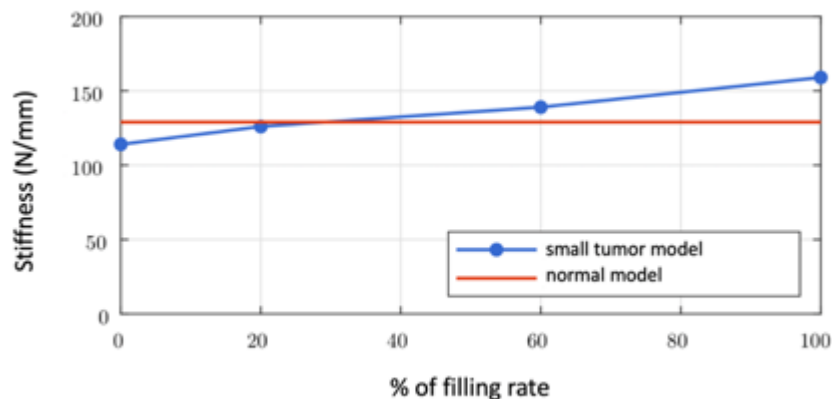
Fig.1 : évolution de la rigidité en fonction du taux de remplissage pour une cavité de faible volume (environ 10 ml)
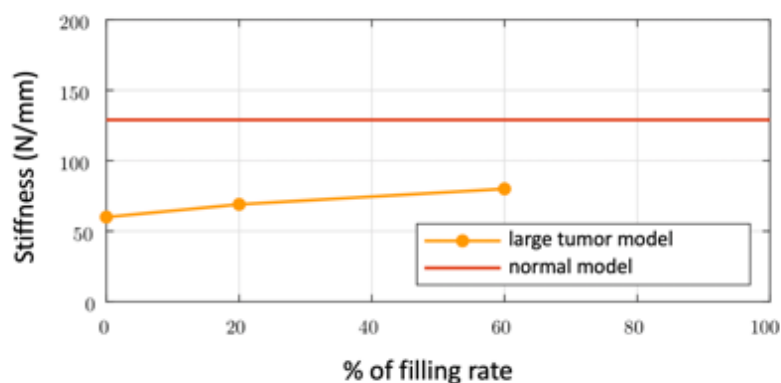
Fig.2 : évolution de la rigidité en fonction du taux de remplissage pour une cavité de gros volume (environ 20 ml)

Analyse par éléments finis

Pour réaliser une simulation numérique, un design assisté par ordinateur d'un bassin a été réalisé selon une méthodologie qui a été affinée progressivement. A partir d'un scanner du modèle de bassin, un fichier stéréolithographique a été généré et utilisé pour les simulations. Les paramètres utilisés (module de Young,

177

coefficient de Poison) pour l'os et le PMMA étaient ceux de la littérature. Ces paramètres étaient simplifiés au maximum (épaisseur constante, propriétés isotropes et homogènes).

Dans un premier temps, le modèle numérique a été validé en le confrontant aux données expérimentales réalisées dans un travail précédent sur un humérus de l'institut d'anatomie cimenté et soumis à un test de flexion 3 points. La corrélation entre les données expérimentales et numériques étant bonne, une analyse a été réalisée au niveau du bassin.

Deux séries de simulation ont été menées sur le bassin, l'une en considérant le promontoire du sacrum comme fixe, l'autre en le considérant partiellement mobile. Dans les deux cas, une force de 500N était appliquée au niveau du fond du cotyle à 45° afin de simuler un appui monopodal. Deux modèles de tumeurs était simulés : une de 20 ml avec atteinte corticale, l'autre de 20 ml également mais sans destruction corticale. Les contraintes de Von Mises et la rigidité étaient calculées. Les résultats pour une tumeur avec atteinte corticale et en considérant le sacrum partiellement mobile sont représentés en fig.3. Pour un remplissage de 50% par le ciment, il existe une normalisation des contraintes de surface alors qu'un remplissage de 100% ne suffit pas à restaurer complètement la rigidité d'un modèle sans tumeur.
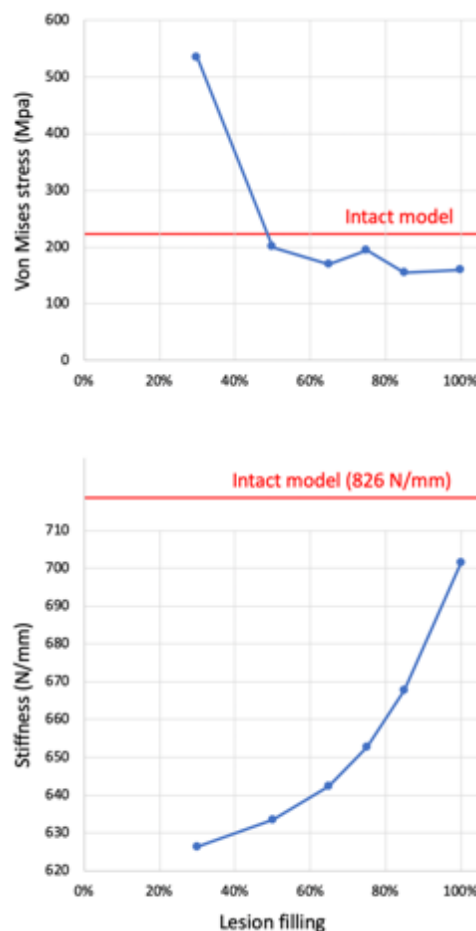

Fig.3 : contraintes de Von Mises et rigidité en fonction du taux de remplissage

178

Au total, les analyses expérimentales et numériques montrent une influence notable du taux de remplissage d'une tumeur ostéolytique sur la rigidité du bassin. Un remplissage maximal devrait être l'objectif lors d'une cimentoplastie extra-rachidienne.

Comparaison des différentes techniques d'injection d'un large volume de ciment

Il existe trois techniques pour injecter un large volume de ciment : la technique séquentielle à plusieurs trocarts, la technique simultanée à plusieurs trocarts et la technique à trocart unique. Au-delà des considérations anatomiques, l'absence de coalescence des différents volumes de ciment pourrait être une limite des techniques à plusieurs trocarts. Pour mieux explorer les avantages et inconvénients de chaque technique, des simulations numériques et des tests sur fantômes de bassin ont été réalisées.

Simulations

La simulation de l'écoulement de ciment a été réalisée sur le logiciel Moldflow qui intègre un modèle de Castro-Macosko associé à un modèle de Cross pour prendre en compte tous les paramètres influant sur la viscosité à savoir la température, le temps et le taux de cisaillement. Après avoir défini les paramètres cinétiques et de viscosité du PMMA, les conditions d'injection (site d'injection, diamètre d'injection, température du PMMA, température du moule dans lequel l'injection est faite, débit d'injection) ont été paramétrées pour reproduire le plus fidèlement possible une injection réelle. La simulation a d'abord été faite pour une sphère de 3 ml puis dans un moule représentant la forme d'une vertébroplastie réalisée en clinique. Ces deux simulations ont permis de démontrer la faisabilité de la simulation à partir d'un seul point d'injection.

La simulation a ensuite été réalisée avec deux points d'injection sur des modèles d'humérus préalablement cimentés dont la géométrie a été extraite à partir de scanners des pièces anatomiques cimentées. Pour le premier humérus, une simulation d'injection de deux volumes de 10 ml de PMMA sur un seul site d'injection avec une pause d'une minute entre les deux injections a été menée. Celle-ci a démontré une augmentation focale de la viscosité du PMMA autour du point d'injection après la phase de pause, suggérant la possible formation de bouchons avec la technique à un seul trocart et plusieurs ciments. Pour le deuxième humérus, deux points d'injection ont été définis et 10 ml de PMMA a été simulé sur chaque site. Cette simulation a montré une différence temporelle de polymérisation au niveau des fronts de ciment, suggérant une possible non-cohésion des ciments en cas de technique simultanée à plusieurs trocarts.

Essais expérimentaux

Plusieurs tentatives de comparaison des différentes techniques d'injection ont été réalisées sur des modèles de bassin en mousse solide et sur os secs. Malheureusement, aucun de ces modèles ne s'est révélé adéquat en raison de l'absence de reproductibilité de la diffusion de PMMA par rapport à une injection réelle. En utilisant des structures lattices, un modèle de bassin a été crée par fabrication additive. Plusieurs modèles d'os trabéculaire ont

été testés pour choisir le plus représentatif de la réalité. Le choix s'est porté sur une structure lattice triangulaire à double porosité, qui permet de reproduire une forme de ciment satisfaisante ainsi qu'une possible lésion grâce à la porosité plus faible au centre.

Sur ce modèle, plusieurs injections ont été réalisées selon le protocole présenté dans le tableau1

Technique	nb of needles	description	delivery device
injection of 20 ml of bone cement			
sequential several trocars	2	1) Insertion of a needle 2) Injection of 10 ml 3) Insertion of 2nd needle 4) Injection of 10 ml	delivery system for vertebroplasty
simultaneous several trocars	2	1) Insertion of 2 needles 2) Simultaneous injection of 10 ml on each needle	delivery system for vertebroplasty
single trocar	1	1) Insertion of 1 needle 2) Injection of 20 ml on the needle	30 ml syringe
injection of 30 ml of bone cement			
sequential several trocars	3	1) Insertion of a needle 2) Injection of 10 ml 3) Insertion of 2nd needle 4) Injection of 10 ml 5) Insertion of 3rd needle 6) Injection of 10 ml	delivery system for vertebroplasty
simultaneous several trocars	3	1) Insertion of 3 needles 2) Simultaneous injection of 10 ml on each needle	delivery system for vertebroplasty
single trocar	1	1) Insertion of 1 needle 2) Injection of 30 ml on the needle	30 ml syringe

Tableau1 : protocole pour la comparaison des différentes techniques d'injection

Un exemple d'injection de 30 ml avec la technique simultanée à plusieurs trocarts est présenté en fig.4. Les résultats apparaissent dans le tableau2
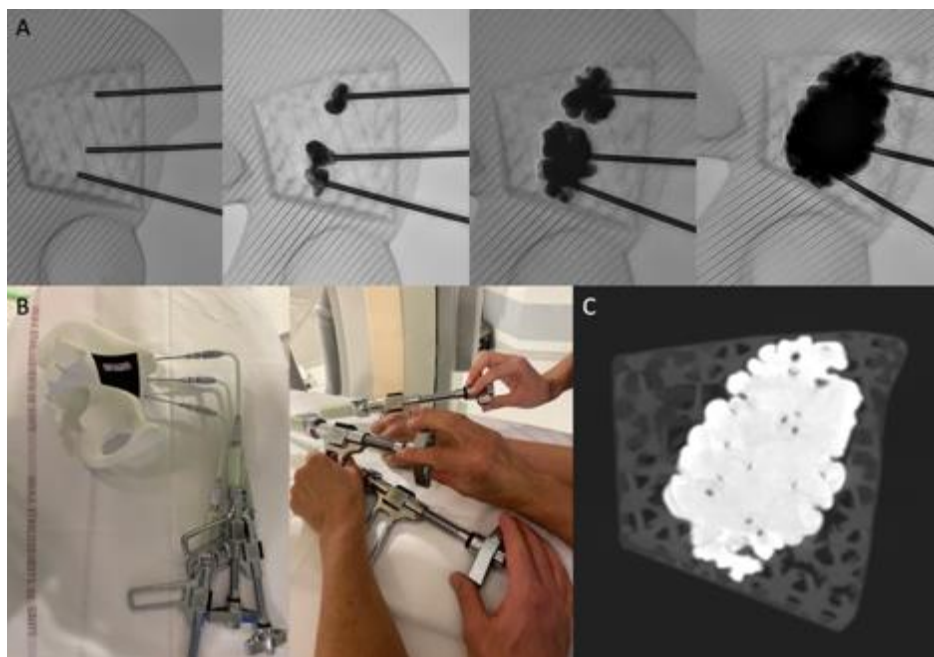
Fig.4 : exemple d'injection de 30 ml avec 3 aiguilles simultanées

technique	confidence of the radiologist in the identification of cement dispersion	force required to perform the injection	height/width ratio	CT aspect of the cement plugs
injection of 20 ml of bone cement				
sequential several trocars	well adapted for clinical practice	well adapted for clinical practice	1.2	partially cohesive
simultaneous several trocars	Poorly adapted for clinical practice	well adapted for clinical practice	1	Completely cohesive
single trocar	well adapted for clinical practice	Poorly adapted for clinical practice	0.9	Completely cohesive
injection of 30 ml of bone cement				
sequential several trocars	well adapted for clinical practice	well adapted for clinical practice	1.5	Completely cohesive
simultaneous several trocars	Not adapted for clinical practice	well adapted for clinical practice	1.3	Completely cohesive
single trocar	well adapted for clinical practice	Not adapted for clinical practice	0.9	Completely cohesive

Tableau2 : résultats des essais expérimentaux

Au vu des résultats, la technique la plus intéressante pour la pratique clinique semble être la technique à trocart unique et large volume unique de ciment. Cette approche nécessite toutefois le développement d'abords anatomiques et d'assistance spécfiques.

Assistance à l'injection d'un large volume de ciment à travers un seul site d'injection

Standardisation anatomique

Au niveau du bassin, l'injection sur un seul site nécessite de définir des abords anatomiques précis.

La technique d'abord antérieur double oblique a été définie sur modèle de bassin et sa réalisation a été standardisée à l'aide de deux points anatomiques : l'épine iliaque antéro-supérieure et l'épine sciatique. Une évaluation de la faisabilité anatomique a été conduite par l'analyse de 60 scanners de bassin (30 femmes/30 hommes, analyse bilatérale). L'analyse radiologique a confirmé la faisabilité de cette approche qui donne accès à la partie postérieure du cotyle et au toit de l'acétabulum avec un seul abord. Sur 120 mesures, seules 4 présentaient un trajet transfixiant l'aile iliaque, et pouvaient aisément être ajustées sur le scanner de repérage.

Une deuxième voie d'abord sur l'axe de transmission des forces a ensuite été évaluée en utilisant deux autres points anatomiqes : l'épine iliaque postéro-supérieure et l'épine iliaque antéro-inférieure. Sur 20 scanners, l'abord antérieur et l'abord postérieur ont été comparés. L'abord postérieur semblait globalement plus facile car sans traversée musculaire et avec une distance similaires entre les deux approches.

Au total, ces deux abord anatomiques permettent d'approcher une lésion du bassin dans son grand axe, ce en se basant sur des repères reproductibles.

Analyse diélectrique de la viscosité

L'étude de la polymérisation des ions et des dipôles d'un fragment de PMMA soumis à un courant électrique alternatif représente la base de l'analyse diélectrique. Le modèle mathématique montre l'existence d'une corrélation entre viscosité ionique et dynamique.

Dans un premier temps, une mesure synchronisée de la viscosité ionique et de la viscosité dynamique a démontré une corrélation entre les deux mesures, ce indépendamment de la température (fig.5)
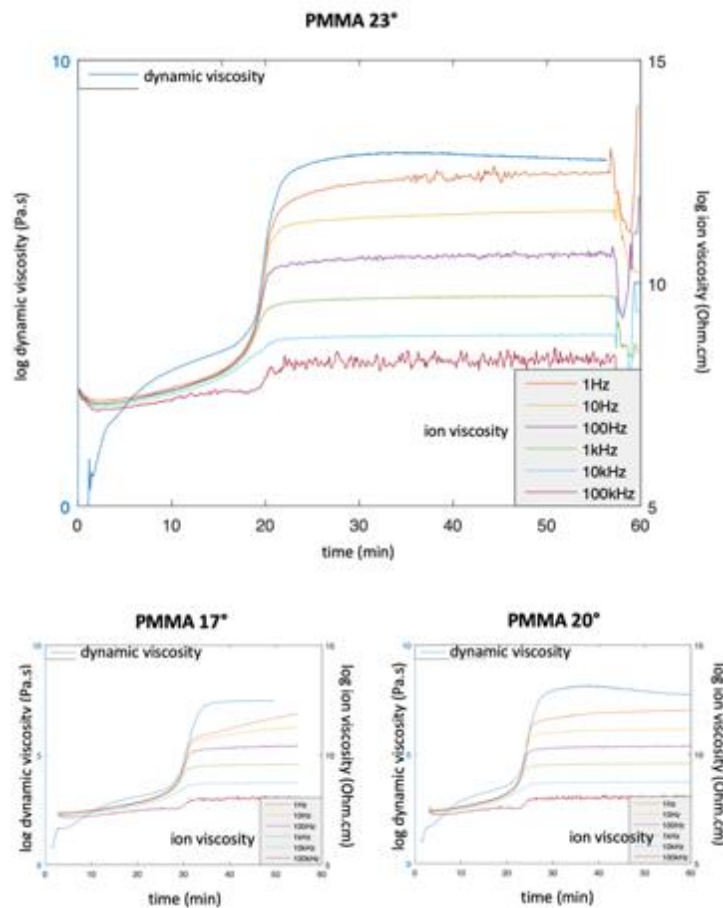
Fig.5 : mesures synchronisées de viscosité ionique et dynamique

Dans un deuxième temps, une mesure in-situ de la viscosité a été testée sur modèle de vertèbre. 5 corps vertébraux ont été préparés afin de pouvoir insérer une électrode diélectrique. Une injection de PMMA a ensuite été réalisée sur chacune des 5 vertèbres. L'analyse d'une vertèbre est présentée en fig.6. La mesure diélectrique montre l'évolution de la polymérisation du ciment avec en particulier le pic lors de la phase de durcissement du ciment.
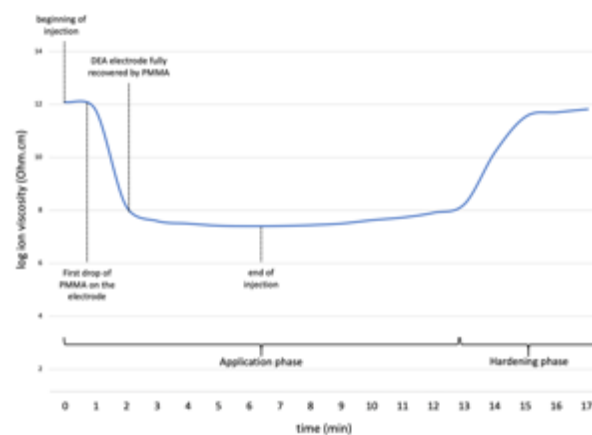

Fig.6 : exemple de mesure in-situ de viscosité ionique

Au total, l'analyse diélectrique permet d'approcher la viscosité dynamique in-situ via la viscosité ionique. Cela pourrait aider à améliorer l'injection d'un large volume de ciment en montrant en temps réel au praticien que le ciment se situe dans une fenêtre de viscosité optimale.

Adaptation du robot S-tronic

Le S-tronic est un robot développé pour l'injection de ciment lors d'une vertébroplastie. En plus d'éloigner le praticien de la source d'irradiation grâce au contrôle téléopéré, ce système permet d'allonger significativement la durée d'injection grâce au refroidissement passif du PMMA. Cela est particulièrement intéressant en cas d'injection d'un large volume car la polymérisation précoce du ciment est la limite majeure à la technique sur trocart unique.

Une seringue de 30 ml en polypropylène a été utilisée comme réservoir pour le large volume de ciment. Un fourreau en aluminium a ensuite été usiné pour permettre à la seringue de résister à une pression interne de 17 MPa qui représente la limite élastique du polypropylène. Une coque en PLA réalisée par fabrication additive et contenant un gel eutectique permet de maintenir le couple seringue – fourreau au froid pendant la durée d'injection et ainsi d'augmenter la durée de la phase d'application de 16 à plus de 30 min.

Un essai sur modèle vertébral a démontré qu'il était possible d'injecter un volume de 30 ml à une vitesse de 1ml/min avec le robot, confirmant que l'adaptation du S-tronic permettait d'atteindre le but recherché d'injecté un large volume de ciment sans polymérisation en cours d'injection.

Conclusion

Les différents travaux menés au cours de cette thèse ont permis de mieux comprendre l'importance mécanique du volume de ciment en cimentoplastie extra-rachidienne, d'évaluer les différentes techniques d'injection d'un marge volume de ciment, et de proposer des solutions d'assistance anatomiques mais également diélectriques et robotiques. Cette thèse ouvre plusieurs voies de développement futures.

Julien GARNON

ASSISTANCE TO THE INJECTION OF A LARGE VOLUME OF ORTHOPEDIC BONE CEMENT

Résumé

La cimentoplastie extra-rachidienne est une intervention percutanée guidée par l'image qui consiste à injecter du ciment acrylique, du polymethylmétacrylate (PMMA) le plus souvent, au sein d'un os pathologique. Le but est non seulement de traiter la douleur mais aussi de renforcer la tenue mécanique de l'os notamment au niveau du bassin. Dans cet optique, le volume de ciment et la technique d'injection pourraient être des facteur prédictifs de succès du geste.

Le but de ce travail est de faire un état de l'art sur la cimentoplastie extra-rachidienne, le PMMA et sur la biomécanique du bassin afin d'identifier les axes potentiels de développement de la technique. Une étude des pratiques cliniques est également réalisée. S'en suit la présentation des résultats de travaux précliniques sur l'influence du volume de ciment et de la technique d'injection d'un volume de PMMA supérieur à 10 ml. Puis 3 axes d'assistance à l'injection d'un volume de plus de 10 ml sont présentés et évalués.

Mots-clés : cimentoplastie extra-rachidienne, rigidité, diélectrique, robotique médicale

Abstract

Extra-spinal cementoplasty is a percutaneous image-guided intervention whereby acrylic bone cement, polymethylmetacrylate (PMMA) most exclusively, is injected inside a pathological bone. The goal is to alleviate the pain and to provide bone consolidation, notably in the osseous pelvis. In this perspective, the volume of bone cement and the technique of injection may predict the outcomes of the procedure.

The purpose of the thesis is to perform a state-of-the-art review of extra-spinal cementoplasty, PMMA and the biomechanics of the osseous pelvis in order to identify technical details that may be improved. A retrospective analysis of the clinical practice is also presented. The mechanical influence of the volume of bone cement and a comparison of the different techniques of injection of a volume greater than 10 ml are then evaluated using numerical simulations and experiments on phantoms. Finally, assistance to the injection of a volume greater than 10 ml is presented and evaluated through 3 different approaches.

Key words: extra-spinal cementoplasty, stiffness, dielectric, medical robotics